



**Flame Propagation Through Different Sizes of Metal Mesh and  
Mitigation Using Fine Water Sprays**

**By**

**ABDULLAHI ALHAJI AHMADU**

**(@00348426)**

**Submitted in accordance with the requirements for the  
Degree of Master of Research**

**Department of Petroleum and Gas Engineering  
School of Computing, Science and Engineering  
University of Salford**

**September, 2018**

## **Dedication**

I dedicated this research study to my parents – Alhaji Ahmadu Nma and Hajiya Jumai Ahmadu and Alhaji Umar Panti and Hajiya Fatima Mohammed (They all sacrificed many things because of my higher education) and to all my siblings.

## **Acknowledgement**

I would like to use this medium to express my deep gratitude to Almighty Allah for granting me good health and strength to withstand all the pressures I went through.

It is unlikely to complete this research study without the help and support of many people. The acknowledgements resulted in the hardest part of writing, because it was not simple to find the right words to express my gratitude for those people, who support and accompany me throughout these years.

First of all, to my supervisors Dr Amir Nourian and Dr Abbas Abubakar, for their tremendous efforts in ensuring that I remained committed, focused and imaginative in my thinking, sayings and even writing. Your humility has given me the courage to be close to you and learnt so much from your vast of knowledge and character. At many stages, I have benefited from your advice, especially in the lab for exploring new ideas, and giving me the freedom to pursue my interests in the combustion group.

I wish to express my heartfelt thanks to colleagues, and friends most especially Mr Aminu Abba Yahaya, Mr Umar Iliyasu Mr Kabir Hassan Jega, Mr Hassan Kabir, Mal. Bala Inyass, Mr Aliyu Mohammed, Mr Adamu Rufai, Mr Yahaya Ibrahim and all those that were there for me knowingly and unknowingly for their encouragement and guidance throughout the period of this research study as well as the preparation of this thesis.

I would also like to express my deep, sincere thanks to my Parents Alhaji Ahmadu Nma and Hajiya Jumai Ahmadu, my siblings especially Mr Tanimu Ahmadu and Mrs Hauwa Kulu Ahmadu for their endless prayers, guidance and financial support during this research study.

I would like to thank Mr Alan Mappin for his assistance in the laboratory experiment and useful discussions throughout the project.

I would like to sincerely give thanks to all the members of Alhaji Ahmadu Nma family for their endless prayers and support throughout the period of these study.

Finally, I also express my profound gratitude to my wife (Mrs. Khadijat Umar Abdullahi) and my children (Ahmad Sultan Abdullahi and Muazu Sherif Abdullahi) for their patience, prayers and also financial support during the past three years.



## **Declaration**

I, Ahmadu Abdullahi Alhaji, declare that this research thesis is my original work, and has not been submitted elsewhere for any award. Any section, part or phrasing that has been used or copied from other literature or documents has been adequately referenced at the point of use as well as in the reference section of the thesis work.

.....

Signature

.....

Date

.....

Supervisor

Dr Amir Nourian

.....

.....

Co-supervisor

Dr Abubakar Abbas Jibrin

.....

## Abstract

Explosion is one of the major problems faced in dealing with flammable hydrocarbon gases. Following the recent tragic incident resulting from gas and vapour cloud explosion around the globe, there has been a great interest in the use of fine water spray to suppress the explosion. The present work is focused on the mitigation of slow-moving deflagration flames flow through various mesh sizes and water spray, with resulting speeds of  $\leq 30$  m/s. Thus, the mesh sizes thickness and droplets within the spray must be small enough to extract heat in the short finite moments that the flame, mesh and droplets interact (approximately 0.03ms for a representative 1mm thick flame front, 0.94mm, 1.31mm, and 6mm diameter meshes). A novel technique, of woven wire steel mesh and perforated steel mesh combined with a high-pressure atomiser known as a Spill Return Atomiser (SRA), was selected, which contained a unique swirl chamber.

The investigation was conducted in three stages including configurations with dry, dry plus mesh and wet plus mesh trials. At the initial stage, the hot trials of homogeneous methane-air mixtures throughout the whole flammable range of 6, 7 and 9% was conducted and the flame speeds observed were 26.32, 27.01 and 30 m/s respectively. The second stage involved flame flow through the mesh. The flame speed observed for the trial was 20.36, 22.75 and 23.31 m/s for 6, 7 and 9% methane-air mixture respectively, for 0.94mm mesh. Mesh insertion into the system reduces the flame speed, and also a decrease in temperature was observed due to the heat loss to the mesh. Similar trend were observed for 1.31 and 6mm meshes. Finally, the flame flow through both mesh and water sprays was investigated, with an average flame speed within the range of 4 – 30 m/s. Whereby a configuration consisting of a steel mesh and a cross flow (X/F) of 4 spill return atomizers at a separation distance of 1000 mm from the mesh in the direction of the flame propagation. The spill return atomizers were configured at 105 mm and 120° apart and opposed to each other, thereby providing a total spray region of 315 mm. The flame speed observed during this trial was 6 and 11.99 m/s for 6 and 7% methane-air mixture respectively at downstream 0.94mm mesh and upstream water spray, and they are fully mitigated. For 1.31mm mesh and water spray, the flame speed observed was 4.49, 5 and 12.42 m/s for 6, 7 and 9% methane-air mixture respectively, and were fully mitigated. This is evidence that as the mesh thickness increases, mitigation of the flame propagation was achieved easily.

Conclusively, the effect of the steel mesh was investigated and shows a good characteristic in influencing the flame propagation and mitigating behaviour, though found to be better while combined with fine water spray.

# List of content

Dedication.....	i
Acknowledgement.....	ii
Declaration.....	iv
Abstract.....	v
List of content.....	vii
List of Figure.....	xi
List of Tables.....	xiv
Appendix Tables.....	xv
Nomenclature.....	xvi
Chapter 1: Introduction.....	1
1.1 Overview.....	1
1.2 Research Contribution.....	2
1.3 Aim and Objectives.....	3
1.3.1 Research Aim.....	3
1.3.2 Research Objectives.....	3
1.4 Thesis outline.....	3
Chapter 2: Background of the Study.....	5
2.1 Overview.....	5
2.2 Explosion.....	5
2.2.1 Types of explosion from the combustion of flammable gases.....	7
2.3 Gas Explosion.....	7
2.4 Formation of Explosive Gas Clouds.....	8
2.5 Accidental Explosion Environment.....	9
2.5.1 Confined Gas Explosion.....	10
2.5.2 Partly Confined Gas Explosion.....	11
2.5.3 Unconfined Gas Explosion.....	12
2.5.4 Blast waves.....	12
2.6 Gas and Vapour cloud explosion.....	13
2.6.1 Type of fuel, properties and storage methods.....	16
2.7 Combustion Chemistry.....	18
2.7.1 Premixed flames.....	19
2.7.2 Flame structure.....	20
2.7.3 The Energy of Activation, $E_a$ .....	21
2.7.4 Mass and Mole Fraction.....	22
2.7.5 Mixture Ratios.....	23
2.7.6 Equivalence Ratio.....	23
2.7.7 Air/Fuel Ratio (AFR).....	24
2.7.8 Fuel/Air Ratio (FAR).....	24
2.7.9 Excess Air, (XSA).....	24
2.8 Governing factors.....	24
2.8.1 Flame propagation.....	25
2.8.2 Flame Speed and Burning Velocity.....	25
2.9 Hydrocarbons Characteristics.....	26
2.9.1 Lower Explosive Limit (LEL) and Upper Explosive Limit (UEL).....	26
2.9.2 Earliest research studies on gas and vapour explosion.....	27
2.9.3 Perforated Sheet/Plate (PS).....	29
2.9.4 Woven wire mesh.....	29
2.9.5 Previous studies on Porous media Combustion.....	30

Chapter 3: Spray and Atomization .....	33
3.1 Overview .....	33
3.1.1 Liquid Droplet Formation .....	33
3.1.2 Liquid Droplet Break-up .....	33
3.1.3 Jet Break-up .....	34
3.1.4 Sheet Break-up .....	34
3.2 Atomization .....	35
3.2.1 Primary Atomization .....	35
3.2.2 Secondary Atomization .....	36
3.3 Basic Spray Properties .....	36
3.3.1 Spray Patternation .....	36
3.3.2 Drop Size Distribution .....	37
3.3.3 Mean Diameter .....	39
3.3.4 Sauter Mean Diameter, SMD or $D_{32}$ .....	42
3.3.5 Factors Affecting Droplet Size .....	43
3.4 Atomizers .....	44
3.5 Fine spray atomizers .....	45
3.5.1 Pressure jet Atomizers .....	45
3.5.2 Pressure swirl atomizers .....	46
3.5.3 Flat fan atomizer .....	46
3.5.4 Rotary Atomizers .....	46
3.5.5 Tow fluid Atomizers .....	47
3.5.6 Spill Return Atomizers .....	47
3.6 Explosion Mitigation by Water Spray .....	48
Chapter 4: Materials, Experimental Apparatus and Procedure .....	53
4.1 Introduction .....	53
4.2 Materials .....	56
4.2.1 Methane .....	56
4.2.2 Air .....	56
4.2.3 Determination of Equivalence Ratio .....	57
4.2.4 Mesh Materials Characterization .....	57
4.3 Experimental Procedure .....	60
4.3.1 Equipment cleaning .....	60
4.3.2 Preparation and set-up .....	60
4.3.3 Experimental runs .....	61
4.3.4 Mixture Preparation .....	62
4.4 Equipment and Description .....	62
4.4.1 Explosion Chamber .....	63
4.4.2 Gas Recirculation System .....	67
4.4.3 Ignition and electrical control System .....	70
4.4.4 SRA's and water Supply system .....	73
4.4.5 Water Storage .....	74
4.4.6 Water Drains .....	75
4.4.7 Methane-Air Supply System .....	76
4.4.8 Electrical Sequence .....	77
4.5 Flame Structure .....	78
4.5.1 Summary of Experimental equipment .....	80
4.6 Video Recording and Data Processing .....	81
4.6.1 Flame Images .....	81
4.6.2 Image Processing .....	82

4.6.3	Thermocouples.....	82
4.6.4	Data Acquisition Box (DAQ) .....	83
4.6.5	Verification of Methane-Air Mixture .....	84
4.6.6	Fuel gas and Air Volumetric Flow rate.....	84
4.7	Perforated steel sheet/Woven wire mesh .....	84
Chapter 5:	Results and Discussions .....	86
5.1	Introduction .....	86
5.2	Dry Trials (No mesh and No sprays) results .....	86
5.2.1	Flame Evolution into PMMA section without obstruction.....	86
5.2.1	Preliminary Flame speed without Mesh and water sprays.....	88
5.2.2	Effect of methane concentration on flame propagation.....	90
5.2.3	Time - Temperature Profile .....	90
5.3	Woven wire Mesh (0.94mm aperture) .....	93
5.3.1	Flame propagation through the mesh at 6 % mixtures .....	93
5.3.2	Flame propagation through the mesh at 7 % mixtures .....	94
5.3.3	Flame propagation through the mesh at 9 % mixtures .....	95
5.3.4	The average Flame speed with 0.94mm Mesh and No water spray .....	96
5.3.5	Time – Temperature Profile with 0.94mm woven wire mesh .....	98
5.3.6	Effect of the Mesh on the flame propagation.....	100
5.3.7	Temperature Comparisons with 0.94 mm mesh and Dry case .....	100
5.4	Woven wire mesh (0.94mm) installed and Water sprays activated.....	102
5.4.1	6 % Flame Evolution with 0.94 mm Mesh and Sprays.....	103
5.4.2	Flame Speed with 0.94mm mesh and water sprays .....	104
5.4.3	Time – Temperature Profile.....	104
5.4.4	Effect of the mesh combined with sprays .....	105
5.4.5	7% Flame Evolution with 0.94 mm Mesh and Sprays.....	107
5.4.6	Time – Temperature Profile.....	107
5.4.7	Time – Temperature Profile at 9% mixture plus sprays .....	108
5.5	Woven wire mesh (1.31mm aperture).....	109
5.5.1	Flame speed with woven wire mesh 1.31mm aperture only.....	109
5.5.2	Flame propagation behaviour at 6% with 1.31mm mesh no sprays .....	110
5.5.3	Temperature – time profile .....	111
5.6	Woven wire mesh (1.31mm aperture) plus water spray .....	113
5.6.1	Average Flame speed.....	113
5.6.2	Flame propagation behaviour at 6% with 1.31mm mesh + sprays.....	114
5.6.3	Temperature – time response at 6% with 1.31mm mesh + sprays .....	114
5.6.4	Comparisons of individual thermocouples .....	115
5.7	Flame propagation behaviour at 9% with 1.31mm mesh no sprays .....	117
5.7.1	Time–Temperature Profile at 9% combustion with 1.31 mm mesh no sprays	117
5.7.2	Average Flame speed at 9% combustion with 1.31 mm mesh + sprays.....	118
5.7.3	Flame propagation behaviour at 9% with 1.31mm mesh + sprays .....	119
5.7.4	Temperature – time response at 9% with 1.31 mm mesh + sprays .....	119
5.8	Perorated sheet, PS (6 mm aperture).....	122
5.8.1	Average Flame speed with 6 mm PS and Dry case .....	122
5.8.2	Flame propagation for 6% & 9% mixture with 6mm mesh no sprays.....	122
5.8.3	Temperature – time profile for 6% & 9% mixture with 6mm mesh.....	123
5.8.4	Flame propagation behaviour for 6% mixture with 6mm mesh + sprays.....	125
5.8.5	Temperature-time profile at 6% combustion with 6 mm mesh+spray .....	125
5.8.6	Flame propagation behaviour for 6% mixture with 6mm mesh + sprays.....	126
5.8.7	Temperature-time profile at 9% combustion with 6 mm mesh+spray .....	127

Chapter 6: Conclusion .....	128
6.1 reccommendations.....	129
References.....	130

## List of Figure

Figure 2.1: Formation of the combustible explosion.....	6
Figure 2.2: Consequences of accidental releases of flammable gas .....	8
Figure 2.3: Internal gas explosion within a vessel.....	10
Figure 2.4: Partly confined gas explosion in a building. ....	11
Figure 2.5: Unconfined gas explosion. ....	12
Figure 2.6: The effect of Blastwave pressure on a structure.....	13
Figure 2.7: Pressure – time history of blast waves (Friedlander wave).....	13
Figure 2.8: a) Overpressure as a function of a distance, b) overpressure effects on people and c) overpressure effects on structures.....	15
Figure 2.9: Buncefield Hertfordshire Oil Storage depot fire incident .....	17
Figure 2.10: Stationary Flame Description.....	20
Figure 2.11: Flame temperature profile and concentration.....	21
Figure 2.12: Activation energy curve .....	22
Figure 2.13: Davy’s safety lamp for coal miners (the earliest flame arrestor). ....	28
Figure 2.14: Apparatus and schematic diagram of burner used.....	32
Figure 3.1: Break-up of a liquid jet.....	34
Figure 3.2: Different stages of liquid sheets break up .....	35
Figure 3.3: Different types of spray pattern.....	37
Figure 3.4: Histogram chart of Drop sizes.....	38
Figure 3.5: Drop size histograms based on Number and Volume. ....	39
Figure 3.6: Locations of Various Representative Diameters .....	43
Figure 3.7: Classification of atomizers .....	45
Figure 3.8: Fuel injection system for diesel engine .....	45
Figure 3.9: Spill return atomizer and angular inlet.....	47
Figure 3.10: Experimental rig used at Spadeadam .....	50
Figure 3.11: Experimental rig 76 mm diameter 5000 mm long pipe.....	51
Figure 4.1: Thermocouple position and flame direction.....	53
Figure 4.2: Schematic representation of the research flow diagram.....	55
Figure 4.3: Woven wire mesh: a) 0.94mm aperture and 0.22mm diameter, and b) 1.31 mm aperture and 0.28mm diameter .....	58
Figure 4.4: Perforated metal sheet 6mm aperture .....	59
Figure 4.5: The position of the mesh within the explosion tube.....	59
Figure 4.6: Schematic diagram of the Experimental Setup system .....	63
Figure 4.7: Mild Steel section of the Experimental Rig .....	64
Figure 4.8: Polymethyl-Methacrylate, (PMMA) Section of the experimental tube .....	65
Figure 4.9: Exhaust outlet.....	66
Figure 4.10: Exhaust block with cling film during the filing period .....	67
Figure 4.11: Gas Recirculation Booster Pump .....	68
Figure 4.12: Gas Turbine Meter.....	69
<b>Figure 4.13:</b> Alarm Portable Gas Detector .....	70
Figure 4.14: Spark Plug Ignition.....	71
Figure 4.15: Magnetic Hinge Outlet .....	72
Figure 4.16: Plunge Type Micro Switches .....	73
Figure 4.17: Pressure pump water supply and Water storage tank.....	75
Figure 4.18: Water Drain System .....	76
Figure 4.19: Electrical control box indicating operator keys and ignition bush button.....	78
Figure 4.20: Temperature profiles through the pre-mixed flame .....	79
Figure 4.21: Thermocouple position and flame direction.....	79

Figure 4.22: Experimental equipment.....	80
Figure 4.23: Nikon cool Camera.....	81
Figure 4.24: Type K thermocouple, (TC Ltd UK).....	83
Figure 4.25: iNet Expandable Modular Data Acquisition (DAQ) System).....	83
Figure 4.26: GMI Gascoseeker Mk2-500 .....	84
Figure 4.27: Perforated steel sheet/plate/woven wire mesh.....	85
Figure 5.1: 6% Flame propagation images (dry) with no water spray and no mesh .....	87
Figure 5.2: 7% Flame propagation images (dry) with no water spray and no mesh .....	87
Figure 5.3: 9% Flame propagation images (dry) with no water spray and no mesh .....	88
Figure 5.4: Average flame speed for three different methane-air mixtures.....	89
Figure 5.5: 6 % methane-air combustion.....	91
Figure 5.6: 7 % methane-air combustion.....	92
<b>Figure 5.7:</b> 9% methane-air mixtures.....	92
Figure 5.8: 6% flame propagation through 0.94mm mesh no water spray.....	94
Figure 5.9: 7 % flame propagation through 0.94mm mesh no water spray.....	95
Figure 5.10: 9 % flame propagation through 0.94mm mesh no water spray.....	96
Figure 5.11: Flame speed for various methane-air mixtures with 0.94mm mesh & no sprays.....	97
Figure 5.12: Methane-air combustion at 6% with 0.94 mm mesh.....	99
Figure 5.13: Methane-air combustion at 7% with 0.94 mm mesh.....	99
Figure 5.14: Methane-air combustion at 9% with 0.94 mm mesh.....	99
Figure 5.15: Comparison of 6% temperature profile with 0.94 mm mesh and dry case. ....	101
Figure 5.16: SRA's Position within the tube 3100mm from the start of ignition .....	102
Figure 5.17: SRA's position and spray water.....	102
Figure 5.18: 6 % Methane-air combustion through 0.94 mm mesh and spray.....	103
Figure 5.19: Time-Temperature profile at 6% CH <sub>4</sub> /Air combustion with 0.94 mm mesh plus sprays .....	105
Figure 5.20: Thermocouple temperature profile comparison with 0.94 mm mesh plus sprays.....	106
Figure 5.21: 7 % Methane-air combustion through 0.94 mm mesh and spray.....	107
Figure 5.22: Temperature profile at 7% combustion with 0.94 mm mesh + sprays.....	108
Figure 5.23: Temperature profile at 9% combustion with 0.94mm mesh + sprays.....	108
Figure 5.24: Comparisons of the average flame speed for various methane-air mixtures, (φ) with 0.94mm and 1.31mm mesh installed .....	110
Figure 5.25: Flame propagation 7% mixture with 1.31mm mesh no water spray.....	111
Figure 5.26: Time-Temperature responses of 6% mixture with 1.31mm mesh no sprays ....	112
Figure 5.27: Comparisons of average flame speed with various methane-air mixtures (6, 7, and 9%) with 0.94mm mesh plus sprays and 1.31mm mesh plus water sprays fully mitigated .....	114
Figure 5.28: Flame propagation 7% mixture with 1.33mm mesh and plus sprays.....	114
Figure 5.29: Time-Temperature profile at 6% combustion with 1.31mm mesh + sprays ....	115
Figure 5.30: The comparison of individual thermocouple temperature-time profile with 1.31mm mesh + spray. ....	116
Figure 5.31: 9% mixture Flame propagation with 1.31mm mesh no water spray.....	117
Figure 5.32: Time-Temperature responses of 9% mixture with 1.31mm mesh no sprays ....	118
Figure 5.33: 9% mixture Flame propagation with 1.31mm mesh and plus sprays.....	119
Figure 5.34: Time-Temperature profile at 9% with 1.31mm mesh + sprays.....	120
Figure 5.35: The comparison of individual thermocouple temperature-time profile at 9% with 1.31mm mesh + sprays. ....	121
Figure 5.36: 6% mixture Flame propagation with 6mm mesh installed no sprays.....	123
Figure 5.37: 9% Flame propagation images with 6mm mesh installed no sprays.....	123

Figure 5.38: Time-Temperature profile for 6% methane/air mixture with 6mm mesh installed no sprays .....	124
Figure 5.39: Time-Temperature profile for 9% methane/air mixture with 6mm mesh installed no sprays .....	124
Figure 5.40: 6% Flame propagation with 6 mm mesh + sprays .....	125
Figure 5.41: Time-Temperature profile for 6% methane/air mixture with 6mm mesh installed plus sprays.....	126
Figure 5.42: 9% Flame propagation with 6 mm mesh + sprays .....	126
Figure 5.43: Time-Temperature profile at 9% combustion with 6mm mesh + sprays.....	127

## List of Tables

Table 2.1: Most Common Material of Flammable Ranges and Spreads .....	26
Table 3.1: Mean diameter and their application .....	40
Table 3.2: Different forms of droplets diameter .....	41
Table 4.1: Methane/Air ratio and filling time .....	54
Table 4.2: Physical properties of methane .....	56
Table 4.3: Characteristics of the woven wire meshes and perforated plate .....	58
Table 4.4: American National Standard Institute (ANSI) 80 pipe table of schedule .....	63
Table 4.5: Properties of Polymethyl-Methacrylate, (PMMA) .....	65
Table 4.6: Specification of the water pump .....	74
Table 4.7: Some Properties of Laboratory Grade C Methane .....	76
Table 4.8: Fill times, flowrates and percentages of methane in air .....	77
Table 4.9: The location of the thermocouples and their intervals.....	82
Table 5.1: Average flame speed for three different methane-air mixtures .....	89
Table 5.2: Average flame speed for various methane-air mixtures .....	97
Table 5.3: Flame speed comparison with mesh installed and no water sprays (dry).....	98
Table 5.4: Exit orifice of SRA's downstream .....	103
Table 5.5: The average flame speed at 6 and 7% methane-air mixtures .....	104
Table 5.6: Flame speed for 6%, 7%, and 9% with 1.31mm mesh no spray .....	109
Table 5.7: Average flame speed for 6%, 7% and 9% methane-air mixtures .....	113
Table 5.8: The average flame speeds with 1.31mm mesh plus sprays for 9% mixture.....	118
Table 5.9: Average flame speed for a various methane-air flame .....	122

## Appendix Tables

Table 6.1.1.1.1-1: 6% methane-air mixtures with no mesh and no water sprays .....	134
Table 6.1.1.1.1-2: 9% methane-air mixtures with no mesh and no water sprays .....	135
Table 6.1.1.1.2-1: 6% methane-air mixtures with mesh and no water sprays data sheet .....	136
Table 6.1.1.1.2-2: 7% methane-air mixtures with 0.94mm mesh and no water sprays .....	137
Table 6.1.1.1.2-3: 9% methane-air mixtures with 0.94mm mesh and no water sprays data sheet .....	138
Table 6.1.1.1.3-1: 6% methane-air mixtures with 0.94mm mesh and water sprays data sheet .....	139
Table 6.1.1.1.3-2: 7% methane-air mixtures with 0.94mm mesh and water sprays data sheet .....	141
Table 6.1.1.1.3-3: 9% methane-air mixtures with 0.94mm mesh and water sprays data sheet .....	143
Table 6.1.1.1.4-1: 6% methane-air mixtures with 1.31mm mesh and no water sprays data sheet .....	144
Table 6.1.1.1.4-2: 7% methane-air mixtures with 1.31mm mesh and no water sprays data sheet .....	147
Table 6.1.1.1.4-3: 9% methane-air mixtures with 1.31mm mesh and no water sprays data sheet .....	148
Table 6.1.1.1.5-1: 6% methane-air mixtures with 1.31mm mesh plus water sprays data sheet .....	149
Table 6.1.1.1.5-2: 7% methane-air mixtures with 1.31mm mesh plus water sprays data sheet .....	151
Table 6.1.1.1.5-3: 9% methane-air mixtures with 1.31mm mesh plus water sprays data sheet .....	151
Table 6.1.1.1.6-1: 6% methane-air mixtures with 6mm mesh no water sprays data sheet....	152
Table 6.1.1.1.6-2: 7% methane-air mixtures with 6mm mesh no water sprays data sheet....	154
Table 6.1.1.1.6-3: 9% methane-air mixtures with 6mm mesh no water sprays data sheet....	155
Table 6.1.1.1.7-1: 6% methane-air mixtures with 6mm mesh plus water sprays data sheet .	156
Table 6.1.1.1.7-2: 7% methane-air mixtures with 6mm mesh plus water sprays data sheet .	157
Table 6.1.1.1.7-3: 9% methane-air mixtures with 6mm mesh plus water sprays data sheet .	160

## Nomenclature

Abbreviation	Description
BLEVE	Boiling Liquid Expanding Vopour Explosion
CO <sub>2</sub>	Carbon dioxide
μg	Dynamic viscosity
μm	Micrometer
°C	Degree Celsius
CH <sub>4</sub>	Methane
Cp	Centipoise
D <sub>0.632</sub>	Characteristics Diameter
D <sub>0.999</sub>	Maximum Diameter
D <sub>10</sub>	Arithmetic Mean Diameter
D <sub>20</sub>	Surface Mean Diameter
D <sub>30</sub>	Volume Mean Diameter
D <sub>32</sub> or SMD	Sauter Mean Diameter
D <sub>i</sub>	Middle Diameter in the Size of range i
D <sub>peak</sub>	Peak Diameter
DV <sub>0.1</sub> , D <sub>0.5</sub>	Mass Median Diameter
EPA	Environmental Protection Agency
GPa	Giga pascal
H <sub>2</sub>	Hydrogen gas
H <sub>2</sub> O	Water vapour
K	Kelvin
kg	Kilogram
kPa	kilo-Pascal
LFL	Lower flammability limit
m	Meter
m	Mass
ms <sup>-1</sup>	Meter per second
ms <sup>-1</sup>	Minutes per second
mm	Millimetre
MPa	Mega Pascal
ms	Millisecond
n	Number of moles
N <sub>2</sub>	Nitrogen gas
N <sub>i</sub>	Number of drops in size range i
O <sub>2</sub>	Oxygen gas
P	Pressure
PMMA	Polymethyl methacrylate
psi	Pound per square inch
P <sub>s</sub>	Peak Explosion pressure
PS	Perforated Sheet
Q	Flow rate
R	Universal gas constant
S <sub>f</sub>	Flame Speed
SRA	Spill Return Atomizer
STP	Standard Temperature and Pressure
T	Temperature
T <sub>f</sub>	Flame temperature

T/C	Thermocouple temperature
$t^*$	Time
$U_{b,u}$	Burning velocity
UPL	Upper Flammability limit
USA	United State of America
V	Volume
V	Volt
$V_g$	Kinematic viscosity
$y_i$	Mole Fraction of component i
$Y_k$	Mass fraction
$\gamma_g$	Specific gravity
$\Theta$	Angle
$\rho$	Density
$\rho_g$	Density of gas
$\Phi$	Equivalence ratio

# Chapter 1: Introduction

## 1.1 Overview

Explosions and fires involving combustible gases and vapours constitute a significant hazard in process industries, and other environments where such materials are produced, used and handled. Therefore, the efforts to minimize the risk of explosions and fires in these industries continue globally, and much work is spent on mitigating accidental gas and vapour cloud explosion. The explosion risk is often defined as the product of the probability of an explosion and its expected consequence [1]. Therefore the basic principle of gas explosion risk management is to minimize the explosion probability as well as the expected explosion loads, which are in turn related to the explosion consequences. Reduced gas explosion consequences can be obtained by active as well as passive measures.

Additionally, when fuel gas is accidentally ignited in pipelines can results in explosions this in some cases causes a transition from deflagration to detonation (DDT). As such, flame arrestors are often used in industry to enhance safety [2]. The typical type of flame arrester is based on the quenching effect of the porous material, which depends on the characteristic pore dimensions and the flame. The operating principles of flame arresters are 'removing heat from the flame as it attends to travel through narrow passages of the holes of the metals or other heat conductive materials.

Combustion of natural gas is much common in domestic appliances such as central heat systems and cooking facilities [3]. However, the reaction of fossil fuels, for example, coal or natural gas with air and oxygen releases heat, which has been utilised for different purposes. On the other hand, natural gas (methane,  $\text{CH}_4$ ) is more advantageous due to its clean nature compared to other fossil fuels because there is no emission of sulphur oxide ( $\text{SO}_x$ ) as sulphur is removed from natural gas before combustion [4]. However, carbon dioxide, ( $\text{CO}_2$ ), carbon monoxides, ( $\text{CO}$ ), and nitrogen oxides ( $\text{NO}_x$ ) can be produced by the combustion of natural gas.  $\text{CO}_2$  emission is intrinsic to the combustion of fossil fuels, which when reduced, improves the efficiency of the combustion equipment.

Natural gas is a naturally occurring hydrocarbon which consists of main methane ( $\text{CH}_4$ ) but also includes varying amounts of other higher alkanes. Natural gas has become one of the major sources of energy around the globe as such, to meet the demand of world energy requirement, the continuous search for it (natural gas) has become of paramount importance.

Transporting this commodity in pipes is a common feature of many process industries. However, the process of transporting this flammable gas (methane) is safe when it contains either no air or air in controlled quantities so that the mixture proportions are always outside the explosive range. Explosion can only occur when these flammable gases or vapour are mixed with sufficient air for the mixture to sustain flame propagation. It is a vastly dangerous commodity, which should be recognised for its hazards and be handled with the proper precautions.

An explosion is a sudden reaction involving a rapid physical, nuclear, or chemical oxidation reaction or decay generating an increase in temperature and/or pressure or both simultaneously. According to Rolf K. Eckhoff, the explosion is an exothermic chemical reaction that, when occurring at constant volume, gives rise to a sudden and significant pressure incidence [5]. While, a gas explosion is a process where combustion of a premixed gas cloud, i.e. fuel-air or fuel/oxidiser causes a rapid increase of pressure [4].

There are various ways of fire mitigation, which include the use of foams, CO<sub>2</sub>, and water, which have significantly indicated promising results over the years, although with limited application depending on the fire source and the surrounding environment. Thus, high-pressured atomised water (regarding drop size distribution, impact force, and spray width) could be an option for such applications. Also, steel mesh sizes heat recirculation inserted in between the flanges of the explosion tube to look into the flow of flame propagation through the porous mesh of different sizes is adopted in this research study.

## 1.2 Research Contribution

Despite the fact that there has been huge research in the use of water sprays for deflagrated explosion mitigation and suppression measure, the contributions to knowledge derived from the present investigation are as follows:

- The influence of perforated sheet and woven wire mesh placed to obstruct the flame flow, thereby reducing the flame speed as well as the heat sink due to convection or conduction between the flame and the wire mesh.
- Structured flame quenching mechanism using steel meshes (woven wire meshes 0.94mm aperture of 0.22mm wire  $\Theta$ , 1.31mm aperture of 0.28mm  $\Theta$  and 6mm hole  $\Theta$  with 6mm hexagonal) combined with Spill Return Atomiser (SRA) that produce single and multiple poly-dispersed sprays of ideal droplet size ( $D_{32} \leq 30\mu\text{m}$ ), mean

droplet velocity (0m/s - 21.4m/s) and liquid volume flux (approximately 0.047 cm<sup>3</sup>/s/cm<sup>2</sup>) to fully mitigate a range of lean, stoichiometric and rich mixtures methane-air explosions system.

## **1.3 Aim and Objectives**

### **1.3.1 Research Aim**

The aim of this research study is as follows:

- To study the effect of steel meshes sizes on flame propagation using the different mesh sizes.
- To study the performance and effects of combining these steel meshes with fine water sprays.

### **1.3.2 Research Objectives**

To achieve the aim of this research work; the following objectives are set to:

- Examine the temperature variation of the deflagrated flame across the tube as it propagates through different mesh sizes as:
  - Perforated metal steel sheet of 6mm holes,
  - Woven wire with 0.94 apertures – 0.22 mm wire diameter, and
  - Woven wire with 1.31mm aperture - 0.28 mm wire diameter.
- Investigate the quenching effects and performance of combining different mesh sizes with a water spray as flame propagates through it.
- To evaluate the flame images using Adobe Photoshop CC 2017 and adobe premiere pro CC 2017 in calculating average flame speeds.

## **1.4 Thesis outline**

This thesis is organised in the form of chapters, consisting of six chapters, with each section presenting the set of information necessary for the completion of these research study.

**Chapter 1:** This chapter highlights the concept, general introduction, reasons and motivations for embarking on this research study and however, briefly explain some the accidental gas explosion in the past and description of the current problem.

**Chapter 2:** This chapter briefly introduces the background of the study, review of Literature provides a literature survey incorporating some fundamental concepts relating to combustion, fire, explosions and flame quenching by water sprays.

**Chapter 3:** This chapter presents a general overview of sprays and atomization process to get a clear understanding of the mechanism associated with sprays and atomization.

**Chapter 4:** This chapter provides detailed experimental setup, apparatus description, required to carry out the entire experimental programme safely. However, the experimental apparatus and experimental structure, procedures and methods of data processing used in this study are discussed.

**Chapter 5:** This chapter includes the experimental observations of methane/air mixtures utilising the apparatus and FPM Rig. The conclusion of the result observed from the experiment of the hot trial of the methane-air mixture for three different concentrations, i.e. 5% 6% and 7% were discussed.

**Chapter 6:** This present the conclusion and recommendation of the research study conducted.

## **Chapter 2: Background of the Study**

### **2.1 Overview**

This chapter concentrates mainly on the essential review of past research studies, which prompt to further avocation in carrying out this study. Moreover, fundamental principles and theories regarding combustion, explosion and flame suppression are explained with further clarification of ignition standards, blast and fire extinguishment.

The advantages, properties and qualities of combustible gases and vapours are highly reported and similarly the potential for uncontrolled combustion cases including rigorous flame, explosion and blasts are likewise basic information. All through current history shows that various spearheading people and institutions that have given a tremendous immense knowledge in explosion suppression and mitigation. However, the chapter also concisely introduce some of the individuals and institutional studies referenced accordingly throughout this research study.

### **2.2 Explosion**

To appreciate what constitutes an explosion mitigation system; it is first necessary to define and understand the characteristics of an explosion. An explosion is an event in which a mixture of combustible materials is giving sufficient energy in other to form reactants further into combustion products while undergoing a violent reaction releasing adequate amounts of heat to generate pressure. Its violence depends on the rate at which the energy is released. In a precise way, the explosion is a rapid release of energy causing pressure development or shock waves. The combustion products will then expand rapidly [3] when this energy is released and create a pressure wave that depends on the various parameters such as the release environment, the type of fuel etc. There are numerous kinds of energy-released results from the explosion, but the three major ones are classified as follows; physical energy; chemical energy and nuclear energy.

Physical energy may be as results of pressure energy in gases, strain energy in metals and electrical energy. For instance, the explosion of a vessel due to high gas pressure and the sudden rupture of a vessel due to brittle fracture are some of the examples of the violent release of physical energy. Furthermore, another important physical form is thermal energy.

Specifically, superheat in a fluid under pressure causes flashing off of the liquid if it is let down to atmospheric pressure. However, this is generally important in creating the conditions for an explosion rather than as a source of energy for the explosion itself.

Chemical energy results from a chemical reaction, for example, the explosion of a vessel due to combustion of explosives gases and reactor explosion caused by decomposition of reaction products in the chemical reaction. Chemical explosion could either be uniform and/or propagating an explosion. However, a blast in a vessel tends to be a uniform blast, while a blast in long pipe results in explosion propagation.

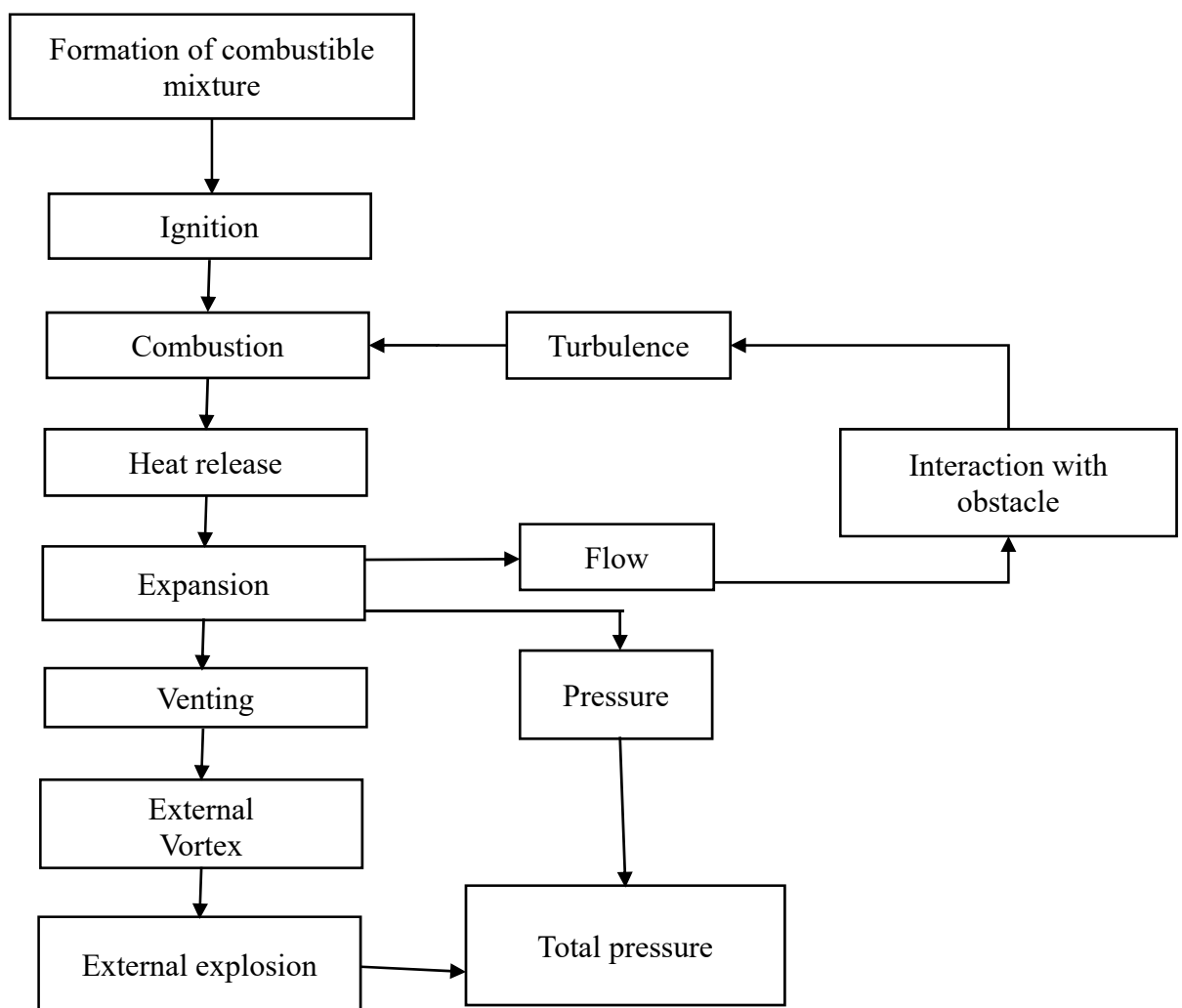


**Figure 2.1:** Formation of the combustible explosion

The pressure wave characteristics determined the primary hazard effect that is associated with explosions, namely damage and injury.

## **2.2.1 Types of explosion from the combustion of flammable gases**

They are two significant types of explosion from the combustion of flammable gases namely, deflagration and detonation which are capable of disastrous consequences. The condition that differentiates one from the other is that the flame position in respect to the aforementioned pressure wave.

### **2.2.1.1 Deflagration**

In a deflagration, the combustible mixtures consume at subsonic velocities. For hydrocarbon and air mixtures, the explosion deflagration speed is in the order of 300m/s. This is the most common type of flame propagation in an accidental gas explosion. However, the peak pressure caused by the deflagration of the hydrocarbon-air mixture in a closed vessel is about 8 bars [6]. A deflagration may transform into a detonation, especially when travelling down a long pipe. Where a change from deflagration to detonation is happening, the detonation speed can briefly surpass the steady-state detonation speed in so-called 'overdriven' condition.

### **2.2.1.2 Detonation**

Chapman and Jouguet were the first to define a theory that describes the supersonic combustion wave, which propagates at a different velocity [7]. In a detonation, the flame front moves as a shock wave took after nearly by a combustion wave, which discharges the energy to maintain the shock wave. At steady state, the detonation front reaches a speed equivalent to the speed of sound in the hot results of combustion; this is substantially more prominent than the speed of sound in the unburned mixture. For hydrocarbon and air blends, the detonation velocity usually is of the order of 2000 and 3000m/s. For correlation, the speed of sound in air at 0°C is 330m/s. A detonation produces more pressures of about 20 bars and is more disastrous than a deflagration. In the present study, natural gas (methane) will be used to form the combustible mixture ranging from lean to stoichiometric.

## **2.3 Gas Explosion**

A gas explosion is a process where combustion of a premixed gas cloud, i.e. fuel-air or fuel/oxidiser is causing a rapid increase in pressure. It can occur inside process equipment or pipes, in buildings or offshore modules, in open process areas or in unconfined regions [8]. Gas explosion can result from gas leaks in the presence of ignition. However, preventing

them from happening is the primary concern of the present investigations. Thus, minimizing or reducing its consequences requires a perfect understanding of what gas explosion is and its formation.

## 2.4 Formation of Explosive Gas Clouds

When combustible gases or evaporating liquids released accidentally into the atmosphere, an explosives fuel-air cloud may be formed.

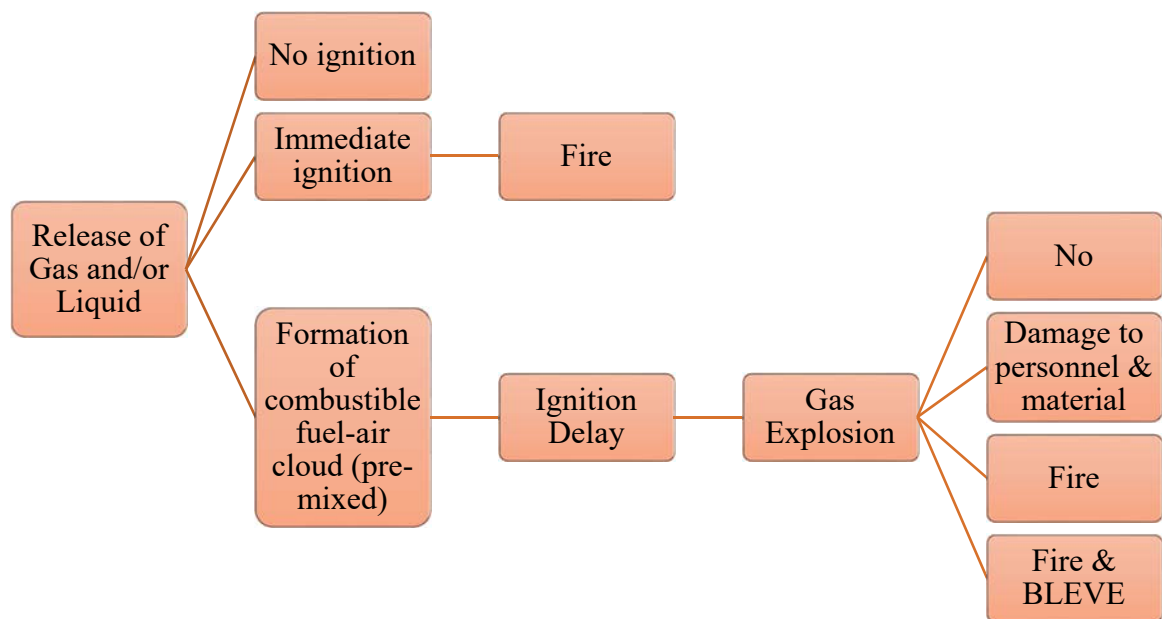


**Figure 2.2:** Consequences of accidental releases of flammable gas [4]

Figure 2.2 described the events resulting from the gas explosion. This could occur when a flammable gas or evaporating liquid is released accidentally into the atmosphere. At the point when the released gas is not within the flammability limits or no ignition source, it might be weakened and vanished. Then, Ignition may occur immediately, or may be delayed by up to tens of minutes; depending on the situations. In the event of an immediate ignition, the fire will occur. The most dangerous situation is when a large flammable premixed fuel-air is formed and ignited. It takes a few seconds to tens of minutes to ignite from its release start time. The pressure generated by the combustion wave will depend on how fast the flame propagates; and how the pressure can expand away from the gas cloud. The pressure build-up caused by the gas explosion can damage personal and material, or it can lead to accidents such as fires and boiling liquid expanding vapour explosion (BLEVE's). Fires are very

common events after gas explosions [4]. The explosion of flammable gases can occur in two different ways. This includes; Deflagration and Detonation. In deflagration, the combustible mixture burns at a subsonic speed. The deflagration velocity for hydrocarbon – air mixture ranges typically in the order of 300m/s and 8bar when in a closed vessel. While in the case of detonation, the flame front travels as a shock wave followed closely by a combustion wave which releases the energy to sustain the shock wave. For hydrocarbon-air mixtures, detonation velocity is on the order of 2000 – 3000m/s and a peak pressure of 20bar [9]. Gas explosion consequences depend on the following factors:

- The type of fuel and oxidizer
- Size and fuel concentration of the combustible cloud
- Ignition location
- The strength of ignition source
- Size, location, and type of explosion vent areas
- Location and size of structural elements and equipment
- Mitigation schemes

## **2.5 Accidental Explosion Environment**

Gas explosion consequence also depends on the environment in which the vapour cloud is contained or engulfed. Therefore, the environment where the gas explosion occurs can be classified as follows:

- Confined Gas Explosions
- Partly Confined Gas Explosions
- Unconfined Gas Explosions

The important to note is that the equipment used in this research work was systematically designed to simulate partly confined and unconfined conditions. In the following Sections, efforts will be made to define each of the environmental explosion categories in order to understand the subject area better.

### 2.5.1 Confined Gas Explosion

This category of explosion environment is also known as an internal explosion. It occurs within tanks, vessels, tunnels, process equipment, pipes, sewage systems, closed rooms and in underground installations [4]. In a totally confined enclosure, the overpressure that is generated in a stoichiometric hydrocarbon – air mixture explosion is about 8 bar; this is because, from the application of the ideal gas law, the absolute flame temperature for the combustion of the hydrocarbon-air mixture is about nine times higher than absolute ambient temperature [10]. A gas explosion consequence depends on the environment in which the gas cloud is contained as depicted diagrammatically in Figure 2.3.

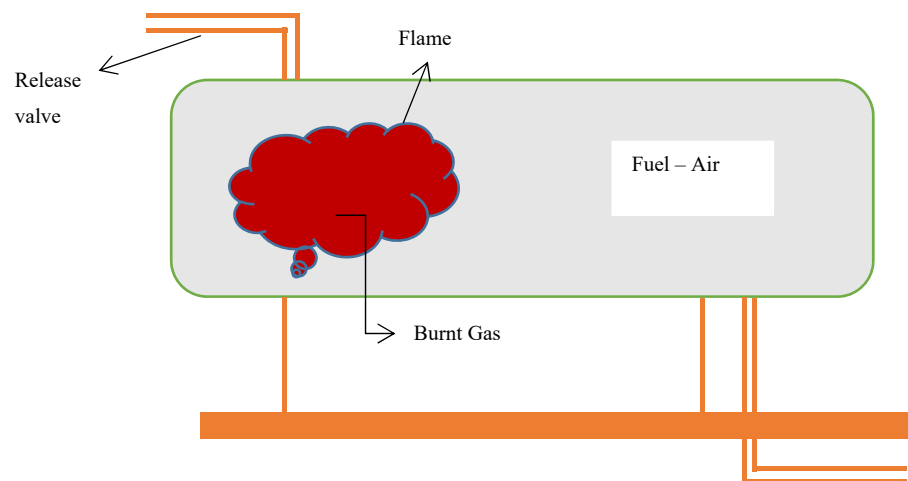


**Figure 2.3:** Internal gas explosion within a vessel [4].

Pengpeng Zhang et al. 2014 studied the effect of ultrafine water fog on the methane/air explosions with different methane concentrations. The result shows that the maximum explosion overpressure and the pressure rising rate decreased after adding water fog. Also, for methane concentrations of 9% and 11%, the maximum flame propagation velocities reduced significantly with the increase of spraying time, and the flame in the burned zone got extinguished earlier than the flame fronts arrived at the top of the vessel. Therefore, the mitigation performance of water fog depends both on the methane concentration and spraying time [11].

Changlong Tang et al. 2014, also investigated explosion characteristics of high methane natural gas/air in a confined vessel under different initial conditions. The result shows that

with an increment in the initial pressure and peak explosion pressure, maximum pressure rate will increase due to a high amount of flammable mixture. Also, with an increase in initial temperature, the peak explosion pressure decreases while increment in pressure during combustion accelerated which indicates a faster flame speed and heat release rate [11].

## 2.5.2 Partly Confined Gas Explosion

As suggested by Khan, et al. 1998 that explosions are considered inside partly confined areas because a number of process plants operate in partially confined areas [12]. Therefore, when fuel is accidentally released inside a building, which is partly open, it is termed a partly confined explosion. The consequences of a gas explosion inside the building will mainly depend on the type of fuel, size and concentration of the gas cloud, ignition and geometrical layout, i.e. confinement, venting and obstructing objects. For instance, in a building with no or little explosion venting, the building will confine the explosion, and high explosion pressures may be generated. Therefore, Vent openings are of key importance in keeping the explosion pressure down as illustrated in Figure 2.4.

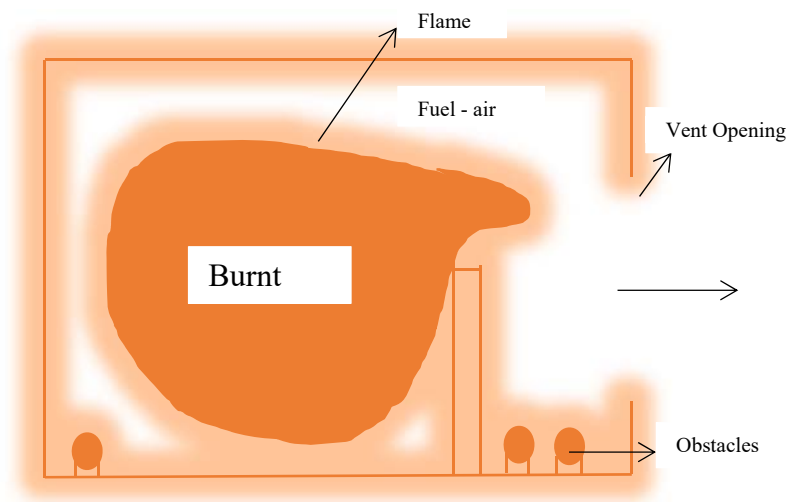


**Figure 2.4:** Partly confined gas explosion in a building [4].

Lee, Park, Green and Park [13] carried out an investigation to assess the effect of different obstacle obstructions in a partly confined rig. The results indicate that explosion pressure decreases in a single obstacle with an increase in blockage ratio rather than the multiple ones due to the formation of a lower volume of unreacted mixtures [13].

### 2.5.3 Unconfined Gas Explosion

The term unconfined was used to describe explosions in open areas such as process plants. It should be carefully used because it has a very high explosion pressure when detonated. In a process plants, there are local areas which are partly confined and obstructed.

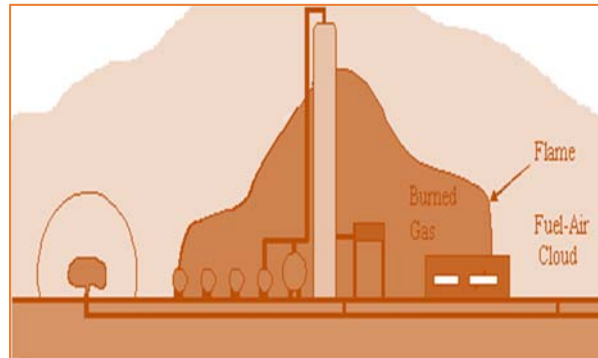


**Figure 2.5:** Unconfined gas explosion [4].

Ibrahim and Masri [14] investigated the effects of obstruction geometry, blockage ratio and venting pressure on overpressures resulting from premixed flame deflagration. The results indicate that deflagration overpressure increases with increasing venting pressure and the maximum overpressure increases, generally with increasing blockage ratio but the rate of increase depends on the obstruction geometry [14]. Acton et al., and Bjerketvedt and Bjrkaug reported in their experiments performed in geometries representative of industrial environments (partial confinement and obstacles). Both studies showed that a considerable reduction of explosion overpressures could be achieved using water sprays. Also, it was shown that the time required to reach the peak pressure could be reduced [15] and [16].

### 2.5.4 Blast waves

A blast wave is a rise in pressure that results from the deposition of a large amount of energy in a small volume. This energy moves forward in the air with a front, and air properties cause this front to shock up or steepen as it progresses further. These shock front moves supersonically, i.e. speed more than the speed of sound in the air ahead of it, with a discontinuity in pressure, density, and particle velocity across the front as shown in Figure 2.6.

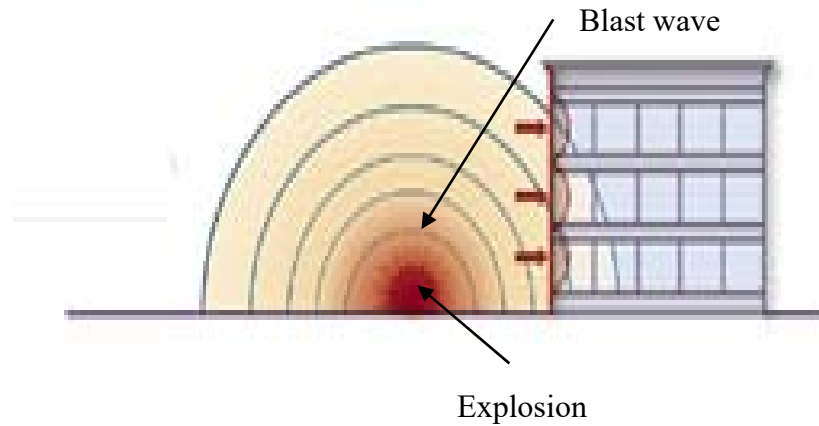


**Figure 2.6:** The effect of Blastwave pressure on a structure [17]

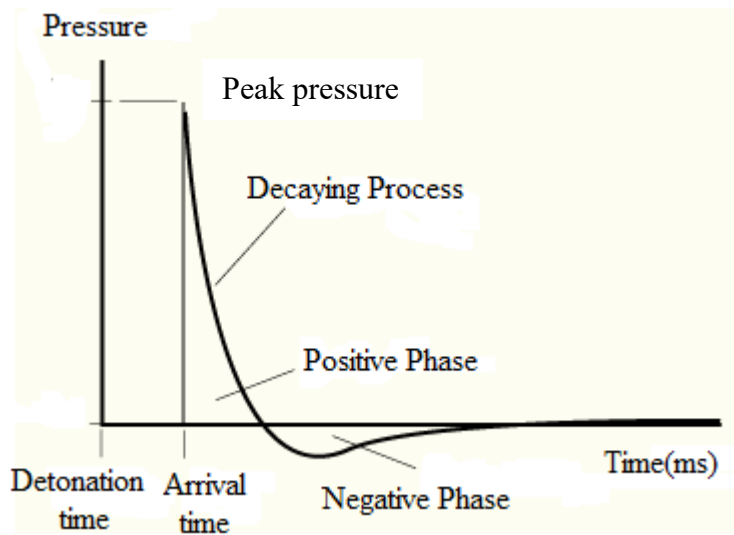


**Figure 2.7:** Pressure – time history of blast waves (Friedlander wave) [18]

Figure 2.7 illustrates that the explosion creates a rapid increase in pressure which gradually decay down to a positive pressure phase during propagation and causes damage to any objects located on its paths and further to a negative pressure phase which causes further damage before pressure returns to atmospheric within a short period of time. Blastwave or overpressures are the fundamental causes of the explosion damage. However, the damage depends on maximum pressure reached, the velocity of propagation and environmental characteristics.

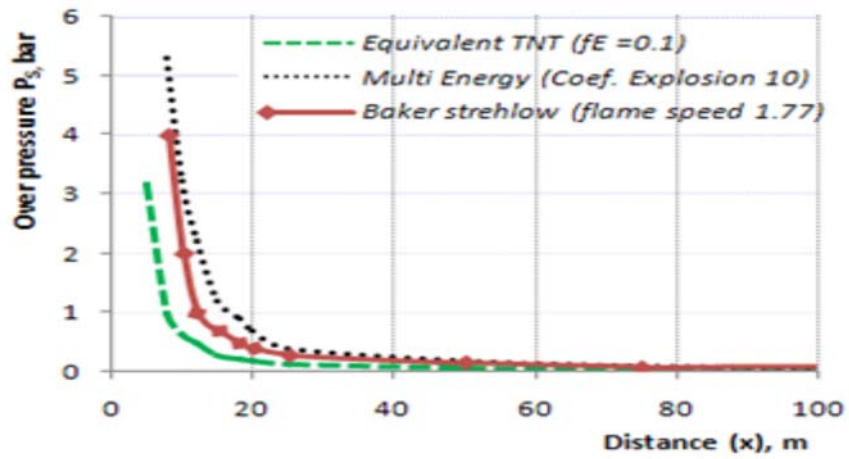
## 2.6 Gas and Vapour cloud explosion

A vapour cloud explosion results from the accidental release of explosive material into the atmosphere which upon ignition will form a catastrophic consequence to the surrounding

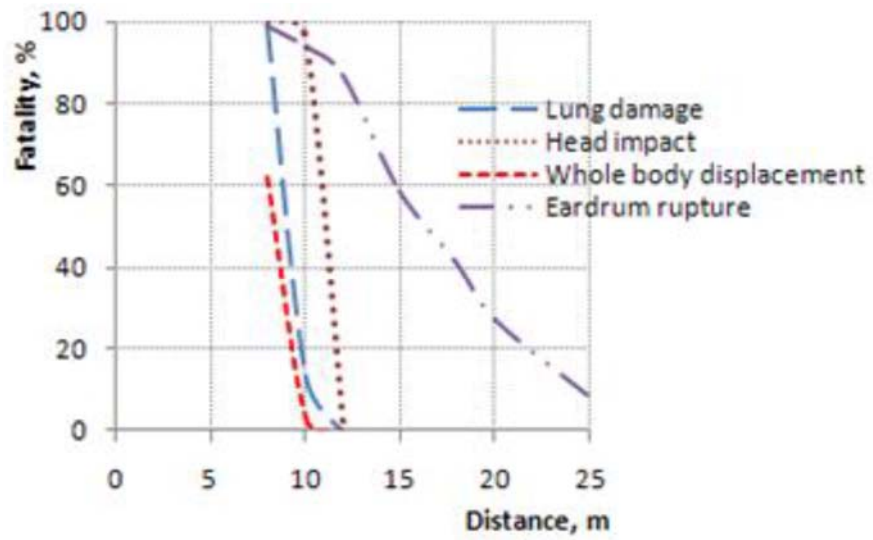
environment or area. Historically, there are various scenarios where these unfortunate incidents occurred as a result of energy release from gas pipe leakage, fittings, vessel, chemical plants, gas storage facilities etc. Mostly, the damaging effects of vapour cloud explosion are due to the overpressure that is generated from the fast expansion of the products of combustion. The overpressure created during vapour cloud explosion is generally the causes of damage to the equipment, people, facilities and the environment at large [19]. This accidental release energy from gas and vapour cloud could result from the following factors:

- ✓ Loss of process containment from the failure of a pipe, reactor, storage tank, or other process vessel containing flammable or combustible liquid, or flammable gas.
- ✓ Rapid discharge of flammable vapour to the atmosphere through a pressure relief system.
- ✓ The release of flammable liquid stored under pressure: for example; Liquefied Petroleum Gas (LPG). The discharged liquid will rapidly boil at atmospheric pressure, forming a flammable vapour cloud.

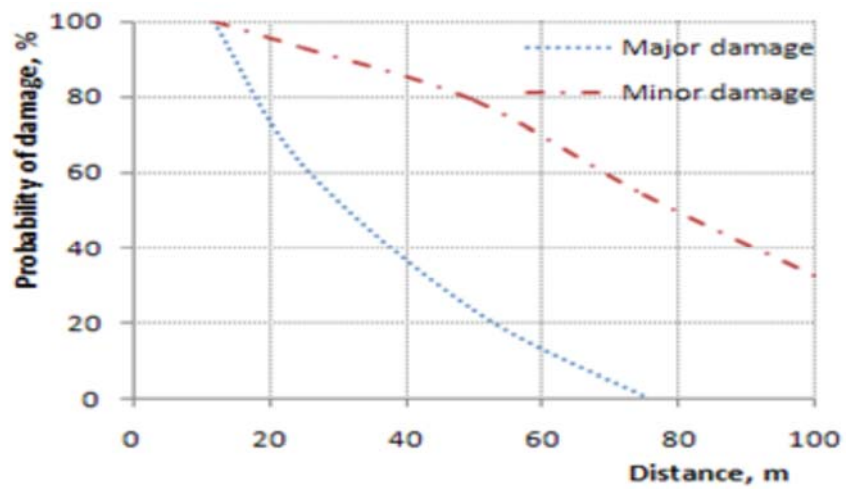
Soman A. R and Sundararaj G 2012, uses Baker-Strehlow models, equivalent TNT (tri-nitro-toluene), TNO multi-energy, as well as probit equation to estimate the overpressure from accidental release of hydrogen explosion from hydrogen holder with a capacity of 120m<sup>3</sup> and the facility damage from overpressure at a different distance from the centre of the explosion. The investigation shows that the proximity of the people working at a radial distance of 2500mm from the centre of the explosion may get affected with different facility ranging from 8% to 100%. However, the structure at a radial distance of 10000mm from the centre of the explosion may get minor damage with different probability from 32 to 100 %. Furthermore, the overpressures generated from TNO multi-energy method are higher than other methods as indicated the Figure 2.8.



(a)



(b)



(c)

**Figure 2.8:** a) Overpressure as a function of a distance, b) overpressure effects on people and c) overpressure effects on structures [19].

## **2.6.1 Type of fuel, properties and storage methods**

The significances and the possibility of gas explosion occurrence depend on the fuel type. However, under similar experimental conditions, different fuel-air mixtures will generate different explosion pressures.

In spite of the fact that they have been numerous damaging explosion episodes involving natural gases, they occurred because of the presence of the degree of confinement. However, natural gas has relatively lighter density than air as such when releases in an unconfined area, it tends to diffuse into the atmosphere which may result in flash fires rather than an explosion. Thus, heavier hydrocarbons with densities similar to or higher than air are more likely to be involved with unconfined vapour cloud explosions.

### **2.6.1.1 Past explosion event in Industries**

Hazards associated with an explosion are found historically in several industrial workplaces particularly in industries like mining, chemical, oil & gas exploration and production (E&P), steel manufacture and aeronautical industries etc. Due to the dangerous nature of hazards associated with an explosion, industries have endeavoured to make the workplace a safer place usually with help from their governing bodies. The primary application of work in this thesis lies in the oil & gas industries.

### **2.6.1.2 Middletown, 2010**

The large explosion occurred in the natural gas power plant in Middleton and claimed six lives, and at least 50 were injured on 7<sup>th</sup> February 2010. The explosion was caused by an automatic ignition of a gas cloud inside the plant. Approximately 11000 Sm<sup>3</sup> was released and formed an explosive cloud [20]. The source of ignition has not been found yet, but construction works were going on around the area which might have caused the ignition of the mixture. This area was within the building, and then, of course, the building contained process equipment that causes an increase in burning rate and gives rise to pressure build-up.

### **2.6.1.3 Buncefield, 2005**

The occurrence of an explosion resulted in the amount of fire in a fuel depot in Buncefield, England on Sunday 11<sup>th</sup> December 2005. Gas overfilled a storage tank, and fluid fuel began to overflow on the top of the tank. Around 300 tons of fuel got away and evaporated butane

and droplets from less volatile components formed a flammable cloud that was ignited [21]. A strong tank exploded that leads to the destruction of buildings, facility damage and cars within the area due to the ignition gas cloud. However, there are speculations that a lane of trees accelerated the deflagrated flame up to detonation. About 43 people were injured. Some of the facility damage as a result of the explosion is shown in Figure 2.9.



a) Before



b) Before



c) During



d) After

**Figure 2.9:** Buncefield Hertfordshire Oil Storage depot fire incident [21]

Figure 2.9 also present some of the results of the fire and explosion that occurred in Buncefield, 2005 before, during and after the explosion incident.

#### 2.6.1.4 Flixborough, 1974

On Saturday 1<sup>st</sup> June 1974, an explosion in Nypro plant at Flixborough occurred. It is one of the most serious accidents in the history of the chemical industry, which resulted in the death of 28 workers with a further 36 sustaining serious injuries. The explosion was caused by a release of 20.78m<sup>3</sup> of Cyclohexane, which attributed to the temporary failure of pipe

equipment. The flammable cloud was ignited about 1 minute after the release. A very violent explosion occurred, and several properties were damaged, many were injured, and many lost their lives, [22] and [4].

#### **2.6.1.5 Haltenbanken, Norwegian Continental Shelf, 1985**

The 1985 uncontrolled blowout occurred on semi-submersible drilling rig West Vanguard at block 6407/6 at the Haltenbanken in the Norwegian oil platform [23]. It was a result of gas leakage, which escapes into the engine room and very violent explosion developed. All the workers on-board were saved, but the damage to the rig facility causes them a huge amount of money.

#### **2.6.1.6 Piper Alpha, 1988**

The explosion and fire on the Occidental's Piper Alpha platform occurred in 1988. The explosion started in compressor module resulted in large fire due to the rupture of a riser, and a subsequent inquiry suggested that the fire was a result of uncontained gas release that found the source of ignition, making it the world worst offshore oil disaster. This disaster claimed 167 lives and destroyed most of the platform [24]. The estimation of overpressure generated by the initial explosion was about 0.3bar.

However, due to the catastrophic nature of damage attributed to the explosion, mitigating, suppressing and quenching explosions have been an important concern. The main objective of suppressing fire is to provide means of cooling it to prevent it from spreading and to provide extinguishment for the fire incidents. There are different types of fire suppression method available to protect facilities, properties and loss of lives. Water is the most useful and vital fire suppression medium due to its relatively low cost and its availability [25].

## **2.7 Combustion Chemistry**

To understand the formation of pollutants in combustion systems, we must first understand the nature of the fuels been burned, the thermodynamics of the combustion process, and some aspects of the flame structure. However, Combustion is the rapid exothermic reaction, which liberates a substantial amount of energy as heat and flames as combustion reactions with the ability to propagate through a suitable medium. Alternatively, combustion is the conversion of a substance known as fuel into chemical compounds known as products of combustion by

combination with an oxidizer. That is combustion usually involves the oxidation of a (hydrocarbon  $C_mH_n$ ) fuel to form products of oxidation. For example, in complete combustion, the global reaction in air is expressed in Equation 2.1.



The process of combustion is an exothermic chemical reaction that is energy is been released as it occurs. Moreover, either the chemical energy released is transfer to the surrounding as it is produced. It remains in the combustion products in the form of elevated internal energy (temperature).

Generally, in combustion processes, the focus is to break the chemical bond that exists between fuel and oxidizer that is the complex reaction chain and chemical kinetics generating light and heat in form flame or fire. However, the chain reaction in combustion comprises hundreds of transitional steps where hydrogen and oxygen decompose and break up to form hydroxyl radicals. To quench or suppress combustion flames, this chains or bond must be broken down which affects further propagation due to the dissociation of these radicals which forces the reaction to early termination. This research study focuses on the combustion of a fuel with air. The amount of heat or energy released per unit mass or per mole during combustion of the fuels is termed as the heat of reaction or heating value measured in the calorimeter. The three main parameters which have a very strong influence on combustion: temperature, turbulence and time. Meanwhile, from the perspective of combustion science, there are two main types of flames that are regularly encountered these includes; premixed and diffusion flames.

### **2.7.1 Premixed flames**

In many processes of fire protection engineering involves premixed flame. A premixed flame is the self-sustaining propagation of a localized combustion zone at subsonic velocities [26]. The gas flow into the combustion chamber is taken to be laminar, and uniform across the diameter of the tube and the flame is planar and perpendicular to the flow [27]. The flame produced after the ignition of quiescent fuel-air mixture conditions is considered to be a laminar deflagration wave. For instance, when two planes are considered ahead of and behind the flame as illustrated in Figure 2.10.

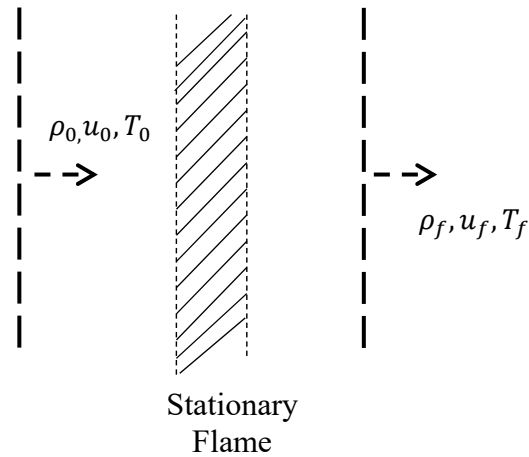


**Figure 2.10:** Stationary flame Description [27]

Then, the following conservation relations (i.e. conservation of mass and momentum) can be applied.

$$\rho_0 u_0 = \rho_f u_f = m \quad (2.2)$$

$$P_0 + \rho_0 u_0^2 = P_f + \rho_f u_f^2 \quad (2.3)$$

Rearranging the equations 2.2 and 2.3 gives;

$$\frac{P_f - P_0}{\left(\frac{1}{\rho_f} - \frac{1}{\rho_0}\right)} = -m^2 \quad (2.4)$$

$$\frac{P_f - P_0}{(u_f - u_0)} = -m \quad (2.5)$$

Where;  $P_0$  = Initial pressure of the gas,  $\rho_0$  = Initial density of the gas,  $u_0$  = Initial velocity of the gas,  $P_f$  = Final pressure of the mixture,  $\rho_f$  = Final density of the mixture,  $u_f$  = Final velocity (speed) of the mixture and  $m$  = Mass flux through the transition.

Equation 3.4 shows that the decrease in pressure increases deflagrations flame velocity. That is; the burnt gases leaving the flame front travelled at a higher velocity with lower pressure and density than the initial gas reactant. Taken into account the release of chemical energy with a great rise in temperature produces a very low pressure typically to around 1/1000<sup>th</sup> of the total pressure and usually neglected [27].

## 2.7.2 Flame structure

A simplified structure of laminar premixed flames can be identified as the preheat zone, the reaction zone, and the product zone, as shown in Figure 2.9. The preheat zone is governed by

the diffusion process of heat and mass while in the reaction zone, the chemistry of combustion takes place.

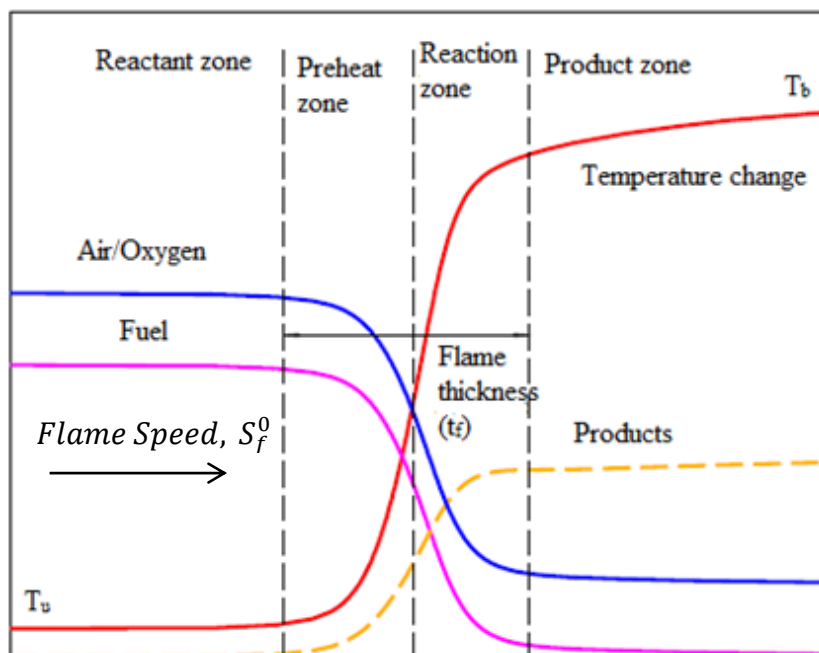


**Figure 2.11:** Flame temperature profile and concentration [26]

In the observation of the flame structure, it is noticeable that the temperature increases smoothly through the flame together with the product concentration. Thus the concentration of fuel molecules must decrease in a corresponding manner. The unstretched laminar flame speed ( $S_f^0$ ) usually defined as the velocity of flame front relative to a stationary observer. The flame front follows a preheat zone, where a balance between convection and diffusion exists. The reaction zone is defined as the inner layer, where the fuel is consumed and the radicals are depleted in a usually branched chain reactions [26].

### 2.7.3 The Energy of Activation, $E_a$

For sustainment of a combustion reaction, there must be enough energy levels sufficiently to cracked or break the bonds within the molecules of the fuel and oxidant, which will allow the reactions to occur and products to be formed. That is, activation energy is the amount of energy the reactant particles must have in order to break the old bonds for a reaction to occur. Several saturated hydrocarbons display very similar burning rates, with exceptions including alkenes such as ethylene which has higher activation energy and resultant greater exothermic, due to the presence of a double bond in the molecule. Alkynes such as acetylene contain a triple bond with even greater activation energy.

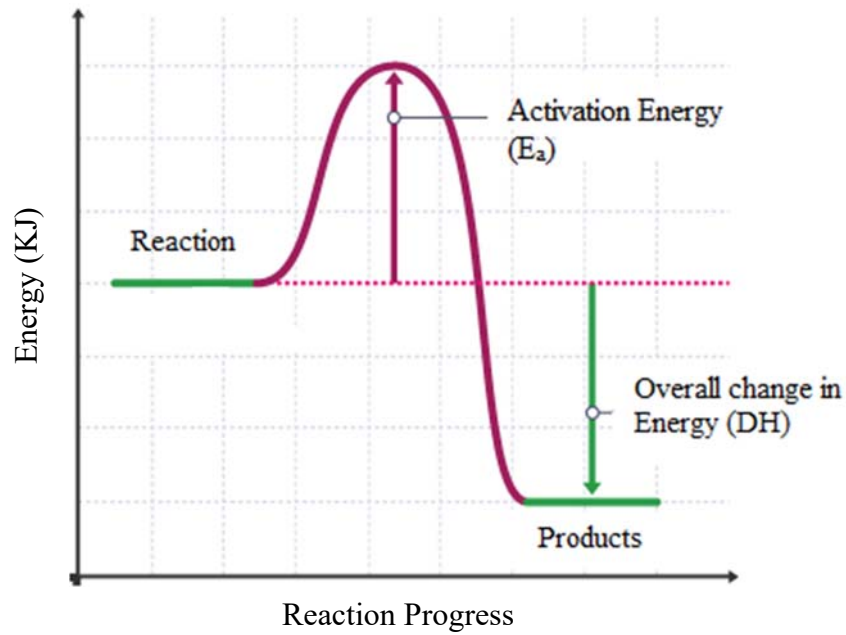


**Figure 2.12:** Activation energy curve [28]

This energy measured in calories (cal) or kilojoules (kJ) per mole, is known as the activation energy [28]. Therefore, this activation energy is defined by the Arrhenius function ( $k$ ), as:

$$K = Ae^{-Ea/RT} \quad (2.2)$$

Where;  $k$  = the rate constant of chemical reactions,  $A$  = the pre-exponential factor,  $Ea$  = the activation energy (kJ),  $R$  = universal gas constant (J/kg K),  $T$  = Absolute temperature (K).

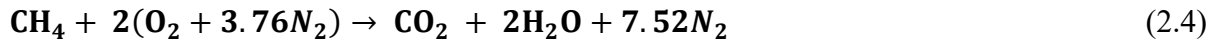
The Arrhenius equation is very simple with remarkable accuracy formula for the temperature dependence of constant reaction rate, and the rate of a chemical reaction.

#### 2.7.4 Mass and Mole Fraction

Mass or mole indicates the amounts of substances present in a sample. A mole is the amount of substance containing the same number of the chemical unit as there are atoms in exactly 12 grams of carbon 12 (i.e.  $6.023 \times 10^{23}$ ). The burning of gas, liquid, or solid in which fuel is oxidised involves heat release and often light emission. For example, equation 2.3 shows the stoichiometric chemical equation of Combustion of methane ( $\text{CH}_4$ ) in air mixtures:



Equation 2.2 indicates that one molecule of methane is oxidised with two molecules of oxygen completely and heat of combustion is generated. From complete combustion of hydrocarbon fuel, CO<sub>2</sub> and H<sub>2</sub>O (vapour) is mainly the chemical products. Furthermore, air consists of about 0.9% by volume of argon, 78.1% nitrogen and 20.9% oxygen. For the purpose of combustion calculations, the composition of air is approximated as a simple mixture of oxygen (O<sub>2</sub>) and nitrogen (N<sub>2</sub>) (21% and 79%). Therefore, re-writing equation 2.2 yields,



Combustion of gaseous fuel in air can occur in two different ways.

- The fire, where fuel and oxygen are mixed during the combustion process.
- The fuel and air (or another oxidiser) are premixed, and the fuel concentration must be within the flammability limits [4].

### 2.7.5 Mixture Ratios

Mixture ratio is one of the most important operating parameters of combustion. That is the ratio of fuel and air present in a system. Mixture ratio can be mixed in the different ways.

### 2.7.6 Equivalence Ratio

The fuel/oxidant ratio is one of the most important parameters for combustion analysis, normally reported in terms of a non-dimensional variable called equivalence ratio  $\Phi$ , which is the actual fuel/oxidant ratio normalized by the stoichiometric fuel/oxidant ratio:

$$\Phi = \frac{(\text{fuel/oxidant})_{\text{actual}}}{(\text{fuel/oxidant})_{\text{stoic}}} \quad (2.5)$$

If equivalence ratio equal to 1 (i.e.  $\Phi=1$ ) is termed as a stoichiometric condition. The condition where there is an excess of oxidant present in the mixture is known as “lean mixture” (i.e.  $\Phi<1$ ). Similarly, mixtures with an excess of fuel are known as “rich mixture” (i.e.  $\Phi>1$ ). Equation 2.2 is valid when the ratio is calculated on both the mass and mole basis, provided that the actual and stoichiometric ratios are calculated consistently. The equivalence ratio may also be defined as:

$$\Phi = \frac{(\text{oxidant/fuel})_{\text{actual}}}{(\text{oxidant/fuel})_{\text{stoic}}} \quad (2.6)$$

### 2.7.7 Air/Fuel Ratio (AFR)

This is the most common method of the mixture. It is simply the ratio of air and fuel by mass at the point of interest. It is expressed as:

$$\text{AFR} = \frac{m_a}{m_f} \quad (2.7)$$

### 2.7.8 Fuel/Air Ratio (FAR)

This is the inverse of the AFR but is not so common because, in the majority of cases, it is significantly less than unity. For example, the stoichiometric fuel/air ratio of methane is 0.0588:1.

### 2.7.9 Excess Air, (XSA)

The majority of combustion operates with a slight excess of air because it prevents the formation of products of incomplete combustion, which can be very toxic. It is the percentage of air in the system by mass that is surplus for the requirement for complete combustion. It is expressed as:

$$\text{XSA} = 100\% * \frac{\text{AFR} - \text{AFR}_{\text{stoic}}}{\text{AFR}_{\text{stoic}}} \quad (2.8)$$

Where,  $\Phi$  = Equivalence ratio, AFR = Air/Fuel Ratio, FAR = Fuel/Air Ratio and XSA = Excess Air.

## 2.8 Governing factors

In the event that a closed vessel containing a combustible mixture of fuel and oxygen at standard temperature and pressure is gradually heated at a controlled rate, a steady state might be achieved without ignition or fire. Experiments conducted by William and Richard revealed that when a combustible mixture of methane and oxygen reached a certain temperature in the range of 300°C – 400°C at the pressures ranges from 2 bar – 2.3 bar, the species involved becomes chemically reactive [29]. However, if there is poor control of the

energy within the closed vessel, then the temperature of the mixture will rise gradually and cause an increase in the reaction rate and would result in pressure increase as well. The exponential increase in collisions would eventually lead to a critical temperature at which ‘ignition’ would occur. An explosion would then follow, and energy in the form of heat and pressure would be released. The energy released as heat in this manner is known as a ‘thermal explosion’.

The ignition temperature is the lowest temperature at which a combustible substance when heated takes fire in air and continues to burn, and the flame will begin to develop, which may then propagate through the remaining unburned mixture. The rate of this propagation depends on the following factors; flame speeds and burning velocity, fuel reactivity, mixture temperature, the equivalent ratio of the fuel and oxidant within the explosive limits, mixture static pressure etc. However, the essential measures for the extinction of a combustion flame or wave is determined by many factors. One of these factors is a non-dimensional quantity known as Damköhler Number (Da). This number is used to relate reaction timescale (rate of reaction) and fluid turbulence timescale to the transport phenomena rate occurring in a system.

### **2.8.1 Flame propagation**

Flame propagation comes from the energy released from an exothermic reaction results either from combustion or exothermic decomposition, or a combination of the two. For example; combustion of methane in air and decomposition of acetylene etc.

### **2.8.2 Flame Speed and Burning Velocity**

Flame speed,  $S_f$ , is the velocity of the flame relative to a stationary observer, i.e. the ground or another fixed frame. While burning velocity,  $U_b$ , is the speed at the flame front propagates through the flammable mixture relative to the unburnt gas immediately ahead of the flame. Note that the flame speed associated with deflagration is always higher than the burning velocity [30]. The relation between flame speed,  $S$ , and burning velocity,  $U$ , is, therefore:

$$\mathbf{S_f = U_b + u_u} \quad (2.9)$$

Where;  $S_f$  = Flame speed (m/s),  $U_b$  = Burning velocity (m/s<sup>2</sup>),  $U_u$  = Velocity of the unburnt gas ahead of the flame (m/s<sup>2</sup>)

## 2.9 Hydrocarbons Characteristics

Hydrocarbon materials have numerous different features that are used to define their level of hazard. The main characteristics of combustible hydrocarbon materials that are of high interest for fire and explosion concerns are described below.

### 2.9.1 Lower Explosive Limit (LEL) and Upper Explosive Limit (UEL)

For the occurrence of fire or explosion, some certain conditions must simultaneously have met. A fuel gas (e.g. methane) and oxygen (air) must exist in certain proportions, along with an ignition source, such as a spark or flame. The ratio of fuel and oxygen that is required varies with each combustible gas or vapour. Lower Explosive Limit (LEL) is the minimum concentration of particular combustible gas or vapour necessary to support its combustion in the air for that gas. Below this level, the mixture is too “lean” to burn. Furthermore, the Upper Explosive Limit refers to the maximum concentration of a gas or vapour that will burn in air. Above this level, the mixture is too “rich” to burn. The range between the LEL and UEL is referring to as the flammable range for that gas or vapour.

**Table 2.1:** Most Common Material of Flammable Ranges and Spreads

Material	Flammable Range (%)		Range Spread
	LEL	UEL	
Hydrogen	4.0	75.6	71.6
Ethane	3.0	12.5	9.5
Methane	5.0	15.0	10.0
Propane	2.37	9.5	7.1
Butane	1.8	8.4	6.6
Pentane	1.4	8.0	6.6
Hexane	1.7	7.4	5.7
Heptane	1.1	6.7	5.6

## 2.9.2 Earliest research studies on gas and vapour explosion

Hazards associated with an explosion found historically in several industrial workplaces particularly in industries like mining, chemical, oil & gas exploration and production (E&P), steel manufacture and aeronautical industries etc. Due to the dangerous nature of hazards associated with an explosion, industries have endeavoured to make the workplace a safer place usually with help from their governing bodies. The primary application of work in this thesis lies in the oil & gas industries.

As far back as 1700's 'hit' was utilized as a part of coal mines as a mechanical method for identifying the presence of oxygen in low levels and increasing levels of explosive gases, for example, methane. Different strategies including conveying little flying creatures, for example, the Canaries, which truly tumbled off their roost if gas levels were not good. On those days, miners conveyed naked flames to the mining location with them as a wellspring of light; nevertheless, to determine different levels of oxygen and methane, they utilized the size and shade/colour of the flame. During 17<sup>th</sup> and 18<sup>th</sup> centuries, due to series of explosions occurring in the European coal mines, the UK's Sunderland Society for safety and preventing an accidental explosion in European coalmines consulted Sir Humphrey Davy to find out the cause of ignition in fire/damp/air mixtures. Davy (The British Chemist) firstly investigated the chemical composition of the firedamp and carried out numerous experiment on the circumstances at it combust. Davy established the limit of flammability of firedamp and suggested that firedamp burns less easily than all other flammable gases and has less heat of combustion [31]. Davy's achievement leads him to the development of a coal miner's lamp known as Davy lamp shown in figure 2.3.



**Figure 2.13:** Davy’s safety lamp for coal miners (the earliest flame arrestor) [31].

Davy’s lamp consists of a flame produced by a wick burning ‘lamp oil’ surrounded by iron gauze. Davy’s work helped him to determine the gauge of the gauze, which surrounded the flame and its ability to prevent flame propagation from one side of the gauze to the other. Davy provided a quota of the early spearheading study in the subject of fire extinguishing [32]. However, Davy’s lamp could be taken into regions of known gas gatherings without fear of ignition.

The U.S. Department of the Interior set up the American Bureau of Mines recommended by the then President Theodore Roosevelt in 1907. However, the Congress refuses to act on his recommendation until series of disasters in the Nation’s coal mines which claimed 3000 lives in 1907 alone. There were 361 coal mineworkers lost their lives in Monongah, WV, on December 6, 1907; 239 killed 2 weeks after Jacobs Creek, PA; 154 killed at Marianna, PA, on November 28, 1908; and 259 killed at Cherry, IL, on November 13, 1909 [33].

Due to this numerous loss of lives, the American Bureau of Mines in collaboration with National Institute for Occupational Safety and Health (NIOSH) in 1910 began to carry out new research centred in Pittsburgh, PA, (the largest of the federal research centres and the oldest). This is in response to the alarming number of fatal explosions and fires in U.S. underground coal mines [34]. The USBM and NIOSH investigation was aimed at providing the mining industry with information on explosion materials and techniques that could be used safely in the presence of flammable mine gases and dust in other to eliminate and reduce fires hazards in mining [35] and [34]. The experimental apparatus used in their investigation include a 30-meter long test section/galley developed to simulate an underground mine

entrance and a 38 acre of land tract rented from the Pittsburgh Coal Company. The scope of the Bureaux includes:

- Investigation concerns with the strategies for mining, particularly in relation to the wellbeing of miners, and the apparatuses best suitable to prevent accidents.
- The possible improvement of the conditions under which mining operations are carried on;
- The treatment of ores and other mineral substances;
- The use of explosives and electricity;

As reviewed by Smith and Thimons, they look into fire research conducted by the USBM and NIOSH from 1910 to 2009. The result of their review demonstrated that the rate of injuries and fatalities reduces drastically in light of the significant advances in mine fire safety. In any case, the risks will keep on evolving because of deeper and gassier mining activities. However, an early interest in fire research was in unconstrained heating during coal storage. Especially in the heating of government structures and powering maritime vessels, this required enormous measures of coal to be stored. Consequently, the sudden ignition prevention research area pulled the focal point of various researchers because of economic reasons [35].

### **2.9.3 Perforated Sheet/Plate (PS)**

Perforated plate/sheet is made primarily for deflagration flame arrester. They are usually metal (stainless steel), but at times incorporate perforated re-factory disk and gauze pads in combination with the metal plates. They are available in different ranges of hole diameter and plate thickness.

### **2.9.4 Woven wire mesh**

Wire mesh is commercially available in a wide range of materials, and there are also numerous wire orientations available in the market. Metallic wire meshes are porous materials consisting of an array of metals forming square, rectangular or circular pore patterns. Wire mesh screens are manufactured in a variety of pore sizes, wire diameters and wire types. Wire meshes are also categorized based on the type of connection between wires

as welded, woven, crimped or molded. Woven wire meshes are manufactured in different pore densities.

### **2.9.5 Previous studies on Porous media Combustion**

This section summarises the review of the previous study by several researchers. Due to the fact that explosion (combustion of hydrocarbons) is a very wide area, there is a numerous number of published, unpublished, conference papers, and even symposium work available; it will be unrealistic to review all of the obtainable literature. However, this Section review and discusses some of the up to date previous published study conducted by researchers.

Donoso-García and Henríquez-Vargas carry out a numerical study on turbulent combustion in a recuperative porous media burners coupled with thermoelectric generation and two-dimensional simulation to investigate the production of thermal NO<sub>x</sub> modelled by the extended Zeldovich mechanism with post-processing computation. They consider variables gas inlet velocity and composition, porous media thermal conductivity and inner wall insulation material. Their results revealed that flammability limits for stable combustion were found alongside with the electric potential generated within the system. Higher values of electrical potential, thermoelectric efficiency and flame temperatures were reached when the gas mixture energy content and heat recovery capacity of the system were increased [36].

Bani et al. (2018) experimentally investigated porous media combustion using hydrogen/Oxygen as fuel to examine the effects of equivalence ratio and conductivity of the solid matrix. The combustor has dimensions of 15 mm in length, 10 mm in width and 1 mm in height with 0.5 mm being the wall thickness. The material for the wall was 316L stainless steel due to its ability to stand high temperatures without physical degradation. The fuel used was H<sub>2</sub>/O<sub>2</sub>, and equivalence ratio was 1.0 and 0.8. The combustor was filled with a mesh made of stainless steel (SS) with a porosity of 0.9. The inserted PM is made by cutting the SS mesh into one ply. The result shows that there was a reduction in combustion efficiency when there is an increase in velocity inlet. The average wall temperature decreased with increase in the solid matrix thermal conductivity. For any 10 K increase in cell temperature, the cell efficiency and power output reduced by 7% and 0.14 W respectively. Projected electrical output power and power density of the complete system were 2.7 W and 0.72 W cm<sup>-2</sup> respectively when the cell temperature is kept at 300 K, and the spacing between the radiant

wall and the PVC is 1 mm. The experiment produced 1:703 W electrical power which was in consonance with what was predicted with the model [37].

Khanna, Goel and Ellzey [38] examined the combustion of methane in a porous medium burner utilising the porosity of 0.87 upstream and 0.84 downstream. Ellzey and Goel [39] use a two-stage porous media burner to measure carbon monoxide and nitric oxides emissions of fuel/air mixtures. Tseng and Howell [40] investigated the combustion of liquid fuels in a porous radiant burner. The focuses these studies were all on burner flames.

Babkin, Korzhavin and Bunev [41], Pinaev [42] and Makris, Oh, Lee and Knystautas [43] investigated steady flame and detonation propagation in vertical tubes filled with sand and spherical beads. The result shows that propagation of flame in porous media at speed greater than 5m/s will produce an increase in pressure ahead of the flame.

Wang and Wen [2] studied the effect of the perforated plate on flame propagation with a porous media using a one-step chemistry model for combustion of the stoichiometric hydrogen/air mixture. The results show numerically that the perforated plate considerably has an effect on the propagated flame in the region downstream from the perforated plate and marginal effect on the upstream region. However, to squeeze the flame front and result in a ring of unburned gas pocket around the flame neck and the perforated plate has an effect of reducing the flame speed downstream of it.

Min and Shin in 1991 tentatively carried out an experiment to investigate the burning of premixed propane-air inside a cordierite honeycomb to provide experimental data for a numerical model. The lean combustibility range was increased from 0.52 to 0.49. The result shows that a maximum inlet temperature occurred at 0.53 equivalence ratio. The heat produced by the burner was higher than the adiabatic flame temperature at the flame front due to heat recirculation from the solid matrix [44].

The experiment carries out by Marbach and Agrawal in 2006 utilising porous media and preheating annulus to provide a heat recirculation premixed burner. Methane gas was used as fuel varying the inlet velocity ranging between 0.5 and 1.0 m/s and measured the performance of the burner with and without porous media and exterior insulation as shown in figure 3.3. The initial gas temperature of the reactant and the final temperature of the products were measured. A peak temperature of the combustion products was observed. The reactant gas temperature was almost the same with porous media in the annulus compared to without it. However, the combustion products temperature slightly higher due to heat loss.

The exterior insulation increases the gas inlet temperature from 150K to approximately 700K. An equality proportion of 0.39 at the lean victory restrict was acquired for the lower gulf speed and emanations expanded at the higher stream rate [45].

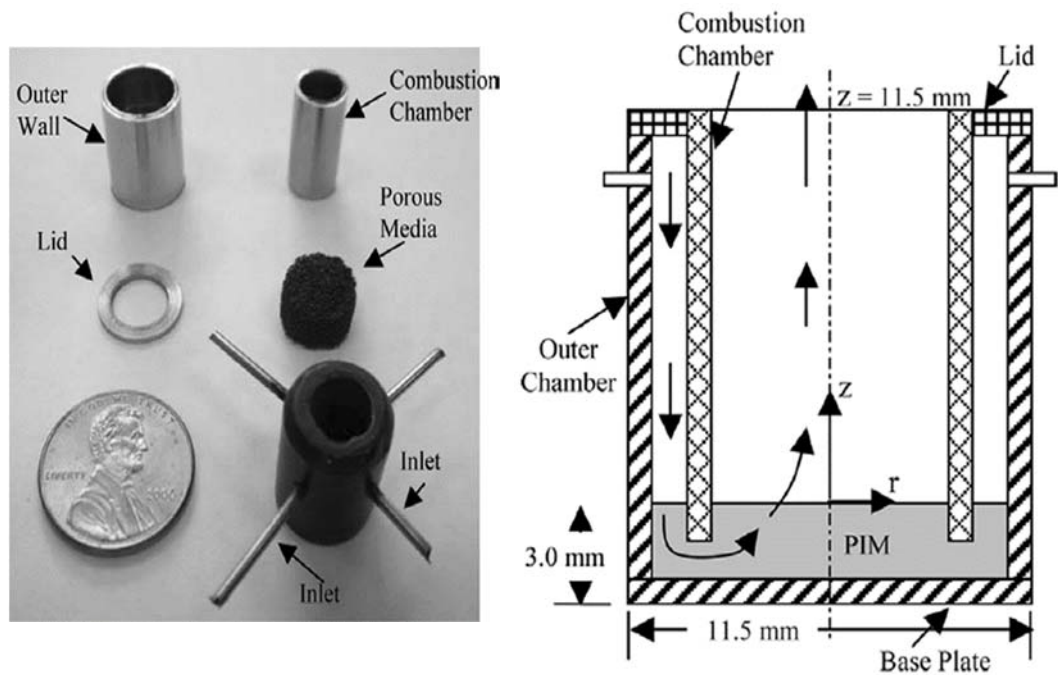


**Figure 2.14:** Apparatus and schematic diagram of burner used [45]

Figure 12 illustrates the apparatus used for the burner. The entire volume of the combustion chamber was 0.364 cm<sup>2</sup>. Methane was burned with air at a varied flow rate between 0.25 to 1.0 m/s and an equivalence ratio between 0.5 and 0.8. From the measurements of CO, the combustion efficiency was calculated to exceed 99.5% with emission levels increasing with equivalence ratio. A peak temperature of 1800 K was recorded in the combustion zone with about 1580 K at the exit.

## Chapter 3: Spray and Atomization

### 3.1 Overview

Spray and atomization are described in three different form of mechanism as follows; liquid droplet break, jet break up and sheet break. Spray can be express as collections of drops formed from bulk liquid source.

#### 3.1.1 Liquid Droplet Formation

The most elementary form of atomization can be exemplified by the slow discharge of a liquid from the end of a burette or a hypodermic needle. If the force of gravity (i.e. weight of the drop) exceeds the surface tension force in the liquid at the orifice lip, the liquid is pulled away from its attachment, and a drop is formed. The mass of the droplet formed can be determined by equating the gravitational and surface tension forces on the droplet [46]. Assume that the entire liquid forms one droplet at the orifice after breaking away from the orifice lip, the size of the droplets is given by

$$D = \left( \frac{6d\sigma}{\rho_l g} \right)^{1/3} \quad (3.1)$$

#### 3.1.2 Liquid Droplet Break-up

The main stresses (force per unit area) acting on the liquid during break up are inertia ( $\mu U/L$ ), viscous ( $\rho U^2$ ) and surface tension ( $\sigma/L$ ), where L is a suitable length scale. Equation 3.1 and 3.2 (Reynold and Webber number) illustrated the relative importance of stresses involved during liquid droplet break up.

$$\text{Reynold number} = \frac{\rho U L}{\mu} \quad (3.2)$$

$$\text{Webber Number} = \frac{\rho U^2 L}{\sigma} \quad (3.3)$$

Where:  $\rho$  = Liquid density (kg/m),  $U_R$  = Velocity (m/s),  $\sigma$  = Surface tension (N/m), L = Length (m). High values of Reynold and Weber number promote more rapid and finer atomization.

### 3.1.3 Jet Break-up

Fuel sprays is an example of high pressure-driven liquid fuel jet breakup when injected through an atomiser insert orifice into the combustion chamber.

Nasr et al. (2002) explained the effects of relative velocity on liquid jet breakup as shown in figure 3.2, the higher the velocity, the disordered nature of the droplets increases as such the prediction of the jet break-up cannot be theoretically predicted at higher velocities [47].

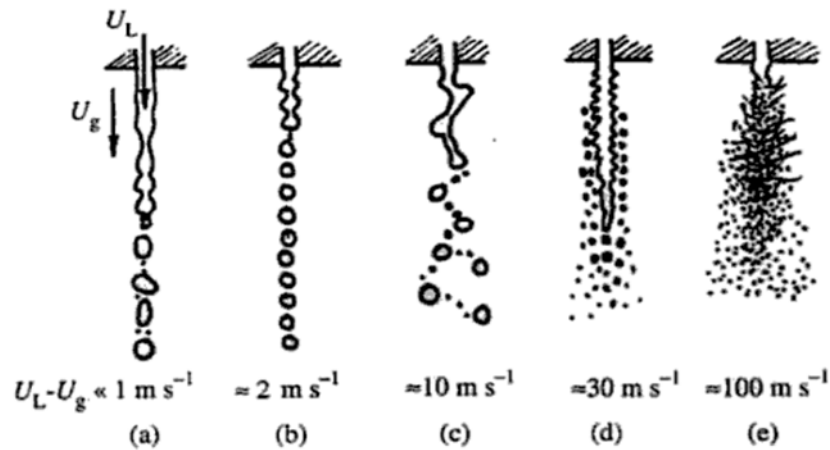


**Figure 3.1:** Break-up of a liquid jet [47]

Moreover, in order to achieve a very fine droplet size from the atomizers, the velocity between the liquid and surrounding gaseous medium must be as high as possible and at high pressure.

### 3.1.4 Sheet Break-up

This is more complex than that of the liquid jet because three-dimensional flow generally occurs.

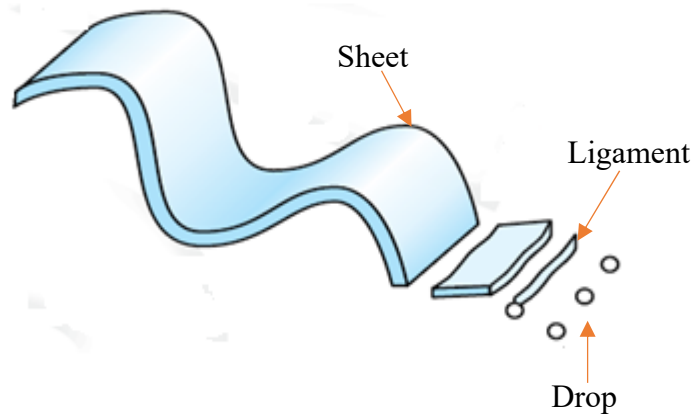


**Figure 3.2:** Different stages of liquid sheets break up

Figure 3.1 elucidate the different stages of liquid sheets break-up. A sheet is being formed when a liquid exit the orifice of the atomizer as a result of high exit velocities of the atomizer depending on the type of atomizer utilized. The sheet then breaks down into ligaments, which are essentially unstable and then break up into individual droplets.

## 3.2 Atomization

Atomisation is the breaking down of atoms into smaller fine particles or converting a substance into very fine droplets in a gaseous medium. There are numerous approaches related to all methods of atomization such as the hydraulics of flow within the atomizers, the development of the liquid jet or sheet and the growth of small disturbance [48]. The two phases of atomization are shown in Figure 3.3, each region characterised by varying aerodynamic interchange of forces.

### 3.2.1 Primary Atomization

These define the liquid formation and disorderliness near the nozzle due to pressure and its mechanism in the flow geometry. That is, at whatever point liquid exit the orifice of the nozzle, a sudden appearance of the smooth jet is observed. As the liquid advanced further away, an unsettling progressive influence in the jet is seen. This increases downstream until the point that the abundance of the aggravation measures up to the jet span, at which beads start to squeeze off from the fluid stream in this way, essential separation was thought to be as a consequences of the flimsiness experienced by the fly surface, prompting the squeeze off

of the drops in reality, turbulent motions of the fluid and hydrodynamic cavitation inside the spout has been distinguished as the controlling system.

Primary atomisation considers the effects of wave growth on the jet surface and turbulence including cavitations and bubble generation.

### **3.2.2 Secondary Atomization**

Secondary atomisation is a process where bulk liquid split to smaller drops at an increased distance downstream of the atomiser insert. Breakup mechanisms consist of two stages, as shown in Figure 2.10. The figure shows the growth of bubbles in the bag type atomiser insert for both low and high Weber numbers.

## **3.3 Basic Spray Properties**

Different uses for sprays have different demands based on their design criteria. The useful properties of the spray are as follows:

- Spray Patternation
- Drop Size Distribution
- Mean Diameters
- Factors Affecting Droplet

### **3.3.1 Spray Patternation**

Spray patternation is an important factor to use in describing spray characterization. Generally, there are four types of the spray pattern, i.e. flat fan, hollow cone, full cone and solid stream. The most commonly used are; flat fan, hollow cone and full cone as illustrated in figure 3.3. Spray patternation depends mainly on the internal geometry and flows within atomizer enclosure. Other factors such as liquid viscosity, the ratio between orifice length and orifice diameter, pressure source, flow rate and aerodynamic forces will also affect spray patternation.

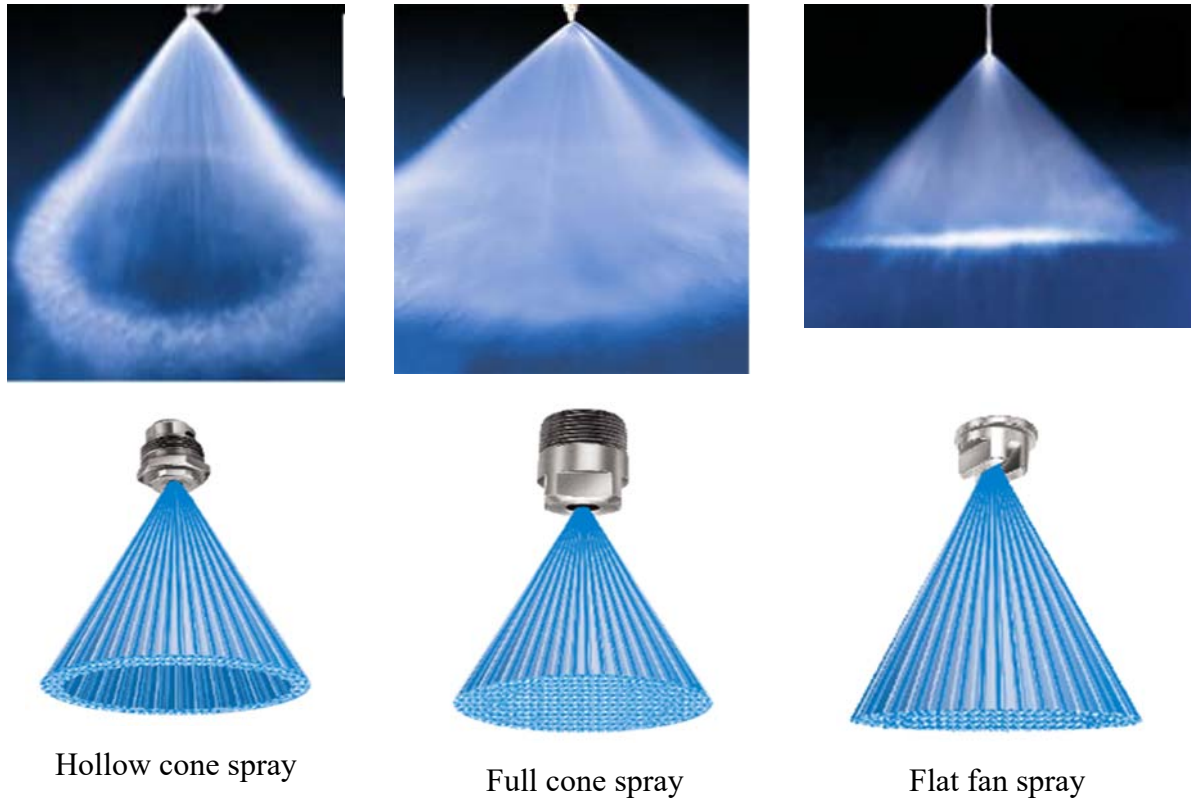
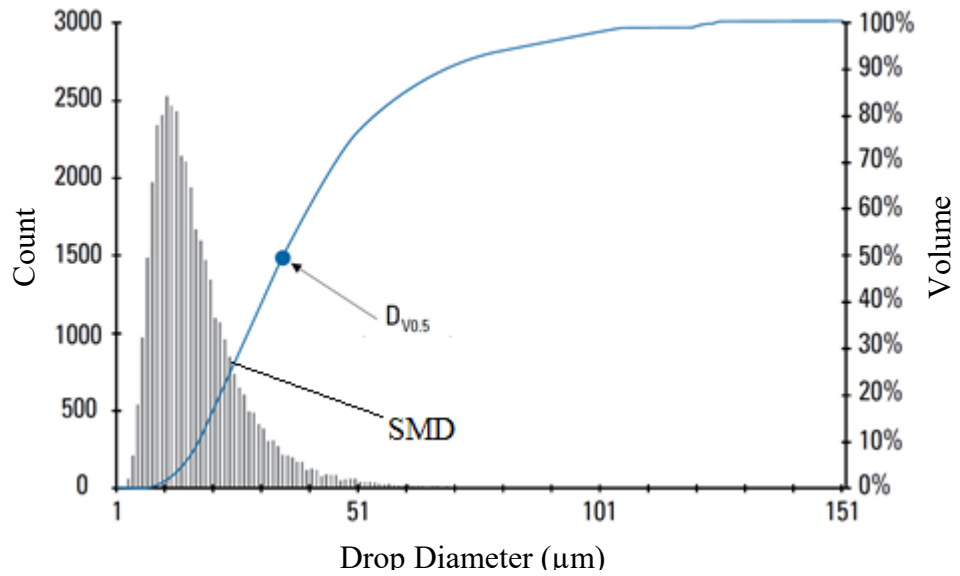


**Figure 3.3:** Different types of spray pattern

### 3.3.2 Drop Size Distribution

Drop size refers to the size of the individual drops that comprises a nozzle spray pattern. Each spray pattern provides a range of drop sizes. This range is known as drop size distribution. Generally, the spray is considered as a system of drops immersed in a continuous gaseous phase. The precise drop size information plays a significant factor in the overall effectiveness of spray nozzle operations. Depending on the type of atomizer used, each spray provides a range of drop sizes, and the range is referring to drop size distribution. Thus, drop size distribution is dependent more on the type of spray pattern utilized.



DV0.5 is the Volume Median Diameter, which is also known as VMD or MVD. DV0.5 is a value where 50% of the total volume of liquid sprayed is made up of drops with diameters larger than the median value and 50% smaller than the median value.

Drop size distribution can be plotted and represented using a histogram of drop size for each ordinate that represents the number of drops whose dimension fall between the limits  $D - \frac{\Delta D}{2}$  and  $D + \frac{\Delta D}{2}$  as illustrated in Figure 3.2.

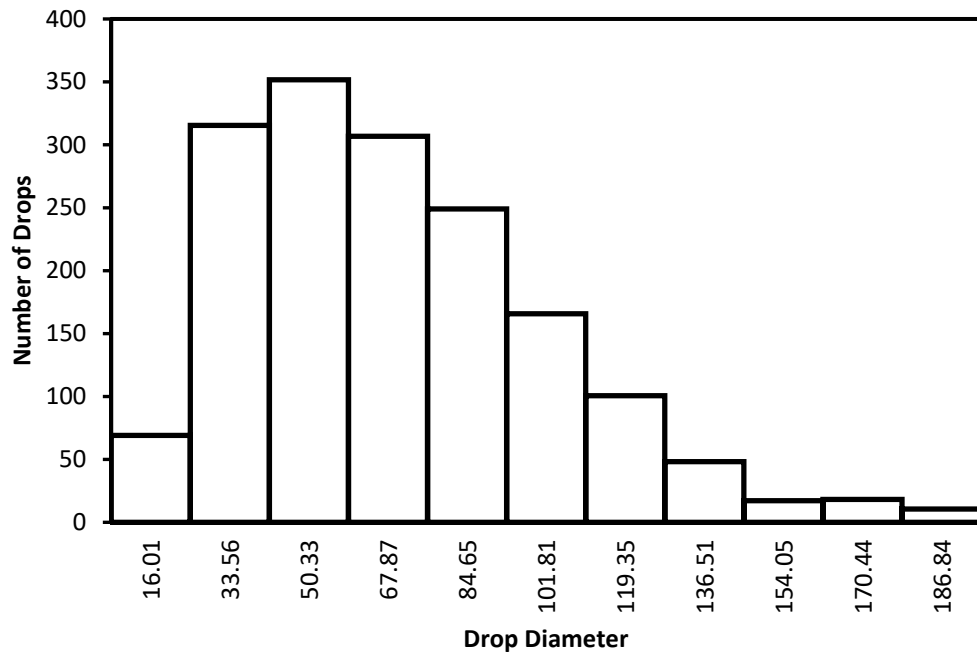


**Figure 3.4:** Histogram chart of Drop sizes [48].

The volume corresponding to a range of drop size plotted as a histogram of drop size between  $D - \frac{\Delta D}{2}$  and  $D + \frac{\Delta D}{2}$  instead of plotting the number of drops, the result of distribution is skew to the right, as shown in Figure 3.3, due to the weighting effect of the larger drops.

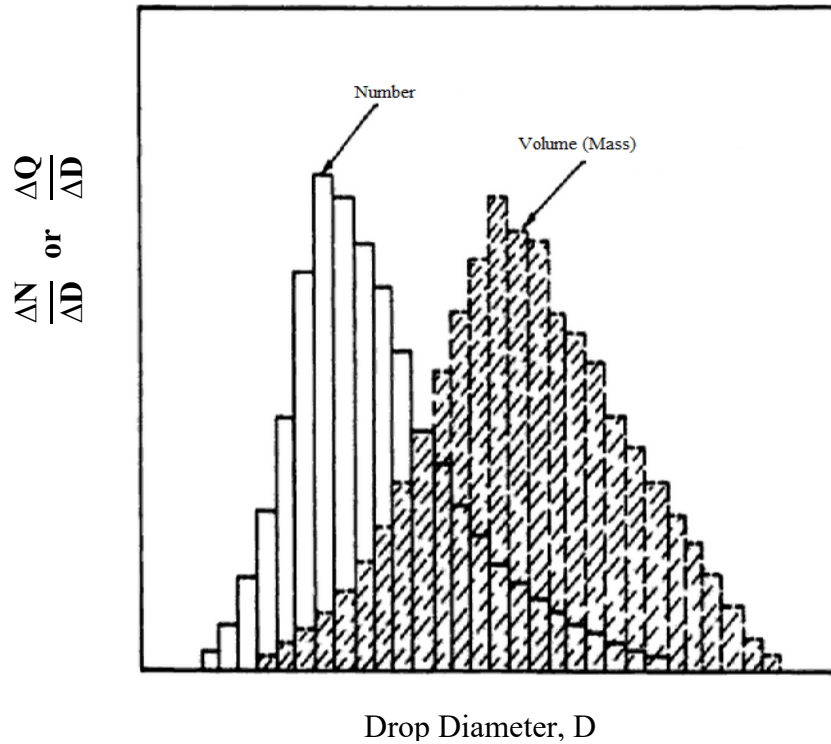


**Figure 3.5: Drop size histograms based on Number and Volume [48].**

As  $\Delta D$  is reduced, the histogram assumes the form of a frequency curve that may be regarded as characteristic of spray, provided it is based on a sufficiently large sample [48]. The frequency distribution curve is shown in Figure 3.3.

### 3.3.3 Mean Diameter

In the most calculation of mass transfer and flow processes, it is appropriate to work only with mean or average diameter instead of using complete drop size distribution. One of the most common average diameters in combustion is  $D_{ab}$ , where:

$$(D_{ab})^{a-b} = \frac{\int_{D_0}^{D_m} D^a (dN/dD) dD}{\int_{D_0}^{D_m} D^b (dN/dD) dD} \quad (3.4)$$

Where  $a$  and  $b$  may take on any values corresponding to the effect investigated, and the sum  $(a + b)$  is called the order of the mean diameter. Equation (3.3) can be written as;

$$D_{ab} = \left[ \frac{\sum N_i D_i^a}{\sum N_i D_i^b} \right]^{1/(a-b)} \quad (3.5)$$

Where  $i$  denotes the size range considered,  $N_i$  is the number of drops in size range  $i$ , and  $D_i$  is the middle diameter of size range  $i$ . Thus, table 3.1 shows the different types of drop diameter.

**Table 3.1:** Mean diameter and their application [48]

<b>a</b>	<b>b</b>	<b>Symbol</b>	<b>Name of mean diameter</b>	<b>Application</b>
1	0	D <sub>10</sub>	Arithmetic mean diameter	Comparison
2	0	D <sub>20</sub>	Surface mean diameter	Surface area controlling
3	0	D <sub>30</sub>	Volume mean diameter	Volume controlling
2	1	D <sub>21</sub>	Relative surface area mean diameter	Absorption
3	1	D <sub>31</sub>	Relative volume mean diameter	Evaporation, Molecular diffusion
3	2	D <sub>32</sub>	Sauter mean diameter (SMD)	Mass transfer, Reaction
4	3	D <sub>43</sub>	Mass, De Brouckere or Hardan	Combustion equilibrium

**Table 3.2:** Different forms of droplets diameter [48]

Symbol	Formula	Terms	Definitions
$D_{10}$	$D_{10} = \frac{\sum_i n_i d_i}{\sum_i n}$	Arithmetic Mean Diameter	This is the average diameters of all the droplets in the spray.
$D_{20}$	$D_{20} = \sqrt{\frac{\sum_i n_i d_i^2}{\sum_i n_i}}$	Surface Mean Diameter ( $d_s$ )	This is the diameter of an assumed particle that has the same averaged surface area as that of the given sample.
$D_{30}$	$D_{30} = 3 \sqrt{\frac{\sum_i n_i d_i^3}{\sum_i n_i}}$	Volume Mean Diameter $d_v$	This is the diameter of a hypothetical particle having the same averaged volume as that of the given sample
$D_{32}$	$D_{32} = \frac{\sum_i n_i d_i^3}{\sum_i d_i^2}$	Sauter Mean Diameter $d_{32}$	This is the diameter of the drop in which the ratio of volume to surface area is the same as that of the entire spray.
DV <sub>0.1</sub>		Mass median diameter 10%	The diameter of the drop is such that 10% of the total liquid volume is in drops of a smaller diameter
D <sub>0.5</sub> or D <sub>50</sub>	$D_{50} = \frac{\sum_i n_i d_i^5}{\sum_i d_i}$	Mass Median Diameter (MMD) 50%	This is the diameter of the drop in which 50% of the total liquid volume is in drops of smaller diameter.
D <sub>0.632</sub>		Characteristics Diameter	This is drop diameter such that 63.2% of the total liquid volume is in drops of smaller diameter
D <sub>0.9</sub>			This is drop diameter such that 90% of the total liquid volume is in drops of smaller diameter
D <sub>0.999</sub>		Maximum Diameter	This is drop diameter such that 99.9% of the total liquid volume is in drops of smaller diameter
D <sub>peak</sub>		Peak diameter	The value of D corresponding to the peak of the drop size frequency curve

Where ; Ni is the number of drops in the size range,  $i$   
 Di is the middle diameter in the size range,  $i$

### 3.3.4 Sauter Mean Diameter, SMD or $D_{32}$

The fundamental quantity used to describe a distribution of fluid particles is the mean particle diameter because it provides basic information about various characteristics of the system, i.e. number, diameter, surface and volume of the particle. It is very useful in engineering calculations of droplet and bubble sizes as well as transport processes. Therefore, Sauter mean diameter (SMD), which is also called Surface Area Moment Mean,  $D(3,2)$  or  $D_{32}$ , is used to evaluate the mean size of given particle distribution. This is defined as the diameter of a sphere that has the same volume/surface area ratio as the particle of interest.

Alternatively, SMD is defined as the diameter of the drop in which the ratio of volume to surface area is the same as that of the entire spray. This is expressed mathematically as;

$$D_{32} = \frac{\sum_i n_i d_i^3}{\sum_i d_i^2} \quad (3.6)$$

Where  $n_i$  equals to a number of drops in range size  $i$  and  $d_i$  equal to the mean diameter range size  $i$ .

The  $D_{32}$  was developed by a German scientist Josef Sauter in the late 1920s. This is also known as Surface Area Moment Mean. It estimates the mean size of a given particle distribution [49]. SMD is widely used in industries as a standard for fire and explosion suppression and Mitigation. SMD is highly significant in calculations where the active surface area is important. Such areas include catalysis and applications in fuel combustion [49].

The locations of various representative diameters on a drop size frequency curve are shown in Figure 3.6.

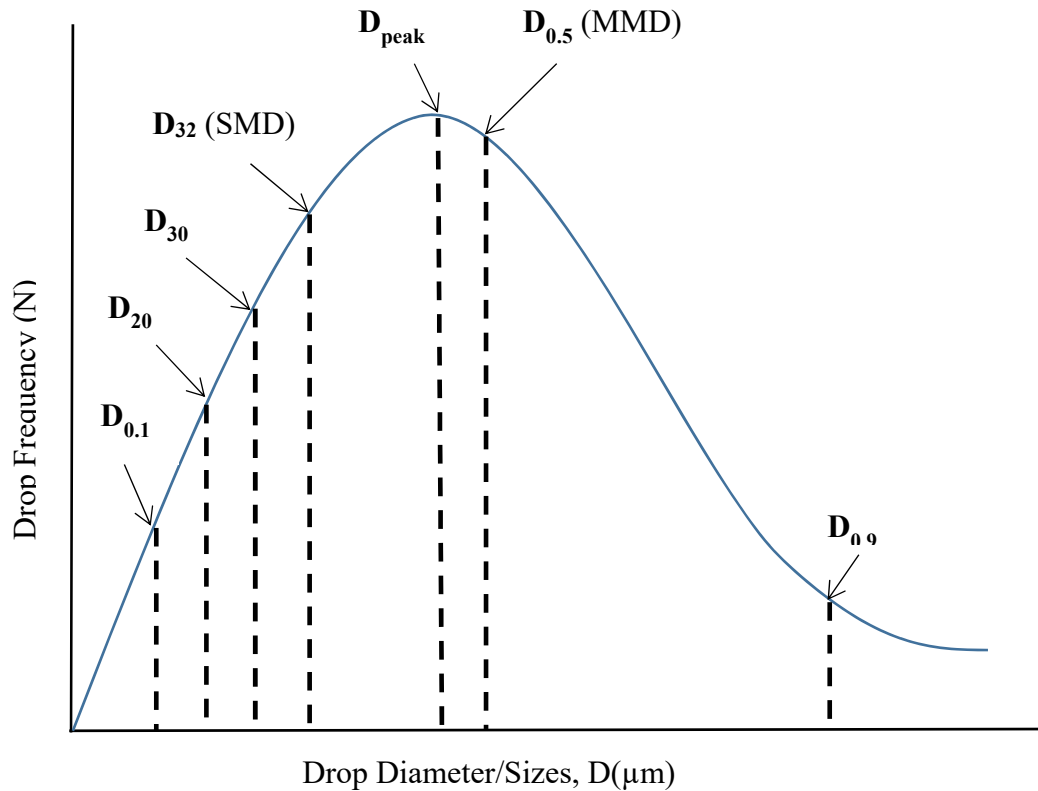


**Figure 3.6:** Locations of Various Representative Diameters [50]

### 3.3.5 Factors Affecting Droplet Size

Fine spray creation is an important parameter for combustion because it penetrates into the flame layer more quickly than larger drops. The following parameters may affect Drop sizes:

- **Flow rate:** An increase in flow rate will reduce droplet size.
- **Pressure:** High pressure reduces droplet size.
- **Velocity:** Liquid velocity depends on energy input to the atomiser. The high-velocity liquid will increase turbulence flows within the atomiser insert and be conducive to small droplet size.
- **Spray Angle:** Spray angle depends on atomiser insert parameter such as input pressure, internal geometry, orifice length/orifice diameter and mechanisms of flow within the atomiser insert.
- **Liquid Properties:** An increase in liquid viscosity or surface tension will require higher aerodynamic forces to produce a liquid break up and so result in larger droplets.



**Figure 3.7:** Classification of atomizers [47]

## 3.5 Fine spray atomizers

### 3.5.1 Pressure jet Atomizers

The pressure jet atomizers utilise a very simple orifice and commonly use in fuel injection applications, mainly for diesel engines. It has very small orifice (usually less than equal to 0.3mm) and operates at a high pressure of about 100MPa that is required to produce fine spray usually for Sauter mean diameter,  $D_{32}$  less than 20-micron meter.

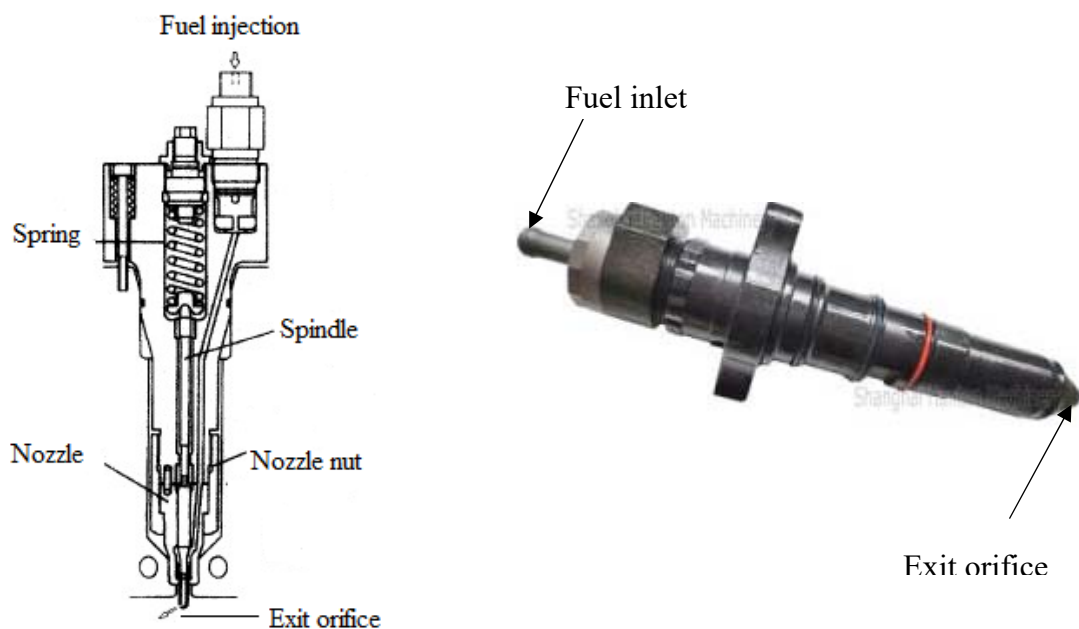


**Figure 3.8:** Fuel injection system for diesel engine [52]

It is proven that the cavitation inside these simple orifices is very significant because it increases the turbulence thereby improving atomization. However, it is very dangerous when there is excess cavitation because it creates a hydraulic flip when the liquid jet separates inside the orifice resulting in poor atomization [53]. This type of atomizers has a poor turndown ratio though very simple to design with good penetration. It has an increasing solid cone angle and very poor vaporization. It is applicable in industrial shower and cleaning, diesel injection and firefighting.

### **3.5.2 Pressure swirl atomizers**

Pressure swirl atomizers sometimes referred to as simplex atomizers by Gas Turbine Company. This type of atomizer is widely used in domestic, water cooling system, combustion systems and many other industrial applications. The liquid is caused to emerge from an orifice with a swirl velocity component resulting from its through tangential passages upstream of the off flee. A thinning conical sheet is produced which interacts with the surrounding atmosphere and subsequently disintegrates into a cloud of drops. It can produce a very fine atomized spray less than equal 20 $\mu$ m.

Pressure swirl atomizer comprises mainly three parts namely; swirl chamber, inlet tangential ports and an exit orifice. The liquid is injected through the tangential ports into the swirl chamber and gain swirl motion and then leaves the exit orifice and spread as conical liquid film outside the atomizer.

### **3.5.3 Flat fan atomizer**

There is a similarity between the flat fan and pressure swirl atomizer; the difference is the flat fan does not use a swirl chamber and makes a flat sheet. The liquid emerges from a wide, thin orifice as a flat liquid sheet which then breaks into droplets. That is the flat fan sprays is the form of a triangular liquid sheet with angles approximately 0° – 120° degrees depending on the orifice shape. Flat fan atomizers are readily applicable in Spray cooling, mineral washing, general product washing, air cleaning and cooling, gas cleaning and cooling, dust control, and rinsing, fire protection.

### **3.5.4 Rotary Atomizers**

This utilises centrifugal force applied to the liquid in order to fling a thin film from a rotating cup, disk or bell. These type of atomizer are often used in spray drying applications because they are able to atomize complex, highly viscous and multicomponent liquids. The basic spray pattern is thus that of a 360° disk, and this geometry generally causes difficulty. The fundamentals of the technique are well known, and the technique has two potential advantages: (1) the possibility of producing very narrow droplet size distributions, and (2) the additional flexibility of the use of mechanical forces to prefilm the liquid rather than relying on small orifices [53].

### 3.5.5 Two fluid Atomizers

Two-fluid atomisation” is a two-phase atomising atomiser insert which feeds gas and liquid from separate sources. “Two-fluid atomisation” could be a combination of **twin-fluid, air-assist, air-blast**, effervescent or flashing atomiser insert. There are huge varieties of design which differ in the shapes, positions and number of internal and external orifices. However, the most common internal and external mixing designs apart from those for some specialised uses such as gas turbine fuel injection use relatively simple concentric liquid and gas jet. Generally, most airblast atomisers’ inserts use external mixing devices; air-assist types can be either internal or external mixing.

### 3.5.6 Spill Return Atomizers

Spill Return Atomiser (SRA) is a type of the pressure swirl atomiser, which holds several advantages. It is a simplex nozzle with a return flow line (often refers as spill line) at the rear wall of the swirl chamber. The high-pressure liquid is injected into the swirl chamber via the tangential ports comprising two streams; one stream discharged outside at high speed and atomised and the other one is spilled back at low pressure to the water storage tank or liquid reservoir through the spill return orifice [54] as illustrated in Figure 4.10.

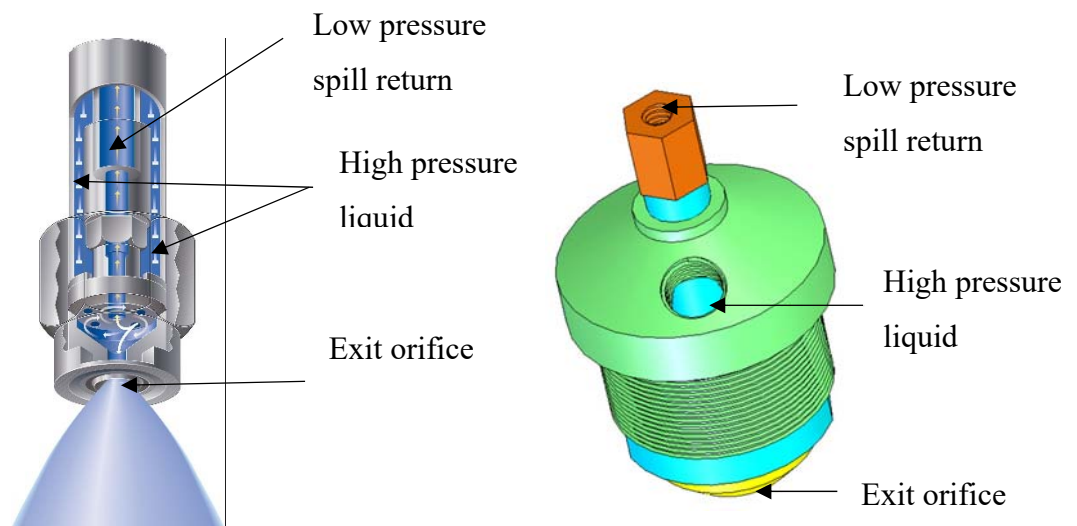


**Figure 3.9:** Spill return atomizer and angular inlet [55] and [54]

Its function allows the SRA to operate under high liquid pressure between 10 – 15MPa (100 – 150bar) at relatively low exit flow rate conditions. Tests have shown that spill return facilities

can return as much as 85% of the total flow rate [56]. This type of atomizer is applicable for spray combustion that utilised finely atomised spray as a cooling agent because it can easily be modified depending on the required flow rate, the cone angle of the spray and volume flux by reconfiguring some of its components. However, the required drop size  $D_{32} \leq 30\mu\text{m}$  can then be achieved. These interchangeability components of the spill return atomizer can result from;

- The diameter of the spill orifice: when the spill orifice is increased, the flow decreases at the orifice exit and equally decreasing the spill orifice increases the flow at the orifice exit.
- The orifice exit: when the exit orifice diameter is increased, the flow rate increases at the exit which could cause a reduction in flow at the spill orifice.
- The two opposing tangential inlet orifices to the swirl chamber: when the tangential diameter of the inlet orifices to the swirl chamber is reduced, the flow velocity increases at a given pressure, thus increasing the turbulence at the exit orifice, resulting in smaller mean droplet size.
- The swirl chamber: as design previously by Nasr, Yule and Lloyd [54] the integral machined component supplied by two 0.6mm tangentially opposed inlet orifices. The length and diameter of the swirl chamber were optimised to ensure maximum turbulence within the swirl chamber and at the exit orifice.

### **3.6 Explosion Mitigation by Water Spray**

Water is given much consideration today in a fighting explosion due to its favourable physical properties of fire mitigation. It has high heat capacity and high latent heat of evaporation that can absorb a significant quantity of heat from flames. However, water can expand up to 1700 times when it evaporates to vapour that result in the dilution of the surrounding oxygen concentration. The formation of fine water droplets has increased the effectiveness of water droplets in fire mitigation, which is a result of its availability for heat absorption and evaporation. Thus, the primary mechanism of extinguishment should be due to heat extraction and oxygen displacement, which leads to the theoretical consideration of water vapour/air dilution and kinetic effects at the molecular level [57]. Moreover, water is used in fire mitigation nowadays compared to other mitigating agents because it has the following advantages such as; No toxic and suffocation problems, Environmental friendly,

Low cost and highly available, Limited and no damage and High efficiency in mitigating certain fires [58].

In the effort to solutions and proffer explosion mitigation strategies, researchers, academia, and institutes are still carrying out numerous investigations on minimizing the level at which explosion occurs. Such investigations are carried out in laboratories in various countries such as United Kingdom, United States and Norway with the objective of developing methodological frameworks that would be more effective in using fine water spray to mitigate gas and vapour cloud explosion.

Several researchers have conducted investigations on explosion suppression, prevention, and mitigation utilizing water sprays in arrays of drop sizes. This is due to a tragic incident that occurred on the Piper Alpha oil platform which claimed lost lives, damage to facilities and environmental pollution as briefly in chapter subsection 1.2.5. Since then, a rapid interest in the use of water spray to produce further explosion protection to save lives, damage to industrial facilities and the environment at large [59]. Although there are various means of controlling explosion, this includes; CO<sub>2</sub>, Foam, and water which have significantly shown promising results over the years. However, water sprays seem to be an obvious choice of mitigating explosion because water is not harmful to the environment, no toxic, cost-effective and readily available [58]. However, there have been different means in which the effectiveness of water has been studied; these techniques include small-scale laboratory studies, shock-tube studies, full-scale offshore studies and lastly computer simulations.

British Gas Research and Technology conducted a series of experiments in the 1980's at Spadeadam site in the United Kingdom in a large/full and small scale to investigate the causes and consequences of gas and vapour cloud explosion. Quite a bit of their research work was centred on circumstances where gas and vapour leakage had happened in an outside climate and ignition had been delayed for a limited period. However, the delay in ignition gives room for gas and vapour to travel and spread within site, which engulfs the areas that are closely packed, with repeated obstacles as in arrays of pipes.

Confined region &  
Ignition point

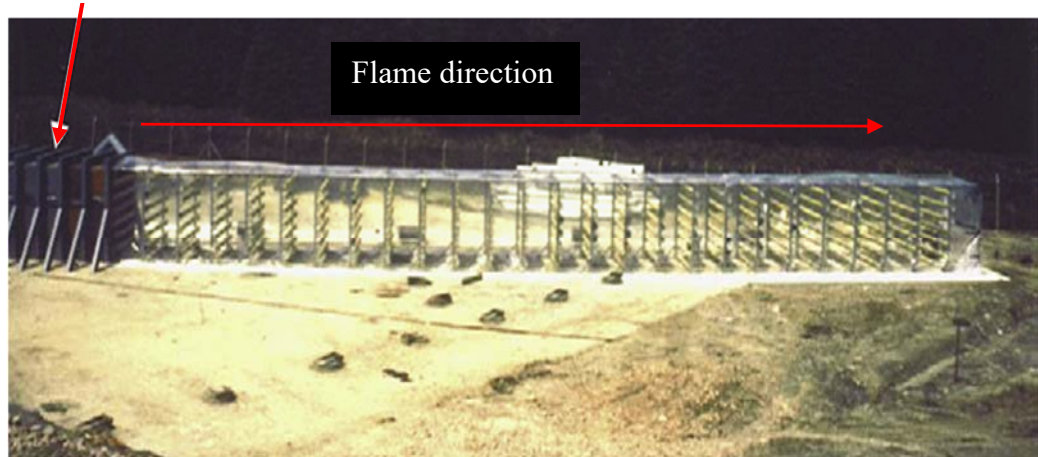


**Figure 3.10:** Experimental rig used at Spadeadam [60]

The large-scale experimental equipment used as shown in figure 2.5 comprised of a 9000mm long, 3000mm square, cross-sectional area confined region and 36000mm long polythene was used to secure the external congestion. 180 mm diameter pipe was used as varieties of obstacles situated at intervals 1500mm all through the length of the enclosure section. Inside and simply outside the confined region, these arrays had an area blockage of 42%. The ignition point is located at the one end of the experimental rig that is within the confined section of the rig.

Wang, Yu, Wen, Deng and Pei [61] investigated the effect of droplet size of water mist and pipe sizes on methane/air suppression explosion in pipe via water mist; the result shows that for droplet diameter 45 mm and 100 mm it was impossible to suppress the explosion. Instead, it promoted the explosion and the larger the diameter, the more easily the gas exploded. The work demonstrated a theoretical background in order to design a water mist explosion suppression system in many industry occasions.

An investigation carried out by Thomas and Breton shows that high-speed flame was mitigated in a horizontal 5000 mm long pipe and 76 mm internal diameter tube with a total internal volume of 0.023 m<sup>3</sup> as shown in Figure 3.13. Flame speed was accelerated using duralumin liners (68 mm inner diameter) with the corrugated internal surface was inserted at 200 mm distance. Three different atomizers were used namely; Delevan BIM8's, Lurmark 0.8fn's and Woolworth garden nozzles. The nozzles mean droplet sizes (142.7 μm, 87.6 μm, and 52.0 μm). Water was introduced into the tube via the nozzles installed in three pairs of diametrically opposed ports of a distance of 2.11, 2.21, and 2.31 m from a pump at the

pressure 100 psi. The results revealed that mitigation of propagated flame could be achieved using water sprays and droplets with a Weber number greater than 12 gave a higher mitigation success rate [62].

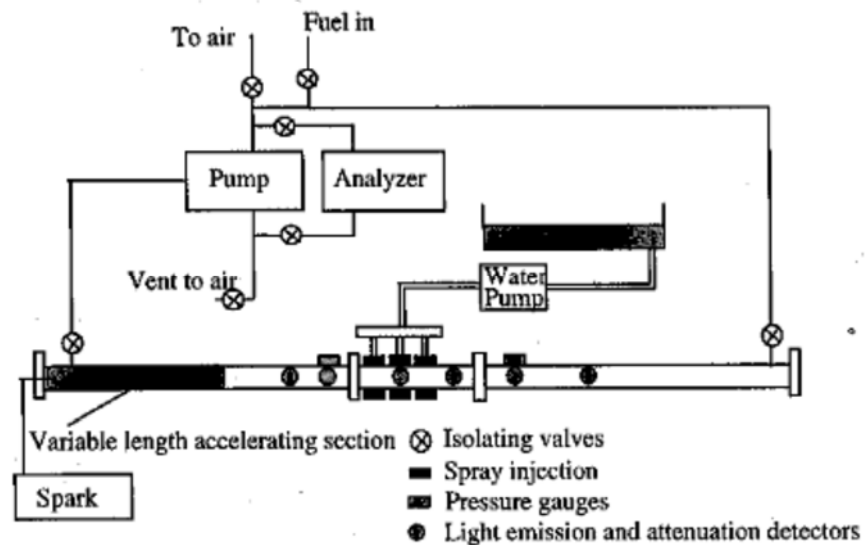


**Figure 3.11:** Experimental rig 76 mm diameter 5000 mm long pipe [62].

Tang, Zhang, Si, Huang, Zhang and Jin [11] experimentally studied the influence of using ultrafine water sprays in methane/air explosion in a fully sealed visual vessel with the following methane concentrations 8%, 9.5%, 11% and 12.5%. The mist was generated with the aid of two nozzles, and Sauter mean diameter droplets of 28.2  $\mu\text{m}$  and 43.3  $\mu\text{m}$  respectively. Phase Doppler Particle Anemometer (PDPA) was used to measure the droplets sizes. The results revealed that the maximum explosion overpressure, pressure rising rate and flame propagation velocity of methane explosions in various concentrations increased significantly after spraying. Furthermore, their result also revealed that the brightness of explosion flame got much higher after spraying.

Tang, Zhang, Si, Huang, Zhang and Jin [11], investigated the characteristics of a high fraction of methane gas in a constant volume combustion vessel at different initial conditions. They found that increasing initial pressure causes an increase in peak explosion pressure due to a higher amount of flammable mixture, which generates also a high amount of heat. An increase in initial temperature decreased the peak explosion pressure but accelerated the pressure rise during combustion, which indicates an increase in flame speed and heat release rate.

Thomas [63], and Wingerden and Wilkins [64] described experimentally the influence of turbulence generated on the gas explosion and the effect of water sprays on gas explosion

under certain circumstances. They suggested that the increase in flame speed does not depend on the size of the droplets generated by the various nozzle types.

Sapko., Furno and Kuchta [65] and later Zalosh and Bajpai [66] the results show that the water volume required to inert an environment is much less than those required in quenching propagating flame. They suggested that droplets of  $<10\mu\text{m}$  are as effective as vapour when being used as an inerting agent. They suggested that fine water spray could mitigate combustion in two ways;

- Fine sprays can inert a gaseous mixture preventing flame propagation away from an ignition source.
- Secondly, with sufficiently dense sprays, it is possible to quench an already well-established propagating flame.

Qin and Chow study the effect of water mist set up on a bench-scale solid fuel PMMA fires in a confined area under different external radiant heat fluxes. Water mist was generated by a single nozzle pressure in a calorimeter. The result shows that water mist would suppress the diffusion flames induced by burning PMMA in a confined space by oxygen displacement, evaporation cooling and radiant heat attenuation. Combustion might be enhanced through expansion of the mixture and chain reaction. Suppression plays a dominating role when water mist of sufficient volumetric flow rate is applied. The flame can be suppressed more easily under poorer ventilation [67].

However, the mechanism of these processes is still yet, poorly understood, and further research needs to be conducted in order to ensure that a certain level of safe approaches is implemented. Moreover, this research study tends to mitigate methane/air explosion with ultra-fine water sprays with the droplet size less than equal to  $30\mu\text{m}$  and the installation of the different sizes of steel meshes (0.94mm, 1.31mm and 6mm diameter) in between the flanges to evaluate the effects and performance of the steel meshes alone and when combined with water sprays; flame temperature and average flame speed when passing through the mesh aperture.

# Chapter 4: Materials, Experimental Apparatus and Procedure

## 4.1 Introduction

This chapter discusses the materials, procedure, experimental setup, and methods of data processing utilised during these trials. The experimental equipment is located at the petroleum laboratory (G90) in Newton Building where all the experiments were runs.

The experiment was carried out in three different stages, comprising of dry (no mesh and no spray), dry plus mesh material and wet (water spray) plus mesh material combined together. Three different methane/air mixtures of 6, 7, and 9 % concentration are used in the experimental trial. The entire experiment was carried out in 190 mm internal diameter and 6300 mm long tube. The temperature of the flame was monitored using a thermocouple K mounted at five different locations as shown in Figure 4.1. The thermocouples were coded as TC-1, TC-2, TC-3, TC-4 and TC-5 respectively. Gas-co-seeker was used to measure the concentration of methane in the mixture. However, further to the filling process, the methane/air mixture was circulated using a booster pump to have an equal distribution of the mixture in the tube. During these runs, the percentage concentration of the methane-air and the filling time used shown in Table 4.1, and the table also presents the equivalence ratio calculated for each methane/air concentration.

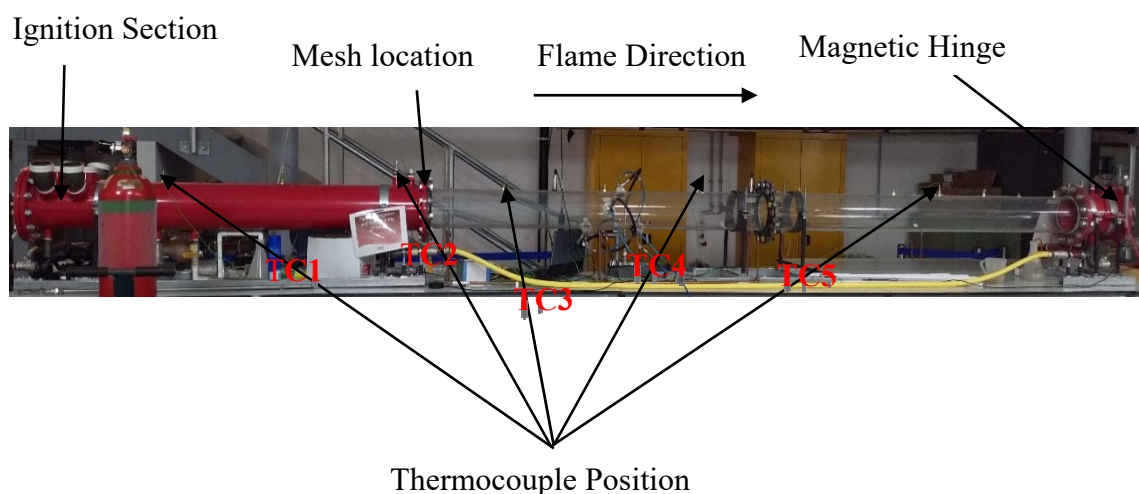


**Figure 4.1:** Thermocouple position and flame direction

**Table 4.1:** Methane/Air ratio and filling time

<b>Percentage Concentrations</b>	<b>Equivalence Ratio, <math>\phi</math></b>	<b>Filling Time (Minute)</b>
<b>6%</b>	0.61	2:25
<b>7%</b>	0.72	3.45
<b>9%</b>	0.95	4:25

The experimental stages for this research were depicted schematically in Figure 4.2.

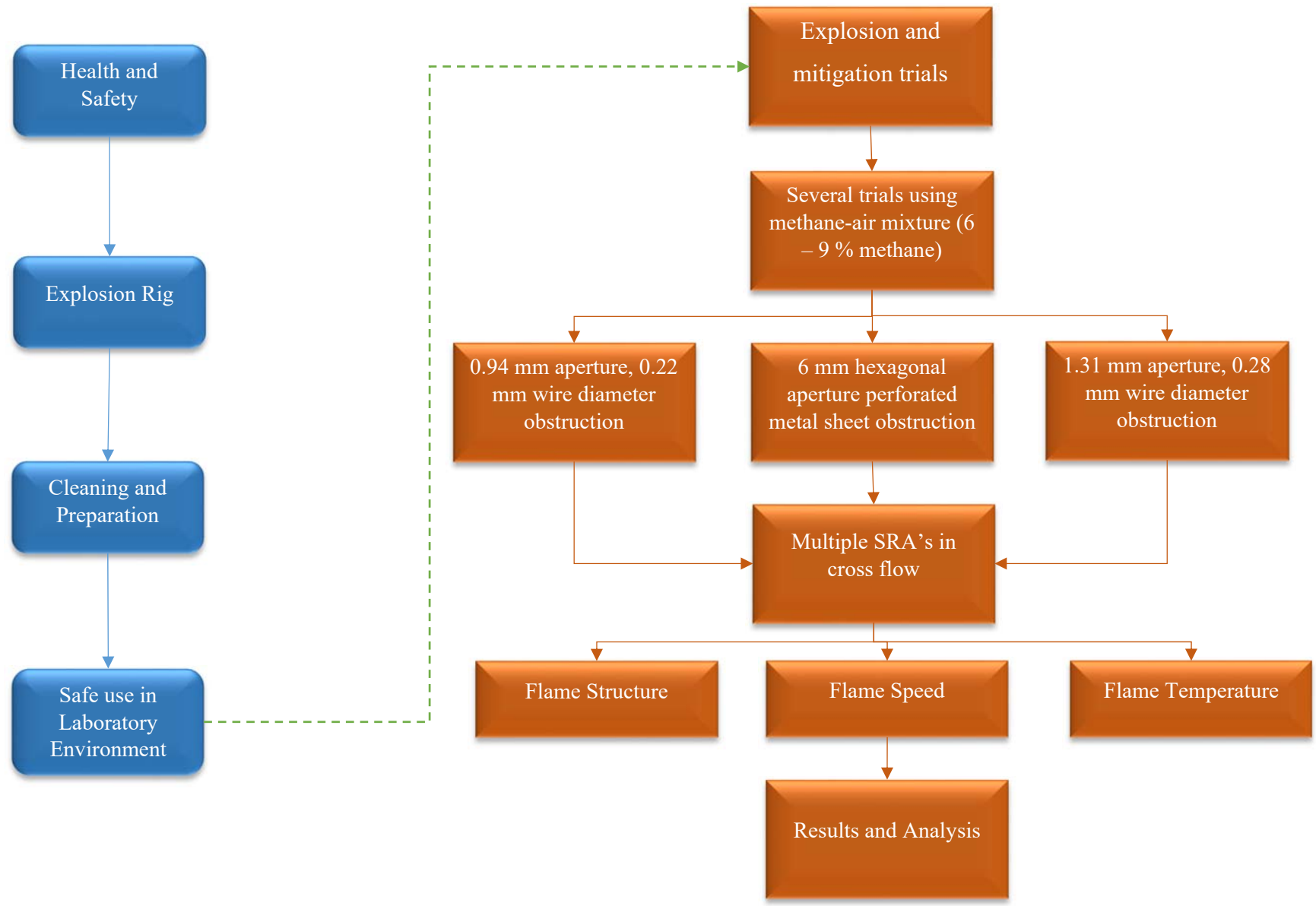


**Figure 4.2:** Schematic representation of the research flow diagram

## 4.2 Materials

### 4.2.1 Methane

Methane is the main constituent found in natural gas pipelines and coal mining industry and is highly flammable. Hence it is used for conducting the present research. Methane is a chemical compound comprising one atom of carbon and four atoms of hydrogen and represented by a chemical formula as CH<sub>4</sub>. Its relative abundance and environmentally friendlier makes it an attractive fuel source, but its higher flammability poses challenges during its transportation, storage and utilization. It is known to ignite within the range of 5vol% – 15vol% CH<sub>4</sub> in air, usually regarded as their Lower Flammability Limits (LFL) and Upper Flammability Limits (UPL) respectively. In conducting this experimental research, high laboratory grade methane with 99% purity supplied by BOC is used throughout. Some of the properties of the laboratory grade methane are shown in Table 4.2.

**Table 4.2:** Physical properties of methane

Fluid Properties	Values	Units
Thermal conductivity, $\sigma$	0.0338	W/m/K
Heat capacity, $C_p$	36.090	J/mol/K
Dynamic viscosity	0.109	mPa.s
Temperature, T	15	°C
Pressure, P	1	atm
Density, $\rho$	0.656	Kg/m <sup>3</sup>

### 4.2.2 Air

Air is a mixture of gases, comprising mainly nitrogen and oxygen, but containing much smaller amounts of water vapour, argon, and carbon dioxide, and very small amounts of other gases. In this study, compressed air is used, and the compositions consist of 79% of nitrogen by volume and 21% of oxygen by volume. Standard industrial grade compressed air was used as the oxidant. An oxidising agent (oxidant, oxidiser) is a substance that can oxidise other

substances—in other words, to cause them to lose electrons. Common oxidising agents are oxygen, hydrogen peroxide and the halogens.

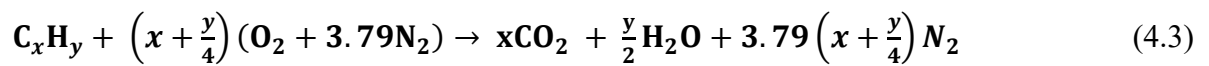
### 4.2.3 Determination of Equivalence Ratio

Equivalence ratio is defined as the ratio of the actual fuel/oxidant ratio normalised by the stoichiometric fuel/oxidant ratio. The following mathematical expression is used to determine the equivalence ratio in this research, given as:

$$\Phi = \frac{(fuel/oxidant)_{actual}}{(fuel/oxidant)_{stoic}} \quad (4.1)$$

$$\Phi = \frac{(oxidant/fuel)_{actual}}{(oxidant/fuel)_{stoic}} \quad (4.2)$$

Also, the reaction equation for the combustion is represented as follow:



Equation (4.3) shows that for every 1 mole of fuel burned, requires 4.79 (x+y/4) mole of air and 4.79(n+y/4) + y/4 mole of combustion products are generated.

### 4.2.4 Mesh Materials Characterization

A mesh is an obstacle made of connected elements of metal, fibre, or other flexible or ductile materials. A mesh has similar features to a web or a net in that it has many attached or woven elements. Three different sizes of meshes were selected from the ranges of the mesh sizes that were suitable in this research study; steel metal sheet mesh was chosen due to its thermal conductivity and its resistance to heat.

In this present experimental research study, different sets of stainless burning plates were analysed and their stability were examined according to three geometric parameters of the burner plate for methane fuel. These parameters are; hole diameter, number of holes and distance between the holes. The different sizes and types of the stainless steel used in the experiment are as follows:

- ✓ 304 Woven wire stainless steel meshes (0.94mm aperture with 0.22mm wire diameter).
- ✓ 304 Woven wire stainless steel meshes (1.31mm aperture with 0.28mm wire diameter).
- ✓ Perforated steel sheet (6 mm Hex, 6 mm Hole, 500mm x 500mm x 0.55mm).

**Table 4.3:** Characteristics of the woven wire meshes and perforated plate

Materials	Hole diameter	Weight	Grade
Woven wire mesh 1	0.94mm	0.5324 kg/m <sup>2</sup>	304
Woven wire mesh 2	1.31mm	0.63 kg/m <sup>2</sup>	304
Perforated sheet	6mm		304

The woven wire meshes were commercial products consisting of stainless steel grade perforated with regularly spaced square holes. The holes had square edges which were perpendicular to the surface of the sheet. While the perforated metal sheet/plate is made up of stainless steel as well with circular holes spaced in a hexagonal pattern with square edges. The details of the dimension and holes spacing are shown in Table 4.3.

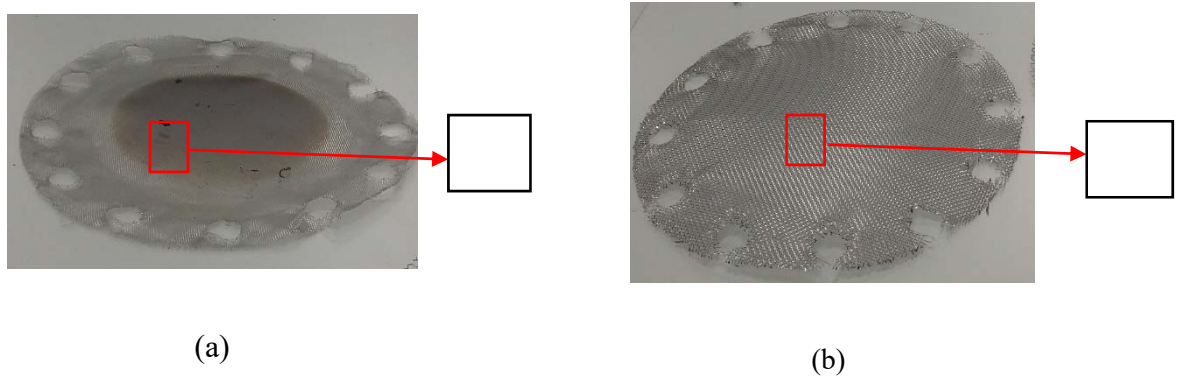


**Figure 4.3:** Woven wire mesh: a) 0.94mm aperture and 0.22mm diameter, and b) 1.31 mm aperture and 0.28mm diameter

These elements as shown in Figure 4.3 (a) and (b) consists of a single woven wire sheet as several metallic wires in a pack form. The manufacture of the wire mesh is firmly controlled to ensure the repeatable accuracy of the aperture size. The woven wire mesh was supplied by the Mesh Company and is commercially available and comparatively very cheap.

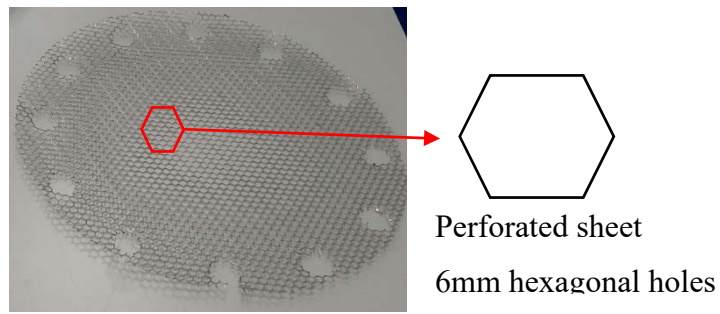


**Figure 4.4:** Perforated metal sheet 6mm aperture

The perforated metal sheet as shown in Figure 4.4 comes in a large variety of forms (hole size, shape and density) as well as material types. It is also readily available and relatively inexpensive. The minimum size of hole though makes this material form on its own impractical for use as a flame arrester element, but it has been used in multiple sheet form. It also has a very low percentage of free area.

Figure 4.5 shows the position of the mesh within the tube from the ignition section of the tube to the transparent section of the tube (i.e. Polymethyl-Methacrylate 'PMMA' section).

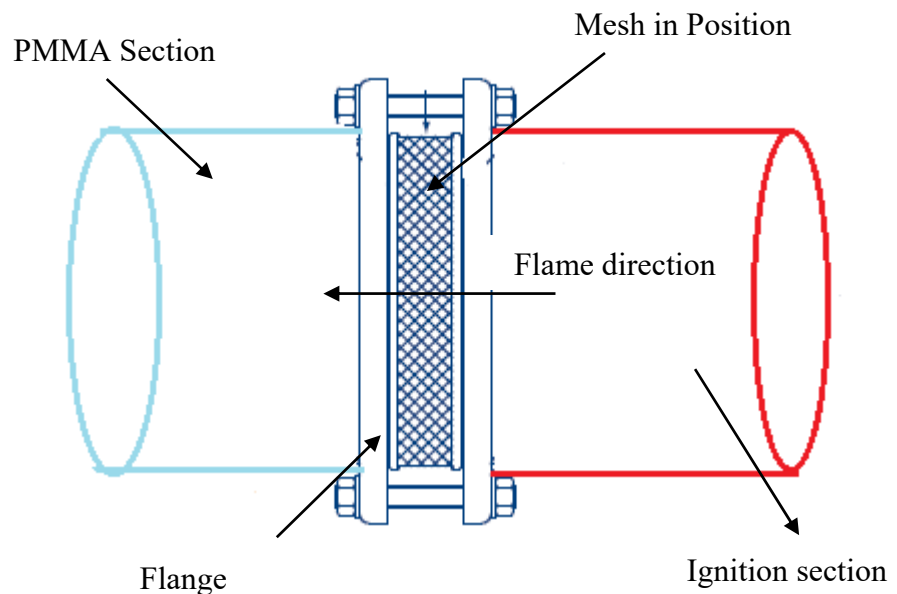


**Figure 4.5:** The position of the mesh within the explosion tube.

## **4.3 Experimental Procedure**

The hot trials are a series of experiments conducted in a petroleum laboratory using Flame Propagation and Mitigation Rig (FPMR). To ensure the experiments are run successfully, the following procedure is deduced and summarized as:

### **4.3.1 Equipment cleaning**

The experimental equipment was cleaned thoroughly before any activity or trials are initiated. These include; the combustion chamber, booster pump, electrical system, water storage system and data acquisition system. The combustion chamber (PMMA tube) was removed and cleaned thoroughly with water and was allowed to dry off. The chamber was then coated with water repellent in order to improve the visibility and water from sticking to the tube. The water storage tank was also checked for any leakage and cleaned weakly and fresh water introduced throughout the duration of the experimental trials. The electrical system was checked to make sure it is safer to use.

### **4.3.2 Preparation and set-up**

After cleaning the experimental rig, the rig was set-up as depicted in Figure 4.6. Further, to ensure adequate safety in the laboratory, only the technician and the researcher were allowed in the laboratory during the experimental trials. Therefore, an appropriate sign and warning were placed at the laboratory entrance to keep other students and staffs away for safety reasons during the explosion experiments.

After which, all the valves and fittings at the fuel source were checked to make sure they are in a safe position, and then air was injected into the combustion tube to check the air tightness of the experimental system.

Also for the purpose of quality video recording during the experiment, all light sources directly above the explosion rig and rear-adjacent were switch-off, and the camera was placed appropriately at the opposite side of the rig at 1.6 m. These settings allowed clear visualisation, observation and recording of the explosion path and behaviour in the transparent section (4 m PMMA) of the explosion tube.

### 4.3.3 Experimental runs

After experimental preparation and set-up, the Flame Propagation Mitigation Rig was prepared for the experimental trials using the following steps:

- i. The flange at the end of the explosion tube was opened, and the 'primary key' was turned on to power and energise the magnetic hinge panel section and manually closed and held in place by the electromagnet.
- ii. The six exhaust outlet at the top side of the tube towards the opposite end of the rig were sealed using 'cling film' and Velcro straps.
- iii. After steps i and ii above, the water drainage valves (i.e. valve 1, 2, and 6) were closed, the gas booster key and circulation pump were turn ON. The gas circulations valves (i.e. valve D, E, F and G) were then open.
- iv. After step iii, the methane supply valve was opened, and then the methane was injected via a calibrated solenoid rotameter at 200 L/min into the combustion chamber.
- v. Portable alarm gas detector was used for leakage detection.
- vi. Time was then set and recorded corresponding to each 6, 7 and 9% methane concentration in the chamber using gas-co-seeker.
- vii. After steps iv, v and vi, the data acquisition system and a video camera were switched-on and activated. The mixture was allowed to stabilise for one minute to ensure it became quiescent.
- viii. Before turning on the 'ignition' key and subsequent pushing of the ignition button, a verbal description of the configuration was relayed to the video camera, this includes:
  - a. The concentration of Methane-air mixture
  - b. Mesh size inserted
  - c. Water pump operating pressure and
  - d. The temperature of the WaterThe audible description was used to catalogue video imagery, whereby each file could then be renamed with confidence.
- ix. The ignition key was turn-on, and ignition button was pushed to start the water pump and generate a spark in the following sequence:
  - a. The water pump was activated immediately after the ignition button was pushed,
  - b. After 7 seconds, the mixture was ignited and explosion developed along the tube length.



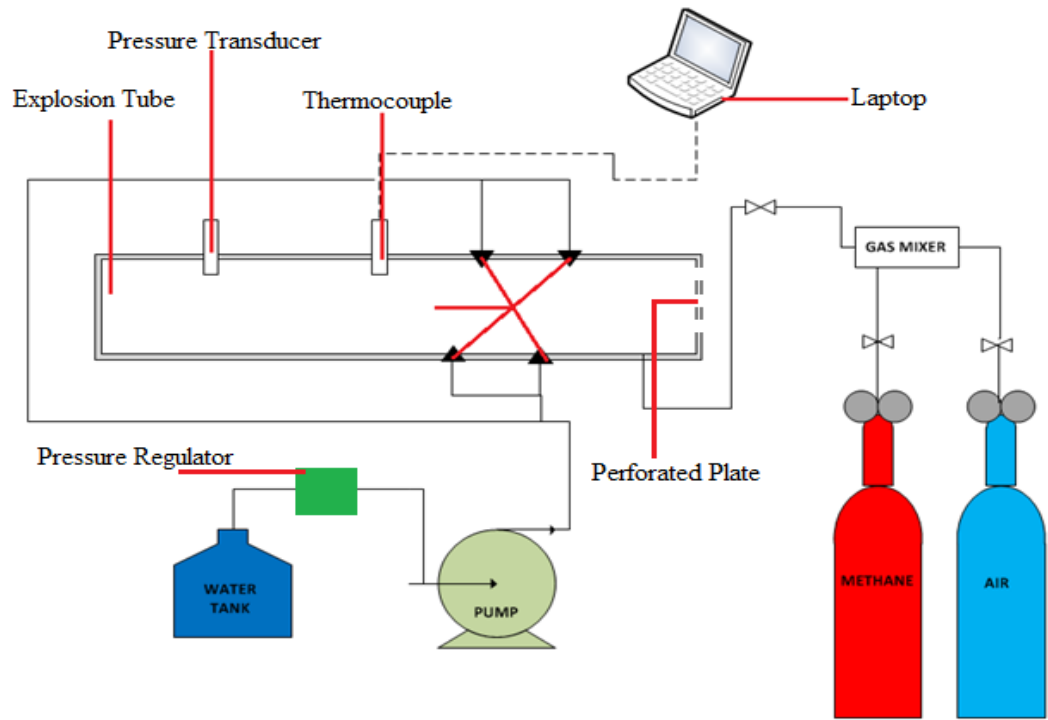


**Figure 4.6:** Schematic diagram of the Experimental Setup system

#### 4.4.1 Explosion Chamber

The tube/pipe used is divided into two sections: 2-meter long with 8-inch diameter mild steel constructed and fabricated according to ANSI-80 design criteria as shown in Table 4.4, 4-meter long polymethyl-methacrylate (PMMA) situated in the middle of the experimental rig connected to the mild steel and 0.3 m length of the same mild steel with a flange.

**Table 4.4:** American National Standard Institute (ANSI) 80 pipe table of schedule

Pipe Size (in)	Diameter (in)		Nominal Thickness (in)	Transverse Areas (in <sup>2</sup> )			Length of Pipe (per sq. foot of)		Volume (ft <sup>3</sup> /ft)	Weight		Number of Threads per inch of Screw
	External	Internal		External	Internal	Steel	External Surface (ft)	Internal Surface (ft)		lb/ft	kg/m	
1/8	0.41	0.22	0.10	0.13	0.04	0.09	9.43	17.75	0.0003	0.31	0.47	27
1/4	0.54	0.30	0.12	0.23	0.07	0.16	7.07	12.65	0.0005	0.54	0.80	18
3/8	0.68	0.42	0.13	0.36	0.14	0.22	5.66	9.03	0.0010	0.74	1.10	18
1/2	0.84	0.55	0.15	0.55	0.23	0.32	4.55	7.00	0.0016	1.00	1.49	14
3/4	1.05	0.74	0.15	0.87	0.43	0.43	3.64	5.15	0.0030	1.47	2.19	14
1	1.32	0.96	0.18	1.36	0.72	0.64	2.90	4.00	0.0050	2.17	3.23	11 1/2
1 1/4	1.66	1.28	0.19	2.16	1.28	0.88	2.30	2.99	0.0089	3.00	4.46	11 1/2
1 1/2	1.90	1.50	0.20	2.84	1.77	1.07	2.01	2.54	0.0123	3.65	5.43	11 1/2

½												
2	2.38	1.94	0.22	4.43	2.95	1.48	1.61	1.97	0.0205	5.02	7.47	11 ½
2	2.88	2.32	0.28	6.49	4.24	2.25	1.33	1.65	0.0294	7.66	11.40	8
½												
3	3.50	2.90	0.30	9.62	6.61	3.02	1.09	1.32	0.0459	10.30	15.33	8
3	4.00	3.36	0.32	12.56	8.89	3.68	0.95	1.14	0.0617	12.50	18.60	8
½												
4	4.50	3.83	0.34	15.90	11.50	4.41	0.85	1.00	0.08	14.90	22.17	8
5	5.56	4.81	0.38	24.30	18.19	6.11	0.69	0.79	0.1263	20.80	30.95	8
6	6.63	5.76	0.43	34.47	26.07	8.30	0.58	0.67	0.1810	28.60	42.56	8
<b>8</b>	<b>8.63</b>	<b>7.63</b>	<b>0.50</b>	<b>58.42</b>	<b>45.66</b>	<b>12.76</b>	<b>0.44</b>	<b>0.50</b>	<b>0.3171</b>	<b>43.40</b>	<b>64.59</b>	<b>8</b>
10	10.75	9.56	0.59	90.76	71.84	18.92	0.36	0.40	0.4989	64.40	95.84	8

The two sections of the tube were connected via flanges and appropriate gaskets. However, all other joints were coupled with threaded joints using jointing compounds such as recirculation system as shown in Figure 4.7. This table was shown because both of the ends of the rig were constructed using 8 inches (200 mm) diameter mild steel to ANSI schedule 80 with fully welded connections and flanges [68]. The 8'' (200 mm) pipe had an internal diameter of 7.981'' (202.7 mm) and a wall thickness of 0.322'' (8.4 mm) as indicated in Table 4.4.

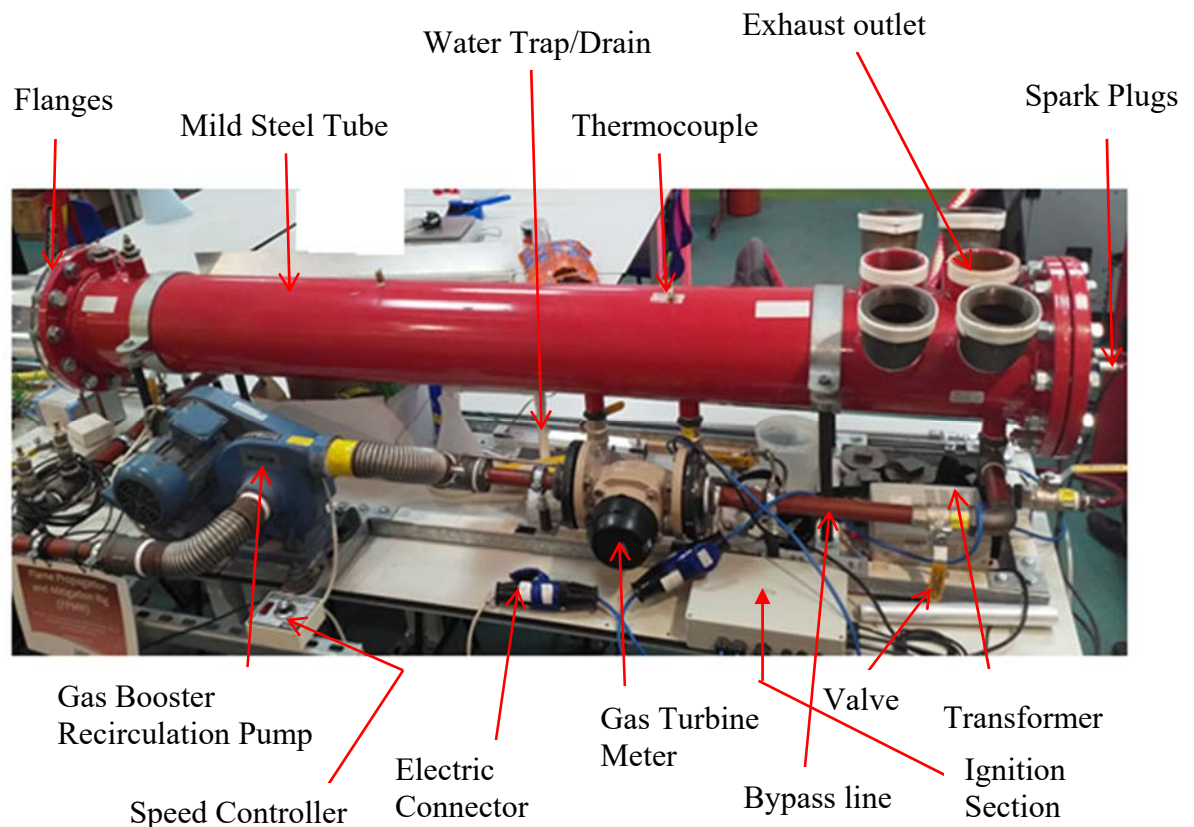


**Figure 4.7:** Mild Steel section of the Experimental Rig

The Polymethyl-Methacrylate, (PMMA) tube is a transparent thermoplastic frequently utilised in sheet form/frame as a lightweight alternative option to the glass. PMMA is used herein other to visualise the propagation of the flame and more importantly, is economically viable when compared to the mild steel tube. It can easily be clean and transported from one point to another. PMMA is regularly alluded to as Acrylic and is sold by numerous exchange names including Acrylic, Acrylic Glass, Acrylite, Acryplast, Altuglas, Limacryl, Lucite, Oroglass, Per-Clax, Perspex, Plazcryl, Plexiglass, Polycast, and R-Cast. The acrylic tube was beforehand utilized effectively and turned out to be a reasonable material for explosion mitigation study and was effectively utilized by researchers as a part of numerous investigations such as [65, 69-71]. Some properties of PMMA are tabulated in Table 4.5 and pictorially shown in Figure 4.8.

**Table 4.5:** Properties of Polymethyl-Methacrylate, (PMMA)

PMMA Property	Formula / Value
Chemical formula	(C <sub>5</sub> O <sub>2</sub> H <sub>8</sub> ) <sub>n</sub>
Density	1.18 g/cm <sup>3</sup>
Melting point	160°C (320°F)
Boiling point	200°C(392 °F)

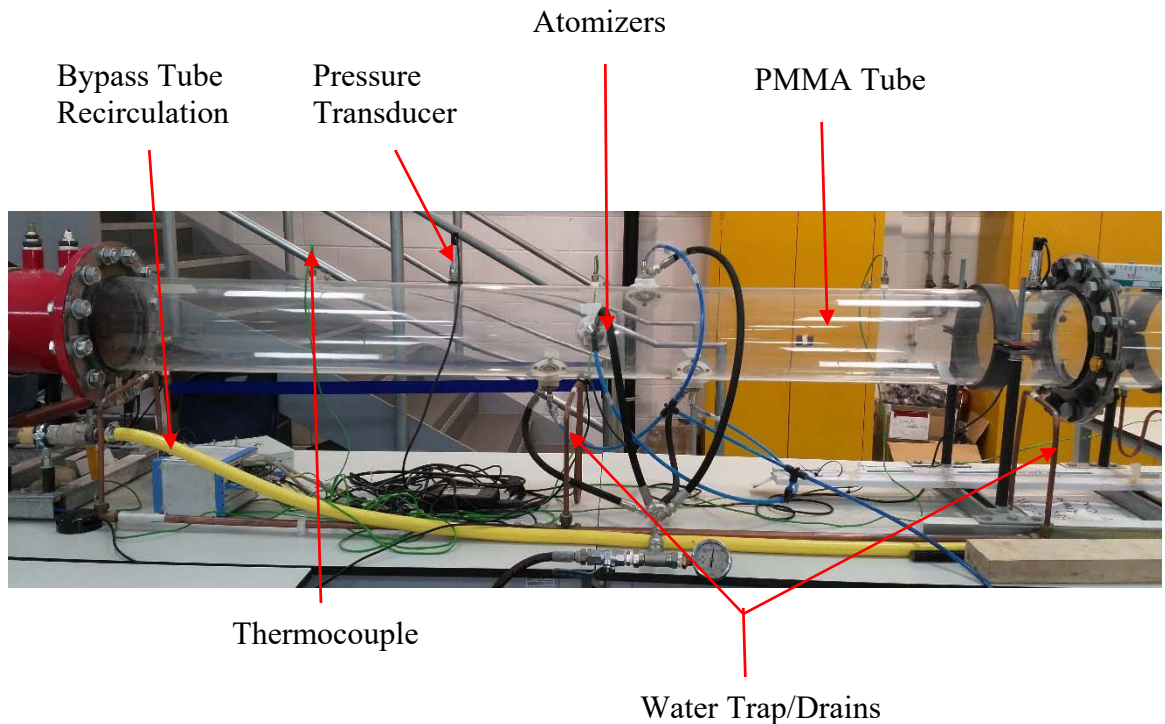


**Figure 4.8:** Polymethyl-Methacrylate, (PMMA) Section of the experimental tube

#### 4.4.1.1 Exhaust Outlet

There are six (6) exhausts opening on top of the tube located at the ignition end of the flame propagation and mitigation rig. The exhaust opening comprises of 88mm hole cut through the wall of the explosion tube and 80mm British Standard Pipe, (BSP) socket welded in position over the hole. However, the exhaust outlets were intended to control the 'blockage ratio' of the burnt gases leaving the apparatus and those driving the flame as shown in

Figure 4.9.

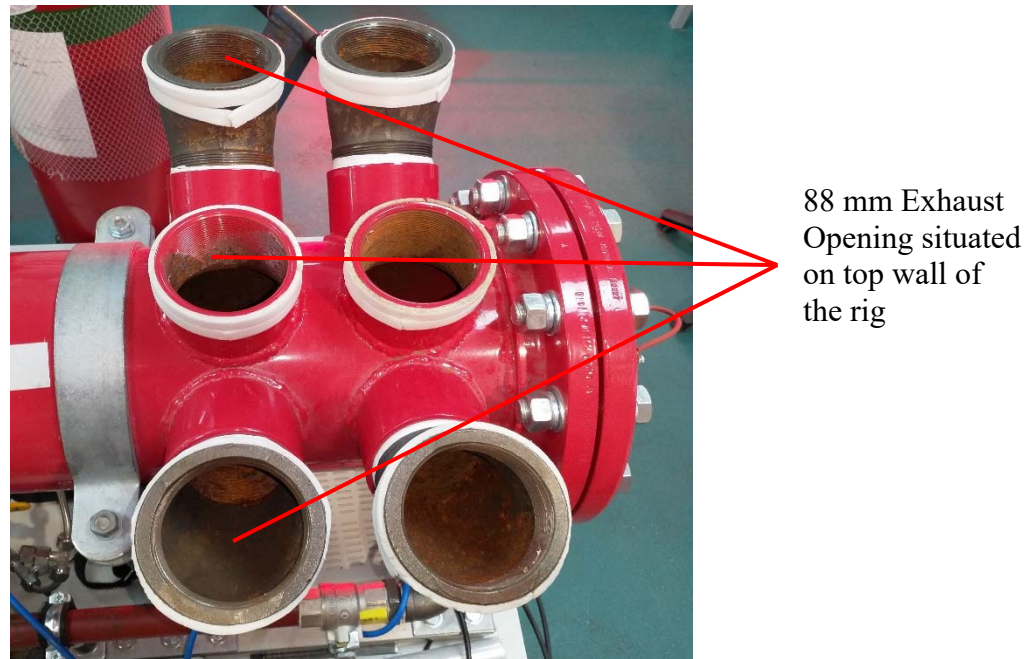


Figure 4.9: Exhaust outlet

#### 4.4.1.2 Bursting Film

The exhaust outlet was sealed using either 80mm BSP threaded plugs or by low-density polyethene sheet 'cling film' to prevent the discharge of the flammable methane-air mixtures during the process of filling. Before each experimental run, 'Cling Film' was secure in position by using adjustable Velcro straps to seal off the six-exhaust outlet that forms a temporary gas-tight seal as indicated in Figure 4.10.



**Figure 4.10:** Exhaust block with cling film during the filing period

The low-density polyethene sheet ‘cling film’ rift off immediately when subjected to an instantaneous pressure differential of about 0.015 – 0.025 bar (15 – 25mbar) within the experimental equipment and outside of the equipment through which the hot-burnt gases are vented out.

#### 4.4.2 Gas Recirculation System

The fuel gas (methane) and air were injected into the combustion tube from one end of the sealed flame propagation and mitigation rig, (FPMR) via a calibrated rotameter. At both ends of the experimental rig, connections were made in other to recirculate the fuel gas (methane)-air mixture via an external recirculation pipe as illustrated in Figure 4.11. The pump (gas booster) was used to increase fluid pressure normally used to the pressure of gas already above ambient pressure. Here, it was installed in a parallel recirculation stream to make a pressure differential through the main explosion tube and recirculate accordingly via bypass circuit stream in other to have homogenous fuel gas-air mixture.

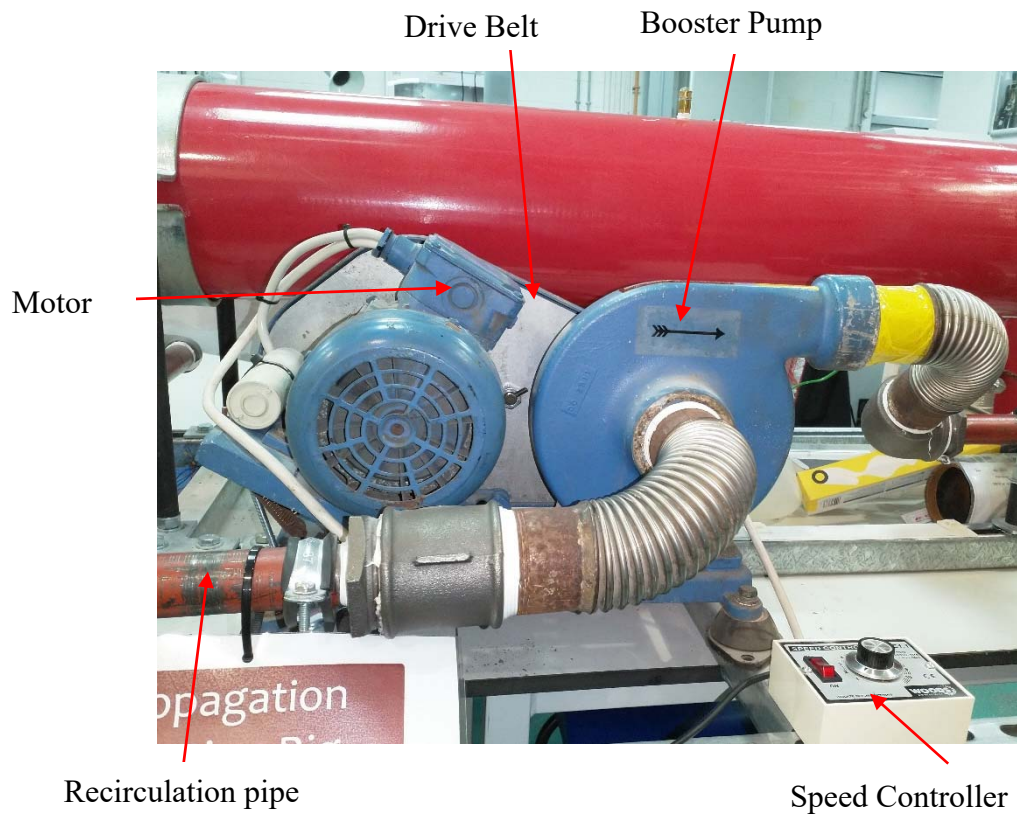


**Figure 4.11:** Gas Recirculation Booster Pump

The recirculation pipe diameter is 25 mm in measurement, which is far smaller than the diameter of the main explosion tube to advance high speed turbulent in mixing in the bypass tube in order to achieve homogenous throughout the main tube.

However, to quantify the volume of the fuel gas-air mixture, a gas turbine meter installed along the bypass tube as shown in Figure 4.12, was used. The meter was based on the principle of velocity measurement of the gas flow. The flowing gas is accelerated and conditioned using the straightening section of the meter. The vanes in the straightening section make the gas flow profile by removing the swirl and asymmetry before the gas flows over the freely rotating turbine wheel. The flowing gas causes the rotor to rotate. The turbine wheel has a helical blade that has a known angle relative to the gas flow. The gas flow drives the turbine wheel at an angular velocity, which, is proportional to the gas velocity. The gas mixture is allowed to stabilise for 1 – 2 minutes. The concentration of the mixture is then measured, verified and recorded using gas-co-seeker. The bypass recirculation circuit was then shut off completely using 5-quarter turn valve, with one located at a beginning section of the explosion tube, two located 2 meters away and the remaining two located at the end section of the explosion tube as indicated in figure 4.6. Part of the recirculation pipework was built utilising 25mm in diameter ridged steel pipe; a segment of reinforced hose was utilized to

connect the two ends of the recirculation pipework also indicated in figure 4.6. However, in other not compromise with the safety, an in-line flame arrestor was installed in the recirculation circuit as secondary measures to mitigate the risk of an explosion from the main flame propagation tube because certainly, it contains gas-air mixtures during filling times.

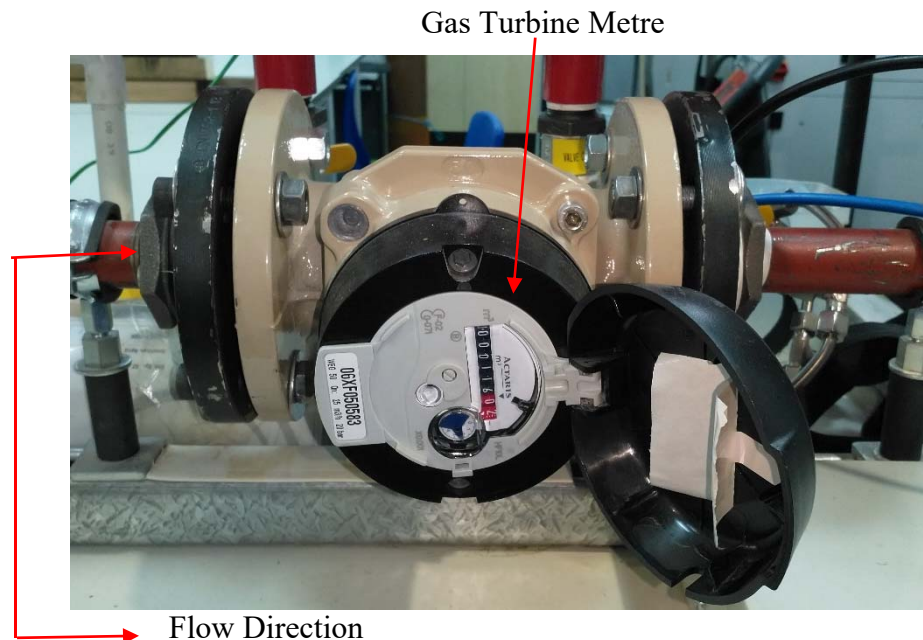


**Figure 4.12: Gas Turbine Meter**

#### 4.4.2.1 Purge Process before Explosion

To achieve accurate results for each experimental run, it was ensured that the equipment was clean and purged with air before injecting new fuel gas-air concentration. The following procedure was followed carefully after each experimental run:

- The experimental rig was fully open at both ends and allowed to stand for at least 20 minutes between each experiment.
- The recirculation system was then purged with air to ensure that the functionality of the equipment is not affected by the contaminants from the surrounding environment.
- The flame propagation tube and recirculation circuit were then tested for gas concentration.

Prior to the filling of the equipment with methane-air time the lock was manually closed and energised by switching on the primary key on the control box. To ensure that the equipment is completely gas-tight, two distinctive gas detectors were used to verify Gas-co-seeker as shown in Figure 4.26 and Alarm Portable gas detectors as shown in Figure 4.13.



**Figure 4.13:** Alarm Portable Gas Detector

### **4.4.3 Ignition and electrical control System**

The ignition system comprises of three main components namely; ignition electrode/spark plug, ignition spark generator and double insulated high-tension ‘HT’ cables. The ignition system is located on the right-hand side of the experimental rig as indicated in Figure 4.14. However, in order to provide adequate safety to the equipment and the entire laboratory, the ignition hardware was completely interlocked which prevents unintentional and untimely ignition start of the mixture.

#### **4.4.3.1 Ignition electrode/Spark Plug**

A spark plug is a device for conveying electric current from an ignition system to the combustion chamber of a spark ignition to ignite the fuel gas-air mixture by an electric spark while containing combustion pressure within the combustion chamber. Here, the spark plug was installed at the centre of the flange plate from the driver section as shown in Figure 4.14. However, two spark plugs were fitted into the experimental equipment, but a single plug was utilised during each trial to make the spark, while the other plug as a stand-by plug.

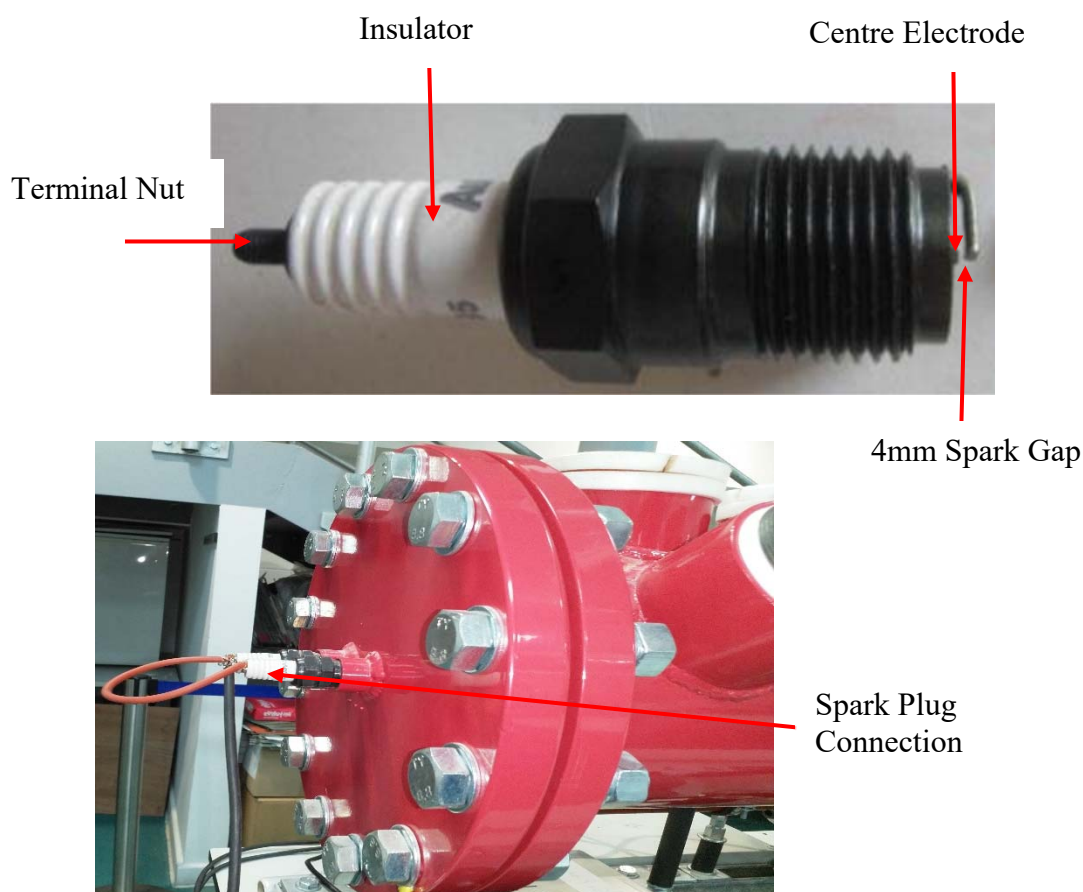


**Figure 4.14:** Spark Plug Ignition

#### 4.4.3.2 Spark Generator and Ignition Transformer

The ignition energy (10 mJ) was utilised throughout the flammability limit in these experimental trials that were sufficient to ignite all the lean, rich and stoichiometry methane-air mixtures. A 10,000 v ignition transformer and spark generator were utilised to supply the required HT spark.

#### 4.4.3.3 Double Insulated HT Cables

Two Universal Durite 19/0.30mm twofold insulated copper core high-tension (HT) leads were utilised to connect the ignition transformer and spark generator to the ignition electrode/spark plugs. Before each experimental trial, these cables should be checked for wear and tear intermittently and replaced where necessary

#### 4.4.3.4 Magnetic Hinge

The component described in section 4.4.5 (Exhaust outlet) allows for the relief of pressures and control of exhaust gas gases upstream of the flame front; another system was needed to

control the end section of the equipment. The magnetic hinge was used to completely seal off the experimental equipment since the equipment needed to be gas-tight during filling, recirculation and mixing period and however, an allowable additional 1-2 minute to ascertain homogeneity of the methane-air mixtures to settle. The magnetic hinge outlet comprises a ‘full bore’ hinged end plate controlled by an electromagnetic locking system as indicated in Figure 4.15.

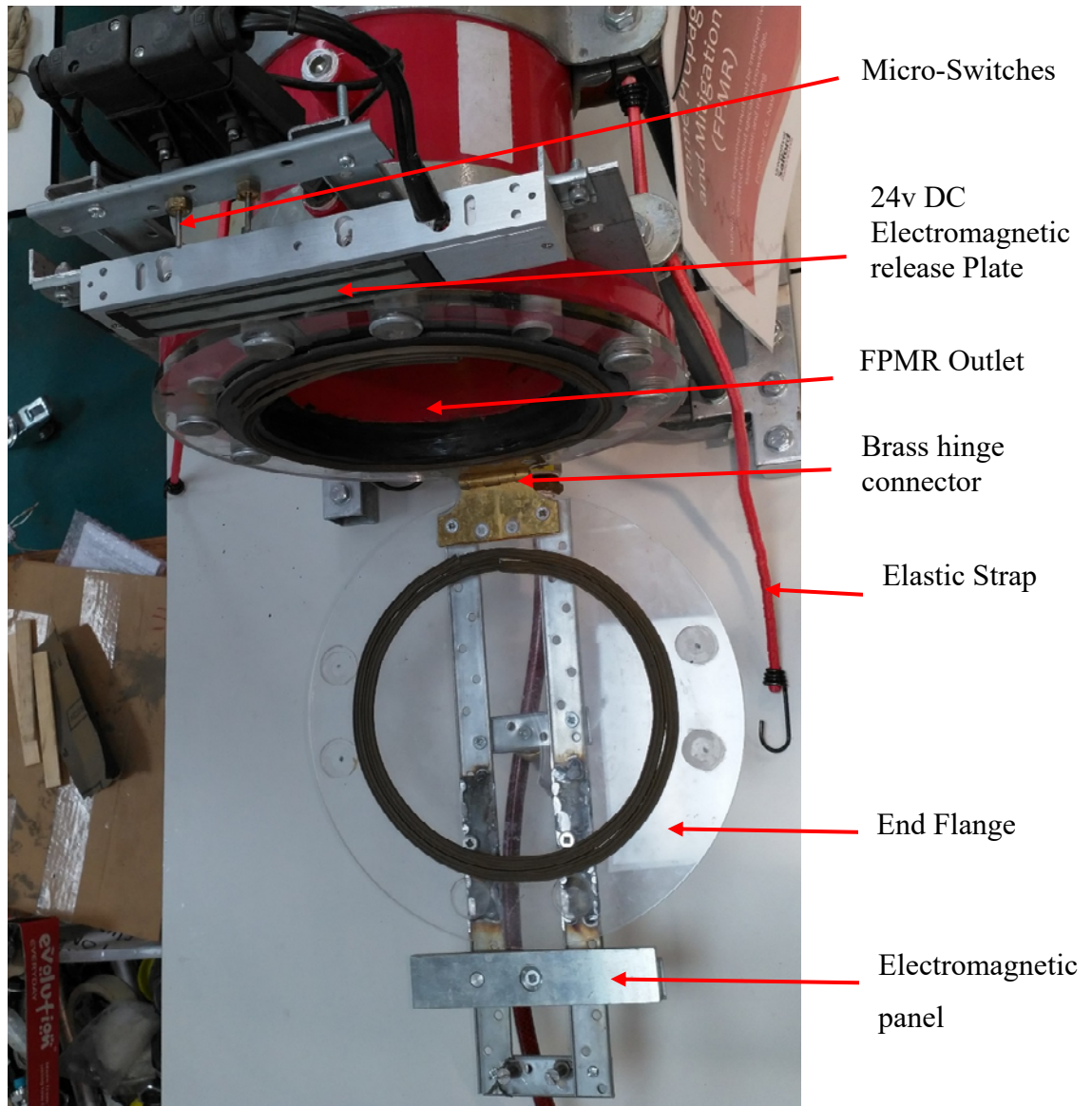


**Figure 4.15:** Magnetic Hinge Outlet

The electromagnetic locking framework was of the sort ordinarily connected with a programmed entryway passage framework. The strength of the direct current, (DC) electromagnetic field, together with the area of the hooking plates was sufficient to hold the end board shut and gas tight. The magnetic lock was controlled by 24 volts, direct current (DC) supply through a ‘time delay’ in the control panel.

#### 4.4.3.1 Plunge Type Micro Switches

To maintain a strategic distance from ignition start inside the shut tube, the magnetic hinge panel has two plunge type micro-switches to avoid ignition within the closed explosion tube. As the end plate is manually closed, the two miniaturised scale switches wired in a series arrangement changed over from their regularly shut to their normally open position. The two switches form part of the ignition system and spark generator interlock circuit. At the point when the timer relay unlocked the magnetic hinge board, the panel board started to open, assisted by the mass of the iron core counterweight. The two micro only operates when the magnet is either energised that is during filling or de-energised during flame propagation, and then the end flange falls off as indicated in Figure 4.16.

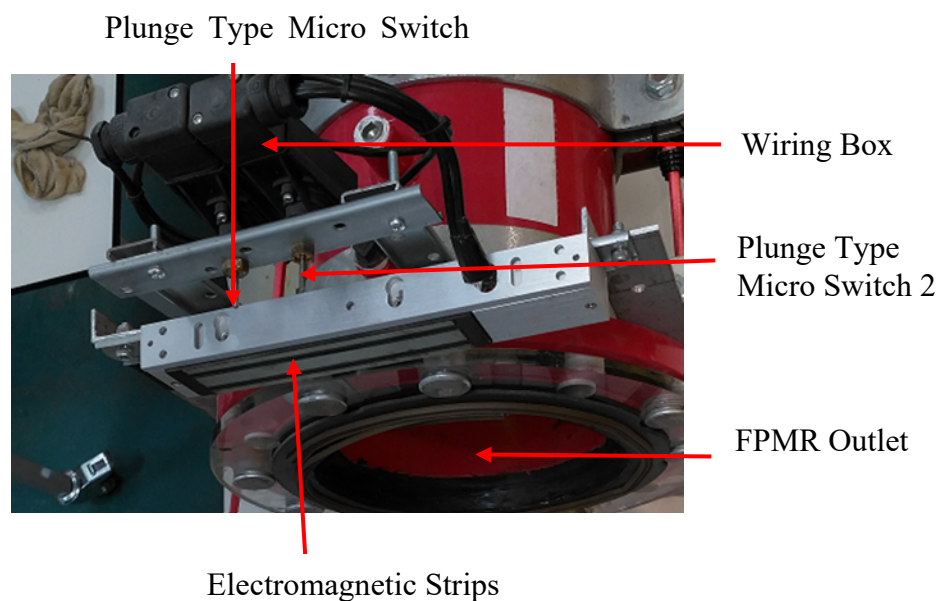


**Figure 4.16:** Plunge Type Micro Switches

#### 4.4.4 SRA's and water Supply system

Water was injected utilising a pump with supply capacity ranging from 5 MPa – 20 MPa. The pump utilised to supply water through the nozzles to the combustion tube (Polymethyl-Methacrylate 'PMMA' tube).

The pressure pump water supply system was manufactured by Interpump Company, which was supplied by industrial pressure washer Supplies Company. This was used to supply the desired water pressure and flow rates required to the SRAs that generate fine water mist to the explosion chamber. Table 4.5 shows the detailed specification of the pressure water pump and the pump and the motor are illustrated in Figure 4.16.

**Table 4.6: Specification of the water pump**

<b>Detail</b>	<b>Specification</b>
Manufacturer	Interpump
Model	W1208
Type	Ceramic plunger pump, oil bath crankcase lubrication
Flow rate	9 L/min
Rotation speed	1450 rpm
Output pressure	17MPa (140 bar) @ 9 L/min

#### **4.4.5 Water Storage**

120-litre wheelie bin was used as a water storage tank that was connected to the cross-spill return atomizers, SRA. The SRAs supply fine water sprays to the combustion chamber and serves as mitigating agents. The motor and pump assembly was obtained from an industrial pressure washer supplies company and was connected to the water storage tank with a pressure gauge to monitor the water supply pressure as shown in Figure 4.17. The bypass regulator was connected via a pump to the water storage tank because the bypass regulator maintains a high flow rate through the pump while returning a low-pressure flow back to the storage vessel.

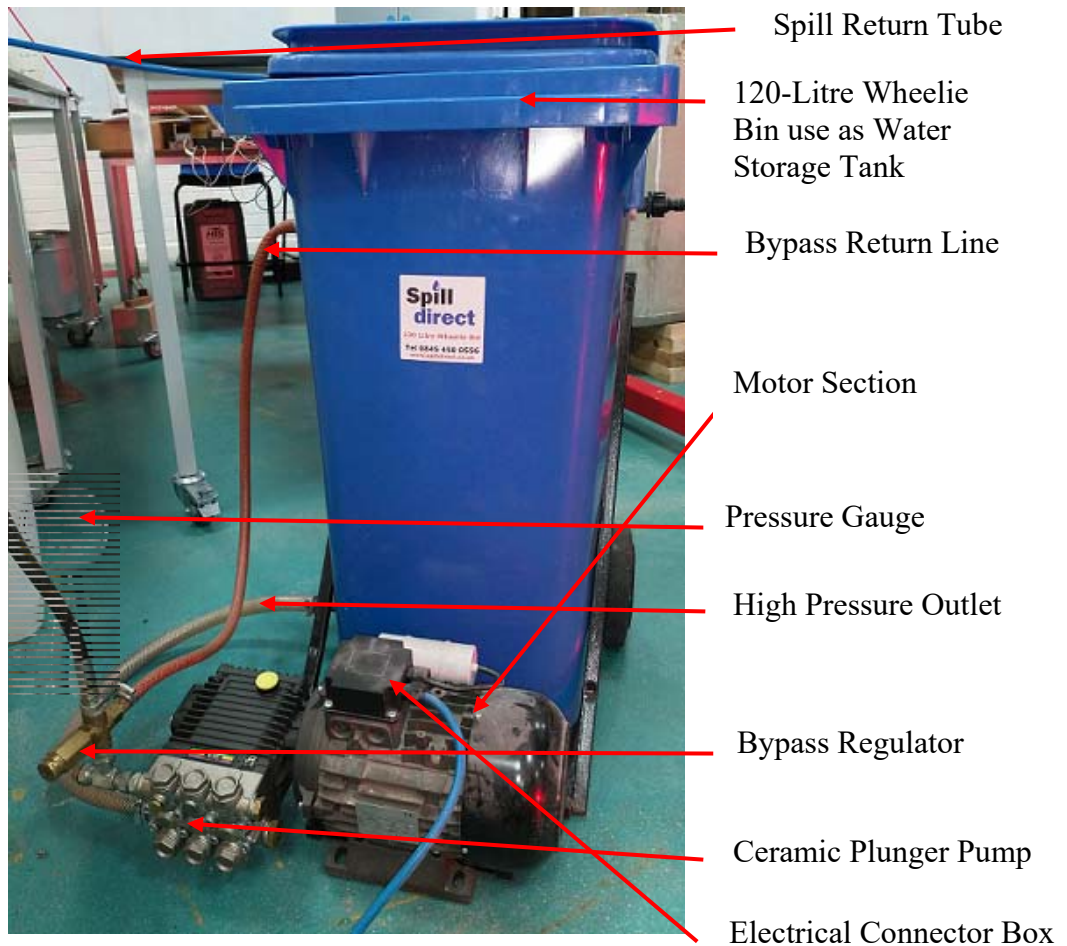


**Figure 4.17:** Pressure pump water supply and Water storage tank

#### **4.4.6 Water Drains**

The 10 mm diameter drains with water traps fixed at three different locations along the clear section (PMMA) of the experimental equipment and a bigger drain of 22 mm diameter and water trap fitted in the mild steel section of the experimental rig. These drain channels fitted were along the tube to ensure that sprayed water is drained out of the equipment quickly and efficiently as pictured in Figure 4.17.

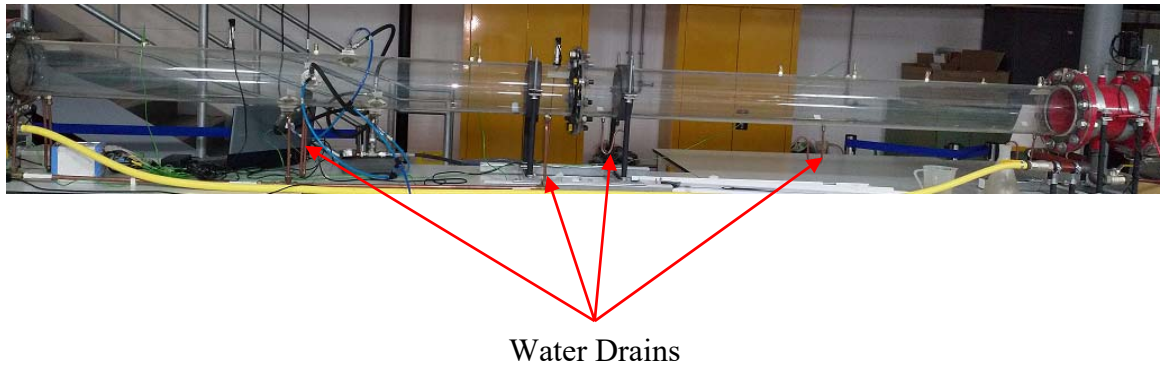


**Figure 4.18:** Water Drain System

#### 4.4.7 Methane-Air Supply System

BOC Company supplied the Laboratory Methane grade, and Industrial grade compressed air in 50 Litre cylinders with necessary connection including regulators and downstream valves. The methane-air was supplied through inlet connections to the combustion chamber via rotameters from the driver section of the experimental equipment; both inlets has a separate valve. Methane gas was supply to the chamber at the initial pressure of 2 bar as regulated from the methane bottle. Some properties of the laboratory methane grade are as shown in Table 4.6.

**Table 4.7:** Some Properties of Laboratory Grade C Methane

Fluid Properties	Values	Units
Thermal conductivity, $\sigma$	0.0338	W/m/K
Heat capacity, $C_p$	36.090	J/mol/K
Dynamic viscosity	0.109	mPa.s
Temperature, T	15	°C
Pressure, P	1	atm
Density, $\rho$	0.656	Kg/m <sup>3</sup>

Furthermore, in other to quantify the gas that flows into the experimental equipment, stopwatch and rotameter were use conjunctionally. The flow rate that was used and found to be very convenient 200 L/min, these provide consistency and reliability. The corresponding

time for each methane-air concentration during the filling period are shown in Table 4.7. To ascertain and verified the final concentration during recirculation circle, calibrated Gas-co-seeker used directly for the measurement, and of course, for safety reason alarm portable gas detectors shown in Figure 4.14 was used to check for any leak before firing.

**Table 4.8:** Fill times, flowrates and percentages of methane in air

Methane-Air (%)	Flow Rate (L/Min)	Filling Duration (Mins)
6	200	2:25
7	200	2:45
9	200	3:25

Before any experimental runs, the laboratory entrance door is lock properly and the experimental rig well checked especially the valves and regulators and then tested before the commencement of any trial, this serves as safety precautions.

#### 4.4.8 Electrical Sequence

Figure 4.18 shows the electrical control circuit used throughout the experimental trial. The electrical control box comprises of the primary key, booster key, ignition key and ignition push button as illustrated in Figure 4.18. The primary key controls 230 V and 24 V circuit; the primary serves as the main control key if turned off, all other electrical keys will not function. The booster key is turned on before the commencement of the filling of the rig with the gas and must be turned off after filling, to allow to the ignition key and ignition button. The ignition key is turned on to allow power to the ignition bush button. Since other students some time used the laboratory, it was ensured that the laboratory entry door was always locked before any experimental trial.

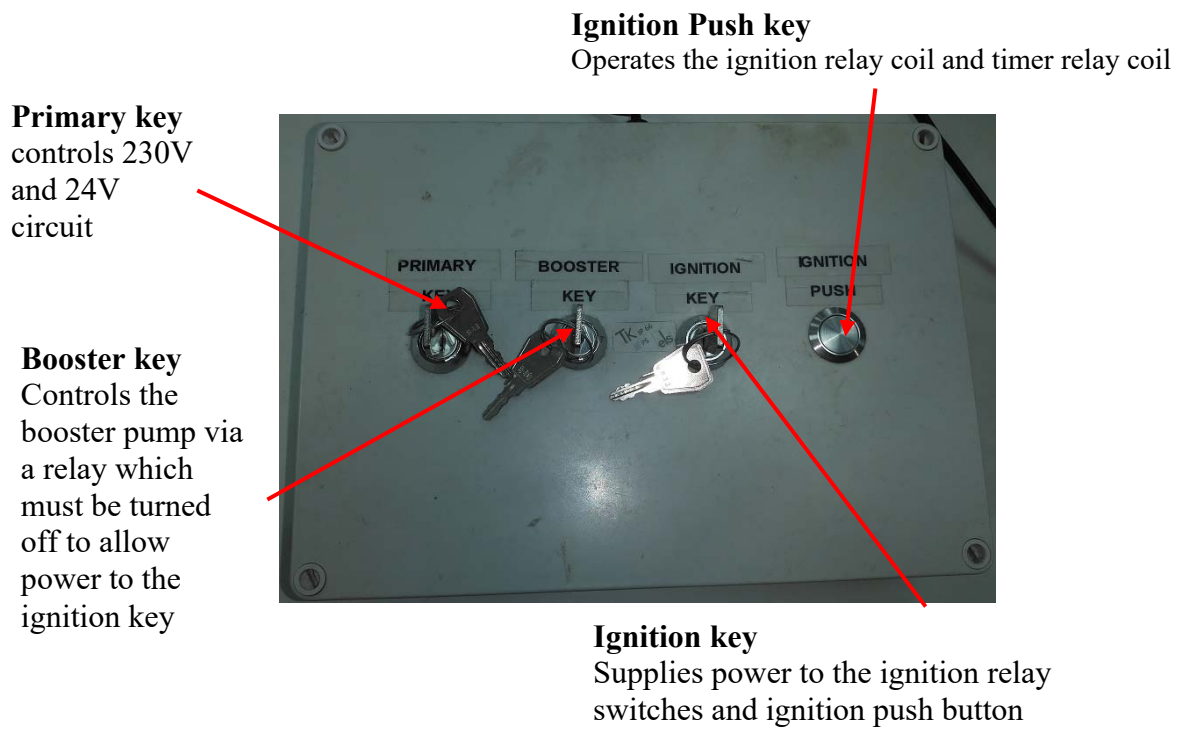
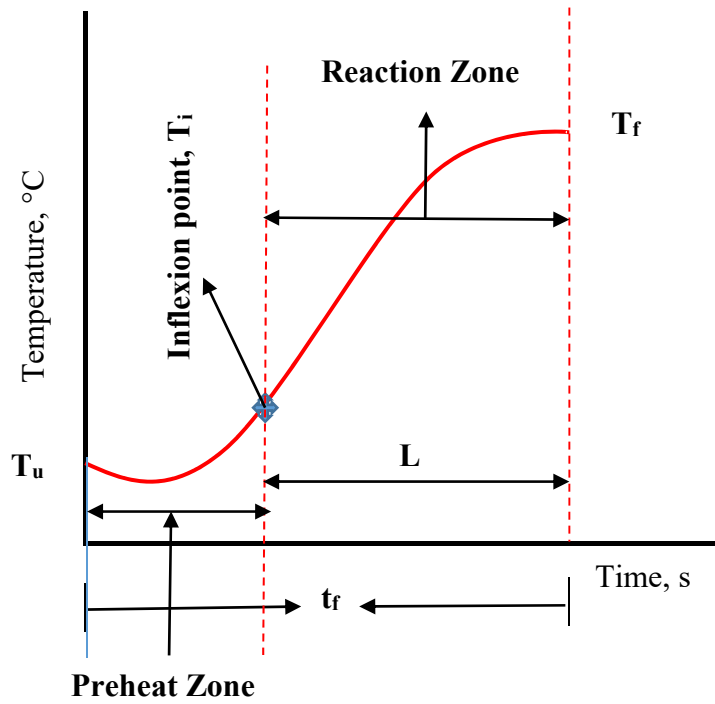


**Figure 4.19:** Electrical control box indicating operator keys and ignition bush button

## 4.5 Flame Structure

Flame may be described as regions of chemically reacting gases which generate heat and light. Figure 4.20 shows schematically the pre-heat and reaction zones regions of a typical concentration and temperature profile through the pre-mixed flame. Preheat zone is the zone in which the cold gases are heated to a particular temperature (autoignition temperature).



Where  $T_u$  = Unburn gas temperature,  $T_f$  = Burnt gas (final) Temperature,  $T_i$  = inflexion point,  $t_f$  = Flame thickness and  $L$  = length.

**Figure 4.20:** Temperature profiles through the pre-mixed flame

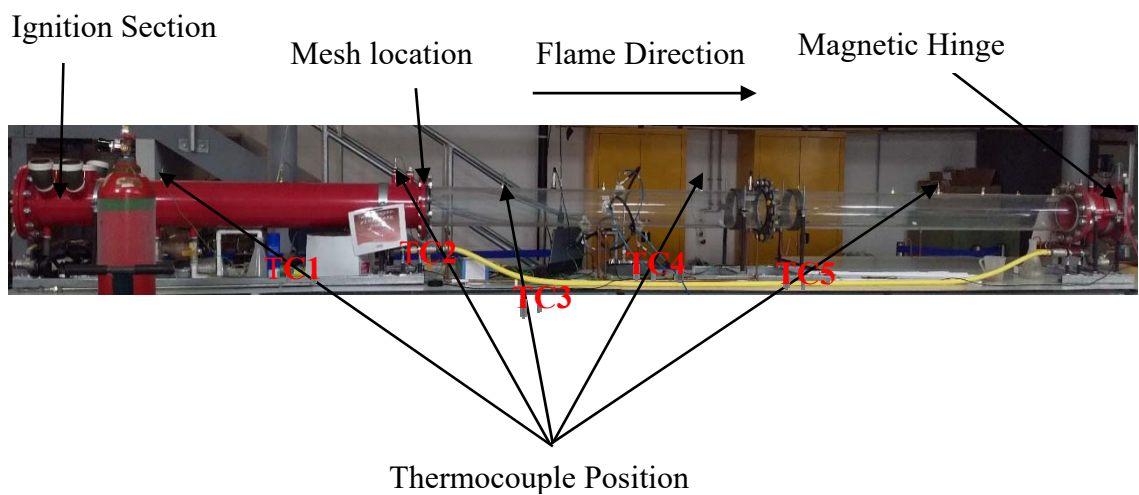


**Figure 4.21:** Thermocouple position and flame direction

### 4.5.1 Summary of Experimental equipment

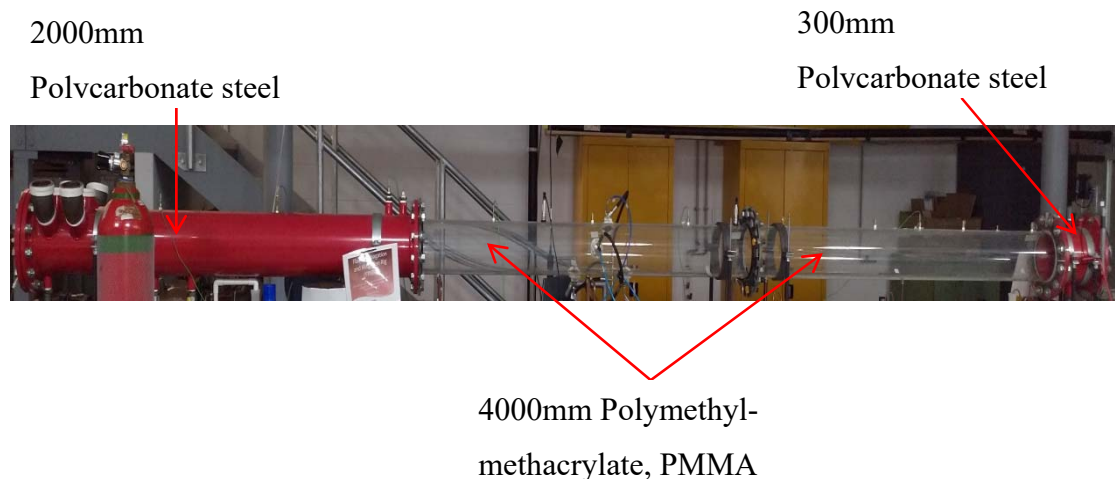


**Figure 4.22:** Experimental equipment

Figure 4.20 shows the complete setup of the experimental apparatus. The system has four sections, namely: explosion chamber, circulation section, ignition source, water supply system and data acquisition system. The explosion chamber was designed to withstand the pressures and temperatures normally associated with propagating deflagrations in unconfined and partly confined situations.

The chamber has two cylindrical compartments that are made up of polycarbonate steel pipe, and polymethyl methacrylate (PMMA) joined using a flange jointing technique. The tube has a total length of 6.3 m (6300 mm) with both inner and outer diameter 202.72 mm and 203.2 mm respectively. The polycarbonate steel pipe is fitted at the beginning and end of the tube with 2 m (2000 mm) and 0.3 m (300 mm).

The first section of the steel pipe has six exhausts (80 mm each) at the top as a gas outlet, and Pete plugs fixed on the closed end section of the tube with an interval of 600 mm. The magnetic hinge is fixed at the open end of the steel pipe with a microswitch.

The polymethyl methacrylate is divided into two with 2 m (2000 mm) each jointed using a flange joint. Spill return atomisers are fixed at PMMA section of the tube at a distance 3 m (3000 mm) away from the beginning of the steel pipe section. The circulation system and gas turbine meter are located on the side of the steel pipe at a distance of about 1800 mm.

The diameter of the recirculation pipe is 25 mm. The ignition box has four switches; primary key (230V and 24V circuit), booster key, ignition key and ignition push button with 10,000 V

transformer. Two Universal Durite 19/0.30mm double insulated copper core high tension (HT) leads were used to connect the ignition transformer and spark generator to the ignition electrodes/spark plugs. The water supply system consists of a water storage tank, bypass return water, single phase motor, and water inlet hose from the tank, bypass regulator, pressure gauge and plunger pump. Figure 4.1 illustrates a schematic diagram of the rig.

## 4.6 Video Recording and Data Processing

### 4.6.1 Flame Images

Nikon cool digital high-resolution (HR) video camera is shown in Figure 4.19, was used to record flame videos. The video recording was used to extract a sequence of images for image processing using adobe premiere Pro CC 2017. The qualitative and quantitative information regarding images of the flame structure, flame temperature, and average flame speed process during the experimental trials were then analyses. The camera has a glass lens with 18x wide-angle optical zoom-NIKKOR ED, 12.1 megapixel CMOS sensor and 3-inch Ultra-High resolution VGA (921,000-dot). It captures 5 shots per second at full resolution with a clear colour displayed. It operates at 29.97 (approximately 30) frames per second (fps).



**Figure 4.23:** Nikon cool Camera

The flame images from Adobe Premiere Pro CS6 and Adobe Photoshop CC 2017, were scaled using the pixel measurement tool. The Adobe pixel measurement tool provided consistent measurements for determining average flame speeds.

#### 4.6.2 Image Processing

The video recordings were used to extract a sequence of images for image processing. The images were then processed using Adobe Photoshop CC 2017 in order to determine the acceleration of the flame front. However, the experimental runs were conducted using three different methane-air mixture concentrations as shown in Table 4.1 As illustrated in Figure 5.5 the selected images from high definition (HD) video camera (Nikon) were processed, edited and time coded using Adobe Photoshop CC 2017. Also, the distance travelled by the flame was obtained using Adobe Photoshop CC 2017. The first images show the onset of the flame emergence from the start of the ignition (that is the propagation of the flame into the clear PMMA section). The remaining three images are observed and referenced to the first image with its corresponding time in milliseconds (ms).

#### 4.6.3 Thermocouples

The exposed junction, mineral insulated K-type thermocouples as shown in Figure 4.21 supplied by Omega Ltd. Manchester was used. Five thermocouples were installed along the pipe length at a different location as shown in Table 4.8.

**Table 4.9:** The location of the thermocouples and their intervals

Apparatus	Location of the Thermocouples
Thermocouple (TC 1)	650mm
Thermocouple (TC 2)	1850mm
Thermocouple (TC 3)	2450mm
Thermocouple (TC 4)	3650mm
Thermocouple (TC 5)	5150mm

The main body had a diameter of 3 mm and was located through the vessel wall so that the exposed 0.6 mm-diameter conduction wires were on the axial centreline of the test vessel.

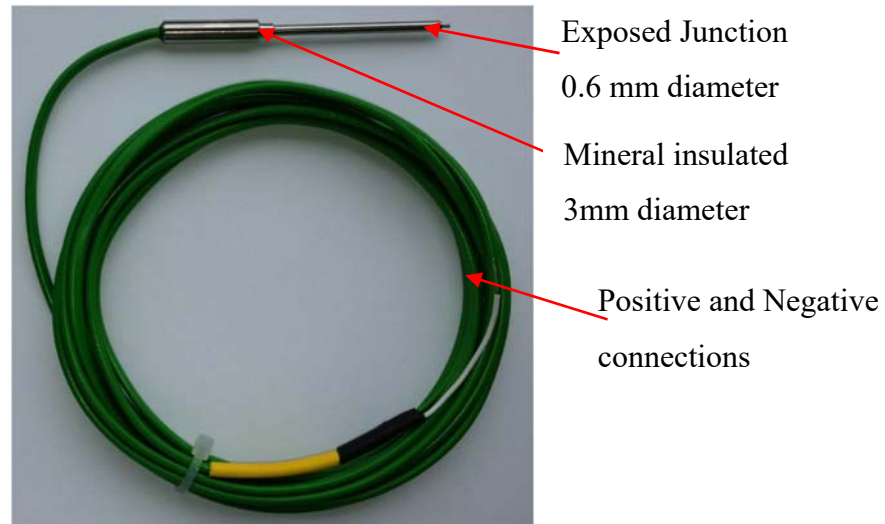


**Figure 4.24:** Type K thermocouple, (TC Ltd UK)

The exposed junction, type K thermocouples were placed along the length of the flame propagation and mitigation rig at different interval intervals as shown in Table 4.21 and held in place using ‘Pete’s Plug’ adapters. These type K thermocouples were connected to instrunet Data acquisition box (DAQ) to record the thermocouple temperatures simultaneously, thereby saving the data file to be further processed.

#### 4.6.4 Data Acquisition Box (DAQ)



**Figure 4.25:** iNet Expandable Modular Data Acquisition (DAQ) System) [72]

The iNet Expandable Modular Data Acquisition System was manufactured by Instrunet as shown in figure 4.22. These was used because of its compatibility and very simple

connectivity to a Windows-based computer. External measurement devices, such as thermocouples, resistance temperature detectors (RTD's), thermistors, strain gauges, load cells, voltage, current, resistance and accelerometer inputs can be connected to the iNet510 Wiring Box [72]. This is, however; the iNet software is designing to supply a real-time data display, which is highly compatible with Ms Excel.

#### 4.6.5 Verification of Methane-Air Mixture

To maintain safety due to numerous mixture of methane-air, which was formulated, and well mixed before the explosion and mitigation testing; the GMI Gascoseeker 500 was used to ascertain the final mixture percentages.



Figure 4.26: GMI Gascoseeker Mk2-500 [72]

#### 4.6.6 Fuel gas and Air Volumetric Flow rate

To know the amount of fuel gas that goes into the combustion chamber, Solartron Mobrey rotameters were used to fill in the desired amount needed into the flame propagation and mitigation chamber.

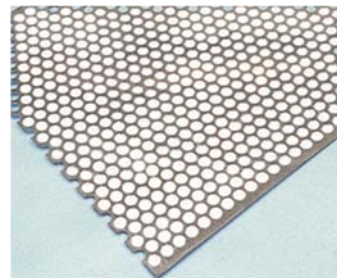
#### 4.7 Perforated steel sheet/Woven wire mesh

The heat recirculation medium used in the experimental work were of two types: perforated plate/sheet with hexagonal aperture 6 mm made of stainless steel material and woven wire meshes with a square aperture 0.9.4mm and 1.31mm aperture made of stainless steel material as well shown in Figure 4.24. The perforated plate supplied by Rs online company while the woven wire mesh was supply by the mesh company. The arresters were cut in the form of a circular disc with a diameter the same as that of the outside diameter of the explosion tube.

The arrester was held in between the two flanges of the tube that was sealed into position using the nut and bolts of the flanges.



Woven wire mesh



Perforated metal sheet

**Figure 4.27:** Perforated steel sheet/plate/woven wire mesh

# Chapter 5: Results and Discussions

## 5.1 Introduction

The chapter provides the series of the experimental results obtained from explosion trials of methane/air mixtures utilising Flame Propagation and Mitigation Rig (FPMR) as described in chapter 4. The results were presented in three different stages according to the experimental setting as explained in schematically in chapter 4, section 4.1.

These stages were due to the experimental setting involves during each runs and includes: dry (no mesh and no spray) runs using methane-air, dry with mesh obstruction runs, and wet (water spray) with mesh obstructions combined. Each experiment was run using 6, 7 and 9% methane concentration in the methane-air mixture with the corresponding equivalent ratios of 0.61, 0.72, and 0.95  $\Phi$  respectively.

## 5.2 Dry Trials (No mesh and No sprays) results

The sequence of experimental runs without any means of flame suppression and obstruction that is, there is no steel mesh installed nor water sprays activated. The following series of results were obtained and analysed.

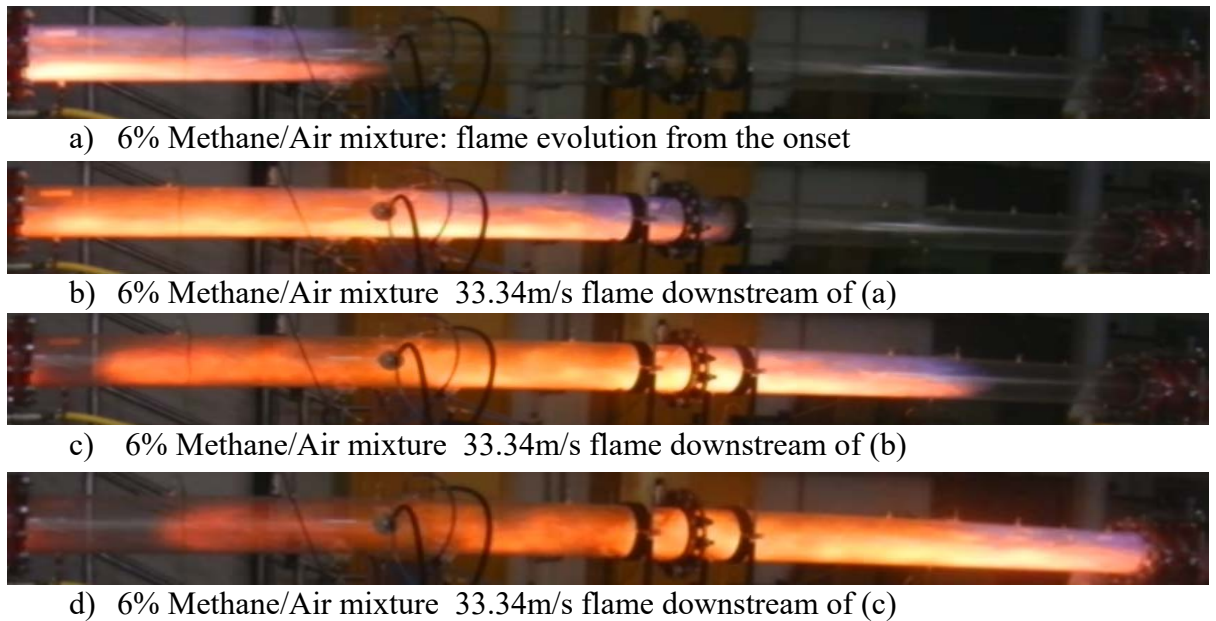
- Flame images from the flame propagation,
- Flame speed and
- Flame temperature.

### 5.2.1 Flame Evolution into PMMA section without obstruction

A sequence of high-speed video images of flame propagation for 6, 7 and 9 % methane/air mixture in the combustion chamber without any obstruction were shown qualitatively in Figure 5.1, Figure 5.3 and Figure 5.3.

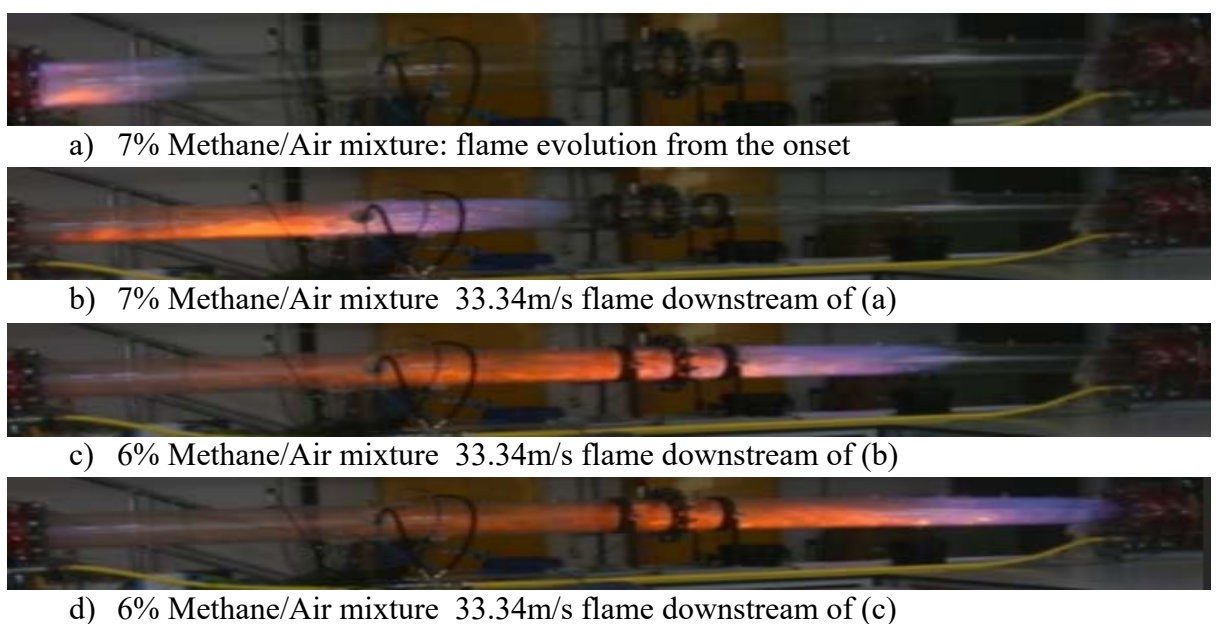
The observation from Figure 5.1, which represents the 6% methane-air mixtures combustion, indicates that the flame front appeared to be slightly dark (bluish in character) from the onset which represents a complete combustion region of the system. This shows the emergence of the flame into the clear section of the tube as the system ignited (Figure 5.1 (a)). The flame continues to propagate along the tube as the mixtures in the chamber continue to burn. These are shown in Figure 5.1 (b), (c), and (d). Additionally, the colour of the flame at the middle appears yellowish, and as the flames propagate further, the unset point which now becomes

the flame back appears to be dark yellow which indicates a lower temperature region. This is because there is not enough oxygen present in the region and combustion is incomplete.



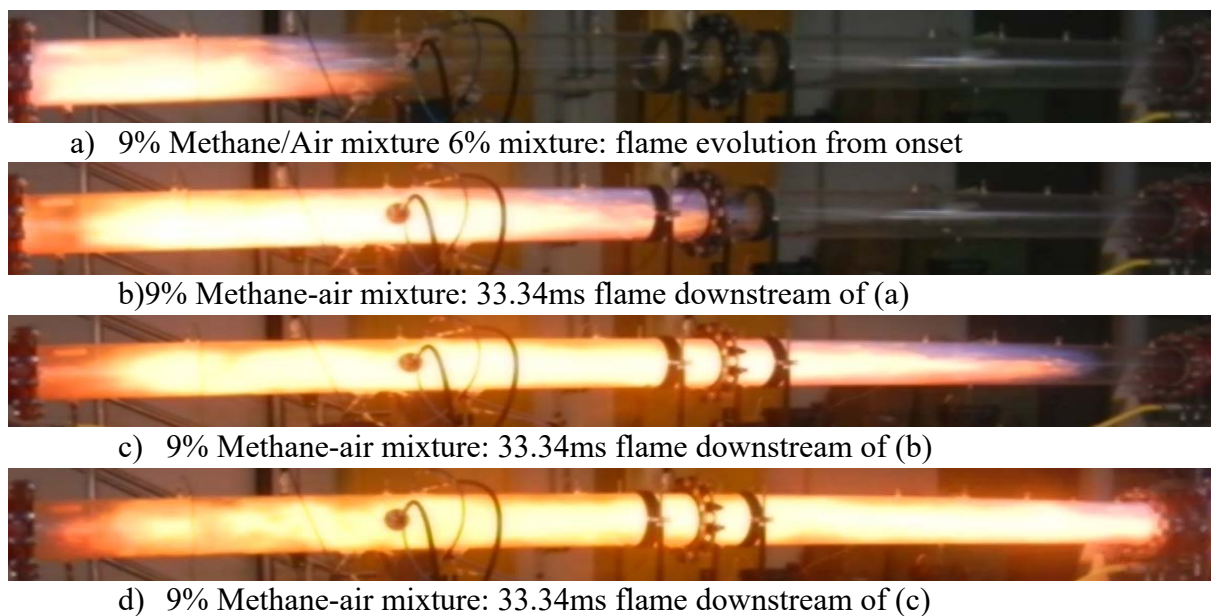
**Figure 5.1:** 6% Flame propagation images (dry) with no water spray and no mesh

Figure 5.2 pictorially present the flame images of 7% methane/air combustion. It was observed that the flame front appeared to be bluish in character and wrinkled as the flame arrives the clearer section (PMMA) of the tube from the point of ignition (Figure 5.2 (a)) resulting from the conduction effects combined with the flame stretch at the flame front. The flame continues to propagate along the tube as the mixtures in the chamber continue to burn. These are shown in Figure 5.2 (b), (c), and (d).



**Figure 5.2:** 7% Flame propagation images (dry) with no water spray and no mesh

Figure 5.3 shows the flame images of 9 vol% methane/air mixture explosion. It can be seen that the flame exhibit similar character when compared to Figure 5.1 and Figure 5.2, but the colours varies greatly at different times. Though, as depicted in Figure 5.3, the beginning of the flame appears in light blue, and a very brighter (Yellow) coloure appears at the middle, and the flame appears in the form of a cone with a smooth flame front. This is because the propagation speed on the flame edges is smaller than those on the middle as a result of the friction of the pipe wall and cohesion of gas which is similarly reported by [73]. As the flame propagates further, the flame back appears in dark brown. This is because a great amount of energy was released at higher methane/air combustion. This behaviour also clearly indicates the pre-heat and reaction zones as the flame propagates further which is also in agreement with Mallard and Le Chatelier theory [74]. The preheat zone which is the period between the ignition point and the first heat release in the system. While the subsequent heat loss is exceeding the heat gain representing the reaction zone. This is because, from the literature point of view, the blue colour of the flame is the hottest part compared to the yellow colour.



**Figure 5.3:** 9% Flame propagation images (dry) with no water spray and no mesh

### 5.2.1 Preliminary Flame speed without Mesh and water sprays

The speed of the flame were obtained from the video recordings as presented in Figure 5.1, Figure 5.2, Figure 5.3 flame images of three (6, 7 and 9 vol%) methane-air combustion. This resulting flame speeds will be used for comparisons to other average flame speeds throughout the result discussion in this thesis.

As observed from Figure 5.1 to Figure 5.3, though not seen in the video recordings (film), it is assumed that the flame expanded spherically until it reaches the wall of the pipe and burning rate was assumed to decrease when the flame hit pipe wall. Due to this, the flame speed and structure becomes unstable as the flame continues to propagate within the tube length.

It was observed that as the concentration of methane in air increases, the average flame speeds increases. This behaviour is due to more fuel (methane) availability to participate in the combustion tube, similarly reported by Steve Johnson in his thesis. The results presented in Table 5.1 shows the average flame speeds for each of the methane-air concentrations also, displayed graphically in Figure 5.4. The calculation is previously shown in Table 5.1 and Figure 5.4 and similarly reported by Steve Johnson in his thesis [75].

**Table 5.1:** Average flame speed for three different methane-air mixtures

Methane/air mixture (%)	Distance travelled by flame (m)	Time travelled (s)	Average flame speed (m/s)
6	3.400	0.133	25.56
7	3.600	0.133	27.07
9	3.000	0.100	30.00

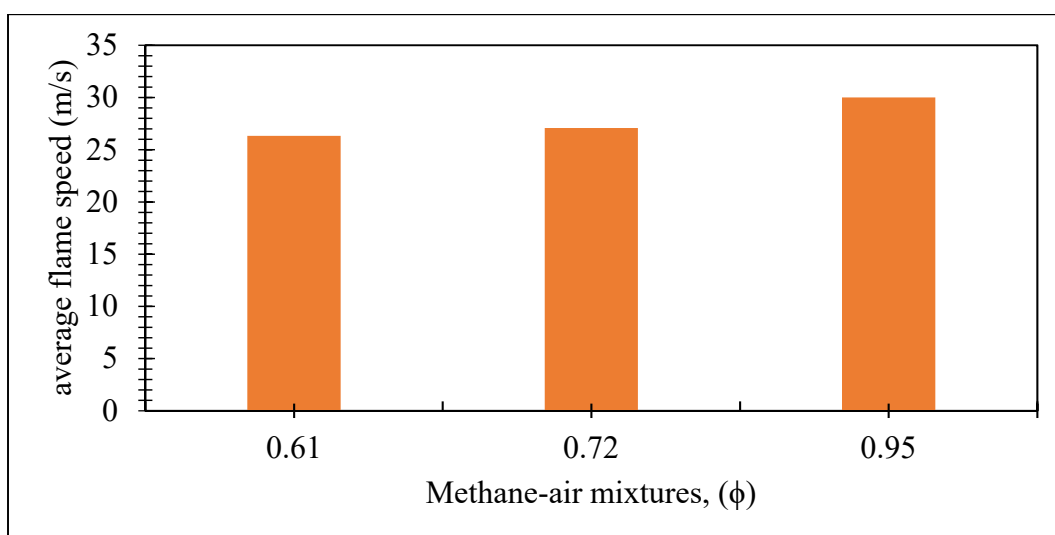


**Figure 5.4:** Average flame speed for three different methane-air mixtures

## **5.2.2 Effect of methane concentration on flame propagation**

The concentration of methane-air mixtures considered in this present study is 6%, 7%, and 9% respectively. As illustrated in Table 5.1 and graphically represented in Figure 5.4, the flame speeds with various methane-air mixtures. At 6% concentration, the flame speed was about 25.56 m/s with an increase methane concentration to 7 %; the flame speed increases 27.07 m/s and subsequent increase in methane concentration to 9%, shows an increase in flame speed to 30 m/s. This behaviour indicates that the energy released by the chemical reaction is lower when close to the lower explosive limit and thus lower the flame temperature which declines the burning rates.

## **5.2.3 Time - Temperature Profile**

The temperature variation across the five labelled thermocouples TC-1, TC-2, TC-3, TC-4, and TC-5, has been investigated to understand the trends of the flame energy exothermicity as well as predicting the amount of opposing forces required to quench the flame. The results of the thermocouple output data for 6, 7 and 9 % methane-air are presented in sub-sections 5.2.3.1, 5.2.3.2 and 5.2.3.3. These three sections described the phenomena observed with each of the methane-air combustion considered.

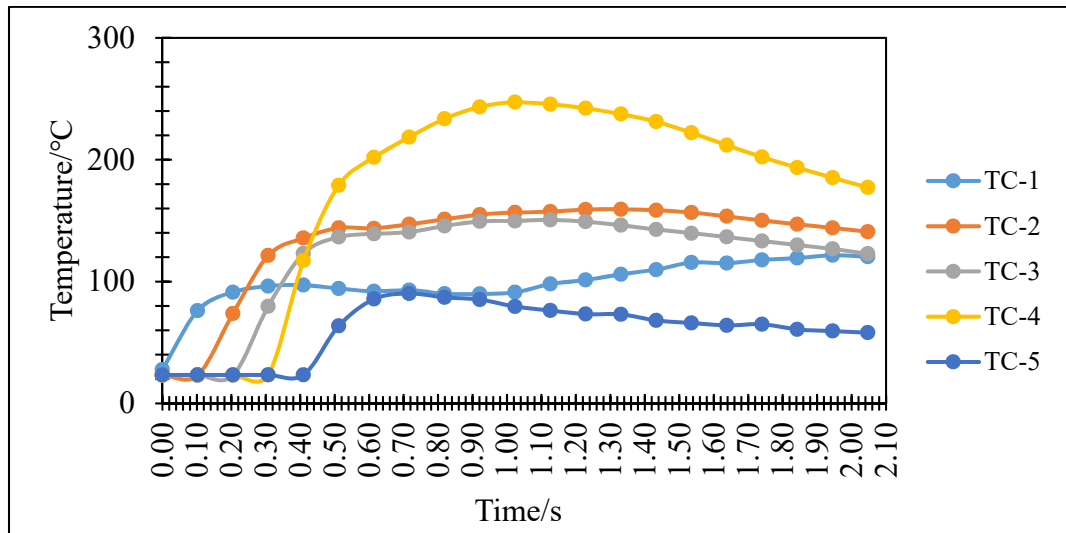
### **5.2.3.1 Temperature profile at 6 % methane/air combustion**

Figure 5.5 shows the results obtained from various thermocouple output data for 6% methane/air combustion. It was observed that after TC-1 trigger point; there is a rapid increase in the propagated flame temperature (hot gases) from 23.40°C to about 91.2°C with the corresponding time to be 0.20s.

Figure 5.5 shows that the highest temperature was achieved at TC-4 (243°C and 0.92s). This is because the concentration of methane could not obtain all the air requirements at the beginning of the combustion tube. Therefore, the series of explosion occurred as the flame expands and propagates further through the pipe length thereby gaining access to more un-combusted methane. Thus, exothermically releasing further heat due to the series of reactions of the un-combusted methane which leads to more temperature rise at the TC-4 compared to TC-1.

Additionally, understanding the general trends of temperature change was observed to be similar for all thermocouples and these shows that there is a gradual decrease in the extent of reactions and exothermic heat evolution across the length of the tube. The temperature

recorded from all the thermocouples is very similar with TC-2, TC-3 and TC-5 having a maximum temperature of 135.69°C, 136.51°C and 90.18°C with their corresponding time 0.41s, 0.51s and 0.72s respectively. Additionally, TC-5 recorded the lowest temperature because the temperature continues decreasing as the flame propagates to the end of combustion and more heat was loss to the surrounding as the flange falls off.



**Figure 5.5:** 6 % methane-air combustion

### 5.2.3.2 Temperature profile at 7 % methane/air combustion

Figure 5.6 depicts the temperature-time curve at 7 % methane in air combustion. It can be seen from Figure 5.6 that the trends of results obtained as expected exhibit similar behaviour when compared with Figure 5.5 (6 % methane-air combustion). After the mixture was ignited, it was observed that the temperature increases gradually from TC-1 (91.28°C and 0.20s) but TC-4 recorded the maximum temperature (247.22°C and 1.02s). This observation is detailed in subsection 5.2.3.1.

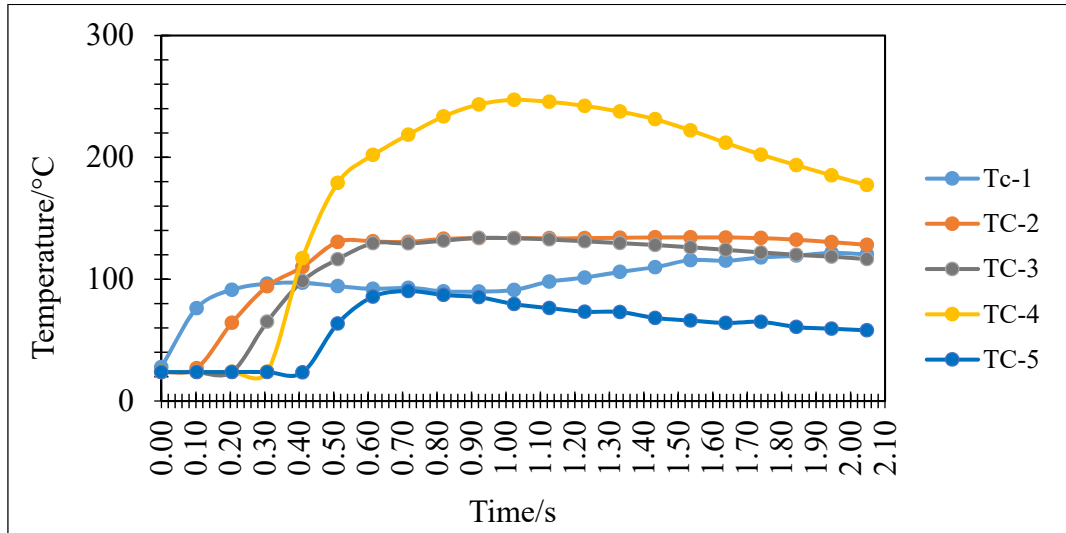


**Figure 5.6:** 7 % methane-air combustion

### 5.2.3.3 Temperature profile at 9 % methane/air combustion

Figure 5.7 shows the changes in the combustion temperature with the variation in time. All the temperature-time recorded exhibit similar behaviour compared with Figure 5.5 and Figure 5.6. It was observed from Figure 5.7 that as methane concentration increases, the temperature increases as well because more energy liberated.

However, other thermocouples indicate a lower temperature sequentially compared to TC-4 with a further decrease from TC-2 to TC-3, TC-3 to TC-1 and TC-1 to TC-5 respectively. All the temperature-time curve obtained displays the ranges of temperature of the flame propagation in a pipe which is in agreement with the literature .

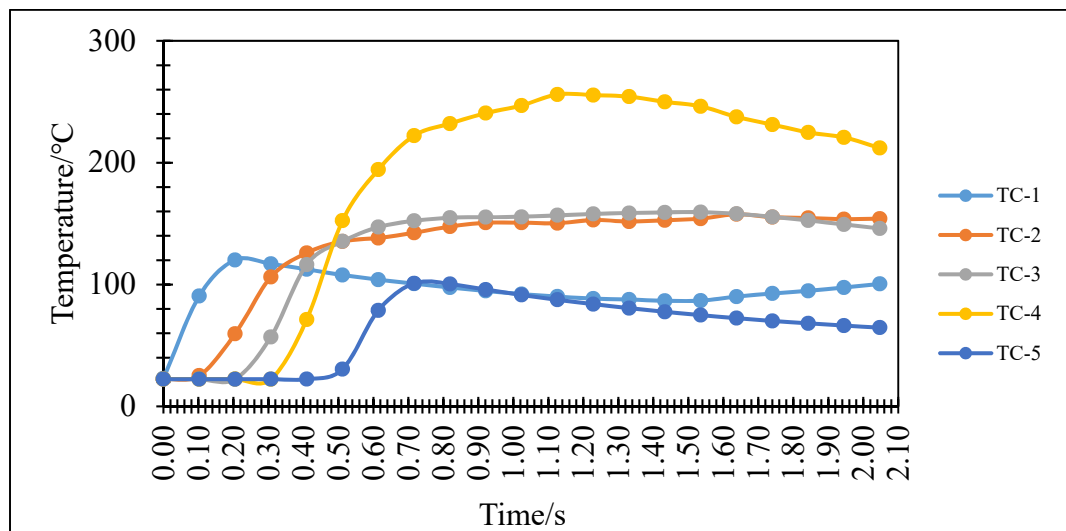


**Figure 5.7:** 9% methane-air mixtures

The results of these preliminary experimental runs will be used to compare with subsequent trials including a dry test with mesh in place and mesh plus water sprays scenarios. The following subsequent result section shows the set up with 0.94mm aperture installed but no water sprays.

### **5.3 Woven wire Mesh (0.94mm aperture)**

The experimental rig was reconfigured with 0.94 mm aperture installed in between the steel pipe and the PMMA tube at 2000 mm distance from the point of ignition (driver section). This is described and detailed in section 4.3.

#### **5.3.1 Flame propagation through the mesh at 6 % mixtures**

Figure 5.8 (a, b, c, and d) shows a sequence of images of the flame propagation through wire mesh at 6 % methane-air combustion. The woven wire mesh (0.94 mm aperture) was installed at 2000 mm distance from the start of ignition (that is immediately after the second thermocouple). It was observed that after the ignition of the methane-air, it takes about 20 – 30 milliseconds for the flame to propagate and vanished away from the explosion tube.

The observed trends from the flame propagation through the woven wire mesh indicate that the colour of the flame varies gracefully as it moves along the tube. At the onset, an unstable combustion region appears which was represented by the different colours appearing at the same time. The blueish flame head dominates the region, and this shows that more of the methane fuel was burnt completely at the beginning of the explosion. Additionally, it was observed that the flame obstruction due to the wire mesh installed, causes flow resistance of the methane-air mixture. This obstruction led to the reduction in the flame front speed and burning rate as it emerges into the transparent tube. A clear separation of the regions appears as the flame propagates further into the transparent tubes, for example, as shown in Figure 5.8 (b, c and d).

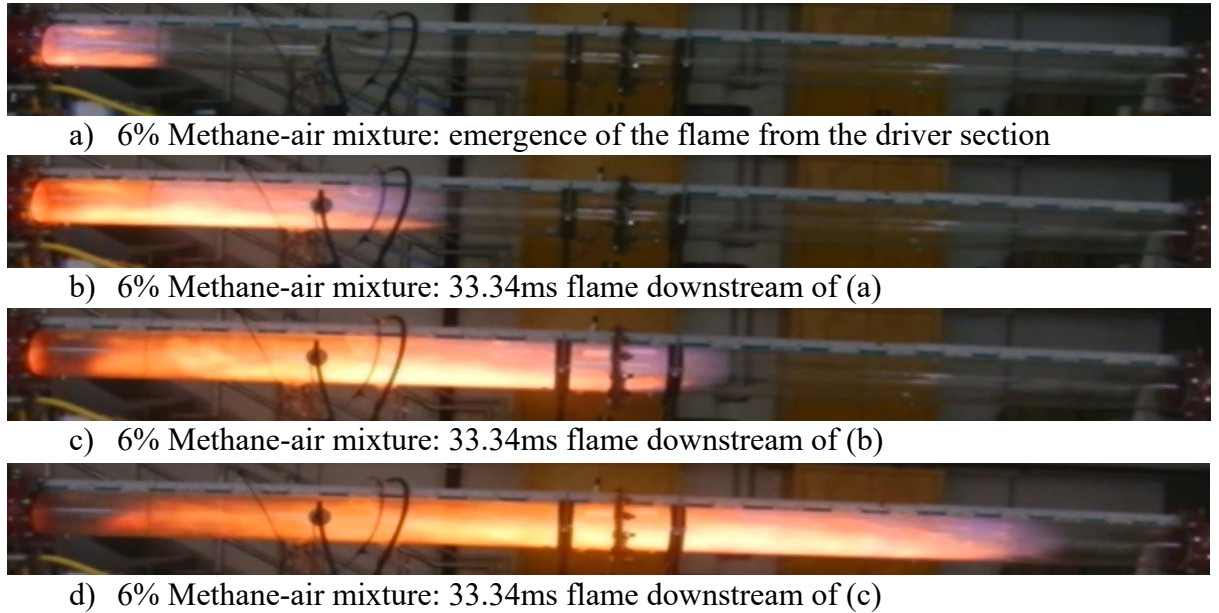


**Figure 5.8:** 6% flame propagation through 0.94mm mesh no water spray

The complete and incomplete combustion regions were the two distinct separation regions observed as indicated in the figures. The flame front profile formed a cone-like structure as the flame rejuvenates after passing through the obstruction. This behaviour of the flame rejuvenation can be observed in Figure 5.8 (b, c and d) presented.

### 5.3.2 Flame propagation through the mesh at 7 % mixtures

Figure 5.9 (a, b, c, and d) presented qualitatively the results obtained for the methane-air combustion at 7 %. It was observed that the trends of the flame propagation through the same size (0.94 mm) wire mesh shows a similar behaviour while compared with the combustion of 6% methane-air mixture. In Figure 5.9 the appearance of the flame into the clear section of the combustion tube is separated in two distinctive regions. However, the effect of the obstruction due to wire mesh was more pronounced in this case. This effect due to obstruction can be seen in Figure 5.9 (a), as the flame front emerges into the transparent section of the tube, a slow movement of the flame was observed. The two distinct regions of complete and incomplete combustions were indicated in this case by a short pale blue zone and a trailing yellowish flame respectively. Although, the flame shape changes are roughly the same, though there are some differences due to the flame scattering and rejuvenation dynamic which results from the effect of steel wire mesh installed.

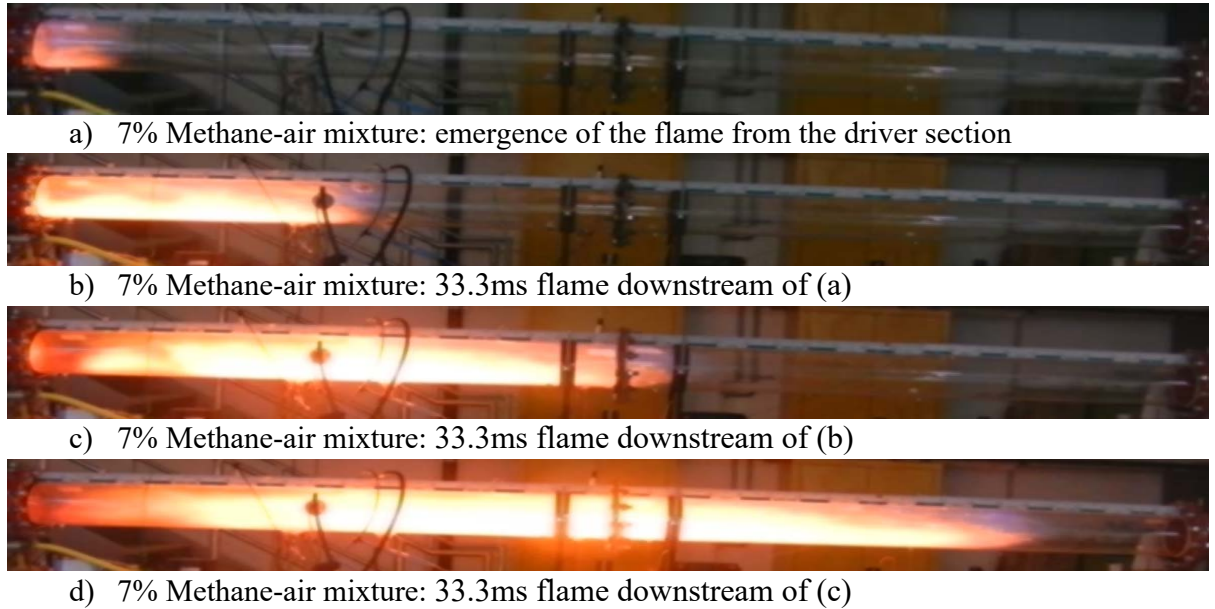


**Figure 5.9:** 7 % flame propagation through 0.94mm mesh no water spray

### 5.3.3 Flame propagation through the mesh at 9 % mixtures

Figure 5.10 (a, b, c, and d) shows a sequence of the flame images at 9 % methane-air combustion passing through 0.94 mm wire mesh.

As presented in Figure 5.10, the observed trends from the flame propagation through the woven wire mesh indicate that the colour of the flame varies significantly with an increase in methane concentration. Also, it can be seen from the onset that as the flame propagates through the mesh, an unstable combustion region appears which was represented by the different colours appearing at the same time.

It can be seen from Figure 5.10 (a) that the flame appears to be very bright from the onset with traces of dark yellow at the middle with the top of the flame (flame front) being blue. The flame appears in a cone-like shape with a fairly smooth flame front. This behaviour indicates incomplete combustion occurred as the flame hit the mesh and methane fuel were burnt completely at the tip of the flame. Additionally, it was observed that the flame obstruction due to the wire mesh installed, causes flow resistance of the methane-air mixture. This obstruction led to the reduction in the flame front speed and burning rate as it emerges into the transparent tube.

As flame propagates further as illustrated in Figure 5.10 (b, c, and d), the brightness of the flame continues to increase, and flame front remains blue until the end of combustion where the end flange had fallen off, and the flame diffuses into the surrounding. The behaviour is

affected by the scattering nature of the flame as it passed through the wire mesh, high turbulent intensity and high energy were released.

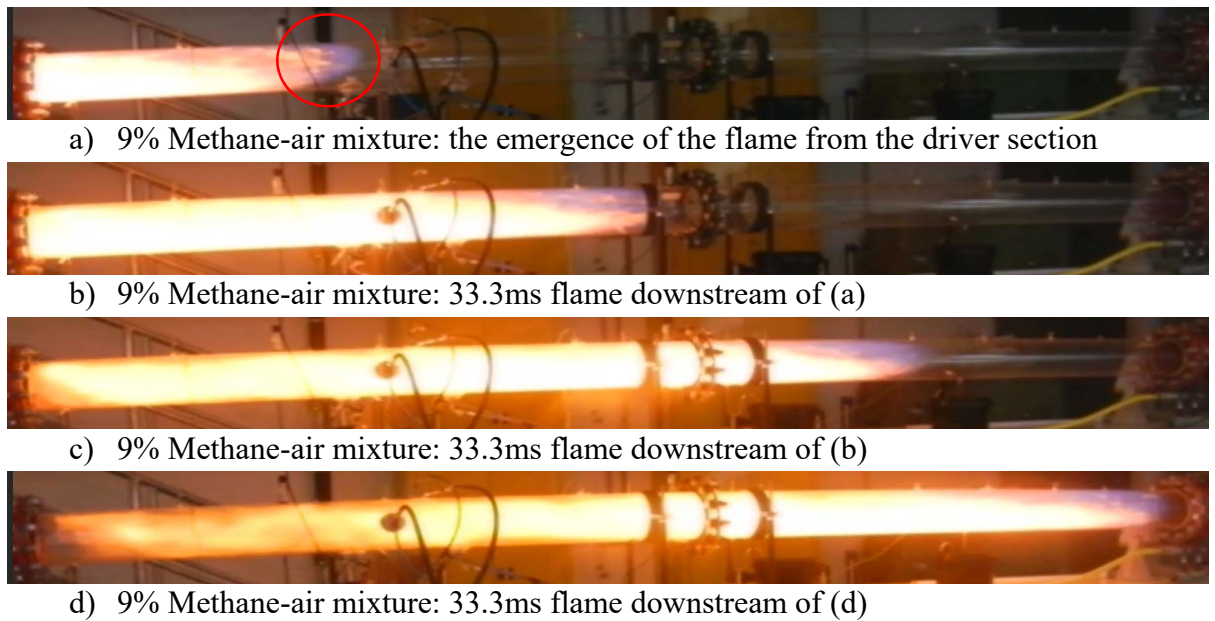


**Figure 5.10:** 9 % flame propagation through 0.94mm mesh no water spray

### 5.3.4 The average Flame speed with 0.94mm Mesh and No water spray

The average flame speed was obtained with the insertion of the woven wire mesh 0.94 mm. The series of results obtained provide flame images and the results relating to the effect and performance of the mesh on the propagated flame. That is, the flame propagated in the presence of an obstacle travelling from the right-hand side of the FPMR to the left-hand side of the rig. However, this is still a dry experimental trial without water spray.

Table 5.2 shows the average flame speed for various methane-air flames with woven wire mesh 0.94mm aperture installed. Using the same technique for measurement and calculation of flame speed as described in subsection 5.2.1, it is obvious that the insertion of the mesh shows a decrease in flame speed, when compared to the previous runs (that it no obstructions). This is a result of a heat sink due to the steel mesh and to the pipe wall. Figure 5.11 and Table 5.3 represents the comparison of the average flame speed with and without mesh installed.

The decrease in flame temperature and subsequent decrease in flame speed is also observed comparing TC-4 temperatures in figure 5.7 and figure 5.10. For instance, comparing TC-4 thermocouple temperatures for each scenarios, the maximum temperatures recorded in figure 5.7 (a) and (b) 247°C and 256°C in TC-4 thermocouple respectively while in figure 5.10 (a),

(b) and (c) shows the peak temperatures in TC-4 thermocouple 134°C, 136°C, and 149°C respectively. However, comparing TC-3 thermocouples temperatures in figure 5.5 and 5.10, TC-3 maximum temperatures recorded in figure 5.5 (a), and (b) are 149°C, and 152°C while TC-3 peak temperature in figure 5.10 (a), (b), and (c) are 42°C , 38°C, and 37°C respectively. The great reduction in temperatures in TC-3 thermocouples is due to heat loss to the steel mesh by conduction. As the flame pass through the aperture of the mesh, the flame will scatter thereby causing a decrease in the flame speed.

**Table 5.2:** Average flame speed for various methane-air mixtures

Methane/air mixture (%)	Distance travelled by flame (mm)	Time travelled (ms)	Average flame speed (m/s)
6	3.400	0.167	20.36
7	3.800	0.167	22.75
9	3.100	0.133	23.31

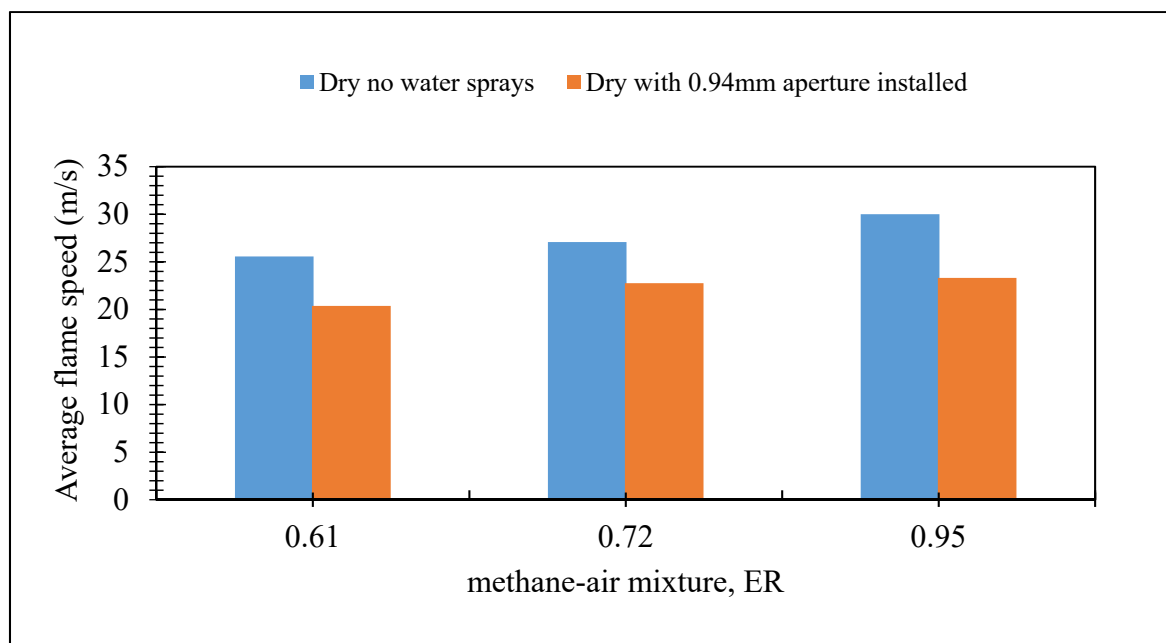


**Figure 5.11:** Flame speed for various methane-air mixtures with 0.94mm mesh & no sprays

**Table 5.3:** Flame speed comparison with mesh installed and no water sprays (dry)

<b>Methane/air mixture (%)</b>	<b>The average flame speed with no mesh and no sprays (m/s)</b>	<b>The average flame speed with 0.94mm mesh installed (m/s)</b>
6	25.56	20.36
7	27.07	22.75
9	30.00	23.31

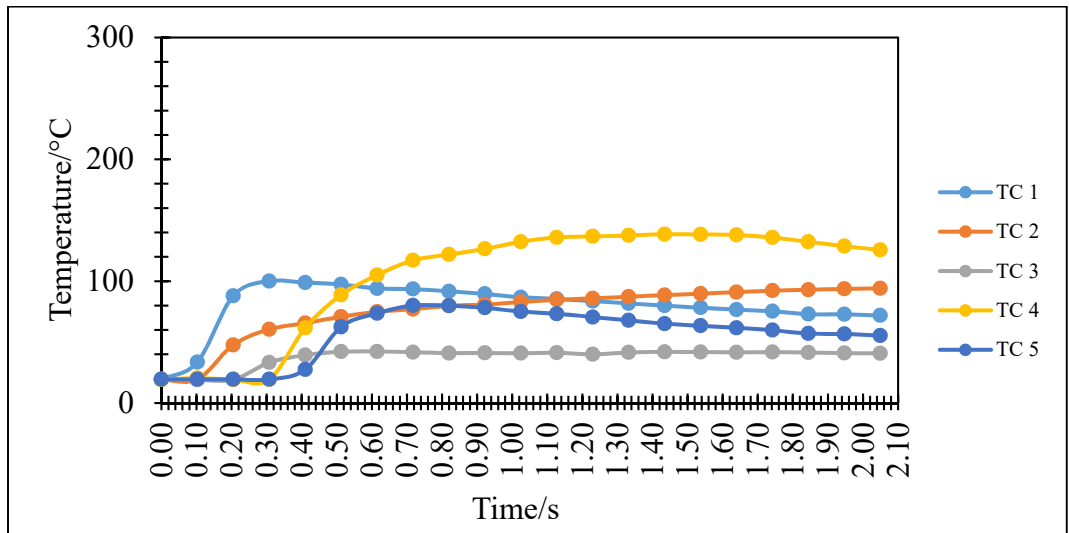
### **5.3.5 Time – Temperature Profile with 0.94mm woven wire mesh**

The thermocouple data reading for the dry experimental test but with 0.94mm diameter mesh in position for three different methane/air concentrations as shown in figure 5.5, 5.6, and 5.7 revealed the temperature of the hot gas with the corresponding time frame. However, it can be seen that in each scenario, the flame produce similar temperature profile with the exception that slightly higher temperatures were recorded in the fourth thermocouples (TC-4). This is due to the development of the flame from a flash fire to the fully developed flame which gradually declines down until a stable temperature was recorded.

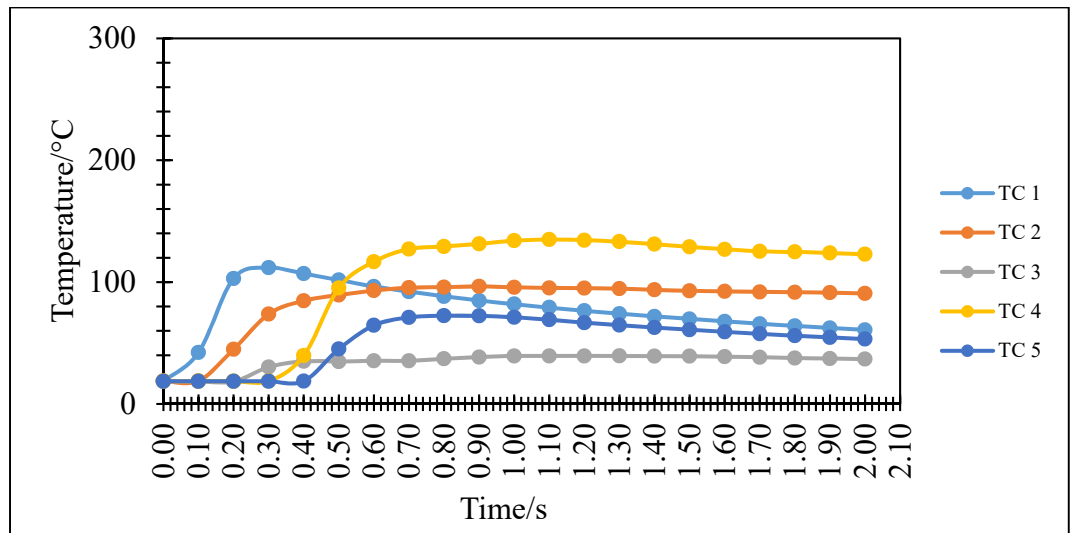
#### **5.3.5.1 Temperature profile at 6, 7 and 9 % methane-air combustion**

Figure 5.12, Figure 5.13 and Figure 5.14 present the thermocouple output data at 6, 7 and 9 % methane-air combustion with 0.94 mm steel wire mesh inserted. The time-temperature profile across the five thermocouples (TC-1 to TC-5) fixed along the length of the tube spaced at a specified interval are used to obtain the flame temperatures.

It can be seen from Figure 5.12, Figure 5.13 and Figure 5.14 that the maximum temperature was observed at TC-4 (105.05°C, 116.78°C and 130.62°C with their corresponding times 0.61s, 0.61s and 0.61s respectively). This observation is due to flame scattering as it passes through the mesh and some heat sink to the mesh and pipe wall and flame regeneration before exiting the combustion tube causes a rise in temperature in TC-4. As the flame temperature decreases, in the presence mesh, it then increases as the flame was not extinguished, but it can clearly be seen from the Figure 5.12, Figure 5.13 and Figure 5.14 f that the effect of the mesh is noticeable. The temperature of flame which passes the steel wire mesh is lower than the temperature of flame before the metal wire mesh similarly reported by [73].



**Figure 5.12:** Methane-air combustion at 6% with 0.94 mm mesh



**Figure 5.13:** Methane-air combustion at 7% with 0.94 mm mesh

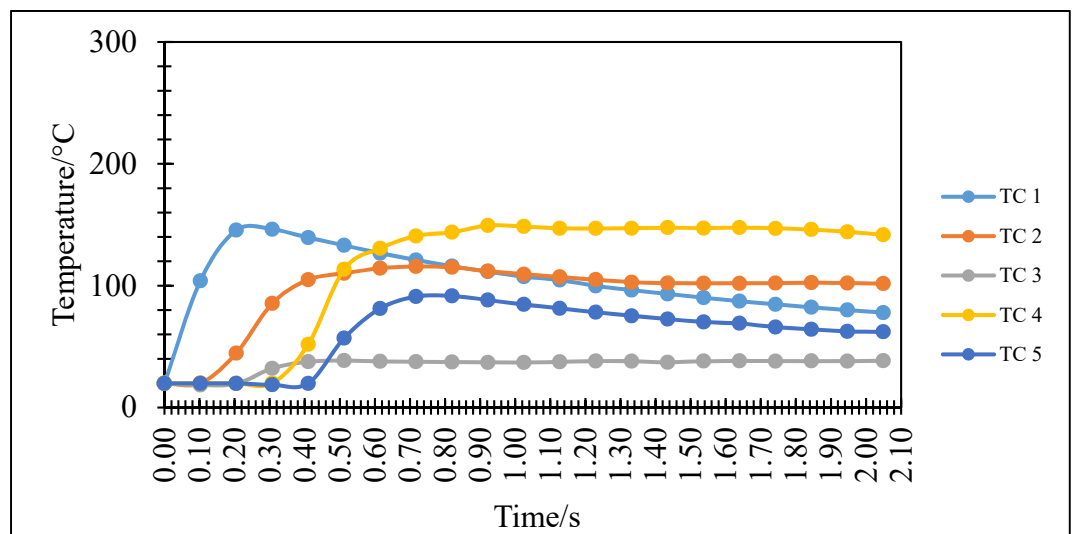


**Figure 5.14:** Methane-air combustion at 9% with 0.94 mm mesh

### **5.3.6 Effect of the Mesh on the flame propagation**

The flame temperature (the temperature of the hot gases) that passes the woven wire mesh is lower than the temperature of the flame before the wire mesh as in the case of TC-1 and TC-2. As shown in Figure 5.12, Figure 5.13 and Figure 5.14, TC-3 recorded the minimum or lowest temperatures of (39.28, 39.78 and 37.61°C with 0.41, 0.41 and 0.41s). This behaviour shows that there is a great decrease in temperature when compared with the dry scenario which has a maximum temperature of 149°C. This behaviour is attributed convective heat loss to the wire mesh, and considering the fact that the beginning part of the combustion tube is made up of carbon steel metal, some heat could be driven to the wall by conduction since the beginning of the tube is made up of mild carbon steel.

The overall flame speed in the presence of an obstacle (i.e. 0.94mm mesh installed), are lower when compared with the free flame propagation (i.e. without any obstruction). The decrease in flame temperature decreases the flame speed as well. As shown in figure 5.6, the flame speed decreases greatly from 25.56m/s to 20.36m/s, 27.07m/s to 22.75m/s and 30m/s to 23.31m/s for 6%, 7%, and 9% mixtures respectively.

### **5.3.7 Temperature Comparisons with 0.94 mm mesh and Dry case**

Figure 5.15 shows the comparisons of thermocouple temperatures with free flame propagation (no obstruction) and flame propagation with an obstruction (0.94 mm mesh). It can be seen that TC-1 temperatures are very similar, but there is a significant difference in TC-2 temperatures. This difference is attributed to convective heat loss to steel wire mesh. While in TC-3 temperature, there is a rapid decrease in temperature. While this drastic drops in TC-3 temperature are completely attributed to the wire mesh because some heat was a loss to the wire mesh. The mesh also affected TC-4 temperatures because as the flame passes through, it takes a few milliseconds to rejuvenate thereby causing an increase in TC-4 temperature. However, TC-5 maintains a similar flame temperature as can be seen from

Figure 5.15.

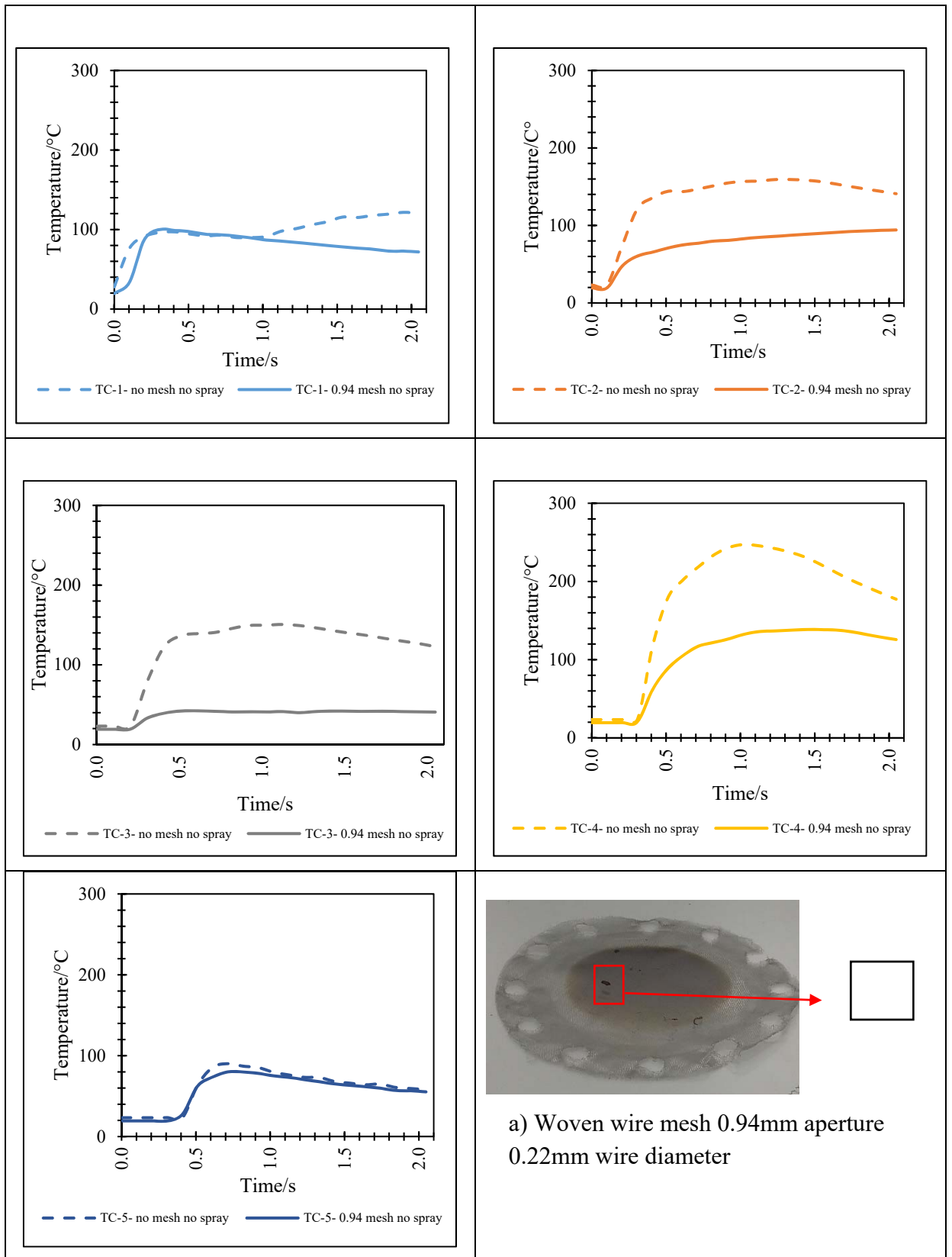


**Figure 5.15:** Comparison of 6% temperature profile with 0.94 mm mesh and dry case.

## 5.4 Woven wire mesh (0.94mm) installed and Water sprays activated

In this experimental trial, woven wire mesh (0.94mm aperture) was installed in combination with four cross flow spill return atomisers activated. The mesh position is indicated in Figure 5.16, and Figure 5.17 illustrates the cross flow SRA's configuration.

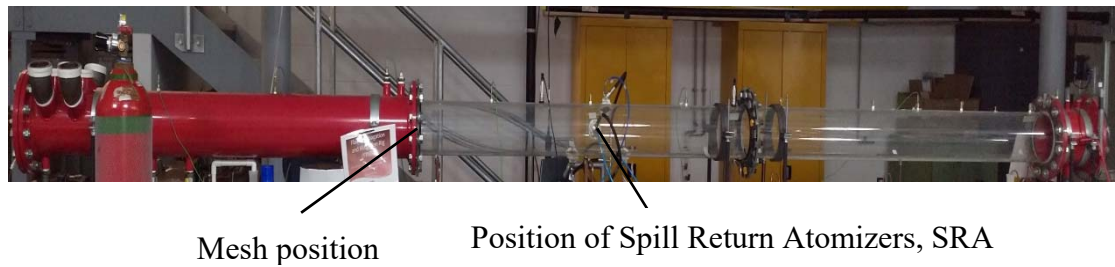


**Figure 5.16:** SRA's Position within the tube 3100mm from the start of ignition

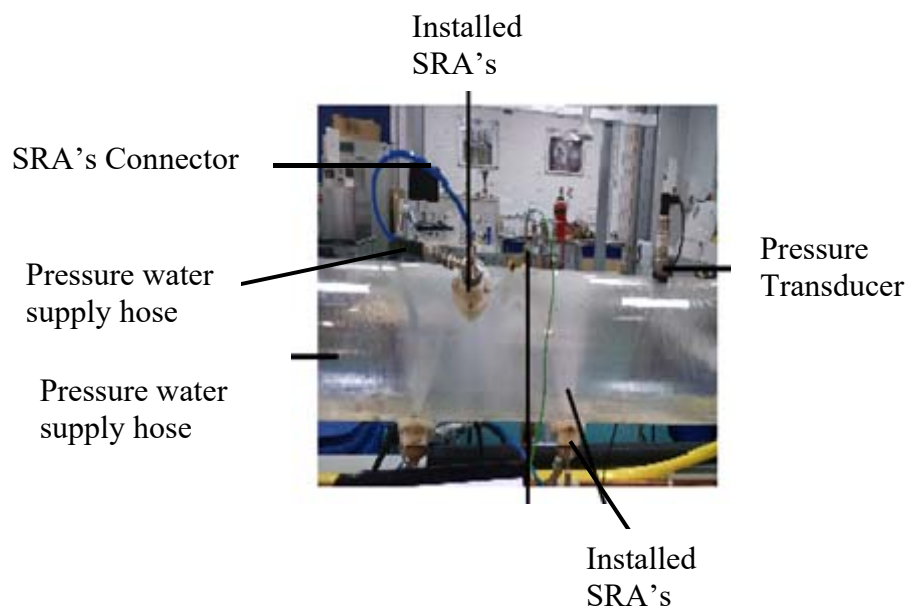


**Figure 5.17:** SRA's position and spray water

In this configuration, the mesh and the SRA's were subjected to three different methane-air mixtures of 6%, 7%, and 9%. With the 0.94mm mesh installed, the SRA's were supplied with water at the pressure of 130bar. The experimental rig was then filled with various (6%, 7% & 9%) methane-air mixtures and allowed to become quiescent for a minute. Table 4.1 shows the Sauter mean diameter  $D_{32}$ , liquid volume flux, mean droplet velocity and the woven wire size.

**Table 5.4:** Exit orifice of SRA's downstream

Mean $D_{32}$ ( $\mu\text{m}$ )	Mean liquid volume flux ( $\text{cm}^3/\text{s}/\text{cm}^2$ )	Mean droplet velocity (m/s)	Woven wire mesh (mm)
26	0.024	21.4	0.94mm

The experiment was conducted sequence with a mesh in position and atomisers, (SRA's), the following series of results were obtained which provides series of data, images from the flame propagation, and the results relating to the flame propagation passing through an obstacle in a confined area. The selected images from high definition (HD) video camera (Nikon) were processed, edited and time coded using Adobe Photoshop CC 2017.

#### 5.4.1 6 % Flame Evolution with 0.94 mm Mesh and Sprays

Figure 5.18 shows qualitatively a sequence of flame images at 6 % methane-air combustions with 0.94 mm mesh and water sprays. It can be seen from Figure 5.18 that as the flame propagates into a clear section of the combustion tube, it appears in three colours: dark yellow from the onset, pale blue at the middle and bluish flame front. According to literature, a blue flame indicates a region of complete combustion while a yellow colour indicates a region of incomplete combustion [76]. Since the flame propagates through the steel mesh, there is convective heat transfer to the wire mesh and to the pipe wall. This observation gives move advantage to flame been quenched upon reaching the spray position, and the flame dies off completely as shown in Figure 5.18.

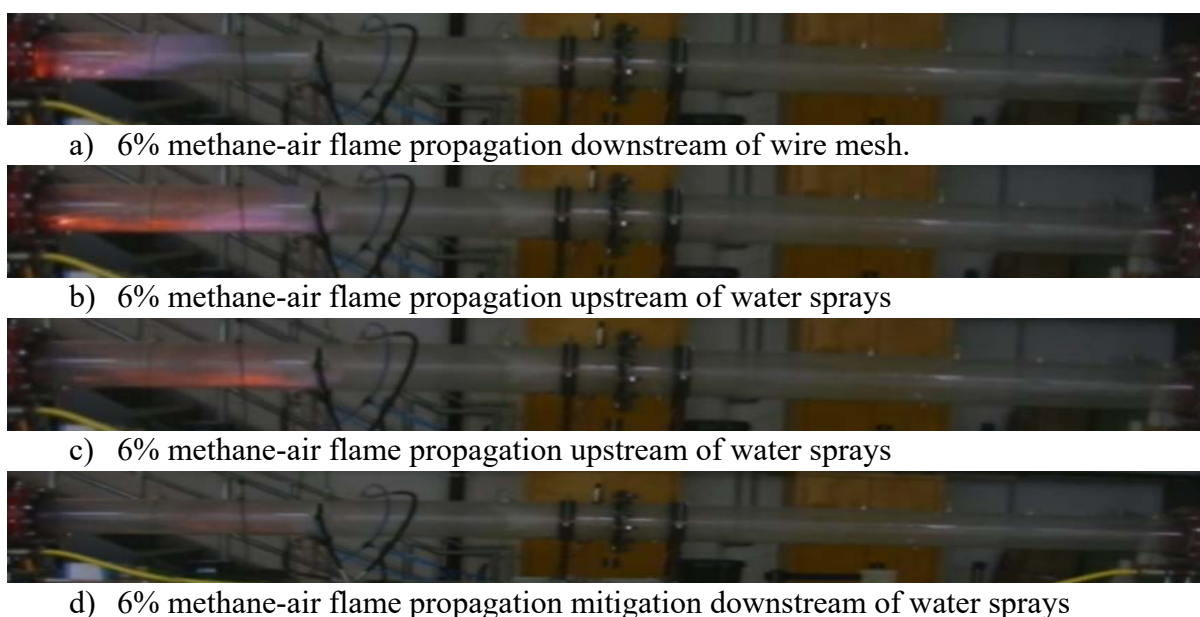


**Figure 5.18:** 6 % Methane-air combustion through 0.94 mm mesh and spray

### 5.4.2 Flame Speed with 0.94mm mesh and water sprays

The average flame speed was measured at downstream of the mesh and both upstream and downstream region of water spray as shown in Table 5.5.

In 6 and 7% methane-air mixtures, with the 0.94mm mesh installed and water sprays activated, the average flame speeds were 6m/s and 10.45 m/s. The methane-air of 6 and 7% were fully mitigated with no further flame propagation downstream and a great decrease in flame speeds, when compared to the runs involving 0.94mm wire mesh only and dry (no obstruction) cases as discussed in sections 5.6.1 and 5.7.2.

**Table 5.5:** The average flame speed at 6 and 7% methane-air mixtures

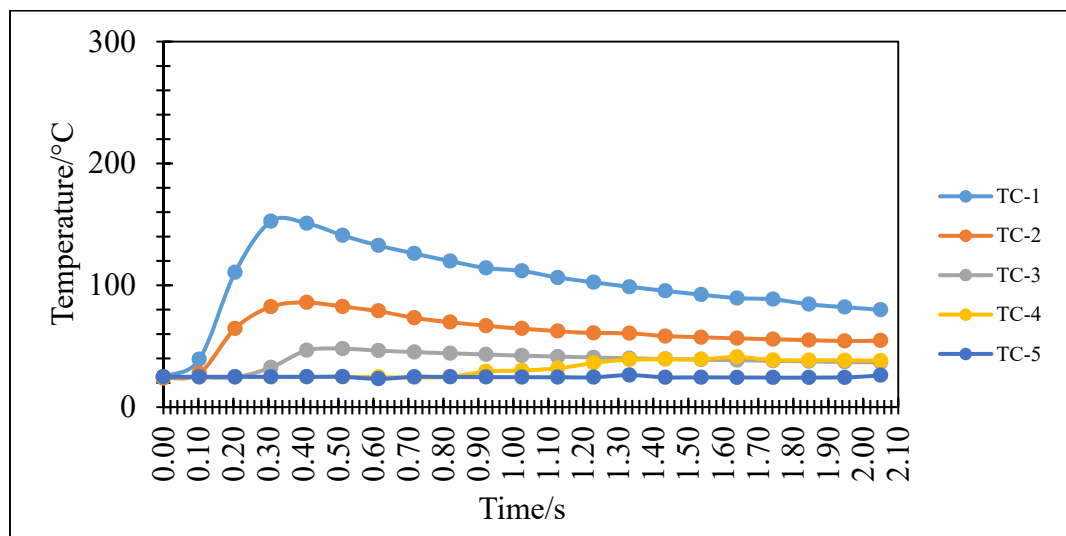
Methane/air mixture (%)	Distance travelled by flame (m)	Time travelled (s)	Average flame speed (m/s)
6	0.800	0.133	6.00
7	0.700	0.067	10.45

### 5.4.3 Time – Temperature Profile

Figure 5.19 shows the temperature variation across each thermocouple TC-1, TC-2, TC-3, TC-4 and TC-5 with 0.94 mm woven wire mesh and fine water sprays activated. The results obtained presents similar trends of time-temperature profile reported in sub-section 5.2.3 and 5.3.5.

It is observed from Figure 5.19 that a sudden rise in temperature from room temperature to about 152°C for TC-1 as the ignition commences, and then gradually decaying until the temperature stabilised at 79°C. However, other thermocouples located along the 6300mm long indicated a lower temperature sequentially, with a further decrease from TC-1 to TC-2, TC-2 to TC-3, and afterwards, a uniform temperature was recorded from thermocouples TC-4 and TC-5. However, the behaviour of the trends as the expected increase in temperature when the ignition commenced which resulted in the temperature for TC-1, which is due to excessive energy released as reported in similar studies [77, 78]. The overpressure growth in the explosion resulted in the flame moving towards the remaining parts of the tube with lower pressure, and as a result, the temperature begins to decline due to sudden expansion.

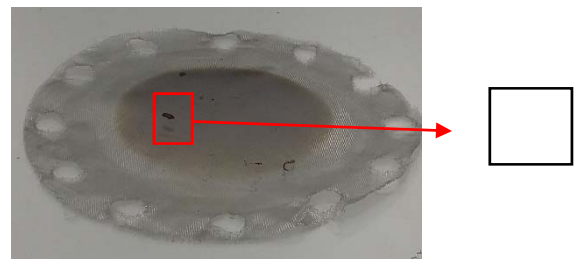
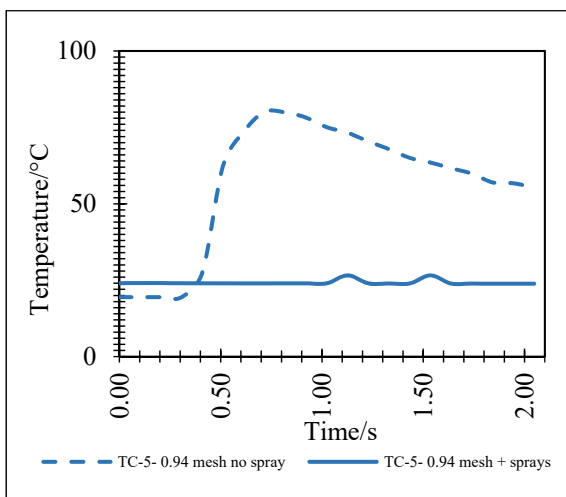
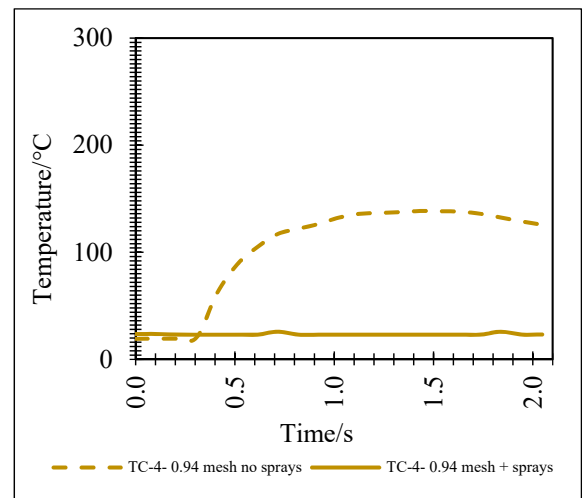
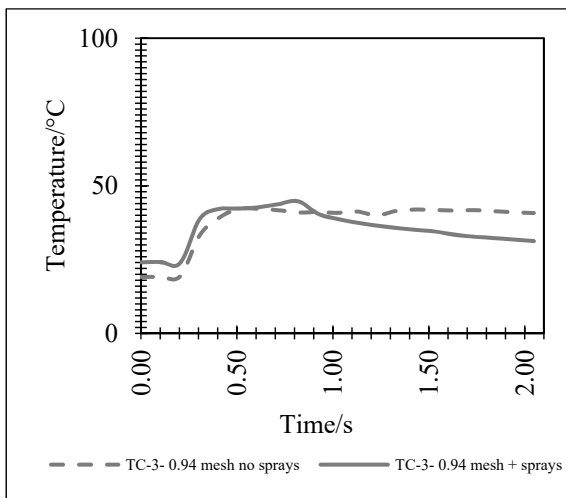
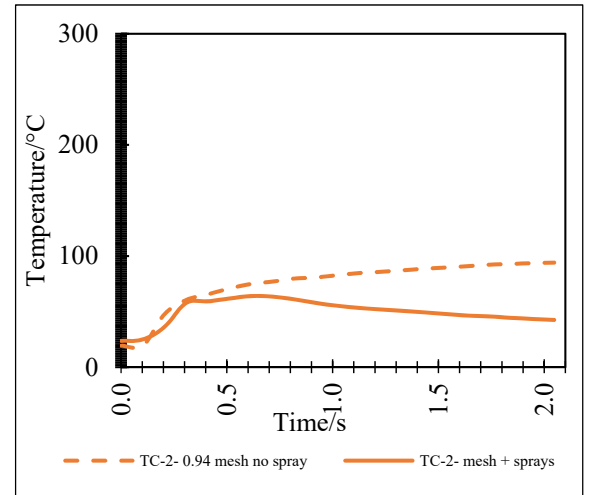
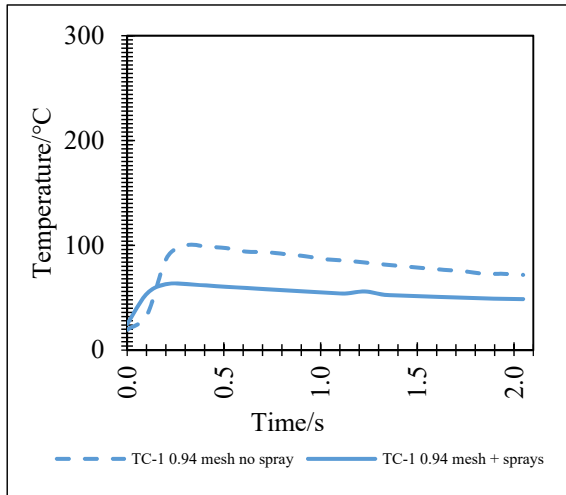
As flame propagates from the upstream of the wire mesh, through the mitigation zone and then quenches due to the influence of the fine water sprays. Therefore, the flame was not captured downstream as illustrated in Figure 5.19. As the flame propagated through the aperture of the mesh, it could be scattered and decreases the flame speed to some specific amount, and upon meeting the fine sprays barriers, the flame extinguished and greatly reduces the flame speed to 6.00m/s. Also, it indicates a significant fall in TC-3 temperature to about 46°C. This is due to heat loss wire mesh and to the wall of the tube and considering the fact the beginning section of the pipe is made up of carbon steel metal, which could drive some significant heat loss by conduction.



**Figure 5.19:** Time-Temperature profile at 6% CH<sub>4</sub>/Air combustion with 0.94 mm mesh plus sprays

#### 5.4.4 Effect of the mesh combined with sprays

It is clearly observed that the heat loss to the woven wire mesh has drastically reduced the flame temperature and as such enhance the quenching effect of 6 % mixture when the flame meets the fine sprays barrier. However, the retardation in flame speeds upon coming in contact with the flame put the off flame and quenches completely.



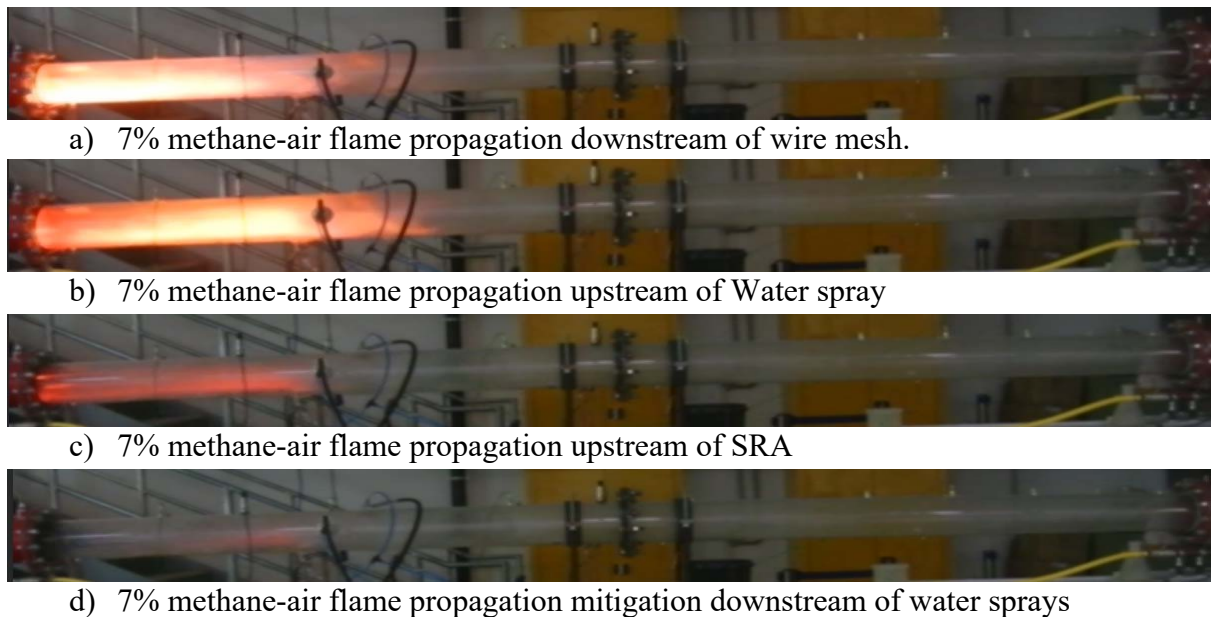
a) Woven wire mesh 0.94mm aperture  
0.22mm wire diameter

Figure 5.20: Thermocouple temperature profile comparison with 0.94 mm mesh plus sprays.

### 5.4.5 7% Flame Evolution with 0.94 mm Mesh and Sprays

Figure 5.21 shows qualitatively a sequence of flame images at 7 % methane-air combustions with 0.94 mm mesh and water sprays. It can be seen from Figure 5.21 that as the flame propagates into a clear section of the combustion tube, a very brighter (yellow) flame appears from the onset and this behaviour results from incomplete combustion.

As the flame propagated through the aperture of the mesh, it's scattering nature decreases the flame speed to some specific amount, and upon meeting the fine sprays barriers, the flame extinguished.



**Figure 5.21:** 7 % Methane-air combustion through 0.94 mm mesh and spray

### 5.4.6 Time – Temperature Profile

It can be seen from Figure 5.22 that a similar trend of temperature profile are observed. At the time 0.31 s, the peak temperature of about 123.71°C was observed at TC-1 and then gradually decaying until the temperature stabilised. However, other thermocouples located along the 6300mm long indicated a lower temperature sequentially, with a further decrease from TC-1 to TC-2, TC-2 to TC-3, and afterwards, a uniform temperature was recorded from thermocouples TC-4 and TC-5. However, the behaviour of the trends as the expected increase in temperature when the ignition commenced which resulted in the temperature for TC-1, which is due to excessive energy released as reported in similar studies [77-80].

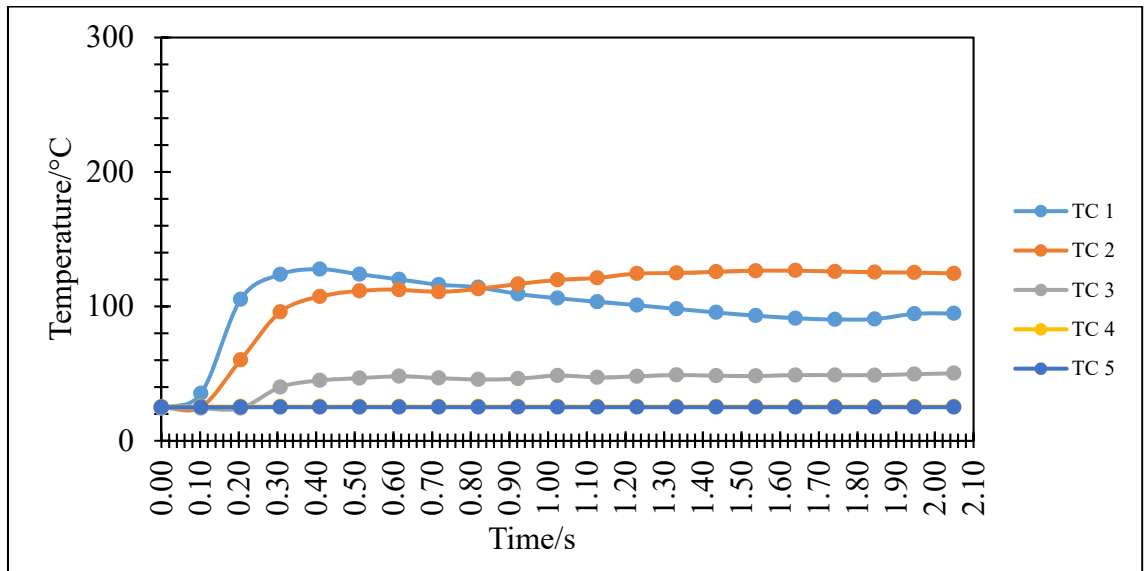


**Figure 5.22:** Temperature profile at 7% combustion with 0.94 mm mesh + sprays

### 5.4.7 Time – Temperature Profile at 9% mixture plus sprays

Figure 5.23 illustrates the temperature-time variation across each thermocouple TC-1, TC-2, TC-3, TC-4 and TC-5 with woven wire mesh 0.94mm installed and fine water sprays activated. The results obtained presents similar trends of time-temperature profile reported in sub-section 5.3.5 and Figure 5.14. Although, the flame was not extinguished, but the effect of the mesh is clearly observed.

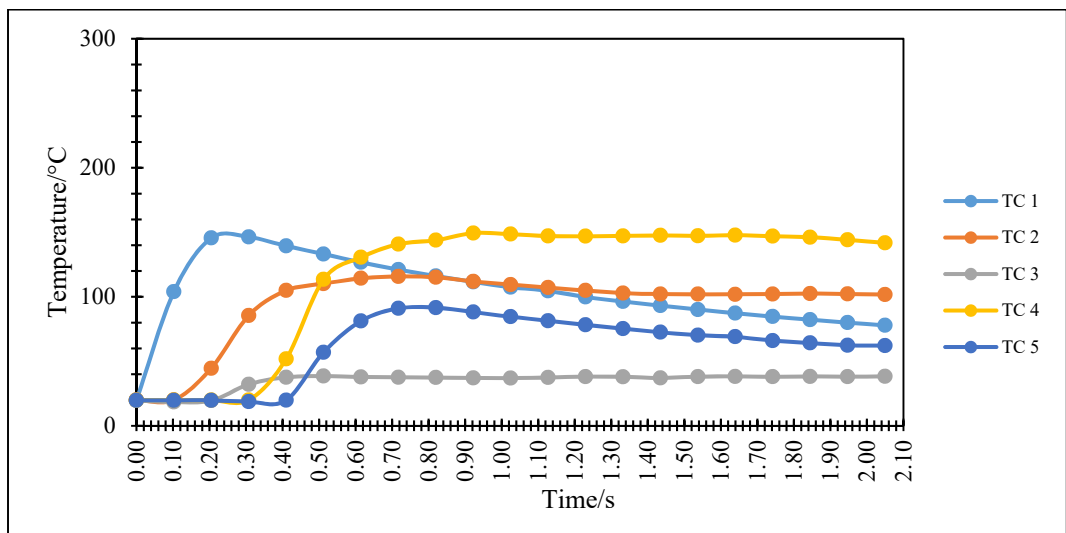


**Figure 5.23:** Temperature profile at 9% combustion with 0.94mm mesh + sprays

## 5.5 Woven wire mesh (1.31mm aperture)

The experimental rig was reassembled with the insertion of the woven wire mesh 1.31mm aperture. This trial was conducted without fine water sprays (the four-cross SRA's were deactivated).

### 5.5.1 Flame speed with woven wire mesh 1.31mm aperture only

The average flame speed was measured downstream of the mesh. Table 5.6 shows the average flame speed of three different methane-air concentrations. The average flame speed varies for each methane-air concentration. The flame accelerates upon the start of the ignition and decelerate to about 20.24m/s for 6% mixture, 19.04m/s for 7% mixture and 19.35m/s for 9% mixture when coming in contact with the mesh compared to flame propagation without an obstacle (mesh). During this period, the woven wire mesh (1.31mm mesh) has a significant influence or effect on flame propagation when compared with the free flame propagation. This is due to the scattering nature of the flame when passing through the mesh and heat conduction of the mesh material.

**Table 5.6:** Flame speed for 6%, 7%, and 9% with 1.31mm mesh no spray

<b>Methane/air mixture (%)</b>	<b>Distance travelled by flame (m)</b>	<b>Time travelled (s)</b>	<b>Average flame speed (m/s)</b>
6	3.400	0.168	20.24
7	3.200	0.168	19.04
9	3.250	0.168	19.35

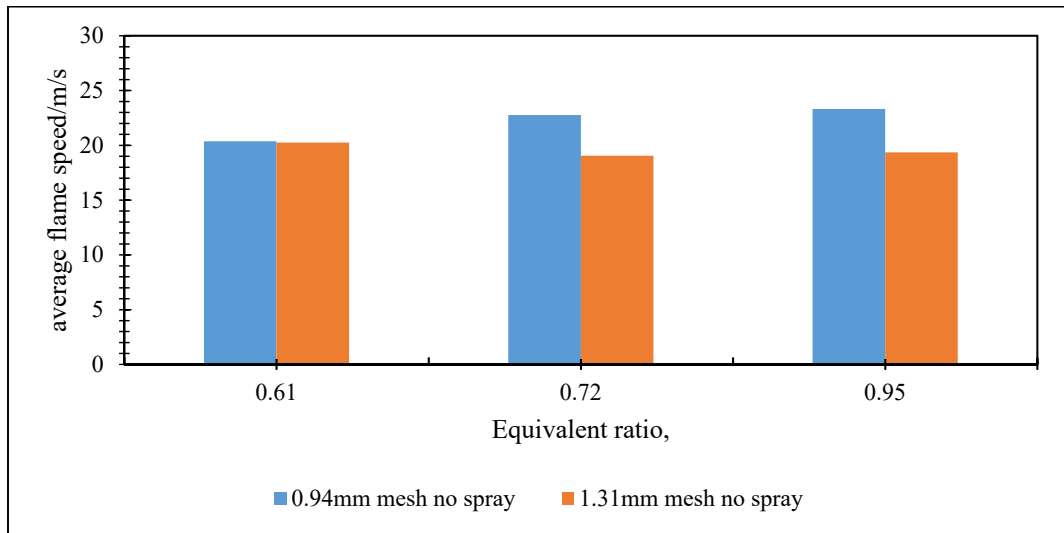


**Figure 5.24:** Comparisons of the average flame speed for various methane-air mixtures, ( $\phi$ ) with 0.94mm and 1.31mm mesh installed

Figure 5.24 and Table 5.6 shows the results of the average flame speed for three various methane-air mixtures of 6%, 7%, and 9% respectively. It was observed that changing the mesh sizes resulted in a decrease in the average flame speeds when compared with 0.94mm mesh previously discussed in section 5.7. This is attributed to the increase in the thickness of the mesh from 0.22mm to 0.28mm. A similar trend of increasing flame speed with a corresponding increase in concentration noticed when compared with the previous observation with 0.94mm mesh; it found that the average flame propagation speed varies with changes in equivalent ratios.

### 5.5.2 Flame propagation behaviour at 6% with 1.31mm mesh no sprays

Figure 5.25 shows a sequence of high-speed Nikon images of 6% methane-air flame propagation in a closed tube. The first image shows the onset of the flame through the woven wire mesh (1.31mm) (downstream of the mesh) into the transparent section of the tube (PMMA section).

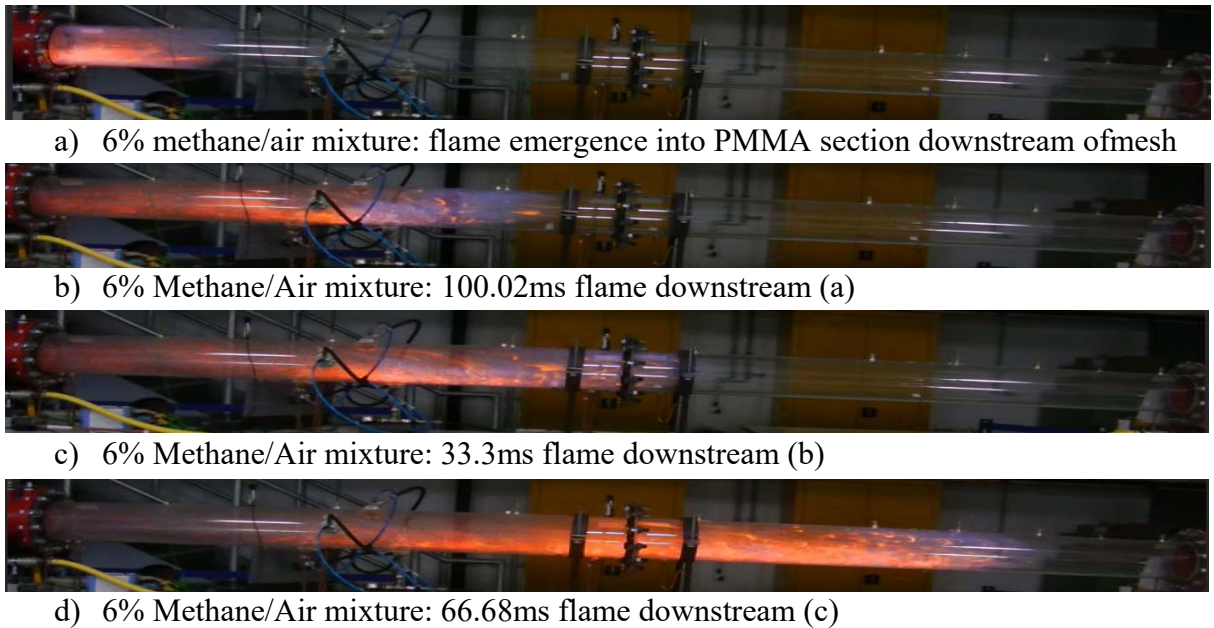


**Figure 5.25:** Flame propagation 6% mixture with 1.31mm mesh no water spray

### 5.5.3 Temperature – time profile

The time-temperature profile shown in Figure 5.26 presents the temperatures recorded over a short period of time approximately two seconds which was extracted from the raw temperature data. At the start of the ignition, there is a rapid increase in temperature to about 8°C measured at TC-1. This point illustrates the onset of combustion which is referred to as the ‘trigger point’. After this point, the inflexion point was established. Inflexion point is the point at which the heat is received from the hot zone refers to as pre-heat zone. (The distance between the trigger point and inflexion point is known as preheat zone).

As shown in Figure 5.26 the thermocouple output data at 6 % methane-air combustion with 1.31 mm woven wire mesh inserted. After the triggered point, the flame propagated through the narrow aperture of the woven wire mesh, which shows a profound effect because the flame decelerated due to the scattering of the flame when passing through the woven wire mesh.

It can be seen from Figure 5.26, when the flame propagated through the mesh, the temperature falls drastically from 95°C in TC-1 to 31°C in TC-3 which shows that there is a specific heat loss by conduction to the woven wire mesh and to the pipe walls across the length of the pipe until a stable temperature reached. At about 0.71 seconds, there was a great increase in temperature TC-4 to about 134°C. This is because the flame has rejuvenated and gained back some of its momentum.

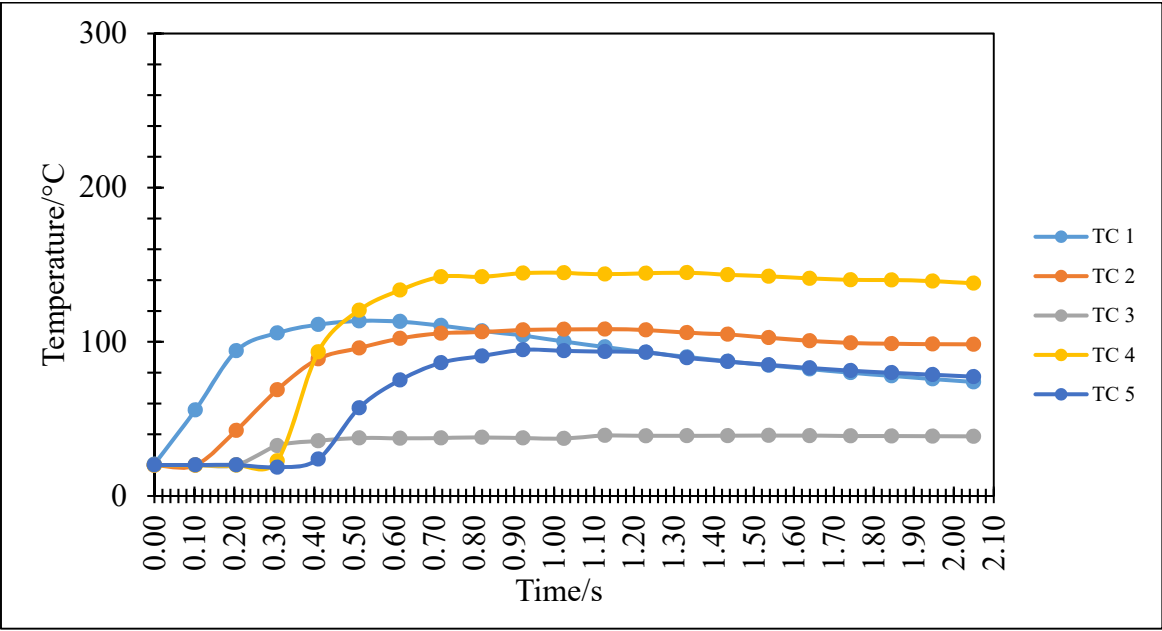


**Figure 5.26:** Time-Temperature responses of 6% mixture with 1.31mm mesh no sprays

## 5.6 Woven wire mesh (1.31mm aperture) plus water spray

Here the experiment was run with 1.31mm aperture installed with four cross spill return atomizers used for high-pressure water sprays activated as shown in figure 5.12. The mesh (1.31mm aperture) and SRA's were subjected to three different methane-air mixtures of 6, 7, and 9% methane concentration respectively. The atomizers were supplied with ordinary water at 20°C, and at the operating pressure of 130bar.

### 5.6.1 Average Flame speed

The average flame speeds were measured from the downstream of the mesh and upstream and downstream of the region of the water sprays as illustrated in Figure 5.28.

In 6, 7 and 9% methane-air mixtures, with the 1.31mm mesh installed and water sprays activated, the average flame speeds were found to be 4.49, 5 and 9 m/s as shown in Table 5.7 and Figure 5.28. The methane-air of 6, 7, and 9% were fully mitigated with no further flame propagation downstream and great decrease in flame speeds when compared to the previous runs discussed in sections 5.3, 5.3.1 and 5.3.2.

**Table 5.7:** Average flame speed for 6%, 7% and 9% methane-air mixtures

Methane/air mixture (%)	Distance travelled by flame (m)	Time travelled (s)	Average flame speed (m/s)
6	0.300	0.067	4.49
7	0.500	0.100	5.00
9	0.900	0.100	9.00

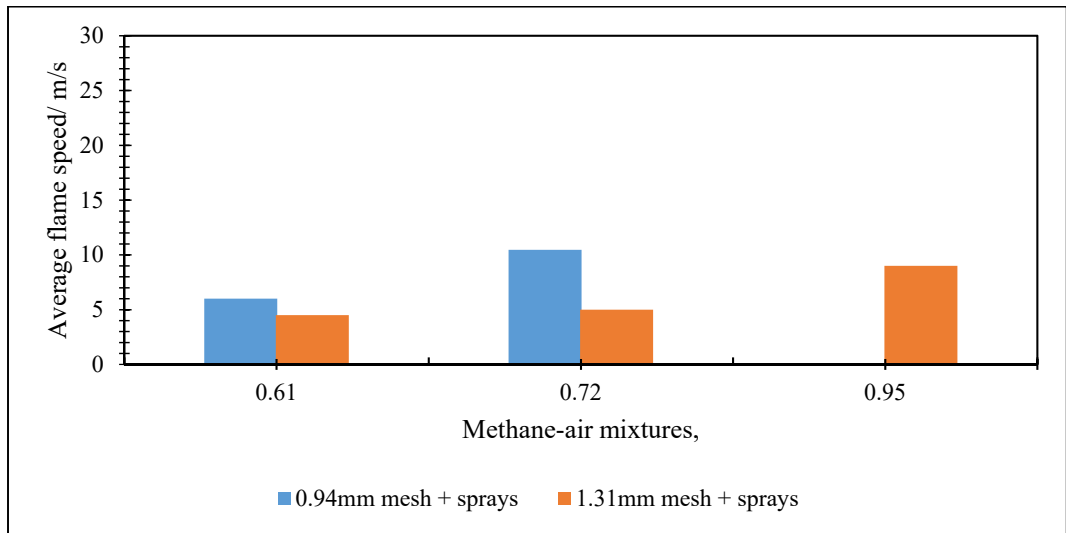


**Figure 5.27:** Comparisons of average flame speed with various methane-air mixtures (6, 7, and 9%) with 0.94mm mesh plus sprays and 1.31mm mesh plus water sprays fully mitigated

### 5.6.2 Flame propagation behaviour at 6% with 1.31mm mesh + sprays

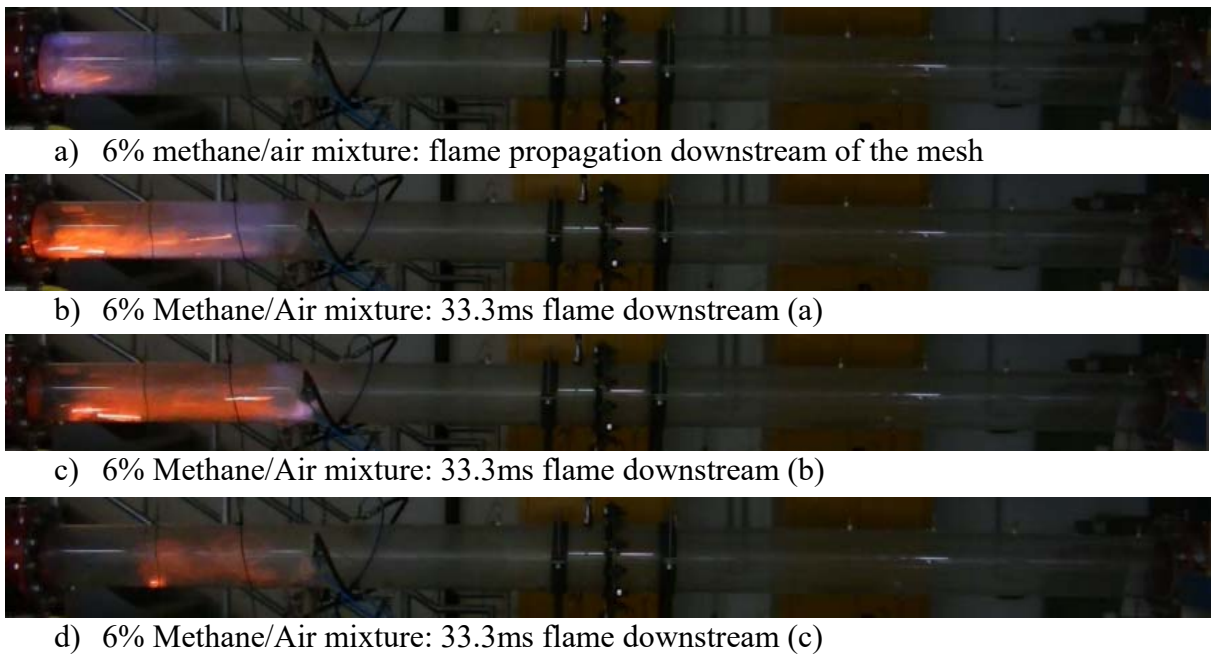


**Figure 5.28:** Flame propagation 6% mixture with 1.33mm mesh and plus sprays

### 5.6.3 Temperature – time response at 6% with 1.31mm mesh + sprays

Figure 5.29 indicates a similar trend of temperature variation shown in Figure 5.18. Thermocouple (TC-3) has maintained a similar range of temperature during the 2.0ms duration. This is particularly relevant as propagating flame were not allowed beyond the atomizers position, thereby limiting its speed, at the same time enabling thermal

accumulation around the initial length of the tube due to ineffective heat transfer compared to the non-mitigated propagating flames. As the flame passes through the mesh and subsequently the third thermocouple which decreases the flame temperature to 39.0°C due to heat loss by conduction to the mesh. The energy balances around the water sprays and the opposing flame were reduced by the cooling sensation of the water spray, and more significantly, the latent heat of vaporization of the water, which was transferred from the flame, thereby causing a significant reduction in temperature at those two thermocouples. Since the flame did not propagate further the TC4 and TC5 maintain stable temperatures when compared to figure 5.13.

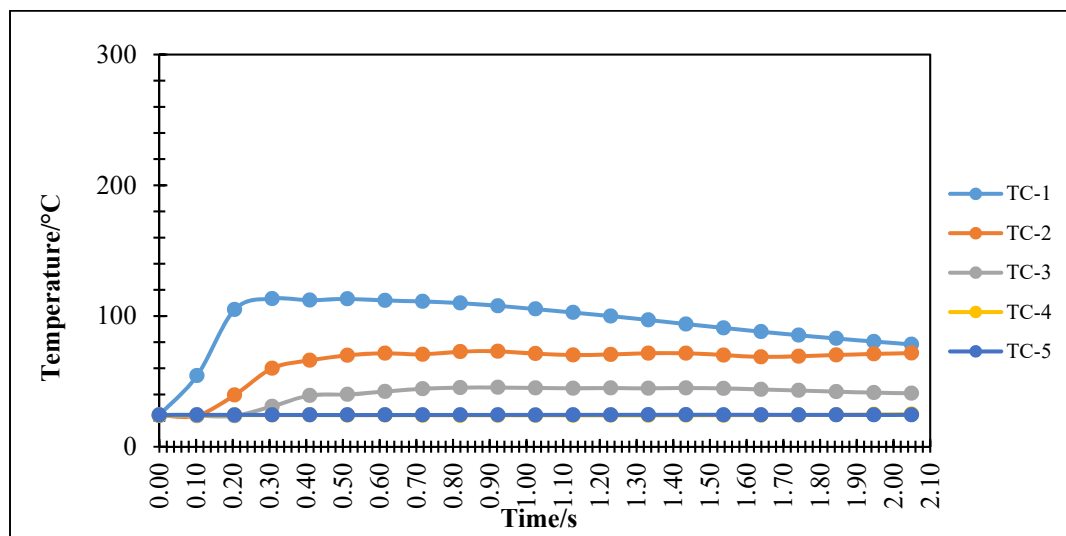
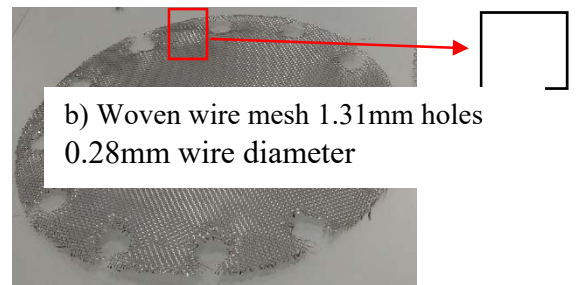
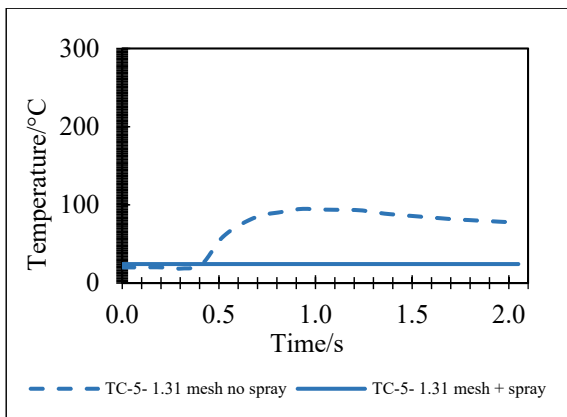
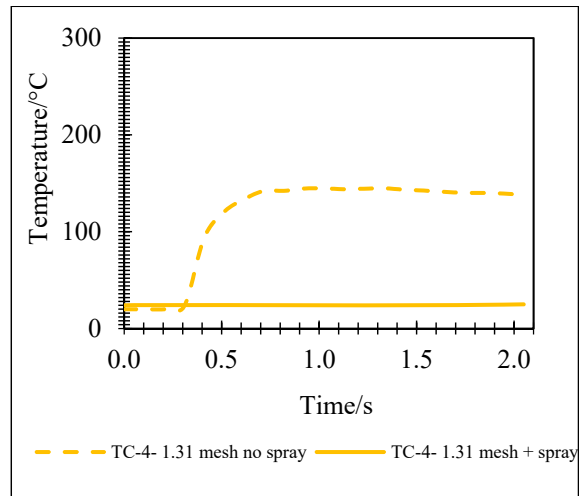
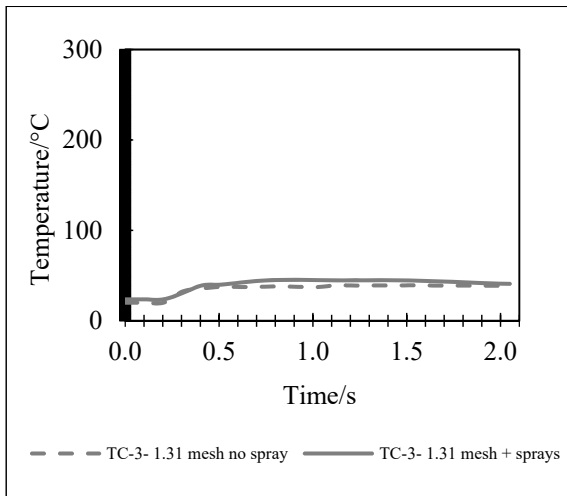
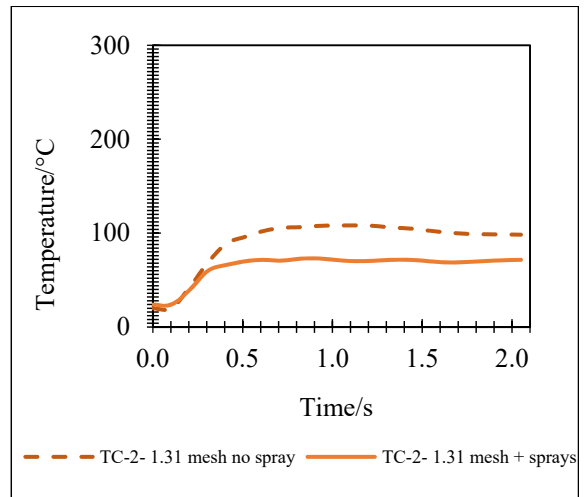
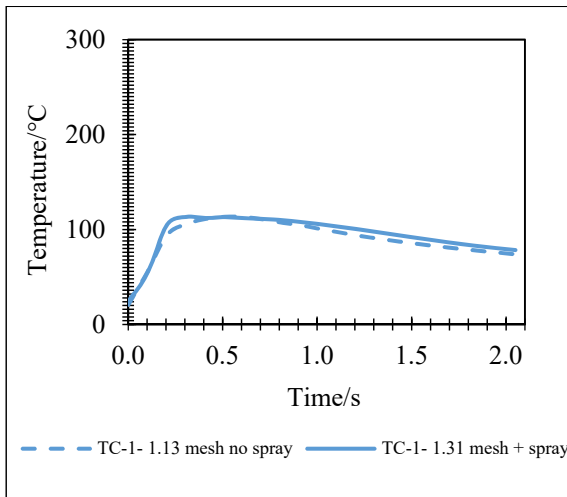


Figure 5.29: Time-Temperature profile at 6% combustion with 1.31mm mesh + sprays

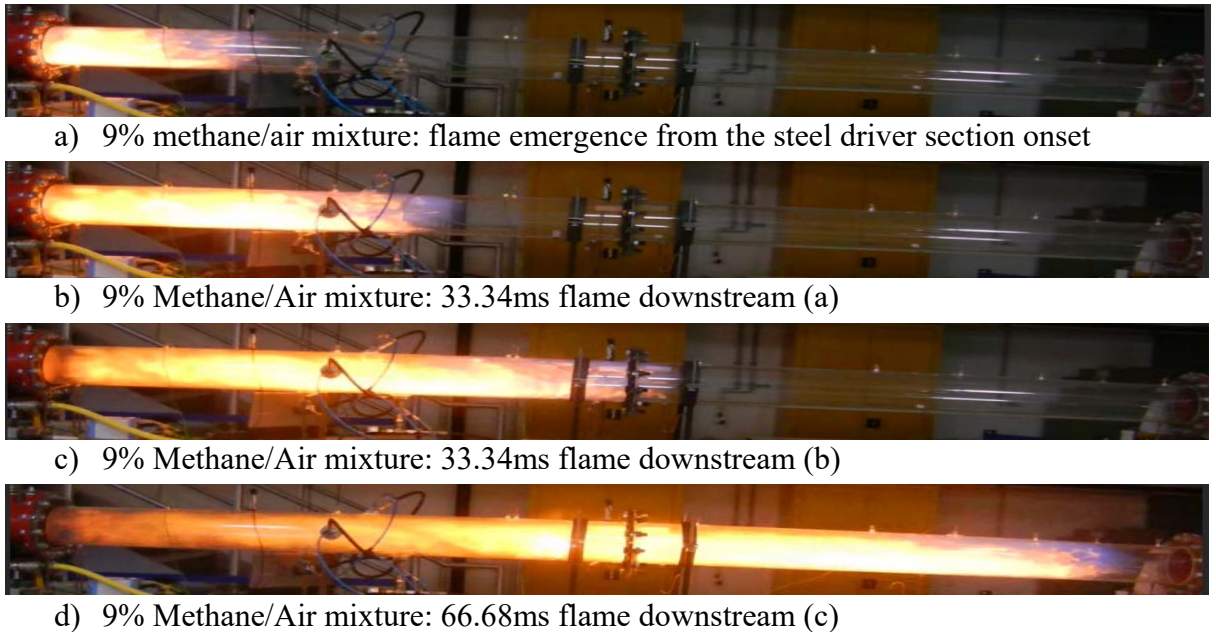
### 5.6.4 Comparisons of individual thermocouples

Figure 5.30 shows the comparisons of the individual thermocouples with 1.31mm mesh and mesh plus water sprays. The dot lines indicate the trials were run with the mesh alone while the second line indicates the trials with both mesh and water sprays activated.



**Figure 5.30:** The comparison of individual thermocouple temperature-time profile with 1.31mm mesh + spray.

## 5.7 Flame propagation behaviour at 9% with 1.31mm mesh no sprays



**Figure 5.31:** 9% mixture Flame propagation with 1.31mm mesh no water spray

### 5.7.1 Time–Temperature Profile at 9% combustion with 1.31 mm mesh no sprays

Figure 5.32 shows the temperature-time response of propagated flame along with a length of 6.3m long with its corresponding time. Figure 5.32 shows the temperature-time profile for 9% methane-air mixture concentration. Although; it shows that the propagated flame was not mitigated. This is because there was no spray but 1.31mm mesh was installed in between the flanges of about 2000 mm away from the start of ignition.

It can be seen that Figure 5.32 exhibit the same character of a high temperature at thermocouple 4 (TC-4) when the meshing material is used alone. It generated a high temperature of about 150°C and rapidly cools down as the flange fall off. Because the mesh is placed before TC-3, the temperature recorded by TC-3 thermocouple shows a lower temperature compared to other. This resulted from heat loss by conduction to the mesh and decreases the temperature to about 40°C.

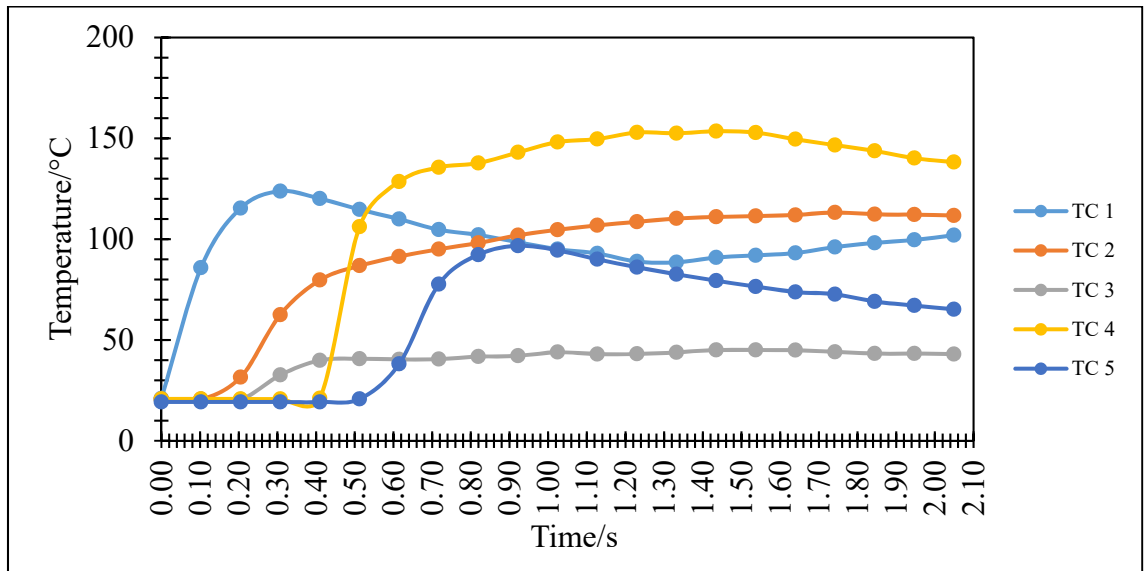


Figure 5.32: Time-Temperature responses of 9% mixture with 1.31mm mesh no sprays

### 5.7.2 Average Flame speed at 9% combustion with 1.31 mm mesh + sprays

The same technique used in section 5.6.1 for measuring average flame speed was utilised. The maximum flame speed measured was 12.42m/s which show a great reduction when compared to the 30m/s flame speed measured previously in section 5.6.1 for 9% methane-air mixtures. The 9% methane-air mixture was fully mitigated with no further flame propagation downstream of sprays, and therefore, no flame image was captured after mitigation as indicated in Table 5.8 and illustrated in Figure 5.33 and Figure 5.34.

Table 5.8: The average flame speeds with 1.31mm mesh plus sprays for 9% mixture

Methane/air mixture (%)	Distance travelled by flame (m)	Time travelled (s)	Average flame speed (m/s)
9	2.900	0.2335	12.42

### 5.7.3 Flame propagation behaviour at 9% with 1.31mm mesh + sprays

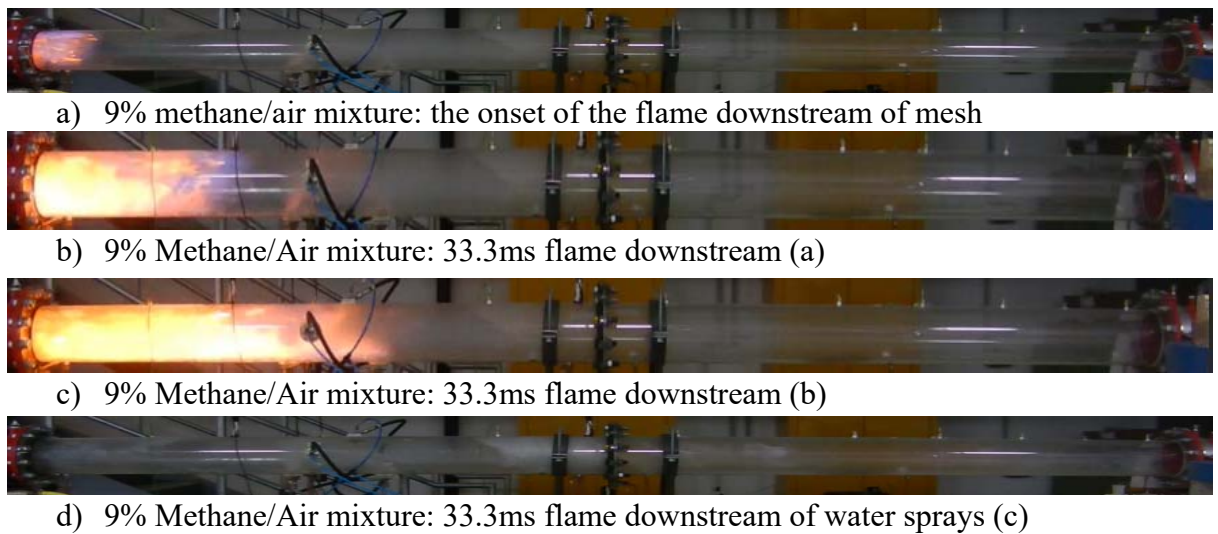
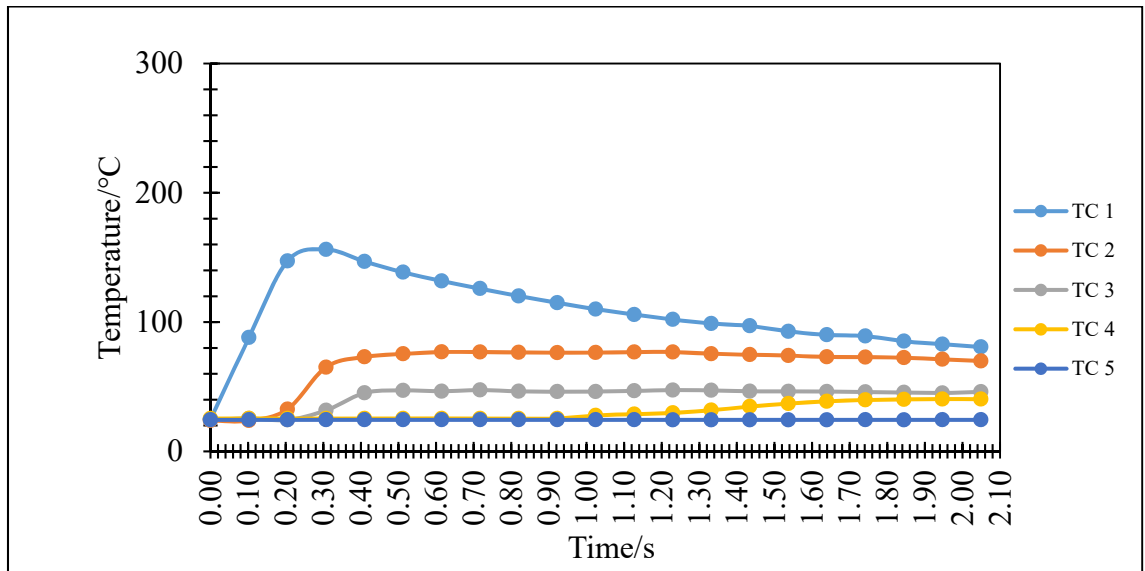


**Figure 5.33:** 9% mixture Flame propagation with 1.31mm mesh and plus sprays

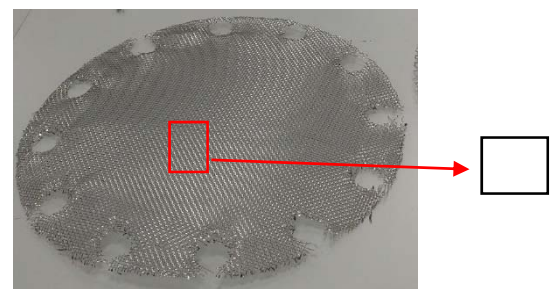
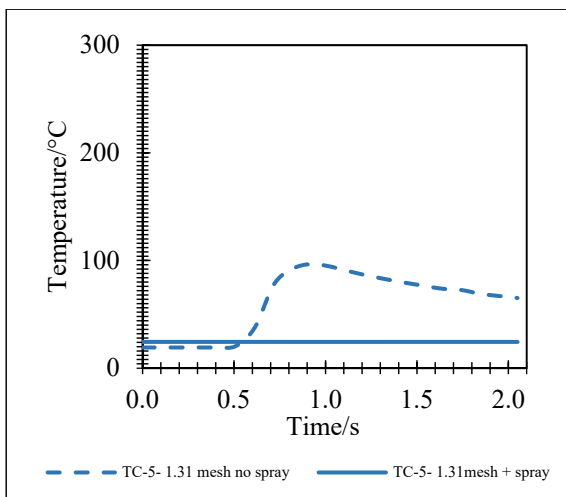
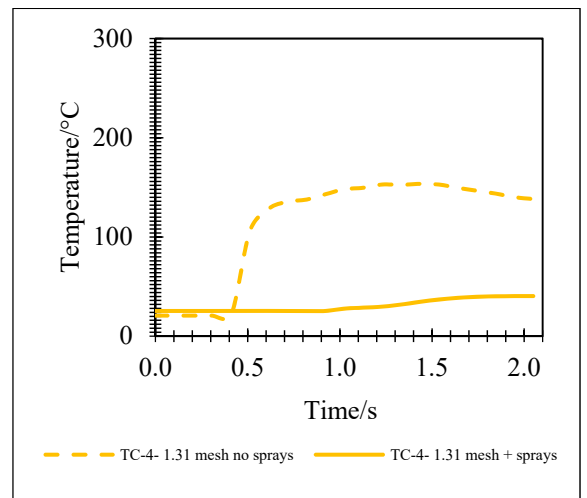
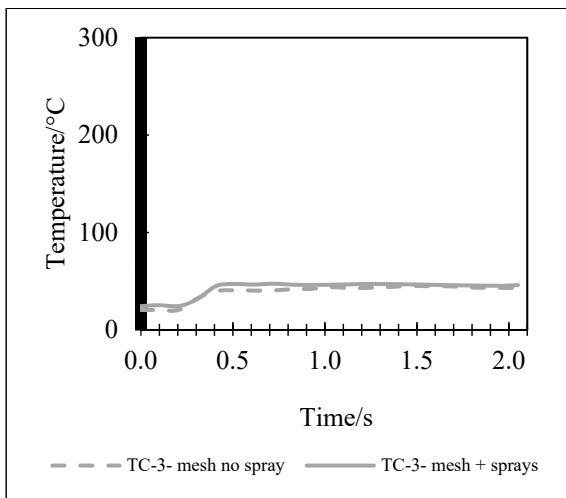
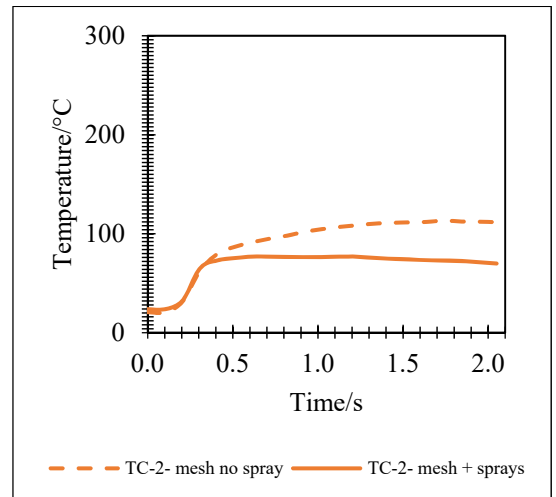
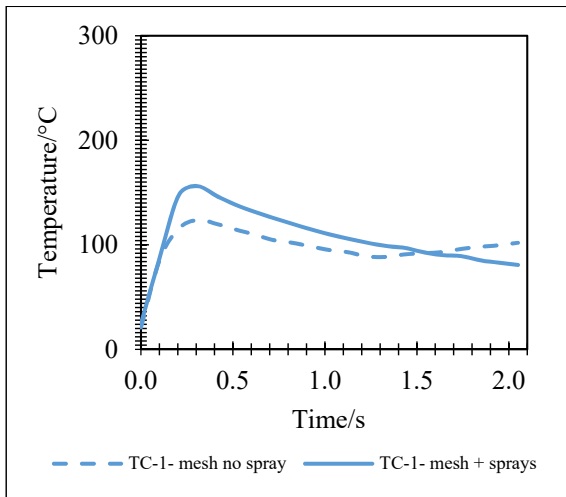
### 5.7.4 Temperature – time response at 9% with 1.31 mm mesh + sprays

Figure 5.34 shows the temperature-time profile with 13.1mm mesh installed and water sprays activated. A similar trend of the temperature profiles was observed presented in subsections 5.4.5, 5.46 and Figures 5.19, and 5.22. It is observed that immediately after the ignition, there was a sudden change in temperature from room temperature to about 156°C for thermocouple A, and then gradually decaying till the temperature stabilised at 80°C.

However, other thermocouples located along the 6300mm long indicated a lower temperature sequentially, with a further decrease from TC-1 to TC-2, TC-2 to TC-3, and afterwards, a uniform temperature was recorded from thermocouples TC-4 and TC-5. Thus, it can be seen that TC-5 shows a little increase in temperature, this could result from large amount of water vapour generated which moves gradually along the pipe length and of course due to the cooling effect of the interaction of water and flame, the vapour generated was warm, and that causes the increase in both thermocouple TC-5 as shown in figure 5.26.



**Figure 5.34:** Time-Temperature profile at 9% with 1.31mm mesh + sprays



b) Woven wire mesh 1.31mm holes  
0.28mm wire diameter

**Figure 5.35:** The comparison of individual thermocouple temperature-time profile at 9% with 1.31mm mesh + sprays.

## 5.8 Perorated sheet, PS (6 mm aperture)

The experimental apparatus was reconfigured with perforated sheet 6mm aperture installed in between the steel pipe and the PMMA tube at 2000mm distance from the point of ignition (driver section). This is described and detailed in section 4.3.

### 5.8.1 Average Flame speed with 6 mm PS and Dry case

The average flame speed results obtained with 6mm perforated sheet installed. The sequence of images obtained from Nikon camera as shown in Figure 5.29 and 5.30 illustrates the flame propagations, and the results relating to the flame temperature and effect and performance of the mesh on the propagated flame

The average flame speed was measured downstream of the mesh. Table 5.11 illustrates the average flame speed for various methane-air concentrations. It is observed that the average flame speed varies for each methane-air concentration.

**Table 5.9:** Average flame speed for a various methane-air flame

Methane/air mixture (%)	Distance travelled by flame (m)	Time travelled (s)	Average flame speed (m/s)
6	2.900	0.1335	21.72
7	3.000	0.1335	22.47
9	3.100	0.1335	23.22

### 5.8.2 Flame propagation for 6% & 9% mixture with 6mm mesh no sprays

Figure 5.36 present's series of flame propagation video images for 6, 7 and 9 % methane-air mixtures with 6 mm perforated sheet installed at 2000mm distance from the start of ignition.

The results obtained with video frames images with the perforated sheet 6mm aperture in position but no sprays activated shows flame propagation frames which were used to calculate the average flame speed as shown in Table 5.9. It was observed that after ignition of the methane-air, it takes just 20 – 30 milliseconds for the flame to vanish away from the explosion tube.

Figure 5.12, Figure 5.13 and Figure 5.14 present the thermocouple output data at 6, 7 and 9 % methane-air combustion with 0.94 mm steel wire mesh inserted. The time-temperature profile across the five thermocouples (TC-1 to TC-5) fixed along the length of the tube spaced at a specified interval are used to obtain the flame temperatures.

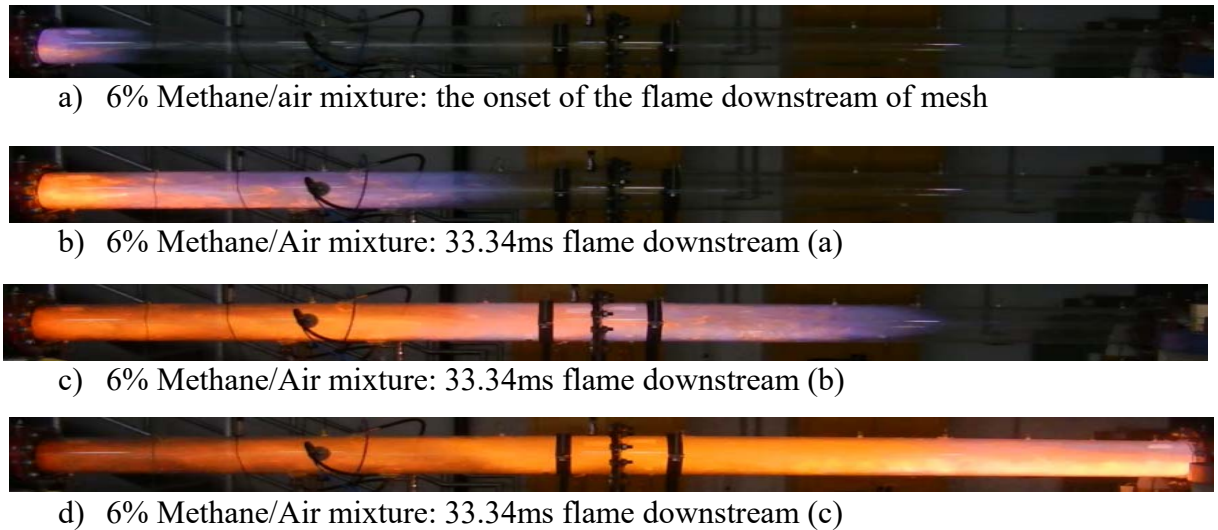


**Figure 5.36:** 6% mixture Flame propagation with 6mm mesh installed no sprays

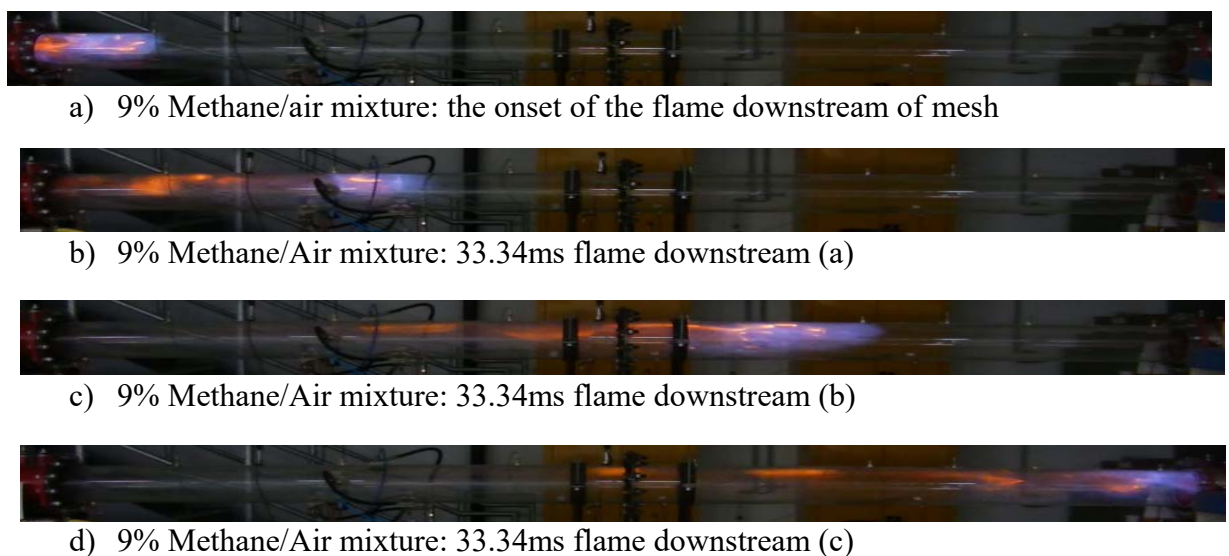
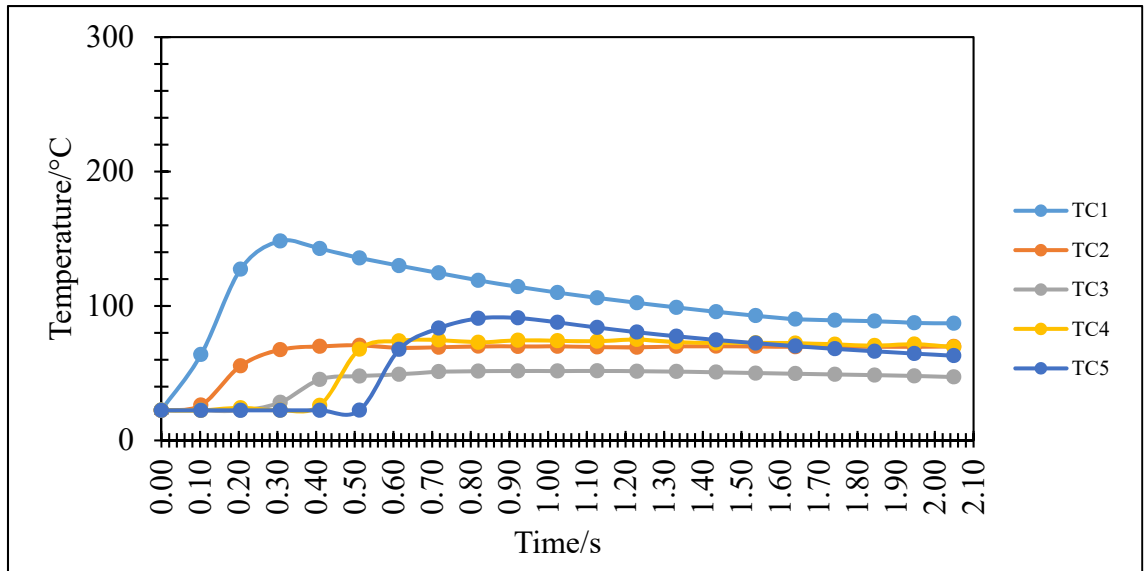


**Figure 5.37:** 9% Flame propagation images with 6mm mesh installed no sprays

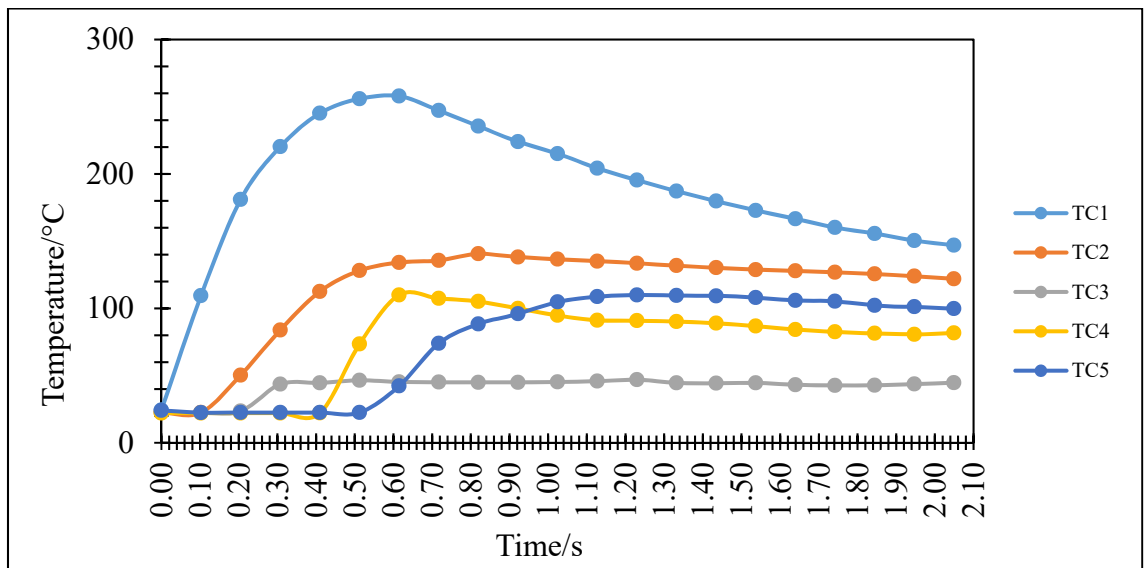
### 5.8.3 Temperature – time profile for 6% & 9% mixture with 6mm mesh

Figure 5.38 shows the thermocouple output data for 6%, methane-air mixtures with 6mm perforated sheet in position. The flame temperature recorded with thermocouple K sensor ranges from TC-1 to TC-5. As seen in Figure 5.38 and Figure 5.39, the temperature measured encompasses the same trends as the previous runs presented in sub-sections 5.3.5, 5.3.7, 5.4.6, 5.4.7, 5.5.3, and 5.6.3. The TC-1's recorded the maximum temperature of 148°C and

257°C which then declined down as flame propagates further to about 87°C and 146°C for 6, 7 and 9% mixture also reported by [81]. All other thermocouples indicate a lower temperature sequentially compared to thermocouple TC1 with a further decrease from TC-5 to TC-4 except for the TC3. There was a great drop in temperature in TC3 thermocouples to about 45°C and 43°C for 6% and 9% mixtures which resulted from the mesh inserted due to its heat conductive nature.



**Figure 5.38:** Time-Temperature profile for 6% methane/air mixture with 6mm mesh installed no sprays



**Figure 5.39:** Time-Temperature profile for 9% methane/air mixture with 6mm mesh installed no sprays

#### 5.8.4 Flame propagation behaviour for 6% mixture with 6mm mesh + sprays



a) 6% Methane/air mixture: the onset of the flame downstream of mesh



b) 6% Methane/Air mixture: 33.34ms flame downstream (a)



c) 6% Methane/Air mixture: 33.34ms flame downstream (b)



d) 6% Methane/Air mixture: 33.34ms flame downstream (c)

**Figure 5.40:** 6% Flame propagation with 6 mm mesh + sprays

#### 5.8.5 Temperature-time profile at 6% combustion with 6 mm mesh+spray

Figure 5.41 presents 6 % methane combustion subjected to two different obstructions. The result shows a similar trend in temperature with that of Figures 5.19 and 5.29 respectively. Figure 5.41 indicates that thermocouple (TC-1), has maintained fairly similar range of temperature during the 0.41m/s duration. This is particularly relevant as propagating flame were not allowed beyond the spray position, thereby, limiting its speed, at the same time enabling thermal accumulation around the initial length of the tube due to ineffective heat transfer compared to the non-mitigated flames similarly reported by [81, 82].

As the flame propagate further through the second, thermocouple (TC-2), the energy balances around the perforated sheet and water spray opposes flame propagation thereby causing a reduction due to convective heat loss to perforated sheet and the cooling sensation of the water mist. However, the latent heat of vaporization of the water that was transferred from the flame causes a significant reduction in temperature at TC-2 and TC-3. More importantly, TC-3 recorded a very low temperature compared to TC-1 and TC-2. This is due to the convective heat sink by the propagated sheet. Likewise, at the last two thermocouples TC-4

and TC-5, no major variation in temperature due to the fact that the flame was quenched before reaching the last two thermocouple positions. Because most of the heat was transferred between the perforated sheet and the water sprays vapour.

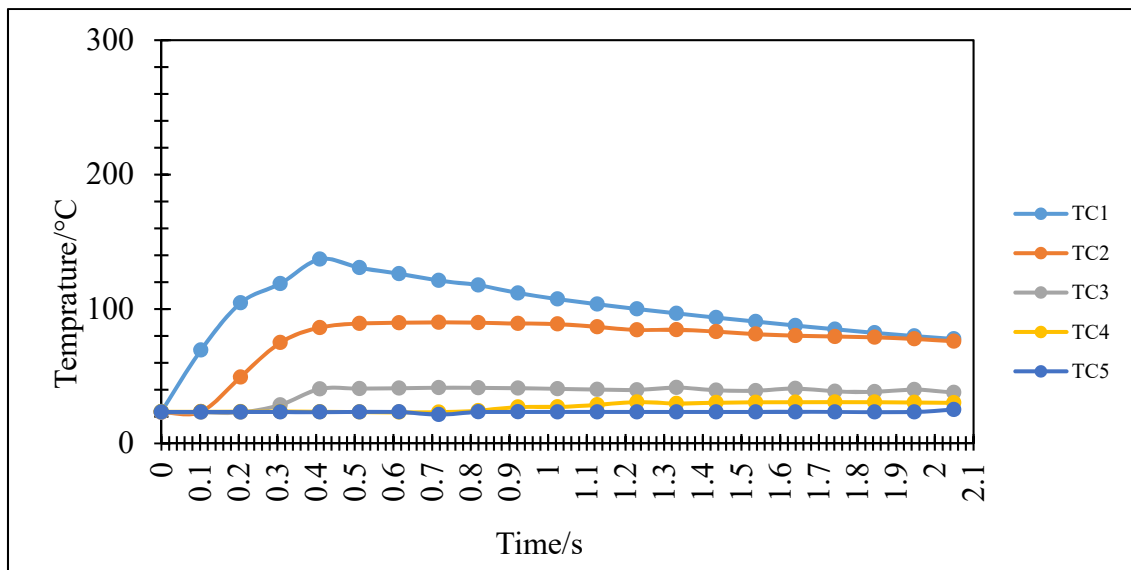
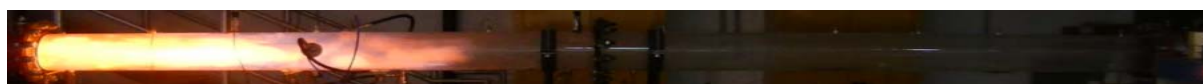


**Figure 5.41:** Time-Temperature profile for 6% methane/air mixture with 6mm mesh installed plus sprays

### 5.8.6 Flame propagation behaviour for 9% mixture with 6mm mesh + sprays



a) 9% Methane/air mixture: the onset of the flame downstream of mesh



b) 9% Methane/Air mixture: 33.34ms flame downstream (a)



c) 9% Methane/Air mixture: 33.34ms flame downstream (b)



e) 9% Methane/Air mixture: 33.34ms flame downstream (c)

**Figure 5.42:** 9% Flame propagation with 6 mm mesh + sprays

### 5.8.7 Temperature-time profile at 9% combustion with 6 mm mesh+spray

Figure 5.43 shows that the highest temperature was achieved at thermocouple TC-1, rather than the usual TC-4 in Figures 5.12, 5.13 and 5.14. However, Figure 5.43 illustrates the temperature-time variation across each thermocouple TC-1, TC-2, TC-3, TC-4 and TC-5 with perforated sheet 6 mm and fine water sprays activated. The results obtained presents similar trends of time-temperature profile reported in sub-section 5.3.5 and Figure 5.14. The propagated flame was not extinguished but the performance and effects of the perforated sheet are clearly observed.

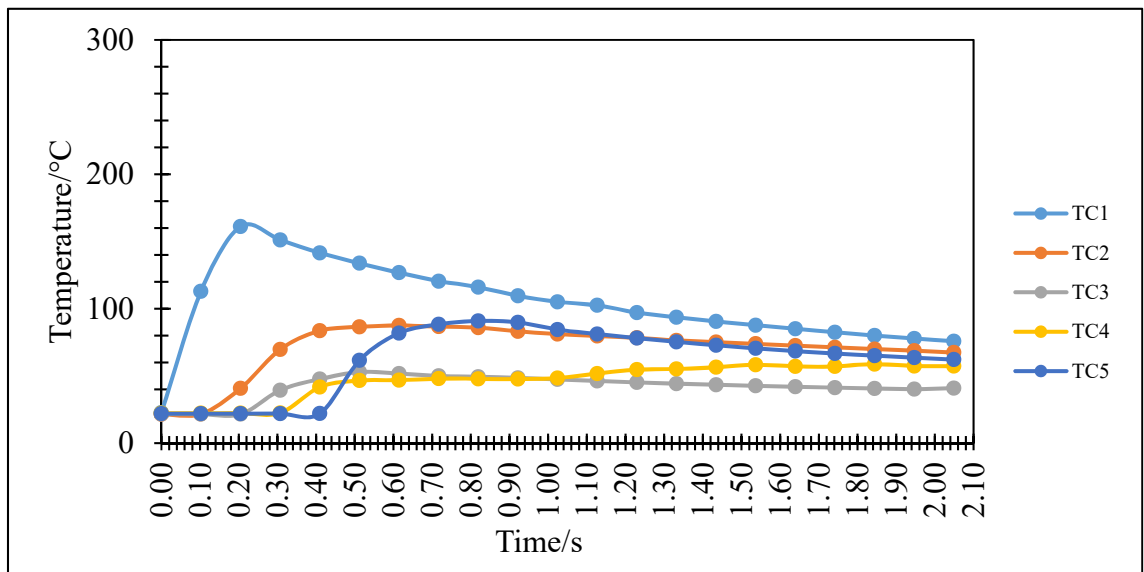


**Figure 5.43:** Time-Temperature profile at 9% combustion with 6mm mesh + sprays

## Chapter 6: Conclusion

The series of experimental trials conducted in this research study encompasses methane-air mixture concentration of 6, 7 and 9 % by volume. The mixture concentrations were used to generate a propagating flame for deflagrated explosion that is aimed to be obstructed with different sizes of steel meshes and mitigated using high pressure water sprays. In the numerous trials for both free flames, flames propagation in the presence of obstructions (steel mesh sizes and fine water sprays) mitigation and no-mitigation scenarios, the following conclusion can be drawn;

- i. The metal wire mesh in the pipeline can decelerate the speed of the flame and the energy of the flame is weakened by the mesh. As such, the steel metal wire mesh can be used to reduce the damage caused by gas explosion.
- ii. The image processing method is effective in calculating the speed of flame propagation. This method was qualitatively used to obtained flame speeds.
- iii. Similarly, 1.31mm mesh size provided more accurate result because a lower average flame speed 19.04m/s and 19.35m/s were obtained for 7% and 9% mixtures. However, it was observed that lean mixtures (6%) initially accelerate faster than rich mixtures (9%) for the same mesh size of 1.31mm aperture.
- iv. It was noticed that the thicker the aperture of the wire mesh size, the better the flame quenching performance. Though, the material also plays a very significant role on the suppressing characteristics of the deflagration flames.
- v. When the concentration of methane was set at 6%, inserting 0.94mm, 1.31mm, and 6mm mesh sizes, a temperature variation of 38°C, 45°C, and 48°C were observed at TC-3 thermocouple. These temperatures decreased gradually until a stable temperature reached, although explosion flame was not mitigated under these conditions but the effect of the mesh was clearly observed.
- vi. Observations indicate that all the recorded temperature – time curves exhibit similar behaviour after the commencement of the ignition. However, average flame speed for various methane-air mixtures obtained, it was observed that for different sizes of mesh used, average flame speed varies for each methane-air mixtures.
- vii. Flame explosion mitigation was easily achieved using 1.31mm mesh size combined with high prssure water sprays for rich mixture of 9% concentration; the mitigated trial also indicated a steady temperature at thermocouple TC-3 during the time of explosion. This was observed to pressure build-up by the obstruction caused by the

water spray, thereby enabling the temperature to be steady around the thermocouple TC-2.

- viii. With 9% methane concentration where mitigation was not achieved, a great temperature decreased were observed at thermocouple TC-3, this was due to the effective heat transfer between the mesh material and hot gases or the flame as it passes through the mesh.
- ix. With the use mesh only for the various methane-air mixtures, the highest temperatures were observed at thermocouple TC-4. But combining the meshes with water sprays, the maximum temperatures were observed at TC-1 thermocouples rather than the usual TC-4.

## **6.1 recommendations**

Based on the results of the present research study, the following are some recommendations for potential improvements on the understanding of flame propagation and quenching.

More experiment should be conducted with perforated metal sheet of different sizes and woven wire meshes in combination with high-pressure water sprays in order to investigate their performance on flame propagation quenching mechanism.

For flame extinction, the combined effects and performance of steel metal meshes and fine water sprays should be theoretically and numerically investigated.

Since pipelines are not always straight, flame propagation around bend (elbow) with different sizes of both wire meshes and perforated sheet should be thoroughly investigated.

## References

- [1] W. E. Baker, P. Cox, J. Kulesz, R. Strehlow, and P. Westine, *Explosion hazards and evaluation*: Elsevier, 2012.
- [2] C. J. Wang, and J. X. Wen, "The effect of a perforated plate on the propagation of laminar hydrogen flames in a channel – A numerical study," *International Journal of Hydrogen Energy*, vol. 39, no. 36, pp. 21335-21342, 2014.
- [3] F. El-Mahallawy, and S.-D. Habik, *Fundamentals and technology of combustion*: Elsevier, 2002.
- [4] D. Bjerketvedt, J. R. Bakke, and V. K. Wingerden, "Gas explosion handbook," *Journal of Hazardous Materials*, vol. 52, no. 1, pp. 1-150, Jan, 1997.
- [5] R. K. Eckhoff, *Explosion hazards in the process industries*: Gulf Professional Publishing, 2016.
- [6] F. Theuretzbacher, J. Lizasoain, C. Lefever, M. K. Saylor, R. Enguidanos, N. Weran, A. Gronauer, and A. Bauer, "Steam explosion pretreatment of wheat straw to improve methane yields: investigation of the degradation kinetics of structural compounds during anaerobic digestion," *Bioresource technology*, vol. 179, pp. 299-305, 2015.
- [7] W. Zeng, H. Ma, Y. Liang, and E. Hu, "Experimental and modeling study on effects of N<sub>2</sub> and CO<sub>2</sub> on ignition characteristics of methane/air mixture," *Journal of advanced research*, vol. 6, no. 2, pp. 189-201, 2015.
- [8] A. L. Kuhl, and H. Reichenbach, "Combustion effects in confined explosions," *Proceedings of the Combustion Institute*, vol. 32, no. 2, pp. 2291-2298, 2009.
- [9] F. Lees, *Lees' Loss prevention in the process industries: Hazard identification, assessment and control*: Butterworth-Heinemann, 2012.
- [10] D. Gardner, and G. Hulme, *A survey of current predictive methods for explosion hazard assessments in the UK offshore industry*: Great Britain, Health and Safety Executive, 1995.
- [11] C. Tang, S. Zhang, Z. Si, Z. Huang, K. Zhang, and Z. Jin, "High methane natural gas/air explosion characteristics in confined vessel," *J Hazard Mater*, vol. 278, pp. 520-8, Aug 15, 2014.
- [12] F. I. Khan, J. D. Rani, and S. Abbasi, "Accident simulation as a tool for assessing and controlling environmental risks in chemical process industries: a case study," *Korean Journal of Chemical Engineering*, vol. 15, no. 2, pp. 124-135, 1998.
- [13] Y. Lee, N. Park, A. Green, and D. Park, "Experimental Studies on Gas Explosions by Different Obstacles in a Partially Confined Region," *Fire Safety Science*, vol. 6, pp. 3a-4--1, 2004.
- [14] S. Ibrahim, and A. Masri, "The effects of obstructions on overpressure resulting from premixed flame deflagration," *Journal of Loss Prevention in the Process Industries*, vol. 14, no. 3, pp. 213-221, 2001.
- [15] V. K. Wingerden, B. Wilkins, J. Bakken, and G. Pedersen, "The influence of water sprays on gas explosions. Part 2: mitigation," *Journal of Loss Prevention in the Process Industries*, vol. 8, no. 2, pp. 61-70, //, 1995.
- [16] M. R. Acton, P. Sutton, and M. Wickens, "Investigation of the mitigation of gas cloud explosions by water sprays." pp. 61-76.
- [17] R. G. Little, "Holistic strategy for urban security," *Journal of Infrastructure Systems*, vol. 10, no. 2, pp. 52-59, 2004.
- [18] Abaqus6.9-EF. "Acoustic and shock loads," 22nd 2018, 2018; <http://130.149.89.49:2080/v6.9ef/books/usb/default.htm?startat=pt07ch30s04aus107.html>.
- [19] A. Soman, and G. Sundararaj, "Consequence Assessment of Vapour Cloud Explosion Involving Hydrogen Release," *International journal of emerging technology and advanced engineering*, vol. 2, no. 11, pp. 291-296, 2012.

- [20] CSBDonHolmstrom. "Statement of CSB investigations supervisor Don Holmstrom updating the public on the CSB's investigation of the catastrophic accident at Kleen Energy, Middletown, Connecticut, CSB " 22nd 2018; <http://www.csb.gov/assets/news/document/CSB>
- [21] T. A. Kletz, *Accident reports may not tell us everything we need to know*, 0950-4230, vol. 22, 2009.
- [22] R. J. Parker, *The flixborough disaster: report of the court of inquiry*, 1975.
- [23] M. Grinrod, O. Haaland, and B. Ellingsen, "A shallow gas research program."
- [24] C. Woolfson, and M. Beck, "The British offshore oil industry after Piper Alpha," *NEW SOLUTIONS: A Journal of Environmental and Occupational Health Policy*, vol. 10, no. 1-2, pp. 11-65, 2000.
- [25] D. P. Nolan, *Handbook of fire and explosion protection engineering principles: for oil, gas, chemical and related facilities*: William Andrew, 2014.
- [26] J. F. Griffiths, and J. A. Barnard, *Flame and combustion*: CRC Press, 1995.
- [27] John N. Bradley, *Flame and Combustion Phenomena*, Great Britain, London: Butler & Tanner Ltd, 1969.
- [28] BBC. "Activation energy and catalysts," 28th April, 2018, 2018; [http://www.bbc.co.uk/schools/gcsebitesize/science/triple\\_aqa/calculating\\_energy\\_changes/energy\\_from\\_reactions/revision/5/](http://www.bbc.co.uk/schools/gcsebitesize/science/triple_aqa/calculating_energy_changes/energy_from_reactions/revision/5/).
- [29] W. A. Bone, and R. V. Wheeler, "I. The combination of hydrogen and oxygen in contact with hot surfaces," *Phil. Trans. R. Soc. Lond. A*, vol. 206, no. 402-412, pp. 1-67, 1906.
- [30] G. Nasr, and N. Connor, *Natural Gas Engineering and Safety Challenges*: Springer, 2016.
- [31] Enardo, "Flame Arrestor Technology," [http://www.enardo.com/products/prod\\_fda.htm](http://www.enardo.com/products/prod_fda.htm), [12th January, 2016, 2016].
- [32] BBC. "History Sir Humphry Davy 1778 - 1829," 25th January, 2018, 2018; [http://www.bbc.co.uk/history/historic\\_figures/davy\\_humphrey.shtml](http://www.bbc.co.uk/history/historic_figures/davy_humphrey.shtml).
- [33] NIOSH. "History of the Mining Program " 26th January, 2018, 2018; <https://www.cdc.gov/niosh/mining/content/history.html>.
- [34] J. T. Robert, and F. B. Ruth, "A History of the Bureau of Mines Pittsburgh Research Center ", 1924, p. 2 and 3.
- [35] A. C. Smith, and E. D. Thimons, "A summary of US mine fire research."
- [36] P. Donoso-García, and L. Henríquez-Vargas, "Numerical study of turbulent porous media combustion coupled with thermoelectric generation in a recuperative reactor," *Energy*, vol. 93, pp. 1189-1198, 2015/12/15/, 2015.
- [37] S. Bani, J. Pan, A. Tang, Q. Lu, and Y. Zhang, "Micro combustion in a porous media for thermophotovoltaic power generation," *Applied Thermal Engineering*, vol. 129, no. Supplement C, pp. 596-605, 2018/01/25/, 2018.
- [38] V. Khanna, R. Goel, and J. Ellzey, "Measurements of emissions and radiation for methane combustion within a porous medium burner.," *Combust Sci Technol*, 1994.
- [39] J. Ellzey, and R. Goel, "Emissions of CO and NO from a two stage porous media burner.," *Combust Sci Technol*, 1995.
- [40] C. Tseng, and J. Howell, "Combustion of liquid fuels in a porous radiant burner.," *Combust Sci Technol* 1996.
- [41] V. Babkin, A. Korzhavin, and V. Bunev, " Propagation of premixed gaseous explosion flames in porous media.," *Combust Flame* 1991.
- [42] A. Pinaev, "Combustion modes and flame propagation

criteria for an encumbered space.," *Comb Expl Shock Waves* 1994.

- [43] A. Makris, T. Oh, J. Lee, and R. Knystautas, "Critical diameter for the transmission of a detonation wave into a porous medium. ," *Proc Combust Inst* 1994.
- [44] D. K. Min, and H. D. Shin, "Laminar premixed flame stabilized inside a honeycomb ceramic," *International journal of heat and mass transfer*, vol. 34, no. 2, pp. 341-356, 1991.
- [45] T. Marbach, and A. Agrawal, "Heat-recirculating combustor using porous inert media for mesoscale applications," *Journal of Propulsion and Power*, vol. 22, no. 1, pp. 145-150, 2006.
- [46] A. J. Yule, and J. J. Dunkley, "Atomization of melts for powder production and spray deposition," *Clarendon press, Oxford*, 1994.
- [47] G. G. Nasr, A. Yule, and L. Bendig, *Industrial Sprays and Atomization: Design*, 2002.
- [48] A. Lefebvre, *Atomization and sprays, combustion: an international series*, 1989.
- [49] L. Filippa, A. Trento, and A. M. Álvarez, "Sauter mean diameter determination for the fine fraction of suspended sediments using a LISST-25X diffractometer," *Measurement*, vol. 45, no. 3, pp. 364-368, 2012.
- [50] A. H. Lefebvre, "Atomization," vol. A, 2006.
- [51] N. Ashgriz, *Handbook of atomization and sprays: theory and applications*: Springer Science & Business Media, 2011.
- [52] MachinerySpaces.com. "The fuel oil injection system for a diesel engine," 14th March 2018, 2018; <http://www.machineryspaces.com/fuel-injector.html>.
- [53] G. G. Nasr, A. J. Yule, and Bendig, "Industrial Sprays and Atomisations: Design, analysis and applications," 2002.
- [54] G. Nasr, A. Yule, and S. Lloyd, "The Characterisation of the Spray from a New Fine Spray Spill Return Swirl Atomiser."
- [55] Lechler. "Engineering your spray solution " 14th March 2018, 2018; [http://www.lechler.de/Products/Environmental-Technologies/Gas-Conditioning/Nozzle-Product-Range/Spillback-Nozzles/-cbbnd\\_AAABwCMAAAEy.t0N2ABm-en\\_US](http://www.lechler.de/Products/Environmental-Technologies/Gas-Conditioning/Nozzle-Product-Range/Spillback-Nozzles/-cbbnd_AAABwCMAAAEy.t0N2ABm-en_US).
- [56] J. A. Stewart, "Investigation into the design and development of a disinfection system utilising a novel spill-return atomiser (SRA)," Salford: University of Salford, 2011.
- [57] H. Naito, T. Uendo, Y. Saso, Y. Kotani, and A. Yoshida, "Effect of fine water droplets on extinguishment of diffusion flame stabilized in the forward stagnation region of a porous cylinder," *Proceedings of the Combustion Institute*, vol. 33, no. 2, pp. 2563-2571, 2011.
- [58] L. Zhigang, and K. K. Andrew, "A Review of Water Mist Fire Suppression Systems - Fundamental Studies," *National Research Council Canada*, vol. 10(3), 2000.
- [59] Thomas G. O, "ON THE CONDITIONS REQUIRED FOR EXPLOSION

MITIGATION BY WATER SPRAYS," *Centre for Explosion Studies*

*Department of Physics*

*University of Wales*

*Aberystwyth UK SY23 3BZ*, 2000.

- [60] D. M. Johnson, "The potential for vapour cloud explosions—Lessons from the Buncefield accident," *Journal of Loss Prevention in the Process Industries*, vol. 23, no. 6, pp. 921-927, 2010.

- [61] F. Wang, M. Yu, X. Wen, H. Deng, and B. Pei, "Suppression of methane/air explosion in pipeline by water mist," *Journal of Loss Prevention in the Process Industries*, 2017/02/08/, 2017.
- [62] G. O. Thomas, and J. R. Brenton, "An Investigation of Factors Relevance during Explosion Suppression by Water Spray," *Health and Safety Executive*, 1996.
- [63] G. O. a. B. Thomas, J. R., "The Dynamics of Explosions and Reactive Systems " *Paper presented at the 14th International Colloquium*, 1993.
- [64] V. K. Wingerden, and B. Wilkins, "The influence of water sprays on gas explosions. Part 1: water-spray-generated turbulence," *Journal of Loss Prevention in the Process Industries*, vol. 8, no. 2, pp. 53-59, //, 1994.
- [65] M. J. Sapko., A. L. Furno, and J. M. Kuchta, "Quenching methane-air ignitions with water sprays," *Report of Investigations RI-8214 (US Department of Interior)*, 1977.
- [66] R. G. Zalosh, and S. N. Bajpai, "Water fog inerting of hydrogen-air mixtures," *Proc. 2nd Int. Conf. on the Impact of Hydrogen on Water Reactor Safety*, pp. 709., 1982.
- [67] J. Qin, and W. Chow, "Bench-scale tests on PMMA fires with water mist," *Polymer testing*, vol. 24, no. 1, pp. 39-63, 2005.
- [68] I. Search. "The Engineering tool box " 13/08/2018, 2018; [https://www.engineeringtoolbox.com/ansi-steel-pipes-d\\_306.html](https://www.engineeringtoolbox.com/ansi-steel-pipes-d_306.html).
- [69] J. Brenton, G. Thomas, and T. Al-Hassan, "Small-scale studies of water spray dynamics during explosion mitigation tests."
- [70] J.-L. Consalvi, Y. Pizzo, and B. Porterie, "Numerical analysis of the heating process in upward flame spread over thick PMMA slabs," *Fire Safety Journal*, vol. 43, no. 5, pp. 351-362, 2008.
- [71] J. Gong, X. Zhou, Z. Deng, and L. Yang, "Influences of low atmospheric pressure on downward flame spread over thick PMMA slabs at different altitudes," *International Journal of Heat and Mass Transfer*, vol. 61, pp. 191-200, 2013.
- [72] S. Internet, 2016.
- [73] B. Nie, S. Hu, L. Yang, L. Wang, and X. Su, "Characteristics of flame velocity of gas explosion with obstruction in pipeline," *Perspectives in Science*, vol. 7, pp. 277-281, 2016.
- [74] J. Jarosinski, and B. Veyssiere, *Combustion phenomena: Selected mechanisms of flame formation, propagation and extinction*: CRC press, 2009.
- [75] S. Johnston, "Mitigation of gas and vapour cloud explosions using fine water sprays," University of Salford, 2015.
- [76] D. Bradley, and C. Harper, "The development of instabilities in laminar explosion flames," *Combustion and Flame*, vol. 99, no. 3-4, pp. 562-572, 1994.
- [77] C. Proust, "Flame propagation and combustion in some dust-air mixtures.," *Journal of Loss Prevention in the Process Industries*, vol. 89-100., pp. 19(1),, 2006.
- [78] C. Y. Wu, and K. H. Chen, "Characterization of hydrogen triple flame propagation in vitiated laminar coaxial flow.," *International Journal of Hydrogen Energy*, vol. 14109-14119., pp. 39(26),, 2014.
- [79] H. Cheikhvat, J. Goulier, A. Bentaib, N. Meynet, N. Chaumeix, and C. E. Paillard, "Effects of water sprays on flame propagation in hydrogen/air/steam mixtures," *Proceedings of the Combustion Institute*, vol. 35, no. 3, pp. 2715-2722, //, 2015.
- [80] X. Chen, Y. Zhang, and Y. Zhang, "Effect of CH<sub>4</sub>-Air Ratios on Gas Explosion Flame Microstructure and Propagation Behaviors," *Energies*, vol. 5, no. 12, pp. 4132-4146, 2012.
- [81] P. Chen, F. Huang, Y. Sun, and X. Chen, "Effects of metal foam meshes on premixed methane-air flame propagation in the closed duct," *Journal of Loss Prevention in the Process Industries*, vol. 47, pp. 22-28, 2017.
- [82] C. Proust, "Flame propagation and combustion in some dust-air mixtures.," *Journal of Loss Prevention in the Process Industries*, , vol. 89-100., pp. 19(1),, 2006.

## Appendices

### 6.1.1.1.1 Data sheet for 6 and 9% Mixtures no mesh and no water spray

**Table 6.1.1.1-1:** 6% methane-air mixtures with no mesh and no water sprays

Time/s	TC-1	TC-2	TC-3	TC-4	TC-5
0.00	27.76	23.12	23.12	23.25	23.39
0.10	76.18	23.19	23.12	23.25	23.43
0.20	91.28	73.81	23.12	23.25	23.39
0.31	96.28	121.39	79.62	23.36	23.43
0.41	97.08	135.69	123.02	117.28	23.43
0.51	94.26	144.00	136.51	179.00	63.59
0.61	92.05	143.69	139.22	202.01	85.67
0.72	92.89	147.10	140.63	218.57	90.18
0.82	90.01	151.10	145.65	233.57	87.04
0.92	89.88	154.97	149.37	243.39	85.23
1.02	91.18	156.77	149.72	247.22	79.52
1.13	98.02	157.39	150.62	245.54	76.25
1.23	101.31	159.15	149.17	242.22	73.31
1.33	105.99	159.33	146.20	237.56	73.05
1.43	109.80	158.50	142.73	231.23	68.17
1.54	115.62	156.66	139.60	222.13	66.03
1.64	115.15	153.62	136.72	211.96	64.06
1.74	117.75	150.17	133.22	202.18	64.96
1.84	119.32	146.99	129.94	193.60	60.78

1.95	121.59	144.03	126.77	185.22	59.38
2.05	120.37	140.94	122.85	177.30	58.07

**Table 6.1.1.1.1-2:** 9% methane-air mixtures with no mesh and no water sprays

<b>Time/s</b>	<b>TC-1</b>	<b>TC-2</b>	<b>TC-3</b>	<b>TC-4</b>	<b>TC-5</b>
0.00	22.99	22.41	22.34	22.44	22.37
0.10	90.60	25.30	22.34	22.44	22.37
0.20	120.18	59.56	22.41	22.44	22.34
0.31	116.96	106.18	57.01	22.34	22.37
0.41	112.52	125.97	116.38	71.26	22.37
0.51	107.79	135.43	135.47	152.50	30.58
0.61	104.05	138.14	147.15	194.35	78.84
0.72	100.72	142.50	152.33	222.22	101.03
0.82	97.57	147.60	154.85	232.11	100.42
0.92	94.75	150.74	155.37	240.70	95.86
1.02	92.14	150.77	155.51	246.94	91.47
1.13	90.23	150.32	156.92	256.02	87.52
1.23	88.46	152.95	157.93	255.44	83.94
1.33	87.75	151.71	158.69	254.25	80.64
1.43	86.65	152.78	159.21	249.98	77.60
1.54	86.82	154.09	159.38	246.25	74.90
1.64	90.13	157.68	158.13	237.61	72.43
1.74	92.71	155.30	155.54	231.29	70.16
1.84	94.82	154.68	152.64	224.81	68.15
1.95	97.60	153.67	149.32	220.80	66.32
2.05	100.56	154.05	146.02	212.08	64.68

### 6.1.1.1.2 Data sheet for various Mixtures with 0.94mm mesh and no spray

**Table 6.1.1.1.2-1: 6% methane-air mixtures with mesh and no water sprays data sheet**

Time (s)	TC 1	TC 2	TC 3	TC 4	TC 5
0.00	19.42	19.33	19.16	19.23	19.43
0.10	33.60	19.39	19.15	20.47	19.43
0.20	87.96	47.64	19.17	19.24	19.43
0.31	100.02	60.45	33.32	19.31	19.44
0.41	98.77	65.56	39.28	61.64	27.52
0.51	97.34	70.80	42.18	88.72	62.46
0.61	94.02	74.94	42.22	105.05	73.63
0.72	93.53	77.06	41.72	117.13	80.07
0.82	91.61	79.76	40.95	121.89	79.89
0.92	89.58	80.76	41.11	126.50	78.20
1.02	86.75	82.87	40.85	132.38	75.07
1.13	85.48	84.75	41.28	135.87	73.27
1.23	83.59	85.85	40.00	136.73	70.44
1.33	81.71	87.23	41.48	137.54	67.87
1.43	79.93	88.61	41.95	138.52	65.02
1.54	78.27	89.72	41.81	138.35	63.51
1.64	76.66	90.94	41.60	137.91	61.62
1.74	75.27	92.21	41.77	135.84	59.87
1.84	72.92	92.94	41.40	132.31	56.99
1.95	72.84	93.66	41.02	128.77	56.70
2.05	71.84	94.15	40.77	125.66	55.31

**Table 6.1.1.1.2-2: 7% methane-air mixtures with 0.94mm mesh and no water sprays**

<b>Time (s)</b>	<b>TC 1</b>	<b>TC 2</b>	<b>TC 3</b>	<b>TC 4</b>	<b>TC 5</b>
0.00	18.58	18.88	18.50	18.76	18.61
0.10	42.27	18.91	18.46	18.72	18.61
0.20	102.99	44.83	18.49	18.73	18.66
0.30	111.79	73.75	30.22	18.81	18.65
0.40	107.02	84.70	34.97	39.72	18.73
0.50	101.78	89.39	34.80	95.14	45.10
0.60	96.34	93.04	35.42	116.78	64.55
0.70	92.15	95.43	35.48	127.08	71.03
0.80	88.21	95.87	37.06	129.20	72.40
0.90	84.81	96.47	38.44	131.39	72.27
1.00	82.03	95.75	39.39	134.07	71.14
1.10	79.27	95.23	39.33	134.94	69.12
1.20	76.52	95.10	39.35	134.39	66.73
1.30	74.05	94.63	39.47	133.26	64.70
1.40	71.82	93.68	39.25	131.16	62.73
1.50	69.73	92.79	39.19	128.95	60.94
1.60	67.77	92.47	38.82	126.83	59.19
1.70	65.80	91.96	38.31	125.31	57.55
1.80	64.08	91.65	37.69	124.84	55.98
1.90	62.40	91.33	37.26	123.90	54.63
2.00	60.80	90.69	36.79	122.89	53.27



e) 7% Methane-air mixture: emergence of the flame from the driver section



f) 7% Methane-air mixture: 33.3ms flame downstream of (a)

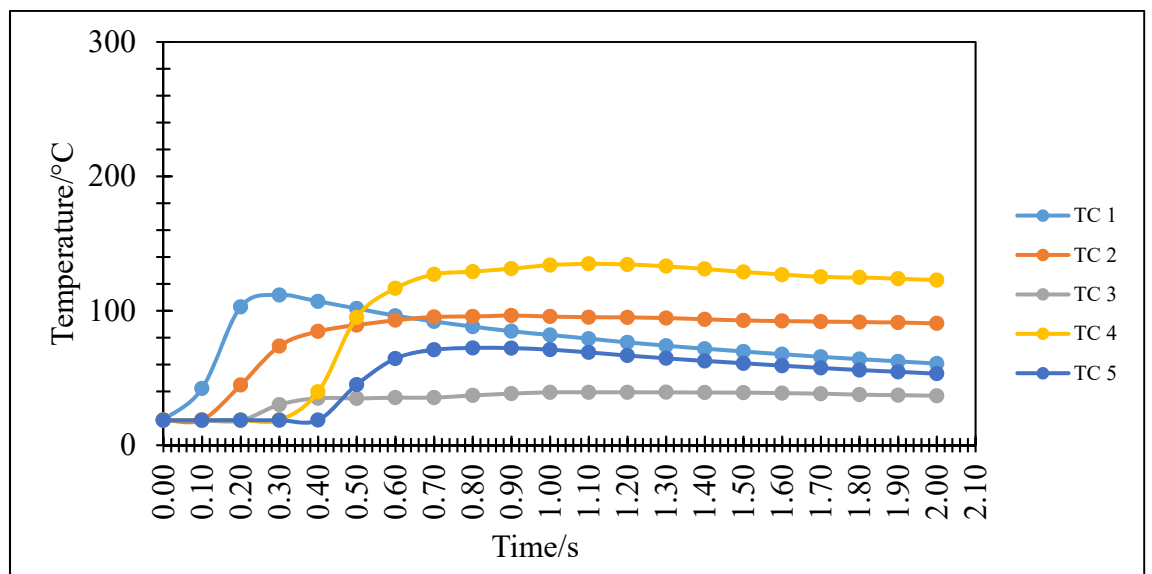


g) 7% Methane-air mixture: 33.3ms flame 33.3ms downstream of (b)



h) 7% Methane-air mixture: 33.3ms flame downstream of (c)

**Figure 6.1.1.2-1:** Average Flame speed of 7% mixture with 0.94mm mesh & no water spray



a) 7% methane-air mixtures

**Figure 6.1.1.2-2:** Time-Temperature responses of 7% mixture with 0.94mm mesh no sprays

**Table 6.1.1.2-3:** 9% methane-air mixtures with 0.94mm mesh and no water sprays data sheet

<b>Time (s)</b>	<b>TC 1</b>	<b>TC 2</b>	<b>TC 3</b>	<b>TC 4</b>	<b>TC 5</b>
0.00	19.88	19.92	19.60	19.90	19.77
0.10	104.00	19.99	18.43	19.91	19.77
0.20	145.58	44.59	19.61	19.91	19.77
0.31	146.32	85.49	32.15	19.98	18.71
0.41	139.40	104.88	37.61	51.79	19.83
0.51	133.16	110.20	38.52	113.48	56.98
0.61	126.73	114.36	37.89	130.62	81.21
0.72	121.03	115.79	37.58	140.79	91.04
0.82	116.10	115.13	37.41	143.84	91.58
0.92	111.55	111.95	37.04	149.38	88.20
1.02	107.37	109.41	37.01	148.57	84.64
1.13	104.60	107.23	37.47	147.06	81.39
1.23	99.82	105.00	38.13	147.03	78.22
1.33	96.39	102.79	38.01	147.10	75.27
1.43	93.20	102.13	37.08	147.66	72.60
1.54	90.12	102.05	38.10	147.24	70.16
1.64	87.30	101.90	38.26	147.76	69.10
1.74	84.70	102.14	38.03	146.95	66.02
1.84	82.28	102.51	38.24	146.18	64.19
1.95	80.00	102.15	38.06	144.19	62.43
2.05	77.87	101.73	38.36	141.80	62.15

6.1.1.1.3 Data sheet for 6% Mixtures 0.94mm mesh plus water spray

**Table 6.1.1.1.3-1: 6% methane-air mixtures with 0.94mm mesh and water sprays data sheet**

<b>Time (s)</b>	<b>TC-1</b>	<b>TC-2</b>	<b>TC-3</b>	<b>TC-4</b>	<b>TC-5</b>
0.00	19.42	19.33	19.15	19.24	19.43
0.10	33.60	19.42	19.16	19.31	19.44
0.20	87.96	47.64	19.39	19.39	19.44
0.31	100.02	60.45	33.32	20.47	19.44
0.41	98.77	65.56	39.28	61.64	27.52
0.51	97.34	70.80	42.18	88.72	62.46
0.61	94.02	74.94	42.22	105.05	73.63
0.72	93.53	77.06	41.72	117.13	80.07
0.82	91.61	79.76	40.95	121.89	79.89
0.92	89.58	80.76	41.11	126.50	78.20
1.02	86.75	82.87	40.85	132.38	75.07
1.13	85.48	84.75	41.28	135.87	73.27
1.23	83.59	85.85	40.00	136.73	70.44
1.33	81.71	87.23	41.48	137.54	67.87
1.43	79.93	88.61	41.95	138.52	65.02
1.54	78.27	89.72	41.81	138.35	63.51
1.64	76.66	90.94	41.60	137.91	61.62
1.74	75.27	92.21	41.77	135.84	59.87
1.84	72.92	92.94	41.40	132.31	56.99
1.95	72.84	93.66	41.02	128.77	56.70
2.05	71.84	94.15	40.77	125.66	55.31

**Table 6.1.1.1.3-2: 7% methane-air mixtures with 0.94mm mesh and water sprays data sheet**

<b>Time (s)</b>	<b>TC 1</b>	<b>TC 2</b>	<b>TC 3</b>	<b>TC 4</b>	<b>TC 5</b>
0.00	24.26	25.09	24.19	25.43	24.97
0.10	35.28	25.12	24.18	25.45	24.97
0.20	105.12	60.12	24.21	25.45	24.97
0.31	123.71	95.85	39.93	25.45	24.97
0.41	127.66	107.28	44.89	25.45	24.97
0.51	123.83	111.50	46.58	25.45	24.99
0.61	120.06	112.35	47.95	25.45	24.97
0.72	116.09	110.76	46.63	25.45	24.97
0.82	114.14	113.02	45.57	25.45	24.97
0.92	109.20	116.61	46.18	25.45	24.97
1.02	106.07	119.67	48.50	25.45	24.97
1.13	103.36	121.13	47.14	25.45	24.97
1.23	100.89	124.38	47.93	25.45	24.97
1.33	98.08	124.82	48.94	25.45	24.99
1.43	95.46	125.70	48.39	25.45	24.99
1.54	93.12	126.39	48.22	25.45	24.97
1.64	91.14	126.64	48.82	25.45	24.97
1.74	90.24	125.81	48.88	25.45	24.97
1.84	90.54	125.36	48.72	25.43	24.97
1.95	94.43	125.14	49.57	25.45	24.97
2.05	94.78	124.44	50.21	25.45	24.99

7% Methane-air mixtures flame propagation images

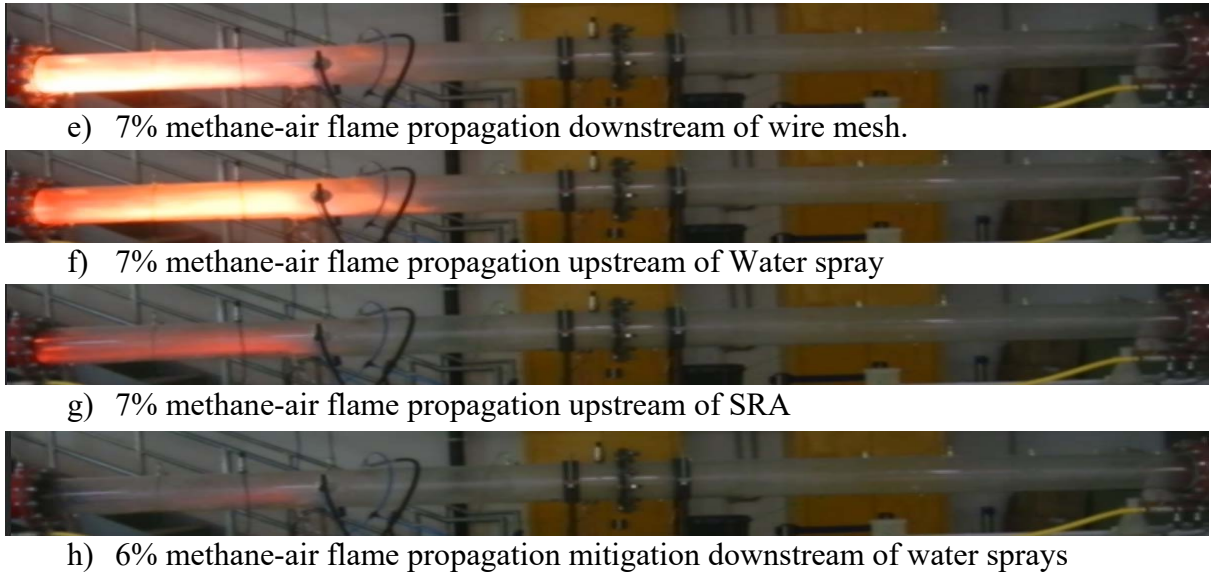


**Figure 6.1.1.3-1: Flame propagating downstream of mesh and upstream and downstream water sprays for 6% methane-air mixtures**

**Time – Temperature Profile**

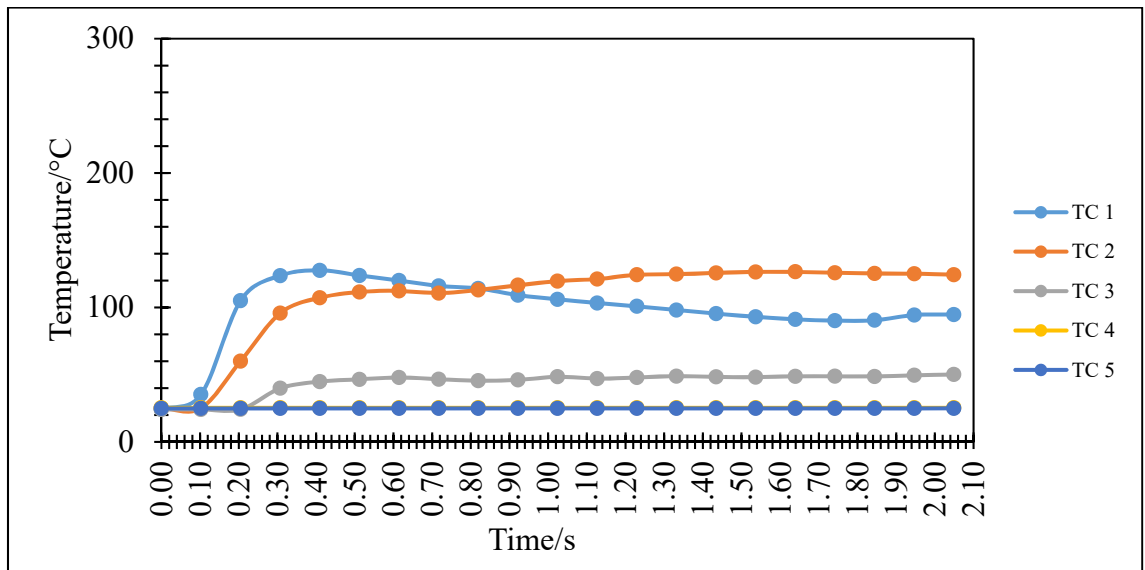


**Figure 6.1.1.3-2: Time-Temperature responses of 7% mixture with 0.94mm mesh plus sprays**

**Table 6.1.1.1.3-3: 9% methane-air mixtures with 0.94mm mesh and water sprays data sheet**

<b>Time (s)</b>	<b>TC 1</b>	<b>TC 2</b>	<b>TC 3</b>	<b>TC 4</b>	<b>TC 5</b>
0.00	19.88	19.92	19.60	19.90	19.77
0.10	104.00	19.99	18.43	19.91	19.77
0.20	145.58	44.59	19.61	19.91	19.77
0.31	146.32	85.49	32.15	19.98	18.71
0.41	139.40	104.88	37.61	51.79	19.83
0.51	133.16	110.20	38.52	113.48	56.98
0.61	126.73	114.36	37.89	130.62	81.21
0.72	121.03	115.79	37.58	140.79	91.04
0.82	116.10	115.13	37.41	143.84	91.58
0.92	111.55	111.95	37.04	149.38	88.20
1.02	107.37	109.41	37.01	148.57	84.64
1.13	104.60	107.23	37.47	147.06	81.39
1.23	99.82	105.00	38.13	147.03	78.22
1.33	96.39	102.79	38.01	147.10	75.27
1.43	93.20	102.13	37.08	147.66	72.60
1.54	90.12	102.05	38.10	147.24	70.16
1.64	87.30	101.90	38.26	147.76	69.10
1.74	84.70	102.14	38.03	146.95	66.02
1.84	82.28	102.51	38.24	146.18	64.19
1.95	80.00	102.15	38.06	144.19	62.43
2.05	77.87	101.73	38.36	141.80	62.15

6.1.1.1.4 Data sheet for various 6% Mixtures with 1.31mm mesh no spray

**Table 6.1.1.1.4-1:** 6% methane-air mixtures with 1.31mm mesh and no water sprays data sheet

<b>Time (s)</b>	<b>TC 1</b>	<b>TC 2</b>	<b>TC 3</b>	<b>TC 4</b>	<b>TC 5</b>
0.00	18.58	16.96	16.76	16.90	17.19
0.10	28.87	16.99	16.77	16.91	17.19
0.20	70.22	35.89	19.80	16.94	17.21
0.31	91.76	57.63	31.05	16.99	17.22
0.41	95.76	77.03	32.40	44.88	20.94
0.51	96.32	89.45	34.73	91.56	50.58
0.61	95.52	96.41	35.05	118.61	74.29
0.72	96.54	100.77	35.09	134.06	87.60
0.82	96.75	102.75	35.64	142.30	94.16
0.92	95.49	103.80	35.49	146.03	96.71
1.02	93.10	104.32	35.81	144.53	96.25
1.13	90.98	103.55	35.58	143.94	94.16
1.23	88.71	102.35	36.31	145.45	91.97
1.33	86.17	102.10	37.63	143.71	89.57
1.43	83.59	102.31	37.31	143.02	86.68
1.54	81.14	102.28	38.00	142.64	85.30
1.64	78.97	101.57	36.13	140.90	81.81
1.74	77.17	100.23	36.47	139.35	79.68
1.84	76.64	99.37	36.37	138.19	77.65
1.95	73.63	98.44	37.40	137.51	76.99
2.05	71.96	97.27	35.79	136.74	73.73

### Flame propagation behaviour for 7% mixture with 1.31mm mesh no sprays

Figure 5.17 shows a sequence of high-speed Nikon images of 6% methane-air flame propagation in a closed tube. The first image shows the onset of the flame through the woven wire mesh (1.31mm) into the transparent section of the tube (PMMA section).

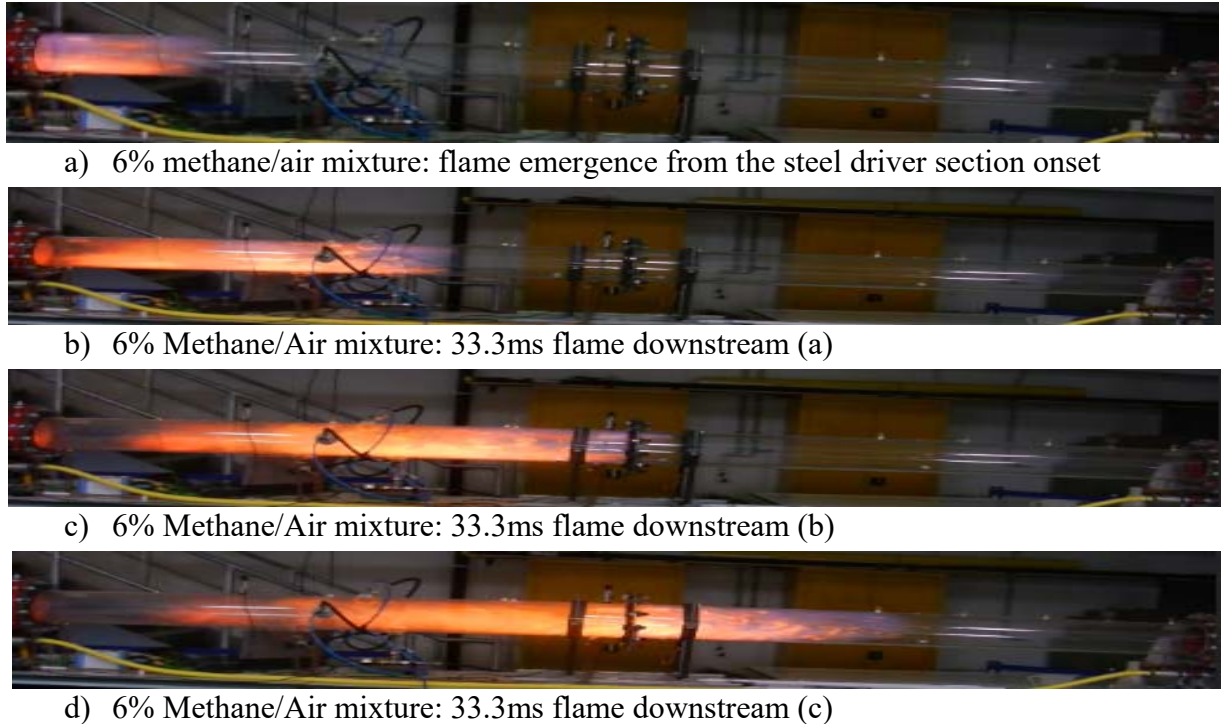


**Figure 6.1.1.1.4-1: Flame propagation 6% mixture with 1.33mm mesh and no water spray**

### Time – Temperature Profile with woven wire mesh 1.31mm

The time – temperature profile shown in figure 5.18 presents the temperatures recorded over short period of time approximately two seconds which was extracted from the raw temperature data. At the start of the ignition, there is a rapid increase in temperature to about 8°C measured at TC-1. This point illustrates the onset of combustion which is referred as ‘trigger point’. After this point, the inflection point was established. Inflection point is the point at which the heat is received from the hot zone refers to as pre-heat zone. (The distance between the trigger point and inflection point is known as preheat zone).

As shown in figure 5.18 the thermocouple output data for 6% methane-air mixture with 1.31mm woven wire mesh installed between the flanges of steel pipe and PMMA tube at the distance 2000mm from the ignition point as shown figure 4.6. After the triggered point, the flame propagated through the narrow aperture of the woven wire mesh, which shows a

profound effect because the flame decelerated due to the scattering of the flame when passing through the woven wire mesh.

As seen in figure 5.18, when the flame propagated through the mesh, the temperature fall drastically from 95°C in TC-1 to 31°C in TC-3 which shows that there is a specific heat loss by conduction to the woven wire mesh and to the pipe walls across the length of the pipe until a stable temperature reached. At about 0.71 seconds, there was a great increase in temperature TC-4 to about 134°C. This is because the flame have rejuvenated and gain back some its momentum.

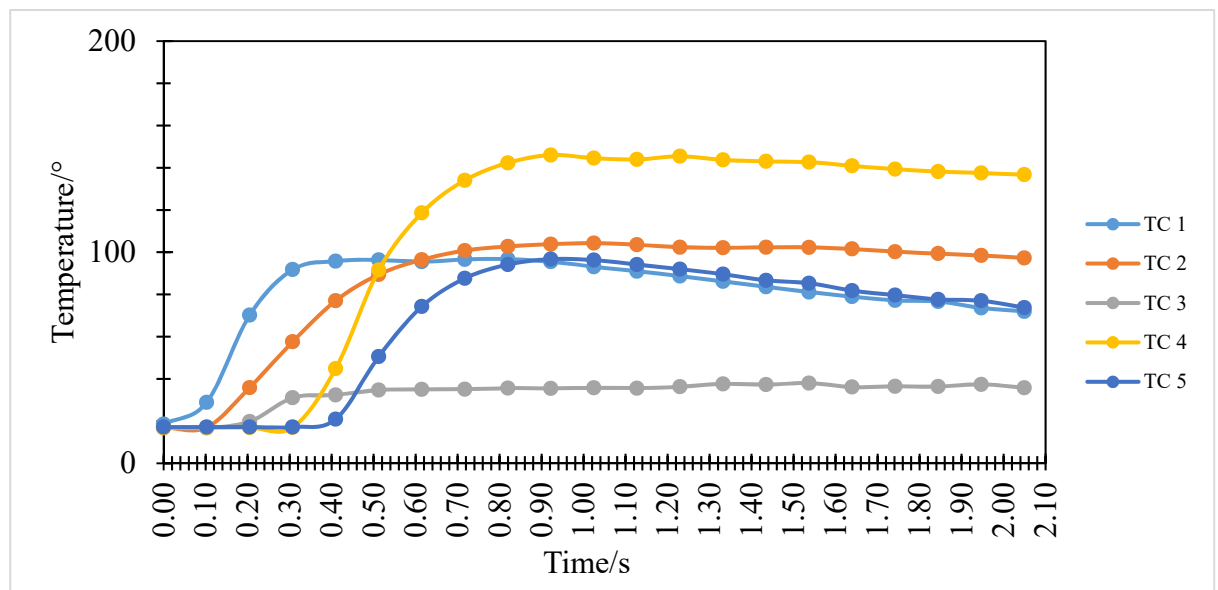


**Figure 6.1.1.1.4-2: Time-Temperature responses of 7% mixture with 1.31mm mesh no sprays.**

**Table 6.1.1.4-2: 7% methane-air mixtures with 1.31mm mesh and no water sprays data sheet**

<b>Time (s)</b>	<b>TC 1</b>	<b>TC 2</b>	<b>TC 3</b>	<b>TC 4</b>	<b>TC 5</b>
0.00	20.55	19.88	20.04	19.92	20.11
0.10	55.73	19.96	20.05	19.94	20.11
0.20	94.13	42.52	20.11	19.93	20.12
0.31	105.75	68.88	32.58	22.78	18.64
0.41	111.16	88.93	35.75	93.47	23.90
0.51	113.49	95.95	37.61	120.46	57.16
0.61	113.17	102.20	37.38	133.54	75.21
0.72	110.54	105.53	37.59	142.18	86.41
0.82	107.01	106.40	38.04	142.17	90.79
0.92	104.18	107.71	37.56	144.57	94.77
1.02	100.24	108.04	37.30	144.77	94.15
1.13	96.65	108.14	39.25	143.86	93.63
1.23	93.17	107.68	38.94	144.41	93.19
1.33	90.16	105.91	39.09	144.84	89.59
1.43	87.38	104.84	39.10	143.46	87.17
1.54	84.74	102.65	39.27	142.50	85.07
1.64	82.32	100.64	39.01	141.15	83.06
1.74	79.98	99.27	38.93	140.21	81.27
1.84	77.88	98.75	38.86	140.08	79.92
1.95	75.87	98.52	38.78	139.36	78.69
2.05	73.94	98.33	38.64	137.96	77.38

**Table 6.1.1.1.4-3:** 9% methane-air mixtures with 1.31mm mesh and no water sprays data sheet

<b>Time (s)</b>	<b>TC 1</b>	<b>TC 2</b>	<b>TC 3</b>	<b>TC 4</b>	<b>TC 5</b>
0.00	20.95	20.68	20.51	20.74	19.25
0.10	85.84	20.68	20.51	20.74	19.25
0.20	115.37	31.55	20.51	20.74	19.25
0.31	123.76	62.51	32.62	20.74	19.25
0.41	120.08	79.69	39.87	21.03	19.25
0.51	114.72	86.81	40.68	106.12	20.74
0.61	109.97	91.37	40.35	128.52	38.15
0.72	104.67	95.03	40.50	135.58	77.63
0.82	102.09	98.09	41.74	137.72	92.27
0.92	98.48	101.93	42.13	143.03	96.71
1.02	95.02	104.64	43.98	148.15	94.44
1.13	92.89	106.83	42.97	149.64	90.00
1.23	88.87	108.58	43.08	152.89	86.04
1.33	88.51	110.22	43.79	152.51	82.56
1.43	90.89	111.02	45.02	153.52	79.40
1.54	91.96	111.44	44.99	152.83	76.48
1.64	93.12	111.96	44.93	149.53	73.77
1.74	96.08	113.20	44.10	146.62	72.64
1.84	98.14	112.35	43.25	143.76	69.08
1.95	99.61	112.16	43.25	140.16	67.06
2.05	101.95	111.70	42.97	138.19	65.19

6.1.1.1.5 Data Series for various 6% Mixtures using 1.31mm mesh plus water spray

**Table 6.1.1.1.5-1:** 6% methane-air mixtures with 1.31mm mesh plus water sprays data sheet

Time (s)	TC 1	TC 2	TC 3	TC 4	TC 5
0.00	24.26	25.09	24.19	25.43	24.97
0.10	35.28	25.12	24.18	25.45	24.97
0.20	105.12	60.12	24.21	25.45	24.97
0.31	123.71	95.85	39.93	25.45	24.97
0.41	127.66	107.28	44.89	25.45	24.97
0.51	123.83	111.50	46.58	25.45	24.99
0.61	120.06	112.35	47.95	25.45	24.97
0.72	116.09	110.76	46.63	25.45	24.97
0.82	114.14	113.02	45.57	25.45	24.97
0.92	109.20	116.61	46.18	25.45	24.97
1.02	106.07	119.67	48.50	25.45	24.97
1.13	103.36	121.13	47.14	25.45	24.97
1.23	100.89	124.38	47.93	25.45	24.97
1.33	98.08	124.82	48.94	25.45	24.99
1.43	95.46	125.70	48.39	25.45	24.99
1.54	93.12	126.39	48.22	25.45	24.97
1.64	91.14	126.64	48.82	25.45	24.97
1.74	90.24	125.81	48.88	25.45	24.97
1.84	90.54	125.36	48.72	25.43	24.97
1.95	94.43	125.14	49.57	25.45	24.97
2.05	94.78	124.44	50.21	25.45	24.99

### Flame propagation behaviour for 7% mixture with 1.31mm mesh + sprays

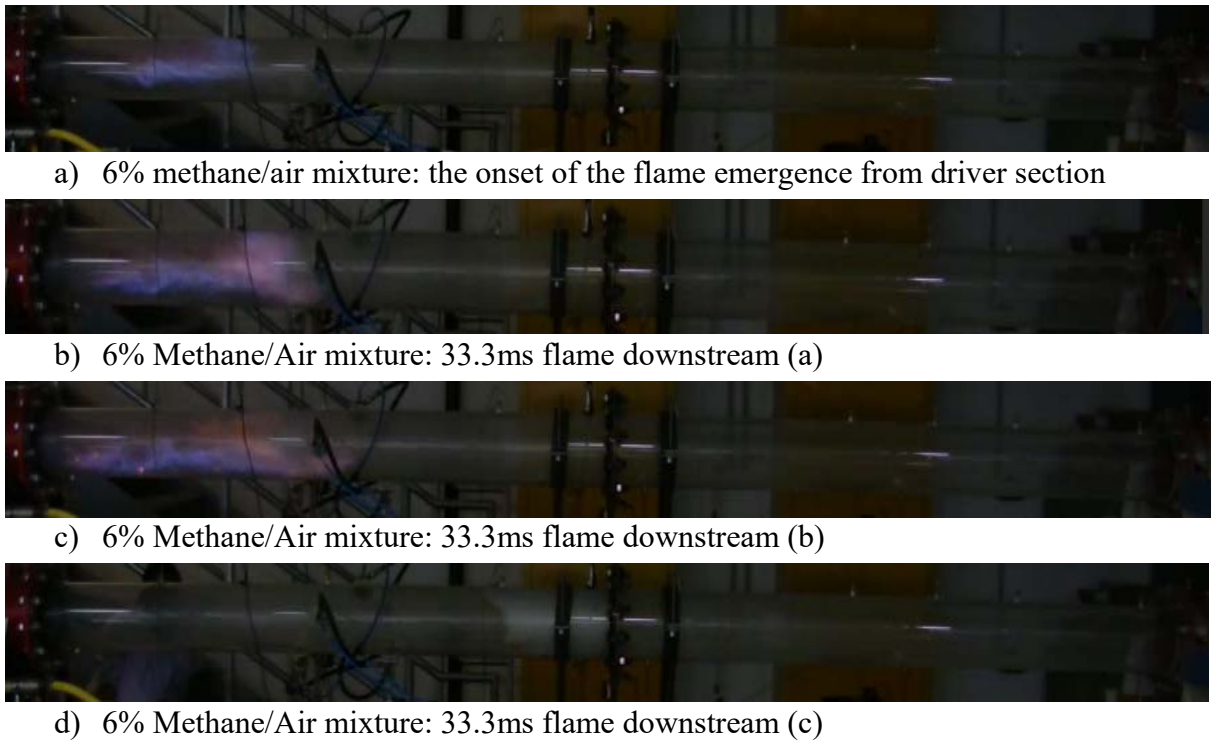


Figure 6.1.1.5-1: Flame propagation 7% mixture with 1.33mm mesh and plus sprays

### Temperature – Time response for 7% mixture with 1.31mm mesh plus sprays

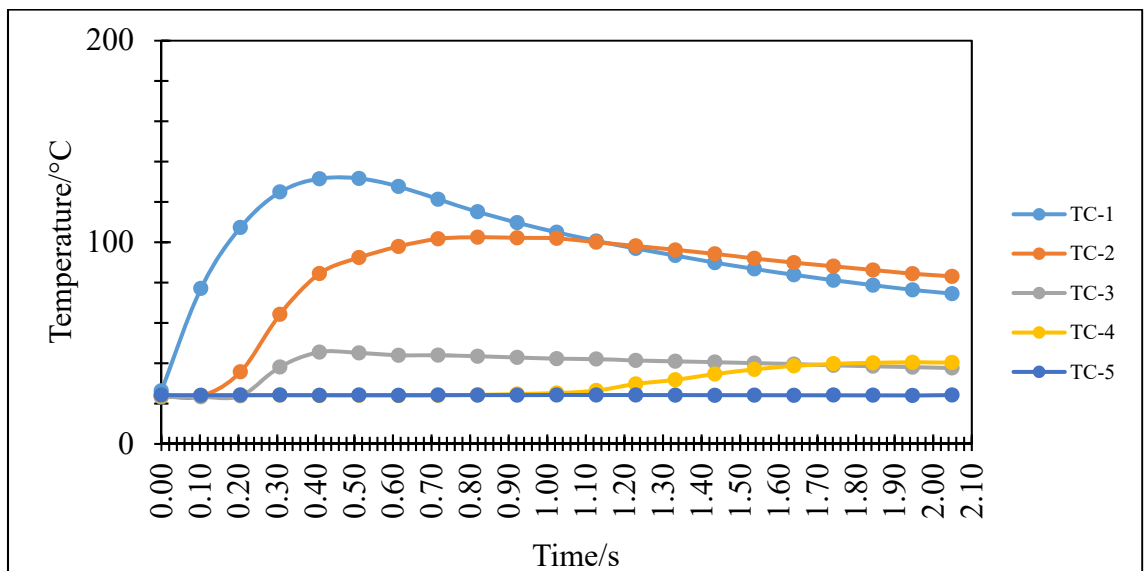


Figure 6.1.1.5-2: Time-Temperature responses of 7% methane/air mixture with 1.31mm mesh

**Table 6.1.1.1.5-2: 7% methane-air mixtures with 1.31mm mesh plus water sprays data sheet**

Time/s	TC-1	TC-2	TC-3	TC-4	TC-5
0.00	26.30	23.67	23.26	23.96	24.22
0.10	77.12	23.71	23.34	24.10	24.14
0.20	107.38	35.73	23.90	24.22	24.26
0.31	124.95	64.28	38.16	24.29	24.22
0.41	131.50	84.47	45.55	24.05	24.09
0.51	131.67	92.43	45.14	24.07	24.29
0.61	127.71	97.92	43.98	23.95	24.09
0.72	121.32	101.74	43.99	24.10	24.24
0.82	115.15	102.51	43.48	24.38	24.19
0.92	109.72	102.24	42.89	24.70	24.21
1.02	104.97	101.94	42.28	25.24	24.29
1.13	100.64	100.02	42.08	26.44	24.29
1.23	96.98	98.23	41.37	29.77	24.29
1.33	93.43	96.20	41.00	31.82	24.17
1.43	89.92	94.25	40.57	34.66	24.12
1.54	86.79	92.02	40.08	36.94	24.21
1.64	83.85	89.87	39.61	38.69	24.09
1.74	81.19	88.14	38.98	39.77	24.24
1.84	78.74	86.22	38.54	40.18	24.19
1.95	76.42	84.45	38.08	40.45	24.03
2.05	74.53	83.10	37.65	40.37	24.24

**Table 6.1.1.1.5-3: 9% methane-air mixtures with 1.31mm mesh plus water sprays data sheet**

<b>Time (s)</b>	<b>TC 1</b>	<b>TC 2</b>	<b>TC 3</b>	<b>TC 4</b>	<b>TC 5</b>
0.00	24.64	23.78	24.33	25.41	24.38
0.10	88.11	23.80	25.48	25.43	24.38
0.20	147.29	32.65	24.33	25.41	24.38
0.31	156.16	65.09	31.74	25.41	24.40
0.41	146.88	73.07	45.21	25.41	24.38
0.51	138.52	75.39	47.14	25.43	24.40
0.61	131.74	76.91	46.49	25.41	24.38
0.72	125.92	76.84	47.46	25.41	24.38
0.82	120.15	76.52	46.43	25.43	24.38
0.92	114.96	76.29	46.19	25.41	24.38
1.02	110.01	76.47	46.26	27.77	24.38
1.13	105.76	76.79	46.78	28.77	24.38
1.23	102.07	76.86	47.37	29.77	24.36
1.33	98.83	75.45	47.15	31.82	24.36
1.43	97.07	74.80	46.53	34.66	24.36
1.54	92.83	74.10	46.36	36.94	24.36
1.64	90.13	73.08	46.28	38.69	24.36
1.74	89.16	72.90	45.95	39.77	24.40
1.84	85.24	72.43	45.58	40.18	24.26
1.95	82.90	71.20	45.14	40.45	24.40
2.05	80.74	69.90	46.09	40.37	24.40

#### 6.1.1.1.6 Data sheet for 6% Mixtures with 6mm mesh no spray

**Table 6.1.1.1.6-1:** 6% methane-air mixtures with 6mm mesh no water sprays data sheet

<b>Time/s</b>	<b>TC1</b>	<b>TC2</b>	<b>TC3</b>	<b>TC4</b>	<b>TC5</b>
0.00	22.54	22.17	22.23	22.38	22.33
0.10	63.80	26.18	22.23	22.36	22.33
0.20	127.29	55.46	22.24	24.19	22.33
0.31	148.25	67.42	28.26	22.38	22.33
0.41	142.65	69.88	45.33	26.03	22.35
0.51	135.69	70.68	47.82	67.79	22.38
0.61	129.97	68.81	49.10	74.03	67.62
0.72	124.58	69.24	51.09	74.72	83.44
0.82	118.99	70.01	51.44	72.95	90.73
0.92	114.31	69.78	51.65	74.43	91.08
1.02	109.94	69.96	51.56	74.05	87.76
1.13	105.99	69.44	51.66	73.78	83.96
1.23	102.34	69.19	51.39	75.03	80.49
1.33	98.86	69.96	51.28	73.10	77.42
1.43	95.66	70.01	50.80	72.36	74.72
1.54	92.76	69.96	49.98	72.56	72.31
1.64	90.15	69.51	49.66	72.33	70.11
1.74	89.33	69.63	49.09	71.46	68.11
1.84	88.71	69.73	48.55	70.48	66.27
1.95	87.37	69.61	47.91	71.54	64.56
2.05	87.02	69.83	47.17	69.44	62.99

7% mixtures with 6mm mesh no sprays



a) 7% Methane/air mixture: the onset of the flame downstream of mesh

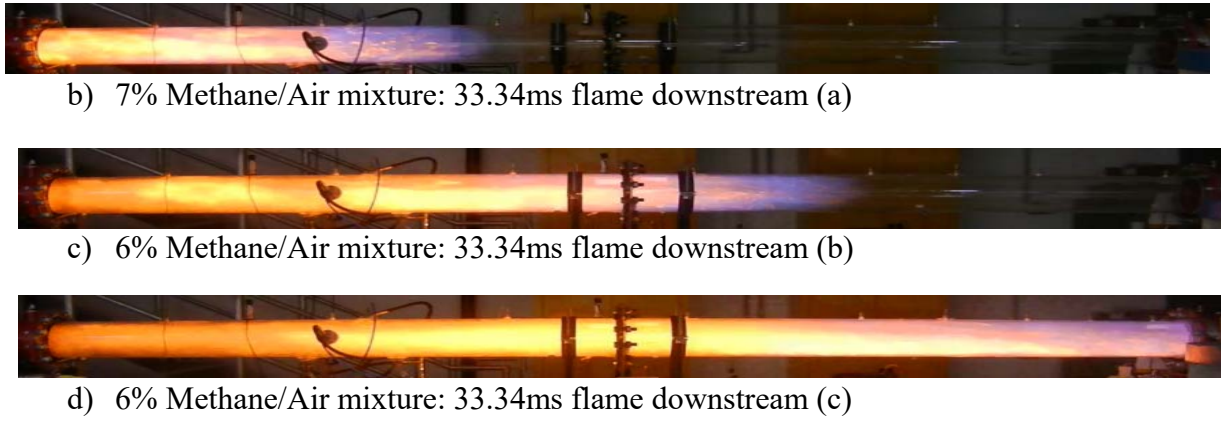


**Figure 6.1.1.6-1:** Flame propagation 7% mixture with 6mm mesh no sprays

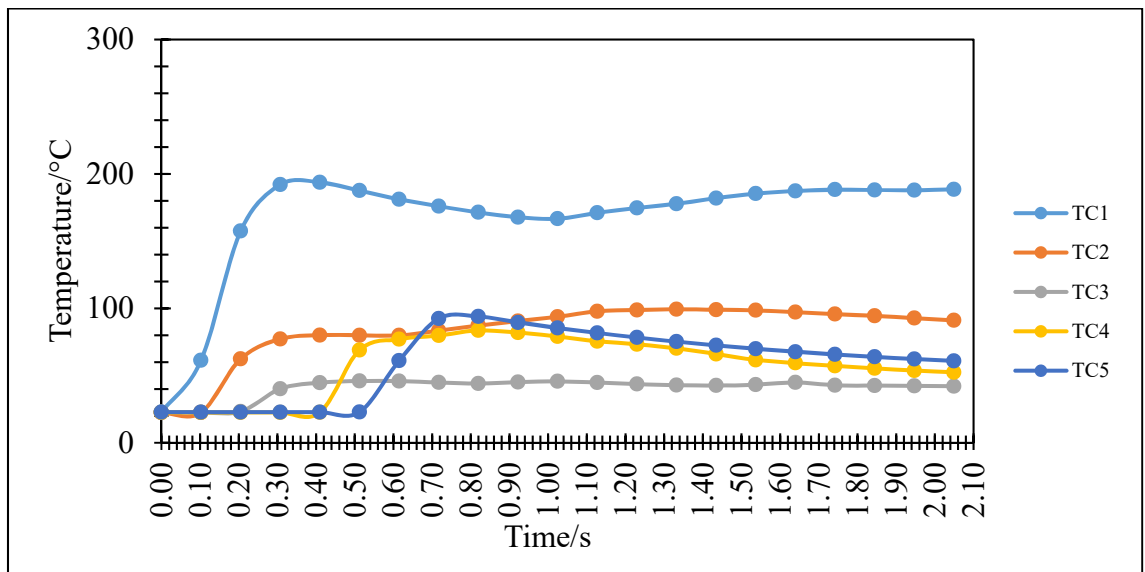


**Figure 6.1.1.6-2:** Time-Temperature responses of 7% methane/air mixture with 6mm mesh no sprays

**Table 6.1.1.6-2:** 7% methane-air mixtures with 6mm mesh no water sprays data sheet

Time/s	TC1	TC2	TC3	TC4	TC5
0.00	22.78	22.44	22.70	22.56	22.82
0.10	61.33	22.51	22.70	22.56	22.82
0.20	157.54	62.35	23.22	22.56	22.82
0.31	192.06	77.21	40.19	22.58	22.80

0.41	193.69	80.07	44.73	22.63	22.82
0.51	187.61	79.96	45.94	68.97	22.85
0.61	181.06	79.88	45.89	77.08	61.06
0.72	175.99	83.30	44.88	79.83	92.40
0.82	171.45	87.38	44.08	83.65	93.94
0.92	167.76	90.46	45.13	81.95	89.47
1.02	166.66	93.72	45.71	79.11	85.38
1.13	171.05	97.80	44.79	75.49	81.70
1.23	174.68	98.77	43.70	73.29	78.35
1.33	177.81	99.34	42.88	70.32	75.33
1.43	182.00	98.94	42.65	65.96	72.51
1.54	185.39	98.55	43.21	61.60	69.97
1.64	187.28	97.16	44.91	59.40	67.70
1.74	188.34	95.73	42.80	57.14	65.69
1.84	187.98	94.44	42.53	55.38	63.94
1.95	187.89	92.73	42.34	53.74	62.32
2.05	188.50	91.06	42.05	52.46	60.89

**Table 6.1.1.1.6-3:** 9% methane-air mixtures with 6mm mesh no water sprays data sheet

<b>Time/s</b>	<b>TC1</b>	<b>TC2</b>	<b>TC3</b>	<b>TC4</b>	<b>TC5</b>
0.00	24.30	22.52	22.37	22.07	24.05
0.10	109.45	22.52	22.38	22.07	22.47
0.20	180.95	50.27	23.56	22.11	22.49
0.31	220.25	83.88	43.57	22.09	22.50
0.41	245.17	112.58	44.60	22.16	22.50

0.51	255.88	128.08	46.50	73.44	22.54
0.61	257.89	134.13	45.25	109.98	42.29
0.72	247.17	135.66	45.13	107.36	73.99
0.82	235.57	140.58	44.94	105.17	88.41
0.92	224.01	138.11	44.96	99.89	95.95
1.02	215.08	136.64	45.26	94.76	104.78
1.13	204.21	135.08	45.82	91.12	108.68
1.23	195.36	133.50	46.92	90.85	109.94
1.33	187.22	131.81	44.60	90.14	109.52
1.43	179.77	130.27	44.27	88.98	109.22
1.54	172.84	128.77	44.60	86.81	108.02
1.64	166.62	127.86	43.18	84.22	105.89
1.74	160.18	126.87	42.71	82.51	105.32
1.84	155.70	125.61	42.83	81.41	102.18
1.95	150.45	123.91	43.69	80.61	101.18
2.05	146.95	121.97	44.69	81.70	99.79

6.1.1.1.7 Data sheet for 6% Mixtures using 6mm mesh no spray

**Table 6.1.1.1.7-1:** 6% methane-air mixtures with 6mm mesh plus water sprays data sheet

Time/s	TC1	TC2	TC3	TC4	TC5
0.00	23.53	23.12	23.07	23.57	23.36
0.10	69.44	23.62	23.07	23.57	23.36
0.20	104.52	49.35	23.08	23.58	23.36
0.31	118.87	75.03	28.63	23.63	23.36

0.41	137.07	86.13	40.53	23.51	23.29
0.51	130.70	89.22	40.75	23.31	23.38
0.61	126.22	89.69	41.06	23.17	23.41
0.72	121.16	90.08	41.45	23.17	21.48
0.82	117.77	89.79	41.28	24.27	23.41
0.92	111.84	89.14	41.13	27.02	23.41
1.02	107.35	88.77	40.58	27.11	23.39
1.13	103.54	86.65	40.09	28.65	23.38
1.23	100.01	84.38	39.82	30.72	23.38
1.33	96.71	84.56	41.50	29.63	23.36
1.43	93.61	83.14	39.55	30.35	23.36
1.54	90.56	81.27	39.23	30.48	23.36
1.64	87.65	80.18	40.84	30.62	23.36
1.74	84.91	79.43	38.75	30.72	23.36
1.84	82.24	78.97	38.43	30.69	23.36
1.95	79.87	77.71	40.01	30.43	23.34
2.05	77.75	76.00	37.83	30.19	25.18

**Table 6.1.1.1.7-2:** 7% methane-air mixtures with 6mm mesh plus water sprays data sheet

Time/s	TC1	TC2	TC3	TC4	TC5
0.00	24.05	23.32	23.63	23.38	23.53
0.10	88.41	23.36	25.32	23.39	23.53
0.20	126.22	34.58	23.63	23.39	23.53
0.31	117.62	67.90	32.19	23.39	23.53
0.41	110.39	82.89	45.20	23.39	23.53
0.51	104.89	89.79	45.46	23.41	23.53
0.61	99.46	87.34	44.24	23.41	23.53
0.72	95.03	82.34	43.92	23.43	23.53

0.82	91.37	78.57	43.62	23.44	23.53
0.92	87.75	75.78	43.33	23.44	23.51
1.02	84.71	72.69	42.80	23.46	23.53
1.13	83.54	70.32	42.23	23.48	23.53
1.23	79.59	68.24	41.65	23.48	23.53
1.33	77.22	66.25	41.06	23.50	23.53
1.43	76.70	64.61	40.47	23.50	23.53
1.54	73.06	62.99	39.92	23.50	23.53
1.64	71.26	61.59	39.41	23.67	23.55
1.74	71.21	60.28	38.94	23.48	23.53
1.84	67.79	59.14	38.50	23.50	23.53
1.95	66.20	58.09	38.11	23.50	23.53
2.05	64.70	57.20	37.72	23.50	23.53

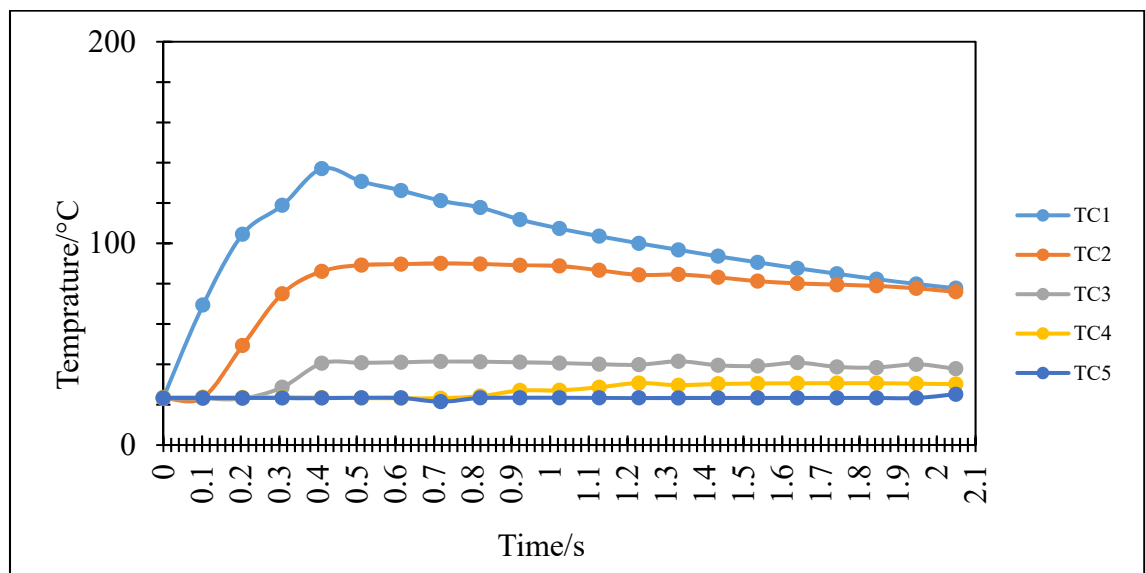


**Figure 6.1.1.7-1:** Time-Temperature responses of 7% methane/air mixture with 6mm mesh plus sprays



**Table 6.1.1.1.7-3: 9% methane-air mixtures with 6mm mesh plus water sprays data sheet**

<b>Time/s</b>	<b>TC1</b>	<b>TC2</b>	<b>TC3</b>	<b>TC4</b>	<b>TC5</b>
0.00	22.64	21.54	21.57	22.30	21.94
0.10	112.95	21.68	21.57	22.32	21.94
0.20	161.11	40.80	21.59	22.33	21.94
0.31	151.17	69.75	39.41	22.47	21.99
0.41	141.51	83.62	47.68	41.80	22.13
0.51	133.84	86.52	52.89	46.58	61.61
0.61	126.82	87.61	51.77	46.87	81.88
0.72	120.47	86.71	50.05	48.00	88.39
0.82	116.06	85.94	49.41	47.79	90.94
0.92	109.55	83.21	48.55	47.69	89.83
1.02	105.12	81.14	47.42	48.42	84.52
1.13	102.53	79.66	46.28	51.78	81.18
1.23	97.07	78.37	45.18	54.69	78.12
1.33	93.68	76.39	44.25	55.14	75.32
1.43	90.50	75.17	43.42	56.53	72.82
1.54	87.74	73.98	42.66	58.34	70.51
1.64	85.08	72.55	41.95	57.10	68.48
1.74	82.48	71.21	41.29	57.10	66.69
1.84	80.06	70.01	40.69	58.80	65.12
1.95	77.86	68.78	40.13	57.37	63.62
2.05	75.80	67.41	40.93	57.29	62.16

### 6.1.1.1.8 Preliminary trials with water sprays only

Here, the explosion temperature generally indicates a sudden rise in temperature from room temperature 20°C to about 92.98°C for thermocouple 2 (TC-2) and then gradually falling until the temperature stabilized at 66.85 °C with corresponding time of 2.76s. This is due cooling sensation of the flame coming in contact with high pressure water sprays that resulted in the flame front been distorted, slowed down and eventually extinguished before reaching the end of the pipe. Thus, other thermocouples located along the pipeline length of 6300mm indicates a lower temperature with a further decrease from TC-2 to TC-3, TC-3 to TC-1 and thereafter, a uniform temperature were recorded at thermocouples TC-4 and TC-5. The trends behaviour projects the expected temperature rise when the ignition commenced between 0.21s to 0.31s for the thermocouple 1(TC-1) which was because of the excessive energy released.

Moreover, as the propagating flame moves towards the end of the 6300mm tube at thermocouples TC-4 and TC-5, the rise in temperature recorded was not significant due to substantial heat transfer, which has effective resulted in heat loss as the flame propagates through the pipe length. This particularly has been relevant considering the beginning of the pipe is made up of carbon steel metal, which could drive some significant heat losses by conduction.

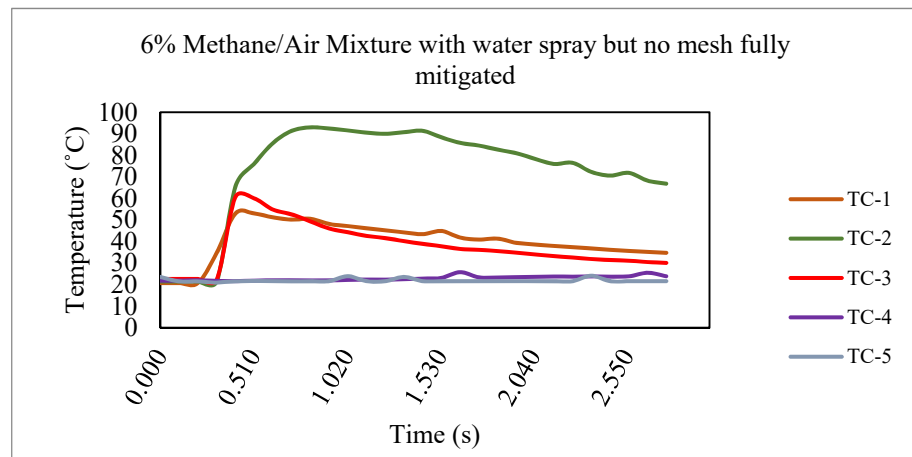


**figure 6.1.1.1.8-1:** Time – Temperature response of 6% methane/air flame propagation with water spray but no mesh

### Time-Temperature variation with 9% mixture using Sprays only

Figure h-1 provides preliminary trials with water sprays only. A similar trend of temperature variation shown previously in figures 5.5, 5.16, and 5.19 were observed. Thermocouple 2 (TC-2) has maintained similar range of temperature during the 2 ms duration. This is particularly relevant as propagating flame were not allowed beyond the atomizers position, thereby limiting its speed, at the same time enabling thermal accumulation around the initial length of the tube due to ineffective heat transfer compared to the non-mitigated propagating flames. As the flame passes through the second and subsequently the third thermocouple, energy balances around the water sprays and the opposing flame was reduced by the cooling sensation of the water spray, and more significantly, the latent heat of vaporization of the water, which was transferred from the flame, thereby causing a significant reduction in temperature at those two thermocouples.

Also, it can be seen that there is a temperature increase in both thermocouples TC-4 and TC-5 to be 62 °C and 38 °C respectively. This is because large amount of water vapour was generated which moves gradually along the pipe length and of course due to the cooling effect of the interaction of water and flame, the vapour generated was warm and that causes the increase in both thermocouple TC-4 and TC-5 as shown in figure 5.12.

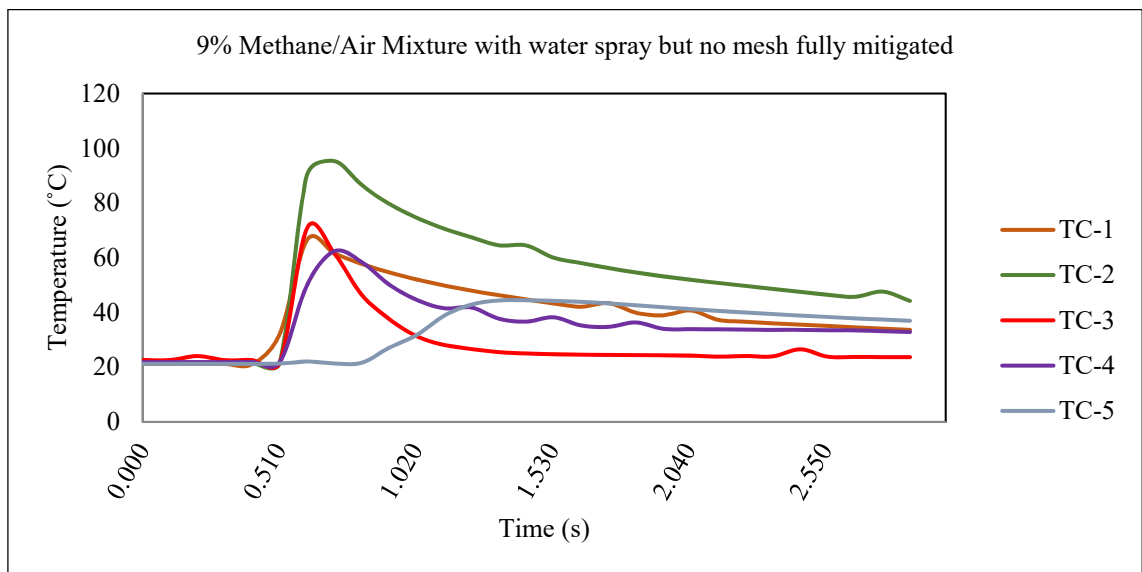


**Figure 6.1.1.8-2:** Temperature profile of 9% Methane/Air mixture with water spray but no mesh



a) Propagating Methane/Air flame at E.R. ( $\Phi$ ) 0.94: interaction with water



b) Propagating Methane/Air flame at E.R. ( $\Phi$ ) 0.94: spray position



c) Propagating Methane/Air flame at E.R. ( $\Phi$ ) 0.94: cooling effect

**Figure 6.1.1.1.8-3:** 9% Flame propagation upstream & downstream with water spray and no mesh